



HAL
open science

Dye and electroactive monomer conjugates for hole transfer material in solid-state dye-sensitized solar cells

Zijun Xu

► **To cite this version:**

Zijun Xu. Dye and electroactive monomer conjugates for hole transfer material in solid-state dye-sensitized solar cells. Other. Université Paris Cité, 2021. English. NNT: 2021UNIP7337. tel-04112087

HAL Id: tel-04112087

<https://theses.hal.science/tel-04112087>

Submitted on 31 May 2023

HAL is a multi-disciplinary open access archive for the deposit and dissemination of scientific research documents, whether they are published or not. The documents may come from teaching and research institutions in France or abroad, or from public or private research centers.

L'archive ouverte pluridisciplinaire **HAL**, est destinée au dépôt et à la diffusion de documents scientifiques de niveau recherche, publiés ou non, émanant des établissements d'enseignement et de recherche français ou étrangers, des laboratoires publics ou privés.

Université de Paris

Ecole doctorale de Chimie Physique et Chimie Analytique (ED 388)

*Laboratoire Interfaces Traitements Organisation et Dynamique des
Systèmes (ITODYS), UMR CNRS 7086*

Dye and Electroactive Monomer Conjugates for Hole Transfer Material in Solid-State Dye- Sensitized Solar Cells

Par Zijun XU

Thèse de doctorat de Chimie

Dirigée par Prof. François Maurel
Et par Prof. Chang-Zhi Dong

Présentée et soutenue publiquement le 05 Mai 2021

Devant un jury composé de :

Présidente :	Claire Mangeney , <i>Professeur</i> , Université de Paris
Rapporteur :	David Kreher , <i>Professeur</i> , Université de Versailles Saint-Quentin-en-Yvelines
Rapporteur :	Yu Pei , <i>Chargé de Recherche</i> , Université Paris-Saclay
Examinatrice :	Corinne Lagrost , <i>Directrice de Recherche</i> , Université de Rennes 1
Directeur de thèse :	François Maurel , <i>Professeur</i> , Université de Paris
Co-directeur de thèse :	Chang-Zhi Dong , <i>Professeur</i> , Université de Paris
Invité :	Mohamed Jouini , <i>Professeur</i> , Université de Paris



Except where otherwise noted, this is work licensed under
<https://creativecommons.org/licenses/by-nc-nd/3.0/fr/>

Acknowledgement

To complete this PhD was really a memorable experience, and certainly non-replicable. One could never achieve such a goal without countless assistance and support.

First of all, I would like to express my gratitude to my thesis supervisor, Prof. François Maurel for your great interest in this work, the vast liberty and kind encouragement I was provided with, for your constant availability and helpful discussions. More preciously, you taught me by your example how to look at the bigger picture from diverse angles (perspectives) and how to communicate more efficiently in different scenarios. Such opportunities are few and far between for a PhD student.

I would like to gratefully acknowledge Prof. Chang-Zhi DONG for your help in the synthesis and long hours you spent to stay late with me in the laboratory.

I would like to express my sincere appreciation to Prof. Mohamed Jouini, not only for the experiments from scientific electrochemical studies to less-scientific welding we conducted together, but also for your constructive discussions and suggestions on both the experimental and written skills provided with your great patience and broad experience.

Dr. Maire-Pierre Santoni is gratefully acknowledged. All the pause-café I took in your office, details we have discussed from synthesis to solar cells are of great importance. You have reminded me of my health and life that should be paid attention to and have always insisted doing things in the right way regardless difficulty and pressure we had to face.

Mr. Sébastien Belynck, it was such a great pleasure sharing the office with you. Many thanks to you for the synthesis work you did, the daily help from chemical purchase to the setup of the defense room. I could not even recall how many times you have been there proposing numerous possible solutions for whatever the problems are. Next pause-café we should take with different choices of chocolate with Mr. Alexandre Chevillot-Biraud, who I would also thank for your help in the preparation of solar cells as well as customized IR analysis training.

I would also like to acknowledge my committee members, Prof. David Kreher, Dr. Yu Pei, Dr. Corinne Lagrost, Prof. Claire Mangeney for your guidance and helpful suggestions.

My deepest appreciation also goes to Dr. Henri-Pierre Jacquot de Rouville who trained me meticulously into a synthetic chemist during the first year of my PhD, indispensable skills that enable me to undertake this project with enough confidence.

Thank you to Dr. Christian Perruchot, the PhD life be totally different without your coffee machine and my favorite shelf in bâtiment Lavoisier filled with chemistry and physics related books, and of course your constant kindness and support should not be forgot.

Dr. Alexis Gosset, who firstly took care of me even before the start. You were and are still there for me even after leaving Paris, along with your spy network. We may not have the office with a view of la Seine anymore, but bavette and beer (or maybe coffee of your choice but not vanille) one day for sure. Cheers.

Dr. Chérif Adouama, special thanks for your kind suggestions in synthesis as well as human relationship which relived me of anxiety and stress.

To Dr. Min Wang for your constant support, I am delighted that it was not too late to get to know you.

I would be remiss to not to thank the amazing people I have the chance encountering, Dr. Nicolas Battaglini, Dr. Samia Zrig, Dr. Jérémy Legall, Dr. Sandra Vasiljevic, Dr. Thomas Groizard, Dr. Sihem Groni, Dr. Bing Ma, Dr. Thamires D.S. Moreira, Dr. Justine Pallu; Doctor- to-be-soon Marie Alvarez , Rabia Djoumer, Samia Mekhmoukhen, Mario Luis Araujo Rocha, Ruwen Wang, Ms. Wanze Wang, and my dear colleagues on the 6th floor and 5th floor, all my friends in France, Belgium, Canada, China, Japan, Singapore, United States, for all the wonderful time we spent together. My thanks to them are covered in alphabetical order so nobody will feel slighted.

I was frequently asked: how could you stick to it? Here comes the answer now, it did not seem that difficult with all of you all by my side. As I said before, I am glad it was you.

This dissertation is dedicated to my family, from whom I inherited the virtues people believe I have. I am who I am mostly because of you. You supported all my decisions in every single way you can, I sincerely believe that I would never have come this far without you. I may not be certain what the future will hold, but who cares as long as we have each other. Afterall, who being loved is poor?

In closing, to myself – What's past is prologue.

Abstract:

The objective of this work is to develop solid-state dye sensitized solar cells (ss-DSSCs) in order to optimize the interfacial charge transfer within the solar cell. Despite of the broad use of liquid electrolyte, stability issues arose from solvent evaporation as well as liquid leakage have limited the large-scale production and commercialization of dye sensitized solar cells (DSSCs). The replacement of liquid electrolyte with solid hole transport materials (HTMs) is indispensable for long-term developments of devices. Conducting polymers is chosen in this work as HTM for its higher hole conductivity, good stability and facile preparation. Part of the newly designed dye molecule (otherwise called sensitizer), the electroactive monomer carbazole is used as initiator for co-polymerization with bis-(3,4 ethylenedioxythiophene) (bis-EDOT) as precursor in the *in-situ* photoelectrochemical polymerization (PEP) process, to ensure the covalent link between the light active center and the generated co-polymer, which serves as HTM. The interface between the dye and HTM is naturally removed as a result. Moreover, the blocking effect of alkyl chain in terms of the performances of ss-DSSCs has also been investigated by altering the molecular structure of dye.

The thesis is composed of five chapters. Chapter 1 gives a general context of photovoltaic solar cells as an introductory chapter. Chapter 2 focuses on the DSSCs including the components, working principle and characterization techniques of DSSCs. Chapter 3 begins by laying out different types of sensitizers and looks at how to design new organic sensitizer which could be covalently linked to the HTM. Chapter 4 presents the results of DSSCs fabricated with originally designed sensitizer. Chapter 5 ties up theoretical and empirical strands with a discussion of the implication of findings to future study in the area.

Keywords: Solid-State Dye-Sensitized Solar Cells, *in-situ* Photo-Electrochemical Polymerization, donor-linker-acceptor organic dyes, covalent link, hole transporting material, conducting polymer

Résumé :

L'objectif de ce travail est de développer des cellules solaires sensibilisées aux colorants à l'état solide (ss-DSSC) afin d'optimiser le transfert de charge interfacial dans la cellule solaire. Malgré la large utilisation d'électrolytes liquides, les problèmes de stabilité liés à l'évaporation des solvants ainsi que les fuites de liquide ont limité la production à grande échelle et la commercialisation de cellules solaires sensibilisées aux colorants (DSSC). Le remplacement de l'électrolyte liquide par des matériaux de transport de trous solides (HTM) est indispensable pour le développement à long terme des dispositifs. Les polymères conducteurs ont été choisis dans ce travail comme HTM en raison de leur haute conductivité de trou, leur bonne stabilité et leur préparation facile. Faisant partie de la molécule de colorant nouvellement conçue (autrement appelée sensibilisateur), le carbazole, monomère électroactif, est utilisé comme initiateur pour la copolymérisation avec le bis-(3,4 éthylenedioxythiophène) (bis-EDOT) comme précurseur dans le processus de polymérisation photo-électrochimique (PEP) *in situ*, pour assurer la liaison covalente entre le centre actif de la lumière et le copolymère généré, qui sert de HTM. L'interface entre le colorant et l'HTM est ainsi naturellement éliminée. En outre, l'effet de blocage de la chaîne alkyle en termes de performances des ss-DSSC a également été étudié en modifiant la structure moléculaire du colorant.

La thèse est composée de cinq chapitres. Le chapitre 1 donne un contexte général des cellules solaires photovoltaïques. Le chapitre 2 se concentre sur les DSSCs, y compris les composants, le principe de fonctionnement et les techniques de caractérisation des DSSCs. Le chapitre 3 commence par présenter les différents types de sensibilisateurs et examine comment concevoir un nouveau colorant organique qui pourrait être lié de manière covalente au HTM. Le chapitre 4 présente les résultats des DSSC fabriqués avec le colorant conçu à l'origine. Le chapitre 5 relie les aspects théorique et empirique et examine les implications des résultats pour les études futures dans ce domaine.

Mots-clés: Cellules solaires à colorant solide, photopolymérisation électrochimique *in-situ*, colorants organiques donneur-accepteur, liaison covalente, matériaux transporteur de trous, polymère conducteur

List of abbreviations

ACN	acetonitrile
ALD	atomic layer deposition
BL	blocking layer
CB	conduction band
CBZ	carbazole
CE	counter electrode
CP	conducting polymer
CV	cyclic voltammetry
DCM	dichloromethane
DFT	density functional theory
DSSCs	dye-sensitized solar cells
D-π-A	donor-linker-acceptor
EDOT	3,4-ethylenedioxythiophene
E_F	Fermi level
E_G	bandgap energy
E_{onset,ox}	onset of the oxidation potential
E_{ox} (dye)	oxidation potential of the dye
EPD	electrochemical deposition
E_{Q-F}	quasi-Fermi level
ETM	electron transporting material
FF	fill factor
FTO	fluorine doped tin oxide
HRMS	High resolution mass spectrum
HTM	hole transporting material
i_c	capacitive current

ICT	intramolecular charge transfer
IPCE	Incident Photon-to-Electron Conversion Efficiency
ITO	indium doped tin oxide
J	current density
J_{sc}	short-circuit current density
LCAO	linear combinations of atomic orbitals
LiTFSI	Li(CF ₃ SO ₂) ₂ N
L_n	electron diffusion length
MLCT	metal-to-ligand charge transfer
Mtoe	Mtoe Million Tonnes of Oil Equivalent
NR	nanorods
OFETs	organic field-effect transistors
OLEDs	organic light-emitting diodes
OPV	organic photovoltaic
PANI	polyaniline
PCE	power conversion efficiency
PEDOT	poly (3, 4-ethylenedioxythiophene)
PEN	polyethylene naphthalate
PEP	(<i>in-situ</i>) photo-electrochemical polymerization
PET	polyethylene terephthalate
PIA	photoinduced absorption spectroscopy
P_{in}	the incoming power
PPy	polypyrrole
PVD	physical vapor deposition
R_{CT}	charge transfer resistance
RE	reference electrode
SCE	saturated calomel electrode

SCN	thiocyanate
ss-DSSCs	solid-state DSSCs
SHE	standard hydrogen electrode
TBP	<i>4-tert</i> -butylpyridine
TCO	transparent conducting oxide
TDDFT	time dependent DFT
TPA	triphenylamine
VB	valence band
V_{oc}	open circuit potential
WE	working electrode
η	conversion efficiency
σ	conductivity

Table of Contents

CHAPTER 1. GENERAL INTRODUCTION OF PHOTOVOLTAIC SOLAR CELLS.....	1
1. GENERAL CONTEXT	1
2. ENERGY FROM THE SUN	3
3. PHOTOVOLTAIC EFFECT AND PHOTOVOLTAIC CELLS	4
4. PHOTOVOLTAIC CELLS GENERATIONS.....	5
4.1. <i>The 1st generation</i>	5
4.2. <i>The 2nd generation</i>	6
4.3. <i>The 3rd generation solar cells</i>	6
5. THESIS OVERVIEW	8
CHAPTER 2. THE DYE-SENSITIZED SOLAR CELL	11
I. THE ARCHITECTURE OF A DSSC	11
1.1. <i>Transparent conductive oxides (TCOs)</i>	12
1.2. <i>Metal oxide semiconductor</i>	12
1.3. <i>The photosensitizer: the organic dye</i>	13
1.4. <i>The redox mediator: The Hole Conducting Material (HTM)</i>	15
1.5. <i>The counter electrode</i>	19
2. DSSC'S OPERATIONAL PRINCIPLE	19
2.1. <i>Operational principle</i>	19
2.2. <i>Thermodynamic requirements</i>	21
2.3. <i>Kinetic aspects in DSSC</i>	22
3. BASIC PARAMETERS TO EVALUATE THE PERFORMANCE OF DSSCs: THE FIGURE OF MERIT OF DSSCs	25
4. EXPERIMENTAL CHARACTERIZATION TECHNIQUES FOR DSSCs	29
5. AIM OF THIS THESIS	30
CHAPTER 3. PRINCIPLE SENSITIZERS IN DSSCs AND NEW DESIGN OF SENSITIZERS.....	39
1. RU COMPLEXES	40
2. PORPHYRIN BASED DYES	46
3. METAL-FREE SENSITIZERS	55
3.1. <i>Coumarin</i>	57
3.2. <i>Triarylamine-based dyes</i>	58
4. DESIGN OF NEW METAL-FREE SENSITIZERS: A MULTIFUNCTIONAL SYSTEM	64
5. RETROSYNTHETIC ANALYSIS.....	69
6. THE SYNTHESIS OF THIOPHENES	71
7. THE STEP OF WITTIG REACTION	72
7.1. <i>Precursors for Wittig reaction</i>	72
7.2. <i>The Wittig reaction</i>	73
CHAPTER 4. ALKYL LINKED DYE-HTM: EFFECT OF LINKER NATURE ON SS-DSSC PERFORMANCES	87
I. INTRODUCTION	87
1.1. <i>Optimization of the Interfacial Charge Transfer</i>	87
1.2. <i>In-situ PEP</i>	88
2. EXPERIMENTAL DETAILS	89
2.1. <i>Dye synthesis</i>	89
2.2. <i>Techniques used for the characterization of dye structures and Dye-sensitized TiO₂ substrates</i> . 89	
2.3. <i>Cell assembly (Fabrication process of ss-DSSCs)</i>	90
3. RESULTS AND DISCUSSION	92
3.1. <i>Optical Properties of the dyes</i>	92
3.2. <i>Fluorescence spectra of the dyes</i>	93
3.3. <i>Electrochemical properties of the dyes</i>	94
3.4. <i>In-situ PEP deposition of PEDOT on the Dye Sensitized TiO₂ Photo-anodes</i>	96

4.	DSSCs DEVICES.....	97
4.1.	<i>Photovoltaic Parameters</i>	97
4.2.	<i>Electrochemical Impedance Spectroscopy</i>	100
CHAPTER 5. THEORETICAL STUDY OF THE ORGANIC TAA-BASED DYES: ZJX4015 AND ZJX4041.		107
I.	FREE DYES ZJX4015 AND ZJX4041	110
1.1.	<i>Conformational properties of the C3 alkyl chain. Study of the ZJX4015 compound</i>	111
1.2.	<i>Energies and geometries of the isomer of ZJX4015 and ZJX4041</i>	114
1.3.	<i>Electronic structures of ZJX4015 and ZJX4041</i>	120
1.4.	<i>Optical properties</i>	126
1.5.	<i>Calculated Photovoltaic Performances using DFT</i>	131
2.	CONCLUSION	135
GENERAL CONCLUSIONS AND PERSPECTIVES.....		149
APPENDIX		153

Chapter 1. General introduction of photovoltaic solar cells

1. General context

From two century and since the industrial revolution the need for energy is continuously growing. For more than several decades, energy production has become one of the crucial challenges for the society. Indeed, the growth of the world's population combined to the increase of life expectancy push the society to produce always more energies. Moreover, technological developments and behaviors are increasingly dependent on energy resources. From 965 million tons of oil equivalent in 1900, the annual global energy consumption raises to 16 billion in 2000. In 2019, it reached 13,9 billion corresponding to approximately to $584 \cdot 10^{18}$ Joules.^{1,2} This eventually resulted in a dramatic increase in population that has not still reached its peak and will cause the global energy demand to double by the year 2040. At the same time, pollution deriving from the emission of side-products from industrial processes such as CO, CO₂, NO_x, are having serious impacts on the climate, causing phenomena like the “greenhouse effect” and the “global warming”. However, since the awareness of global warming generated by human activities, the search for sustainable and renewable energies has become indispensable.

In order to meet this challenge of increasing energetic needs, diverse resources were exploited, such as wood, coal, petroleum and natural gaz. The vast majority of universal energetic consumption is however ensured, at present, by the utilization of non-renewable fossil resources like petroleum, natural gas and coal (see Figure 1.1 and the part of non-renewable energy in energy consumption). Considering the foreseen depletion of these accessible resources as well as their influence over global environment in the relatively near future, it becomes significant and necessary to develop novel renewable resources to guarantee the access to energy for the future generations.

Under this circumstance, the renewable energies including wind, geothermal, hydroelectric, and solar energy are subjects of concerted efforts in order to decrease the cost.

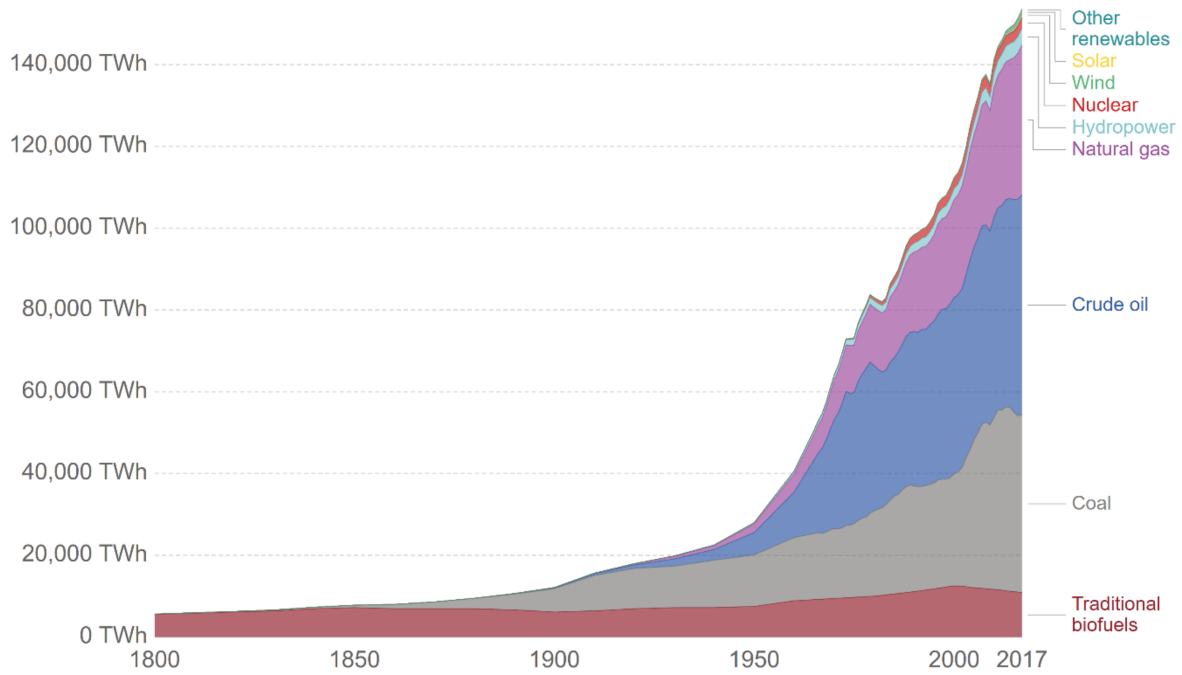


Figure 1.1 Global primary energy consumption measured in tetrawatt-hours (TWh) per year.

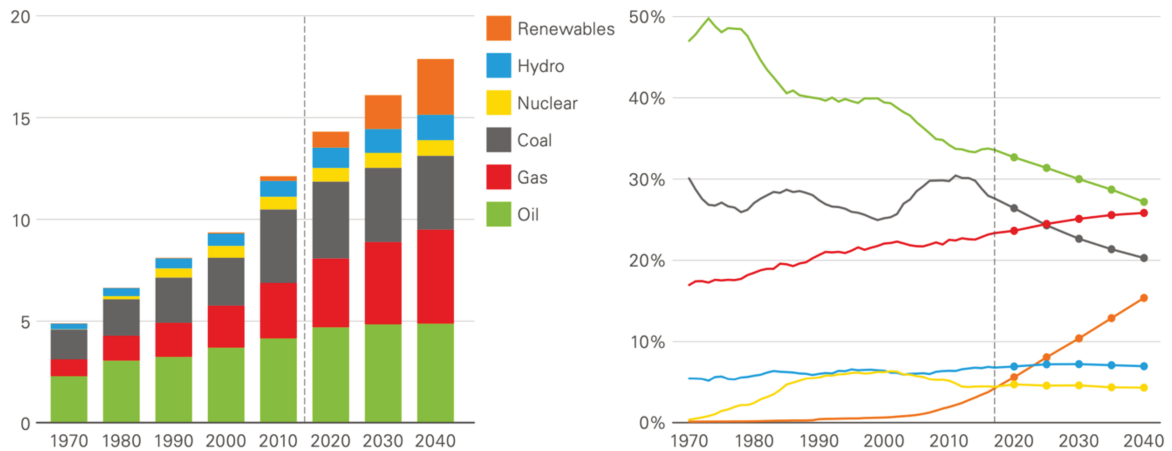


Figure 1.2 Consumption (left) and share (right) energies³.

Photovoltaics, converting the solar energy directly into electricity, has grown considerably in recent years with energy conversion efficiencies in the range of 12% to 17% for current commercial modules (crystallin silicon based). This energy could thereby stand for a promising alternative of fossil energies in the near future. However, many improvements need to be made in this field, particularly in terms of decreasing the production cost of the modules. Indeed, "classic" silicon-based solar cells remain expensive and are hampered by production methods which consume a great amount of energy. Furthermore, crystalline silicon cells are not very efficient under low irradiance, especially in diffuse light when the weather becomes cloudy.

Increasing attention is therefore currently being paid to the development of inexpensive alternatives to solar cells based on crystalline silicon.

Among the newly proposed concepts, the dye-sensitized solar cells are seen as a promising technology to replace the classic solar cells. Numerous researches emerged since the pioneering work by Grätzel et coll. in 1991, who reported hybrid organic-inorganic materials that consisted of semiconducting metal oxide coated with dye molecules.⁴ This type of photovoltaic cells showed an energy conversion of 12% up to date.⁵

2. Energy from the Sun

The solar energy constitutes a gigantic energy source considering $3,186\,000,10^{18}$ joules received by the Earth's surface per year, that is approximately 10,000 times of totality of all kinds of energy currently consumed by mankind. One hour of sunshine would satisfy total annual global energy needs.⁶ The energy of the sun therefore constitutes an almost inexhaustible reserve of energy. Another characteristic quantity used to measure this resource is the amount of energy received by each square meter of the planet, which is 1,700 kWh per year. We can therefore calculate that an area of 145,000 km² would be sufficient to cover human consumption.

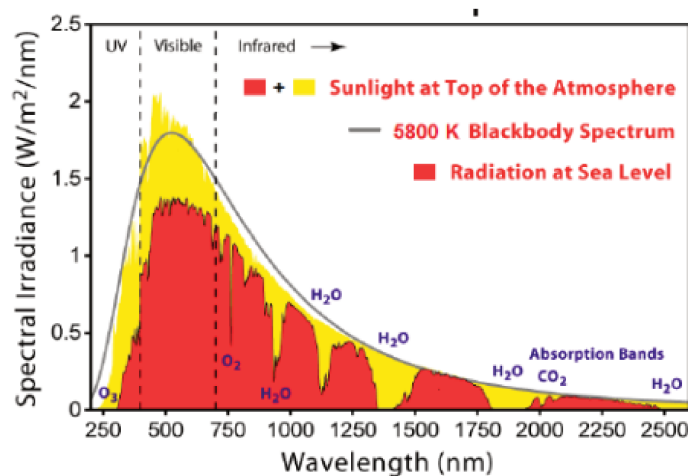


Figure 1.3 Spectrum of solar radiation (similar to black body at 5800K).

The sunlight can be considered as the sum of three components: radiation directly from the sun after passing through the atmosphere, diffuse radiation from diffraction and reflection by clouds, and radiation due to albedo, which is the reflecting power of surfaces.

Solar energy can be exploitable in different ways. Thermal applications include passive exploitation for home heating or water heating, for example, domestic daily use. It is also possible to produce electricity, mainly in two manners (indirect and direct conversion). The first option is through thermodynamic systems *via* concentration of sunlight radiation, transforming heat into mechanic then electric energy. A number of technologies are developed: parabolic trough, Fresnel mirror, Stirling engine. The second possibility is based on the exploitation of photovoltaic effect.

3. Photovoltaic effect and photovoltaic cells

The photovoltaic effect, from the Greek “photo” (φωτος meaning light) and Volta (name of an Italian physicist Alessandro Volta), is a process brought to light for the first time by Alexandre Edmond Becquerel in 1839 when he could “obtain electric currents in the combination or separation of two elements under the influence of chemical rays”.^{7,8} The experiment was conducted in an electrolytic cell in which two platinum electrodes were immersed. He observed that the intensity of the current produced increased when the cell was exposed to sunlight and was also the first one that realized that this effect depended on the wavelength of the incident light. Albert Einstein proposed a theoretical explanation of the phenomena in 1905 with the “quantum energy” carried by the light particles, for which he was awarded the Nobel prize in physics in 1921.⁹

The principle of photovoltaic effect can be described as follows: the absorption of photons in a semiconductor material causes the excitation of the electrons with supplied energy, that leads to the generation of electron-hole pairs, commonly known as excitons. Subjected to an electric field, these excitons will separate into two charges of opposite signs and set themselves in motion: an electric current is generated. The first silicon solar cell was developed in 1954 with a photovoltaic conversion efficiency of 6% reported.¹⁰

Since its discovery, the ability to derive electricity from solar radiation, has aroused increasing worldwide interest and it is still one of the biggest scientific challenges. It should be mentioned that the initial motivation to develop solar cells was strongly connected with the need of being able to provide power for the artificial satellites. The space industry hence drives development of this technology. Photovoltaic research has diversified greatly over time, defining numerous types of devices and applications.

Actually, several technologies based on the photovoltaic effect is developing and reaching various stages of maturity.

4. Photovoltaic cells generations

The development of photovoltaic cells is an extremely dynamic field of research and development and several generations have been developed since the invention of the first devices.

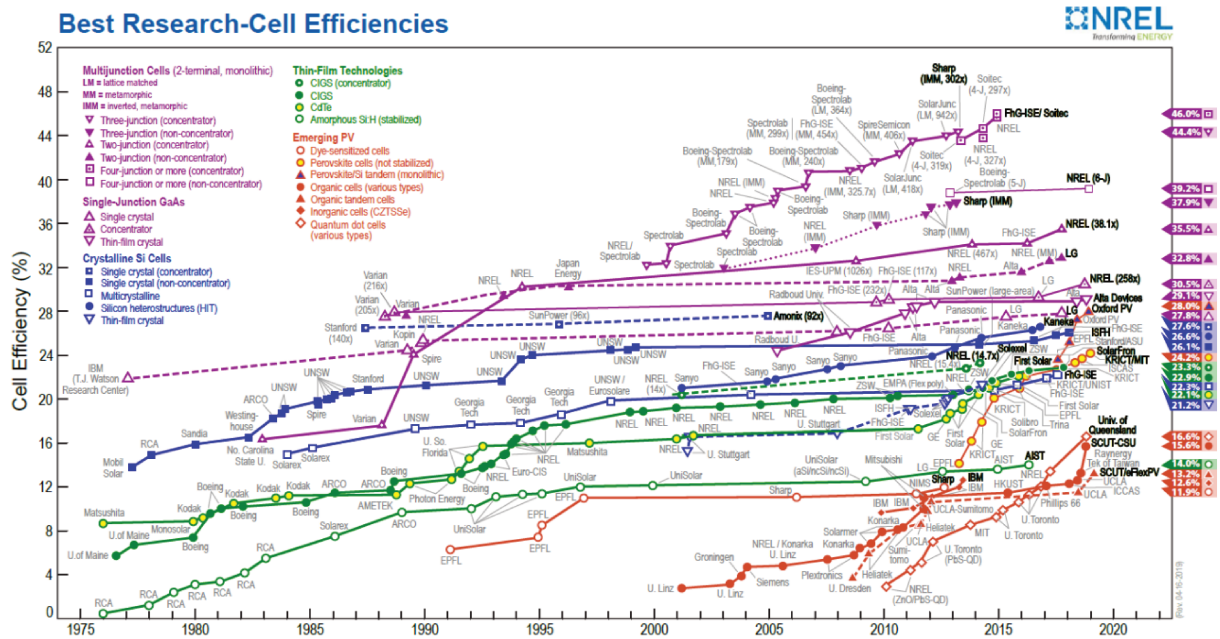


Figure 1.4 The highest confirmed conversion efficiencies for research cells for a range of photovoltaics technologies, plotted from 1976 to the present (crystalline silicon cells in blue, multijunction cells and single-junction GaAs in purple, thin-film technologies in green, and emerging PV in red)¹¹.

4.1. The 1st generation

The first generation of photovoltaic devices exploits a p-n junction between differently doped semiconductors, such as silicon, III-V junctions. The silicon-based devices has always been dominated market of photovoltaic cells covering more than 90% of the world market as the most advanced ones.¹² Developed in the 1960s, monocrystalline silicon accounts for 60% of solar panels on the market. The manufacturing process is mainly based on the fabrication of a homogenous and extremely pure silicon monocrystal of grey/black color with intrinsic semiconducting properties. Nevertheless, the dopants like gallium or bore are added during the manufacture process of crystal to obtain semiconductors of p- or n-type with better conductivity. Solar cells of positively doped silicon photovoltaic is combined with negatively doped silicon (n), allowing the charge separation and transport in the electric circuit. As the most perform materials, the purity and morphology control required and the manufacturing methods involving very high temperature make themselves so costly that limits their application for the general public. However, despite a very high production cost, the market of photovoltaic cells

is still dominated by this type of cells, with the conversion record of 25,6% held by the firm Panasonic,¹³ which is very close to theoretical maximum yield, around 30% determined by Shockley and Queisser.¹⁴

Since the production of monocrystalline silicon is extremely expensive, manufacturing cells from polycrystalline silicon is likely an alternative. In this case, the conversion yield obtained is generally lower (around 20%) due to the heterogeneity of the cell. However, very recently, the German research institute Fraunhofer Institute for Solar Energy Systems (ISE) has shown that the performance of 22.3% (which is a world record) can be achieved with a polycrystalline silicon solar cell. This is a crucial step forward since this technology represents nearly 66% of the worldwide PV production.

Apart from the devices described above, multijunction photovoltaic cells have been also developed and reach performances which could exceed 40% as conversion yield with a record of 44,7% obtained in 2014.¹⁵

4.2. The 2nd generation

The efforts to decrease material costs and reduce the energy payback time, led to emergence of the second-generation photovoltaics founded on the thin-film technology. The conversion yields of the first cells fabricated with amorphous silicon were around 13%. Subsequently, cells based on film of CdTe, Cu-In-Se or Cu-In-Ga were prepared, achieving yields around 20%. The aim of inserting layers within the cell is to improve the charge separation or electron-hole separation. Another advantage possessed by these materials is the relatively high optical absorbance and the accessibility to the utilization of a much thinner film varying from a few nanometers to tens of micrometers, compared with a few hundred μm thickness of crystalline silicon.¹⁶ Nevertheless, it remains true that the thin film technology is still dependent on rare and toxic material sources with increasing concern over their disposal and recycling, for example cadmium.

4.3. The 3rd generation solar cells

In parallel, a number of technologies based on cheaper and environmentally friendly organic compounds have emerged and are undergoing very dynamic development to yield the third-generation cells, including Dyes Sensitized Solar Cells (DSSC), *i.e.*, Grätzel cells which are at the center of the topic of this thesis, perovskite cells derived therefrom, hybrid organic / inorganic cells and Organic Solar Cells (OSC).

The photoconversion properties of perovskites, derived from lead organohalides were brought into view in 2009. The conversion efficiency increased from 3,8% at the time to 20,1% for now with this photosensible material in Grätzel cell. The photovoltaic yields of perovskites has increased rapidly, which could be explained by the synergy found between the exceptional absorption and electron transport of this hybrid material ($25 \text{ cm}^2 \cdot \text{V}^{-1} \cdot \text{s}^{-1}$ for a diffusion length greater than one micrometer) and the hole transport properties of organic materials with which they are now associated. However, obstacles to industrialization remain since perovskites are soluble in water and therefore sensible to air, deteriorate as soon as the temperature exceeds 40°C and contain lead, although in small quantities.

Regarded as one of the protagonist devices, dye-sensitized solar cells are promising in terms of replacing classic solar cells and have inspired global researchers since the early groundbreaking work of Grätzel *et al.* in 1991.⁴ These cells are competitive in the field of new photovoltaic systems because they are low-cost and their photoconversion exceed 12%.^{5,17} As a matter of fact, DSSCs are composed of organic-inorganic hybrid materials and the corresponding manufacturing process is inexpensive. Consisting of a semiconductor where the dye is grafted, DSSCs are immersed in an electrolyte, usually in organic solvent, of I_3^-/I^- , that are trapped between two electrodes, of which at least one is transparent. Under illumination, the dye goes into the excited state and an electron is injected into the inorganic semiconductor then flows into the circuit via the anode. The redox mediator reduces the dye and then diffuses to the cathode where it is reduced in turn. However, although some manufacturers are presently developing products using dye-sensitized solar cells, whether at the stage of prototype or as commercially viable products, this technology remains hampered in its development on a large scale, particularly because the energy conversions are still too low. Various improvements, directly linked to the constituents of this type of device, are thus investigated to overcome current limitations of these devices and to improve their performances.

The dye plays a fundamental and central role in different phenomena that take place in these cells. The development of dyes with the ability collecting more light is an important research area. Another aspect of improvement focuses on the mechanisms involved in the cell. It is hence crucial to ameliorate their properties in terms of increasing their performances. While Grätzel cells, based on the sensitization of n-type semiconductors,^{4,5,17,18} such as TiO_2 and ZnO , have long dominated the world of DSSC, it may be noted that special attention is currently paid to complementary systems based on sensitization p-type semiconductors.^{19,20} However, due to relatively recent developments, DSSCs of p-type have rather low photoconversion efficiencies

compared to their n-type counterparts. New research focus aiming at exceeding the limits of DSSCs is to replace the electrolytic medium in a solid-state fashion. Problems linked to the heating of the electrolyte under illumination (sunlight) and possible leaks, as well as corrosion, could therefore be avoided.

Recent research has involved replacing the liquid electrolyte with an organic solid, which acts as a hole transporter to complete the photovoltaic cycle (Later will be discussed the function principle of DSSCs). In this context, this thesis aims to develop new bi-functional dyes, carrying both photosensitive and polymerization units, so that in the final device, the hole-transporting polymer is covalently linked to the dye.

The objective of this work is to make contribution to the development of Grätzel-type dye-sensitized solar cells by freeing them from the electrolyte. Much of the work has particularly concentrated on the design of solely organic dyes which, in addition to their capacity to absorb sunlight, could also be able to inject efficiently an electron into the semiconductor as well was to recover one-hole transporter grated on to limit current losses.

5. Thesis overview

Chapter 1 has provided a brief introduction to the principle of dye sensitized solar cell, recent progress in DSSCs and the purpose of this research. Chapter 2 will demonstrate in detail the component and working principle of dye sensitized solar cells. Chapter 3 will lay out original dyes used in DSSC and the synthesis of new compounds which combined an alkyl chain, a sensitized unit, and an organic hole transport material as HTM. In the Chapter 4 we will report the main results obtained using the alkyl linked dye-HTM in solid-state DSSC. The Chapter 5 will present theoretical results obtained on the new synthesized dyes and will summarize the research presented and describe the potential direction for further ss-DSSC improvement.

Reference

- (1) Statistical Review of World Energy 2020, BP global. <https://www.bp.com/en/global/corporate/energy-economics/statistical-review-of-world-energy.html>.
- (2) Key World Energy Statistics 2019. <https://www.iea.org/reports/key-world-energy-statistics-2019>.
- (3) Energy Outlook <https://www.bp.com/en/global/corporate/energy-economics/energy-outlook.html>.
- (4) O'Regan, B.; Grätzel, M. A Low-Cost, High-Efficiency Solar Cell Based on Dye-Sensitized Colloidal TiO₂ Films. *Nature* **1991**, *353* (6346), 737–740. <https://doi.org/10.1038/353737a0>.
- (5) Yella, A.; Lee, H.-W.; Tsao, H. N.; Yi, C.; Chandiran, A. K.; Nazeeruddin, M. K.; Diao, E. W.-G.; Yeh, C.-Y.; Zakeeruddin, S. M.; Grätzel, M. Porphyrin-Sensitized Solar Cells with Cobalt (II/III)-Based Redox Electrolyte Exceed 12 Percent Efficiency. *Science* **2011**, *334* (6056), 629–634. <https://doi.org/10.1126/science.1209688>.
- (6) Solar Energy Perspectives 2011. <https://www.iea.org/reports/solar-energy-perspectives>.
- (7) Becquerel, A. E. Recherches Sur Les Effets de La Radiation Chimique de La Lumière Solaire, Au Moyen de Courants Électriques. *Comptes Rendus Acad. Sci.* **1839**, *9*, 145–149.
- (8) Becquerel, A. E. Mémoire Sur Les Effets Électriques Produits Sous Linfluence Des Rayons Solaire. *Comptes Rendus Acad. Sci.* **1839**, *9*, 561–567.
- (9) Einstein, A. Über Einen Die Erzeugung Und Verwandlung Des Lichtes Betreffenden Heuristischen Gesichtspunkt. *Ann. Phys.* **1905**, *322* (6), 132–148. <https://doi.org/10.1002/andp.19053220607>.
- (10) Chapin, D. M.; Fuller, C. S.; Pearson, G. L. A New Silicon P-n Junction Photocell for Converting Solar Radiation into Electrical Power. *J. Appl. Phys.* **2004**, *25* (5), 676. <https://doi.org/10.1063/1.1721711>.
- (11) Best Research-Cell Efficiency Chart <https://www.nrel.gov/pv/cell-efficiency.html>.
- (12) Technology Roadmap - Solar Photovoltaic Energy 2014. <https://www.iea.org/reports/technology-roadmap-solar-photovoltaic-energy-2014>.
- (13) Panasonic HIT(R) Solar Cell Achieves World's Highest Energy Conversion Efficiency of 25.6% at Research Level. <http://news.panasonic.com/global/stories/2014/26881.html>.
- (14) Shockley, W.; Queisser, H. J. Detailed Balance Limit of Efficiency of P-n Junction Solar Cells. *J. Appl. Phys.* **1961**, *32* (3), 510–519. <https://doi.org/10.1063/1.1736034>.

- (15) Dimroth, F.; Grave, M.; Beutel, P.; Fiedeler, U.; Karcher, C.; Tibbits, T. N. D.; Oliva, E.; Siefert, G.; Schachtner, M.; Wekkeli, A.; Bett, A. W.; Krause, R.; Piccin, M.; Blanc, N.; Drazek, C.; Guiot, E.; Ghyselen, B.; Salvetat, T.; Tauzin, A.; Signamarcheix, T.; Dobrich, A.; Hannappel, T.; Schwarzburg, K. Wafer Bonded Four-Junction GaInP/GaAs//GaInAsP/GaInAs Concentrator Solar Cells with 44.7% Efficiency. *Prog. Photovolt. Res. Appl.* **2014**, *22* (3), 277–282. <https://doi.org/10.1002/pip.2475>.
- (16) Green, M. A.; Emery, K.; Hishikawa, Y.; Warta, W.; Dunlop, E. D. Solar Cell Efficiency Tables (Version 45). *Prog. Photovolt. Res. Appl.* **2015**, *23* (1), 1–9. <https://doi.org/10.1002/pip.2573>.
- (17) Hardin, B. E.; Snaith, H. J.; McGehee, M. D. The Renaissance of Dye-Sensitized Solar Cells. *Nat. Photonics* **2012**, *6* (3), 162–169. <https://doi.org/10.1038/nphoton.2012.22>.
- (18) Hagfeldt, A.; Boschloo, G.; Sun, L.; Kloo, L.; Pettersson, H. Dye-Sensitized Solar Cells. *Chem. Rev.* **2010**, *110* (11), 6595–6663. <https://doi.org/10.1021/cr900356p>.
- (19) Odobel, F.; Pellegrin, Y.; Gibson, E. A.; Hagfeldt, A.; Smeigh, A. L.; Hammarström, L. Recent Advances and Future Directions to Optimize the Performances of P-Type Dye-Sensitized Solar Cells. *Coord. Chem. Rev.* **2012**, *256* (21), 2414–2423. <https://doi.org/10.1016/j.ccr.2012.04.017>.
- (20) Odobel, F.; Le Pleux, L.; Pellegrin, Y.; Blart, E. New Photovoltaic Devices Based on the Sensitization of P-Type Semiconductors: Challenges and Opportunities. *Acc. Chem. Res.* **2010**, *43* (8), 1063–1071. <https://doi.org/10.1021/ar900275b>.

Chapter 2. The Dye-Sensitized Solar Cell

In this chapter, the structure and different components of dye sensitized solar cell are firstly introduced. Secondly, the operation principles and fundamental processes that take place in the device will be described in the second part, where also includes the thermodynamic and kinetic aspects. Thirdly, basic parameters to characterize DSSCs as well as usual characterization techniques will be described. In the last part, the aim of the thesis will be presented.

I. The architecture of a DSSC

A standard (n-)DSSC is constituted by three primary parts (Figure 2.1): a counter electrode (cathode), a redox mediator, and a transparent photoanode made of glass substrate coated with transparent conductive oxide (TCO), on which deposited the core of the device: a thin film of nanoporous semiconductor covered by photosensitizer molecules. Five essential components can be distinguished: a transparent conductive substrate, a nanostructured mesoporous semiconductor of wide-band gap, a photosensitizer, a redox mediator (electrolyte for liquid based DSSCs and solid HTM for ss-DSSCs), and a counter electrode. Each element performs a specific function of great importance in the normal operation of the cell (see DSSC's operational principal part) and has received close attention during the last decades.

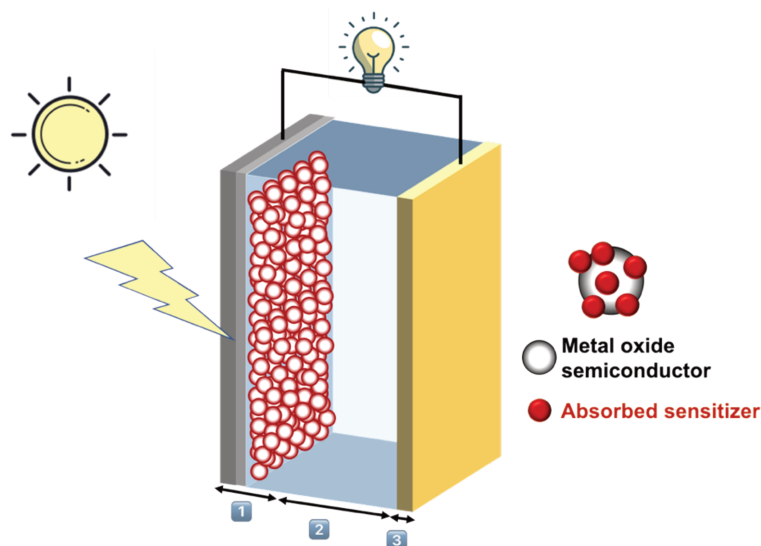


Figure 2.1. Schematic representation of a DSSC: transparent conductive oxide (light grey); transparent conductive glass (dark grey); semiconductor metal oxide covered with sensitizer (red); redox mediator (blue); and counter electrode (yellow).

1.1. Transparent conductive oxides (TCOs)

The substrate needs to satisfy two criteria: (i) high transparency to the solar radiation in the visible-IR range in order to permit the passage of optimum sunlight for light harvest, (ii) high electrical conductivity for efficient electron transport, which can be respectively characterized by transmittance and sheet resistance.

The substrate commonly comprises a bare glass or plastic doped with metal oxide such as FTO (fluorine doped tin oxide, $\text{SnO}_2:\text{F}$) or ITO (indium tin oxide, $\text{In}_2\text{O}_3:\text{Sn}$) to be electrically conductive. Plastic substrates based on polyethylene naphthalate (PEN) and polyethylene terephthalate (PET) are flexible, lightweight, and low-cost. However, its low heat resistance renders the instability in high temperature sintering process of TiO_2 (400-500°C), hence the stability of flexible sheets can be problematic.¹ Therefore, the most popularly used substrates presently are still TCO glass based.

ITO films have a transmittance of above 80% and sheet resistance of $18 \Omega/\text{cm}^2$, while FTO films show a transmittance of about 75% in the visible region and sheet resistance of $8.5/\text{cm}^2$. Since the sheet resistance of FTO glass is independent of temperature up to 500°C,² contrary to ITO glass with low thermal stability; and also FTO is less expensive without price-ever-increasing indium, FTO glass is more privileged.

1.2. Metal oxide semiconductor

Serving as the support for dye loading and transporter of photo-excited electrons from dye to TCO, the photoanode, otherwise namely photoelectrode usually consists of a thin layer of wide-bandgap semiconductor materials deposited on TCO glass, sensitized with dye molecules.

The nanostructured semiconductor layer made of metal oxide (typically TiO_2) necessarily provides a large surface area of high roughness, which endows itself high dye loading capacity that permits a high light harvesting efficiency (LHE).^{3,4}

Several wide-band gap semiconductors available, such as TiO_2 , ZnO , SnO_2 , Sb_2O_5 , and Nb_2O_5 . TiO_2 is the most widely used by virtue of its favorable band positions, high abundance in nature, high chemical stability including exceptional resistance to photodegradation and high thermal stability, non-toxicity, colorlessness, a high refractive index, brightness, and low cost.

Furthermore, TiO₂ is the semiconductor that achieves the best yields today, normally considered as the semi-conductor of reference for the DSSCs.^{5,6}

TiO₂ exists naturally in three crystalline forms, namely anatase, rutile and brookite. Brookite is rarely found in nature and difficult to obtain in the laboratory,^{7,8} consequently only rutile and anatase are of practical interest for DSSCs. Anatase is more popular than rutile due to its superior electron transport than rutile pointed out by Park *et al.* in their previous work on comparison of dye-sensitized rutile- and anatase-based TiO₂ solar cells.⁹

Nanomaterials of different morphologies have been applied in DSSCs, such as nanotubes,¹⁰ nanowires and nanoparticles. TiO₂ nanoparticles with spherical shape are the most commonly used in DSSCs for their larger surface areas for dye adsorption thus higher light harvesting efficiency as well as better charge transport. Hence, in this thesis, TiO₂ anatase nanoparticles are exclusively applied.

1.3. The photosensitizer: the organic dye

As one of the most important elements of DSSCs, dye molecules are used to sensitize the wide-bandgap nanostructured photoelectrode. Two essential tasks are performed by dyes including light absorption and injection of photoexcited electrons into the CB of semiconductor.

The first step in the operation of a solar cell is the absorption of solar irradiation. The dye absorbs part of the incident electromagnetic radiation by harvesting photons, that is why it is crucial to know the nature of the radiation to maximize optical absorption. Before accessing to the cell, the solar radiation undergoes strong absorptions during its crossing of the atmosphere. The light reaching the earth's surface is thus particularly intense in the visible-light region, essentially around 550 nm. The dye must be able to collect the maximum of incident photons and more particularly in the spectral window of the solar absorption spectrum.

Upon illumination, an electron from the ground state (S_0) of the dye gets boosted to the excited state (most often S_1 state populated directly or after a fast relaxation from higher singlet states) and then injected into the conduction band of the nanostructured TiO₂. It should be noted that part of the electron density of the molecule is disturbed by the absorption of the photon and reorganizes itself. In other words, the molecule goes from its ground state to one of its excited states by generating a significant electronic reorganization.

In addition to the harvest of photons emitted by the solar irradiation, the dye also converts the photo-excited electrons into electron flow by charge transfer. A function requires the dye to be bonded strongly to the surface of the TiO_2 in order to ensure efficient electron injection into the conduction band and to prevent gradual leaching from the electrolyte or HTM.

The prototypical structure of organic sensitizers consists of a donor (D), a bridge (typically a π spacer), and an acceptor (A), which are usually combined following a D- π -A rod-like configuration. In n-type DSSCs, the dye is grafted onto the semiconductor so that the electron acceptors of the dye are close to the surface of the anchor group, and the donor group is as far away as possible, and therefore near the electrolytic couple (in conventional DSSC) or HTM (in ss-DSSC). Upon illumination, the electron density moves from the functional group as donors (D) to another functional group or so-called acceptors (A) of the push-pull molecule through a π conjugation pathway. The directional electron flow results in an electron injection of higher efficiency into the CB of semiconductor while diminishing risks of recombination process between semiconductor electrons and oxidized dye molecules. This process is also known as Excited State Intramolecular Charge Transfer (ESICT), identified as one main character of D- π -A type dyes (Figure 2.2).

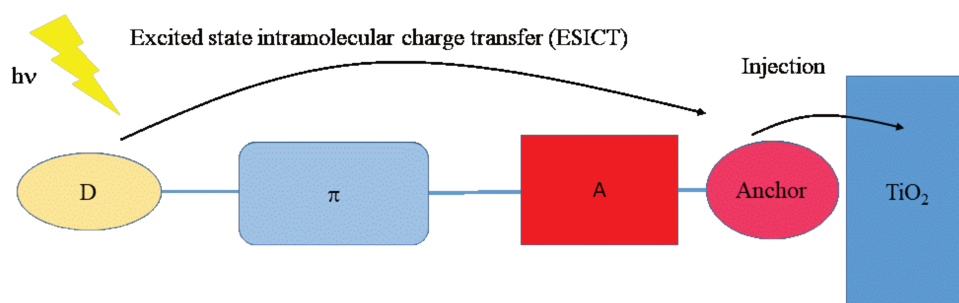


Figure 2.2. Schematic representation of the prototypical structure of a dye used in DSSC. (D: donor; A: acceptor; π : conjugated group)

Following the working principle, several considerations should be undertaken for the organic dyes in order to promote a high light-to-energy conversion efficiency:

- i) To ensure a strong collection of photons, the dye should absorb all wavelengths extending from visible to NIR region, preferably covering a broad range of wavelengths (panchromatic property) with a high molar extinction coefficient ($\epsilon > 10^4 \text{ mol.L}^{-1}.\text{cm}^{-1}$).

- ii) The dye should be stable under sunlight exposure. In general, it should be stable enough to endure 10^8 turnovers corresponding to 20 years exposure to sunlight without apparent degradation.
- iii) The dye must bind strongly to the surface of TiO_2 to ensure efficient electron injection into the photoelectrode conducting band. For this purpose, the sensitizer must carry an appropriate functional group to anchor the surface of mesoporous oxide semiconductor.
- iv) The excited state of the dye must show a strong charge transfer in the excited state to promote the electron into the semi-conductor.
- v) In addition to exhibiting a charge transfer feature, the excited state must be slightly higher than the conduction band of TiO_2 but enough to have a driving force in energy for efficient charge injection into the TiO_2 .
- vi) The ground state of the dye must be sufficiently low in energy for efficient regeneration of dye by the redox electrolyte or HTM.
- vii) The process of electron transfer from the dye to the TiO_2 must be fast enough to compete with excited state decay and recombination of electrons in the semiconductor with oxidized dyes or redox mediator.

Furthermore, it should be mentioned that the dye and HTM fill both the nanopore of the TiO_2 electrode in ss-DSSCs. The layer of the dye plays a crucial role in the performance of the cell since it acts as an isolating layer between the HTM and the electron transport material (ETM), *i.e.*, the TiO_2 . In this configuration, the dye also strongly affects the kinetic of the charge transfer process at these interfaces, including the electron injection and the dye regeneration. Considering the key role of the dye between HTM and ETM, numerous metal complexes and organic dyes have been synthesized and utilized as sensitizers. Given the importance of the dye in the overall device, a presentation of the main inorganic and mostly organic families will be the subject of the chapter 3 of this thesis

1.4. The redox mediator: The Hole Conducting Material (HTM)

A redox shuttle, usually contained in an organic solvent, is crucial for DSSCs to transport charge carriers between a pair of electrodes and to continuously regenerate the dye. The triiodide/iodide (I_3^-/I^-) remains the most widely used redox mediator which was presented in

the pioneering work by O'Regan and Grätzel in 1991 for several beneficial features,³ such as suitable redox potential for most dyes, rapid dye regeneration capacity, and slow back electron recombination along with good solubility and high conductivity. So far, 10.2% was the highest overall efficiency achieved by Wang *et al.* using a metal-free sensitizer,¹¹ and 11.8% was obtained for Ru-based devices.¹²

However, the drawbacks of this redox shuttle are not negligible.¹³ Iodine is corrosive to metals (silver, gold), which are used as current collectors, causing difficult assembling and sealing, thus the long-term stability of the device is troublesome. The iodine has relatively high vapor pressure which makes the device encapsulation problematic. The I_3^- ion absorbs part of visible light, that decreases the photocurrent. In addition, the redox potential of I_3^-/I^- creates a loss in V_{oc} .¹⁴⁻¹⁷ Other alternatives were widely developed since 2010, for instance, Co^{3+}/Co^{2+} -based coordination complexes which lower the voltages loss in the devices and often showed high V_{oc} ,^{18,19} and some other examples such as Br_3^-/Br^- ,²⁰ Fc/Fc^+ ,²¹ $(SCN)_3^-/SCN^-$ and $(SeCN)_3^-/SeCN^-$,²² also showed interesting properties. Nonetheless, the derivatives are all based on organic solvents like acetonitrile. These solvents are toxic and volatile posing problems of encapsulation. Additionally, their relatively low boiling points and melting points make them temperature-dependent: the solvents can freeze at low temperature leading to the insolubility of the salts, and the solvents tend to evaporate rapidly at high temperature.

The replacement of liquid electrolytes with solid-state hole transport materials (HTM) is indispensable for the long-term developments of devices. Dye regeneration is the main difference in operating mechanism between liquid- and HTM-based DSSCs. In liquid-state DSSC, the oxidized dye is regenerated by accepting an electron from the reduction-state species in the electrolyte, and the formed oxidation-state species diffuses to the counter electrode where it will be then reduced by electrons. While in solid state DSSC, the oxidized dye is regenerated by injecting a hole into the HTM and the hole transports to the electrode through the HTM via hopping mechanism. An ideal HTM should meet the following requirements: (i) efficient hole extraction capability, (ii) high mobility/conductivity, and (iii) excellent stability to light, heat, air, etc.

In comparison with inorganic HTMs, organic HTMs possess several advantages, such as facile preparation, relatively low costs, and abundant availability.^{13,23} Organic hole transport materials can be generally classified as either molecular HTMs (molecular hole conductors) or

polymeric HTMs (conducting polymers) based on their composition. In 1997, Hagen *et al.* reported the first solid-state dye-sensitized solar cell which consisted of an inorganic nanocrystalline titanium dioxide layer for electron conduction, a surface-adsorbed Ruthenium dye complex for light absorption, and an organic triphenylamine layer for the transport of holes.²⁴ Despite the IPCE conversion efficiency is low (0.2%), the work initiated ongoing research on replacing liquid electrolyte with solid ones. In 1998, Bach and co-workers published a solid state dye sensitized solar cell based on a spirobisfluorene-connected arylamine hole transporter 2,2',7,7'-tetrakis(N,N-di-*p*-methoxyphenylamine)-9,9'-spirobifluorene (spiro-MeOTAD) with an IPCE of 33% and an overall conversion efficiency of 0.74%.²⁵ The non-doped spiro-MeOTAD has two practical disadvantages: low conductivity and efficient recombination. In 2001, Kruger *et al.* added a combination of TBP and LiTFSI in spiro-MeOTAD to investigate the effect of additives. An open-circuit voltage over 0.9 V, a photocurrent of 5.1 mA, and a conversion efficiency of 2.56% were obtained.²⁶ Snaith *et al.* compared a series of molecular sensitizers utilizing spiro-MeOTAD as organic hole transporter, which resulted in a reduced charge combination and longer electron lifetime by the deblock alkoxy-alkane pendent groups on the sensitizer.²⁷ An overall conversion efficiency of 5.1% was achieved by further increasing the optical path length in the active layer. The efficiency increased to 4,6% and 6% by using dyes with high absorption coefficients as C104,²⁸ and C220,²⁹ respectively. In 2011, the efficiency was improved to 7,2% by increasing the hole mobility of spiro-MeOTAD more than one order of magnitude with FK102 cobalt (III) complex as dopant.³⁰ Besides the most well-known molecular HTM, spiro-MeOTAD, other triarylamine derivatives are also well investigated.

The first study of conducting polymer as HTM in solid-state DSSC was conducted by Yanagida's group in 1997.³¹ The polypyrrole (PPy) was incorporated in an N3-based device archiving an efficiency of only 0,1% under low light intensity of 22 mW cm⁻². The use of a carbon-based counter electrode,³² and a substituted N3 dye,³³ improved moderately the efficiency to 0,62% (light intensity 10 mW·cm⁻²). The poor performance of solar cells based on PPy was owing to the high density and the black color of the HTM, which absorbed the visible light leading to a filter effect.^{31,34} Several other CPs, such as polyaniline (PANI),^{35,36} poly(3-hexylthiophene-2,5-diyl) (P3HT),^{13,37-44} poly(3-octylthiophene-2,5-diyl) (P3OT), and poly(3,4-ethylenedioxythiophene) (PEDOT) are also investigated. PEDOT was shown to be distinctive and versatile. It has sufficient transparency,⁴⁷⁻⁵¹ even it absorbs visible light and owns high conductivity (300–550 S cm⁻¹),^{52,53} as well as exceptional stability under standard

conditions.¹³ In 2004, Saito and co-workers reported the first solid-state DSSC using PEDOT as HTM with an overall conversion efficiency of 0.53%.⁵⁴ Later, various anions such as ClO_4^- , CF_3SO_3^- , BF_4^- , and TFSI⁻ were applied as dopants to improve the overall solar cell performance. Doped anions in the PEDOT hole conductor system have great influences on I-V curves, conductivity, and impedance according to the photoelectrochemical and independence studies. A maximum J_{sc} of $5.3 \text{ mA}\cdot\text{cm}^{-2}$, a V_{oc} of 750 mV, and a conversion efficiency of 2.85% were achieved when the TFSI⁻ anion was used.⁵⁵ The work was then extended to the effect of different perfluoroalkyl chains of bis(perfluorosulfonyl)imides ($\text{N}(\text{CF}_2\text{SO}_2)_2^-$) or perfluorosulfonates ($\text{C}_n\text{F}_{2n+1}\text{SO}_2^-$) on the conductivity of PEDOT.⁵⁶

One ineligible drawback of solid-state HTM is the poor pore filling, that HTM penetration within the mesoporous oxide semiconductor is insufficient. The regeneration of the dye is restrained for the reason that the photogenerated holes cannot be transferred to the HTM by the dye. In order to address this problem, Yanagida *et al.* suggested *in-situ* photo-electrochemical polymerization (PEP) of organic monomers to produce directly CP inside the mesoporous oxide semiconductor layer.³¹

In 2010, Liu *et al.* fabricated efficient polymer-HTM-based DSSCs by *in-situ* polymerization of 2,2'-bis(3,4-ethylenedioxythiophene) (Bis-EDOT) in a thin-layer electrolytic cell using D149 dye as the sensitizer. The corresponding device achieved a remarkable energy conversion efficiency of 6.1% under AM 1.5G illumination.⁵⁷ Later, Kim *et al.* manufactured ss-DSSCs with higher PCE up to 6.8% as a result of enhanced light harvesting from increased transmittance of an organized mesoporous TiO_2 (OM- TiO_2) and good hole conductivity of PEDOT.⁵⁸ Liu and co-workers achieved an even higher conversion efficient of 7.1% with a PEDOT as HTM prepared by photoelectrochemical polymerization (PEP) in conjugation with indoline-type metal-free dye D205.⁵⁹ Moreover, the polymerization was conducted under monochromatic light, unlike conventional PEP under a Xenon lamp. It was observed that the device performance is dependent on the wavelength of monochromatic light used during the preparation of PEDOT. In 2016, Zhang *et al.* reported highly efficient ss-DSSCs with power conversion efficiency of 7.1% and exceptional photocurrent of 13.4 mA cm^{-2} . The *in-situ* PEP process was applied to generate the PEDOT layer, in combination with an organic sensitizer with well-tuned energy levels and a bulky structure, as well as a donor- π -acceptor configuration like LEG4, led to an effective dye regeneration and improved photo-charge injection, resulting in high PV performance.⁶⁰ In this work, a copolymer obtained under *in-situ* PEP with one

monomer (carbazole) as part of the dye and another monomer in solution (Bis-EDOT), is chosen as the HTM.

1.5. The counter electrode

The task of counter electrode (CE) is to collect electrons from the external circuit and transmits them into the cell to reduce the redox electrolyte of liquid DSSCs or collect holes from the hole transport materials in the case of ss-DSSCs so as to complete the process.

The most popular counter electrode for liquid DSSCs is the platinized ones, prepared from a small amount of platinum (Pt) catalyst deposited onto a TCO glass with the purpose of catalyzing the reduction of redox couples in electrolyte, while the plain FTO layer does this rather poorly. The charge transfer resistance of plain FTO counter electrode is of the order of magnitude of $10^6 \Omega \text{ cm}^2$, and that of platinized counter electrode is around $1 \Omega \text{ cm}^2$.⁶¹ Pt is selected due to its high catalytic activity and stability toward the iodide electrolyte. Unfortunately, platinum is very expensive and limited in supply. Great efforts have been devoted to explore alternative counter electrode materials in attempt to replace Pt, including carbon materials, conducting polymers, and transition metal carbides, nitrides and oxides.⁶²

In ss-DSSCs, a layer of gold (Au) or silver (Ag) with thickness of dozens to a few hundred nanometers was deposited on the electrode surface by thermal evaporation in the vacuum chamber to form the counter electrode.^{27,63} In addition to their reflectivity of unabsorbed photons back to the cell which could enhance LHE, silver has a lower cost and shunt resistances while gold exhibit better chemical stability and higher tolerance of minor defects in the HTM layer. Au is selected as the counter electrode for all ss-DSSCs developed in this study.⁶⁴

2. DSSC's operational principle

2.1. Operational principle

The operating principle of a DSSC is schematically shown in Figure 2.3.

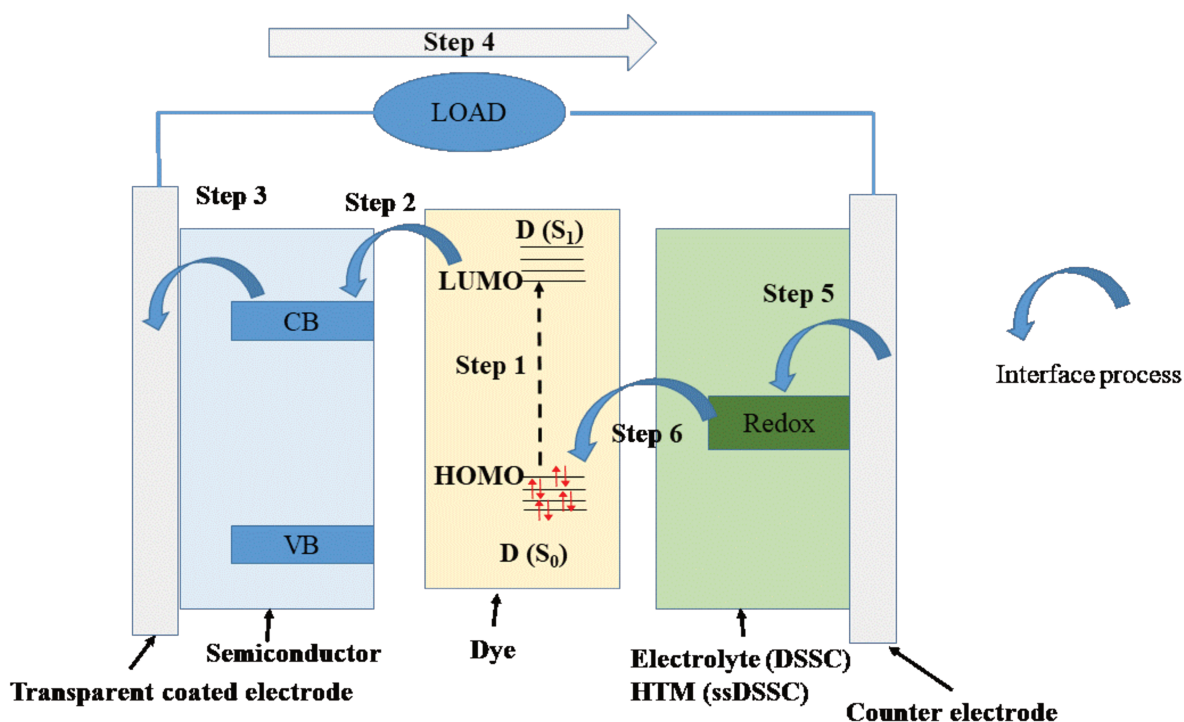
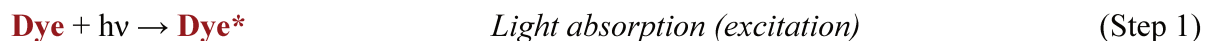


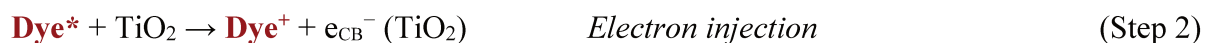
Figure 2.3. Operating principles and interfacial processes in a dye-sensitized solar cell.

The photocurrent yield of a DSSC is the outcome of competitive photo-electrochemical reactions which take place at the semiconductor/electrolyte interface and is summarized below. The primary process in DSSC is the photo-induced charge separation at the metal oxide/dye interface.

In the first step (Step 1), the incident radiation, a photon is absorbed by the dye which is subsequently promoted to the excited state with supplied energy of the photon.



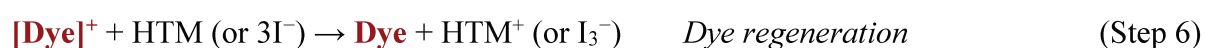
Described as electron injection or charge separation, the electron is injected from the excited-state dye into the conduction band (CB) of a semiconductor material, usually TiO_2 with the consequent oxidation of the dye (Step 2) leaving it in its oxidized state Dye^+ .



The electron in the conduction band flows through the oxide semiconductor toward the TCO of the photoelectrode (Step 3) and is transferred to the external circuit producing an electric current, then reaches the counter electrode (Step 4). Due to the photo-induced charge carrier

transfer from the dye to the semiconductor oxide, the electronic density in TiO₂ increases giving rise to an electrochemical potential difference (ΔV) between TiO₂ and the electrolyte or HTM.

The oxidized dye [**Dye**]⁺ is restored to its ground state **Dye** (Step 6) through a capture of electrons from redox mediator (electrolyte or HTM), whose responsibility is to mediate electrons, in other words to transport charges between electrodes while regenerating the dye in the process. This step is also a redox reaction requiring an electron injection from an electron donor species (I₃⁻ or HTM). The reduced species (I₃⁻ or HTM) are thus oxidized (I⁻ or HTM⁺).



Collecting the electron at the counter electrode, the oxidized redox mediator (I⁻ or HTM⁺) turns into its reduced form (I₃⁻ or HTM). The oxidized form of redox transports positive charges to the counter electrode. In the case of liquid electrolyte, the charge carrier transport occurs through the diffusion of oxidized species while a more efficient hole hopping process takes place in ss-DSSC. The regenerative electric cycle is thus completed.



2.2. Thermodynamic requirements

Following the description of the operating principle, the charge separation in DSSCs can be regarded as a two-step redox cascade. The injection of electrons into the TiO₂ electrode, and the subsequent oxidation of the redox electrolyte, with the latter also resulting in regeneration of the dye in its ground state from oxidized state. Both processes are thermodynamically accessible to allow the cell to operate.

In order to assure an efficient injection into the semi-conductor, the metal oxide and the dye along with the redox couple should achieve a suitable matching. While the excited-state oxidation potential of the dye (E_{ox^*}) must be sufficiently negative but still above the edge of the CB, the ground state oxidation potential of the dye must be sufficiently positive to oxidize the redox mediator (electrolyte or HTM) to assure the regeneration of the dye. These thermodynamic requirements are essential to evaluate the options of different components of the DSSC.

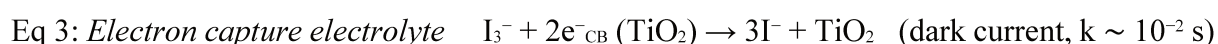
The use of the frontier molecular orbitals formalism, more precisely, the highest occupied molecular orbital (HOMO) and the lowest unoccupied molecular orbital (LUMO) of the

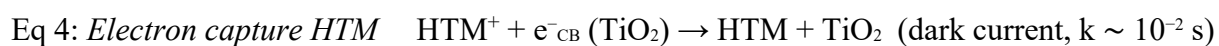
designed cell is a theoretical way to better understand the phenomenon of charge transfer. These orbitals are especially important since they are often involved in the lowest energy electronic transition when the dye is excited by solar radiation. However, it should be pointed out that the transition does not only lie in its HOMO-LUMO gap. Very often, the excitation of a molecule involves both HOMO and LUMO as well as other molecular orbitals such as those just below the HOMO (HOMO-1 or HOMO-2), or just above the LUMO (LUMO + 1 or LUMO + 2), in variable ratios. Be that as it may for most of the dye, the HOMO-LUMO approximation is adopted experimentally to describe the electronic process and we will select this approximation in the rest of this chapter for clarity. As the illumination of the dye promotes an electron into the LUMO, the energy of this orbital should be higher than the conduction band of the semiconductor TiO₂ to favor the injection. From the LUMO level, the electron is injected into the conduction band (CB) of a semiconductor material, usually TiO₂ (Step 2 in Figure 2.3). When the cationic dye is reduced during the regeneration step, an electron provided by the mediator is transferred into the HOMO. It results from the energy matching that the HOMO of the dye should lower than the HOMO of the reducing species of the mediator.

2.3. Kinetic aspects in DSSC

Comprehensive knowledge of the kinetics of different processes is of fundamental importance for better understanding of the structure-function relationship of DSSCs and identification of materials to further optimize the device. An ideal mechanism requires a fast injection of electron into the semi-conductor following by charge transport into the semi-conductor and the dye regeneration by the redox couple (in liquid DSSC) or HTM (in ss-DSSC).

However, several “undesirable” processes affect the performance of the device. Loss pathways include the decay of the excited dye to ground state and the “re-capture” of injected electrons in the semiconductor CB by the oxidized dye (eq 1 and eq 2) or by the mediator (eq 3 and eq 4). The different processes involving electrons and the associated rate time in operating DSSC are shown in Figure 2.4. The kinetic competitions between charge-transfer and loss pathway determine the overall efficiency of the DSSC.





The optimization of DSSCs performance requires that the electron injection and the dye regeneration processes by the electron donor mediator must be more efficient and faster than the decay (radiative or non-radiative) of **Dye*** and the back reaction of the injected electron with the oxidized dye, respectively. In particular, the “dark current” is considered as the main factor of loss for a DSSC. Last but not least, the efficient regeneration of the charge mediator at the counter electrode is non-negligible; otherwise, the device η could be limited.

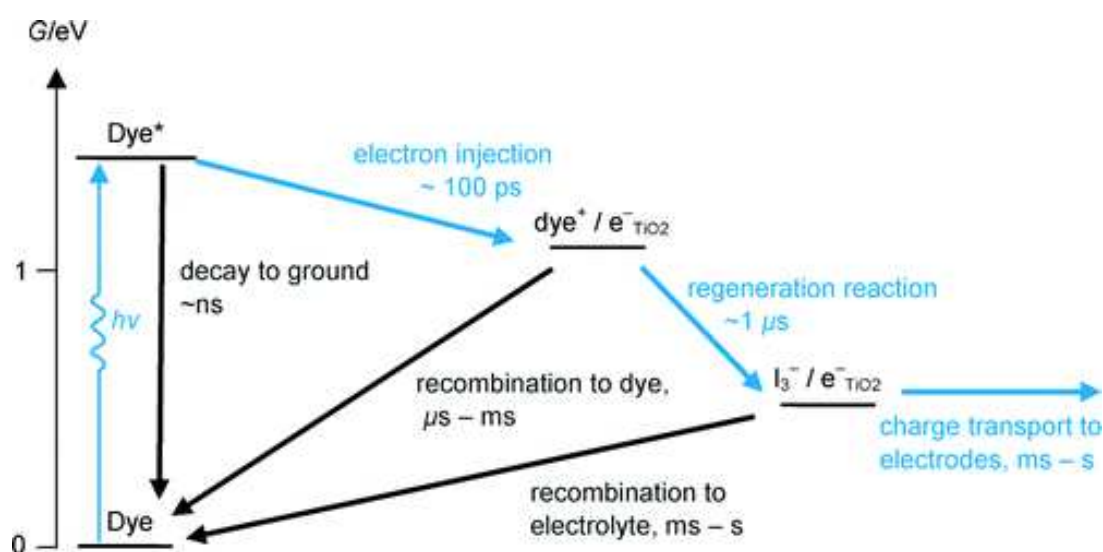


Figure 2.4. State diagram representation of the kinetics processes in operating DSSC.

If we consider the electron injection process, the efficiency of this step depends on the magnitude of the injection kinetics relative to the excited-state decay of the dye to the ground state. Dye with long excited state is thereby favorable. Typical rate of excited-state decay for organic compounds varies from picoseconds to nanoseconds. Another very important requirement for fast electron injection is the electronic coupling between the orbital of the dye that is filled upon photoexcitation, generally the LUMO orbital, and the TiO_2 conduction-band states. These conduction-band states should be also energetically accessible from the dye excited state. In model systems the electron injection rates of $1.0 \times 10^{12} \text{ s}^{-1}$ have been reported for a range of dyes.⁶⁵⁻⁶⁷

Considering the regeneration of the dye, an efficient process requires that reduction of the cation by the redox couple or HTM should be faster than the recombination of injected electrons with the dye cations. This competing recombination is strongly dependent on the electron density in the TiO_2 , the light intensity and cell voltage. In addition, it is also dependent

on the spatial separation between the positive charge of the dye cation and the metal oxide surface. Indeed, consistent with a tunneling theory, the rate constant decays exponentially with the distance.

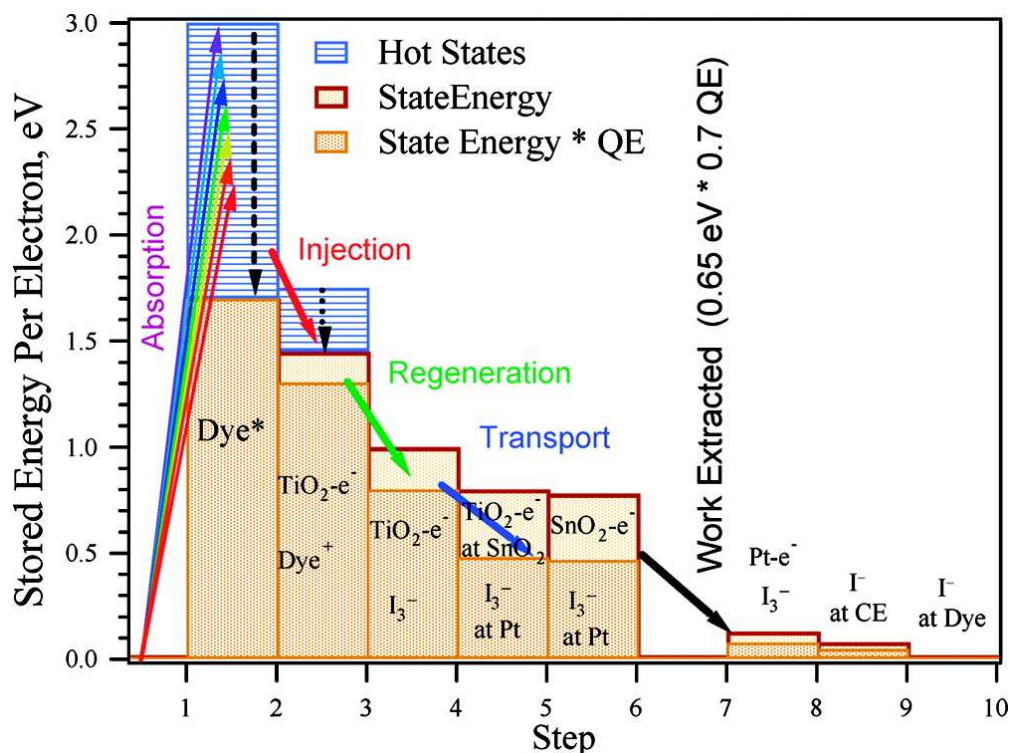


Figure 2.5. State energy diagram of a typical DSSC under 1 sun illumination at the maximum power point. Energy and quantum efficiency values are approximate and will change depending upon dye and electrolyte composition. Figure from the reference by O'Regan and co-workers.⁶⁸ Copyright 2009 American Chemical Society.

Figure 2.5 shows the energy costs of each step of DSSC operation for a typical device achieving an overall power conversion efficiency of $\sim 9.5\%$. The higher-level bars are the state energies given the electron and hole positions after each step. The solid bars are the same energy, reduced by the quantum efficiency (QE) losses up to that point, (State Energy \times QE) specifically for the maximum power point situation (MPP). Also shown (in blue) is the excess energy generated by the absorption of photons at shorter wavelengths than the optical band gap, with this excess energy being lost to excited state thermalization processes. The differences between the successive solid shaded bars show how much each step costs in a real cell under operation. Thus, large steps down indicate a large loss in energy. For the case illustrated, the MPP is assumed to correspond to a device voltage of 0.65 V and a photon to electron quantum efficiency of 0.7, yielding $0.65 \times 0.7 = 0.46$ eV of work extracted per

absorbed photon. For a typical DSSC with the N719 dye, this yields a device efficiency of ~9.5% under AM 1.5 irradiation.

3. Basic parameters to evaluate the performance of DSSCs: the figure of merit of DSSCs

The main parameters that characterize the performances of a DSSC are listed below:

i) The short-circuit photocurrent density (J_{SC}): if the output voltage is zero, the cell is said to be short circuited. The short circuit current I_{SC} refers to the photocurrent generated of the cell under irradiation when short-circuited, it is also the maximum current or total current produced by photon excitation equal to the absolute number of photons converted to hole-electron pairs for an ideal cell. The I_{SC} is dependent upon the area of the solar cell, the number of photons which is directly related to the light intensity, the optical properties of the solar cell and the collection probability which relies on the surface passivation and carrier lifetime. Representing the photocurrent per unit area ($\text{mA}\cdot\text{cm}^{-2}$), the short-circuit photocurrent density (J_{SC}) is usually applied to remove dependence of solar cell area in order to make comparison between devices of different dimensions. The value of J_{SC} relies on the light harvesting efficiency of the dye, its capacity to inject electrons into the semiconductor CB, the ability of the semiconductor to transport electrons to the counter electrode which is strongly linked with the reduction rate of the oxidized dye. The reduction of the oxidized dye to form the original dye should be fast enough so that the dark current could not limit the J_{SC} .

ii) The open circuit voltage (V_{OC}): if the output current is zero, the cell is open circuited, and the voltage of the cell is called the open circuit voltage (V_{OC}). V_{OC} corresponds to the electrical potential difference at open circuit between the two electrodes (photoanode and CE) of the cell under illumination conditions, at which the light-generated current is compensated.

The maximum V_{OC} value of a DSSC (generally around 0.8–0.9 V) is set by the difference between the quasi-Fermi level of the semiconductor (E_F , -0.5 to -0.4 eV vs. normal hydrogen electrode – NHE, for TiO_2), which is approximately the energy level of the conduction-band edge ($E_{C,B}$) and the redox potential of the charge mediator (-0.4 V vs. NHE, for I_3^-/I^- redox couple).⁶⁹ The value is always smaller than the bandgap E_g of the dye.

$$V_{OC} = \frac{E_F - E_{Redox}}{q}$$

Unfortunately, the V_{OC} is lower than the theoretical values due to the recombination of the injected electrons with the oxidized dye and the dark current. As a consequence, experimental V_{OC} can be used to quantify losses due to recombination processes. Moreover, for regenerative photo-electrochemical systems, the V_{OC} can also be expressed using the injection current as follow:⁷⁰

$$V_{OC} = \left(\frac{k_B}{e}\right) \ln \left(\frac{I_{inj}}{n_{CB} k_{red} [I_3^-]}\right)$$

where k_B is the Boltzmann's constant, T represents the absolute temperature, e is the elementary charge, I_{inj} stands for the charge flux resulting from sensitized injection, k_{red} is the reduction rate constant of I_3^- , while n_{CB} and $[I_3^-]$ are the concentration of electrons at the semiconductor surface and oxidized redox mediator (I_3^-) in the (I^-/I_3^-) solution, respectively. It should be noted that the often low open-circuit voltage (typically 0.7-0.8 eV) is a critical issue in DSSC since these values, lower than the band of the light absorber (around 1.5 eV), limit the high driving force both electron injection into TiO_2 and rapid regeneration of the oxidized dye.

iii) The fill factor (FF) is defined by the ratio of actual obtainable peak output power to the product $V_{OC} J_{SC}$. Often expressed in percentage, FF is a convenient means to compare with the theoretical maximum of the cell and is always less than one. High V_{OC} and J_{SC} are essential in achieving high efficiency but paired with low FF factor.

$$FF = \frac{P_{max}}{J_{SC} V_{OC}} = \frac{J_{max} V_{max}}{J_{SC} V_{OC}}$$

where P_{max} is the maximum power output of the cell per unit area, otherwise called P_{mmp} (maximum power point) given by the product ($J_{max} V_{max}$).

In a current density–voltage (J_{SC} vs V_{OC}) curve, the FF describes how well the area under J vs V curve fills-in the maximum rectangle described by the product $J_{SC} V_{OC}$ (see Figure 2.6). The shape of this curve represents a very useful and direct tool to characterize the DSSC performance, i.e., V_{OC} , J_{SC} and η .

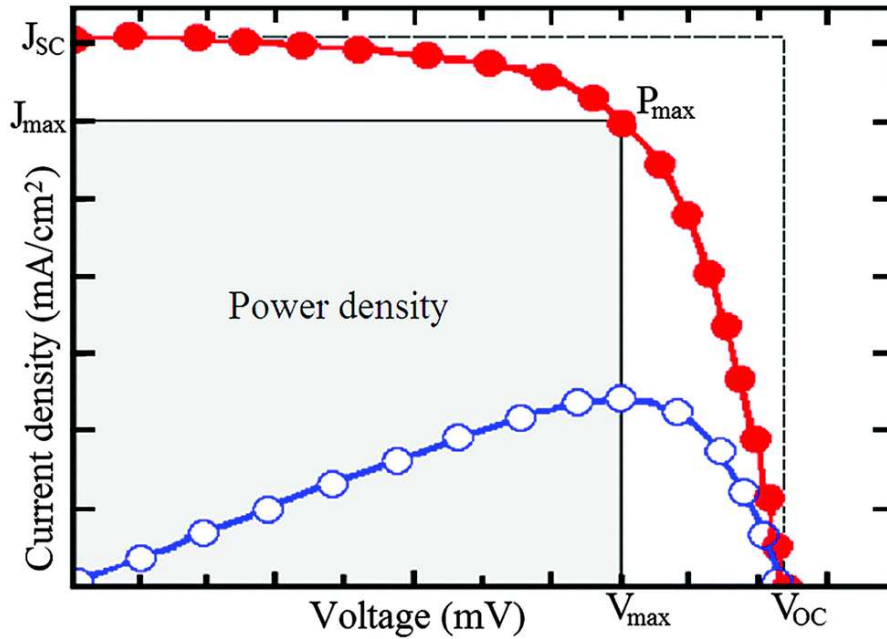


Figure 2.6. Typical current density –voltage curve (filled circles). The FF corresponds to the shaded region, which is delimited by the V_{max} and J_{max} , divided by the area of the region which is delimited by the V_{oc} and J_{sc} . The blue curve (open circles) shows the power as a function of voltage. Figure from the reference by Calogero and co-workers.⁷¹ Copyright The Royal Society of Chemistry 2015.

(iv) The Incident Photon-to-electron Conversion Efficiency (IPCE) or external quantum efficiency (EQE) provides information on the quantum efficiencies of the cell at a given excitation wavelength (λ) and corresponds to the photocurrent density produced in the external circuit per incident monochromatic photons flux that strikes the cell.⁷²

$$IPCE = \frac{\text{number of collected electrons } (\lambda)}{\text{number of incident photons } (\lambda)} = \frac{N_{\text{electrons}} (\lambda)}{N_{\text{photons}} (\lambda)}$$

$N_{\text{electrons}} (\lambda)$ and $N_{\text{photons}} (\lambda)$ can be written as follows:

$$N_{\text{electrons}} (\lambda) = \frac{J_{sc}(\lambda)t}{e}$$

$$N_{\text{photons}} (\lambda) = \frac{P_{in}(\lambda)t}{h\nu}$$

Measured under short circuit conditions, if not specified differently, the value of IPCE can be calculated using the following equation as a function of λ :⁷³

$$IPCE(\lambda) = \frac{\frac{J_{sc}(\lambda)t}{e}}{\frac{P_{in}(\lambda)t}{h\nu}} = \frac{h\nu J_{sc}(\lambda)}{eP_{in}(\lambda)} = \frac{hc J_{sc}(\lambda)}{e\lambda P_{in}(\lambda)} = 1240 \frac{J_{sc}(\lambda)}{\lambda P_{in}(\lambda)}$$

where $J_{sc}(\lambda)$ is the photocurrent (in A.cm⁻²) given by the cell under monochromatic illumination at wavelength λ (nm), $P_{in}(\lambda)$ (in W.cm⁻²) is the photon flux of the incident monochromatic light at wavelength λ (nm), e is the elementary charge, h is the Planck's constant, ν is light frequency, c is the speed of light in vacuum.

The IPCE can also be expressed as the product of the light harvesting efficiency [LHE(λ)] for photons of wavelength λ , and the Absorbed Photon-to-current Conversion Efficiency (APCE) also called Internal Quantum Efficiency (IQE) that refers to the efficiency of charger carrier injection and collection. IPCE includes the effects of optical losses such as transmission and reflection, unlike APCE.

$$IPCE = LHE(\lambda)APCE(\lambda)$$

with $LHE(\lambda) = 1 - 10^{-A}$ and $APCE(\lambda) = \phi_{inj}\phi_{coll}$

where A is the dye absorbance or optical density while, ϕ_{inj} is electron injection efficiency from the excited state of the sensitizer to the CB of the semiconductor and ϕ_{coll} is the charge collection efficiency of the injected electron at the front electrode.

ϕ_{inj} is given by:⁴

$$\phi_{inj} = \frac{k_{inj}}{k_r + k_{nr} + k_{inj}}$$

where k_{inj} is the rate constant for ϕ_{inj} into the semiconductor, while k_r and k_{nr} represent the rate constant of radiative and nonradiative deactivation from **Dye*** to **Dye**, respectively.

(v) Finally, the overall performance of the DSSC can be evaluated in terms of energy conversion efficiency (η) which is defined as the ratio between the maximum output electrical power (P_{max}) and the power of the incident light (P_{light}) given by the relation:

$$\eta = \frac{P_{max}}{P_{light}} = \frac{V_{OC} J_{sc} FF}{P_{light}}$$

A standard measurement condition has been developed to generalize the testing of solar cells at any laboratory, since the efficiency of the solar cell depends on the temperature of the cell and even more on the quality of the illumination, *i.e.*, the total light intensity and the spectral distribution of the intensity. The standard condition used to test a terrestrial solar cell is light intensity of 1000 W/m^2 at AM 1.5 when the temperature of the cell is at $25 \text{ }^\circ\text{C}$. The power output of the solar cell at such conditions is the nominal power of the cell, or module, and is reported in peak watts (Wp).

4. Experimental characterization techniques for DSSCs

The basic techniques to characterize of DSSCs are described as follows:

i) Current-voltage (I-V) measurement: The current-voltage measurement of a DSSC is the most important and conventional technique for evaluating the photovoltaic performance. It is performed on a Keithley 2400 source meter under simulated sunlight. A standard illumination of air-mass 1.5 global (AM1.5) with the irradiance of 100 mW/cm^2 is generally used. A typical I-V curve has been shown in Figure 2.6. From the I-V measurement, four parameters mentioned above (V_{oc} , J_{sc} , FF and η) can be determined.

ii) Incident Photon-to-electron Conversion Efficiency (IPCE) measurement: The sensitivity of a DSSC varies with the wavelength of the incident light. Incident photon-to-electron conversion efficiency (IPCE) measures the ratio of the number of electrons generated by the solar cell to the number of incident photons on the active surface under monochromatic light irradiation is measured under short circuit conditions and displayed graphically versus the corresponding wavelength in a photovoltaic action spectrum. IPCE measurement is also useful for indirect determination of the short circuit photocurrent of a DSSC.

iii) Electrochemical impedance spectroscopy (EIS): Electrochemical impedance spectroscopy measurement is used for characterizing the process of electron transport and ion diffusion at difference interfaces of a DSSC. Impedance is measured both under illumination and under dark conditions. Under illumination the cell is illuminated with a range of intensities and impedance is measured at open-circuit condition. In the dark a bias potential is applied. From EIS, several parameters can be obtained, such as charge-transfer resistance at the CE, electron recombination resistance at the $\text{TiO}_2/\text{dye}/\text{electrolyte}$ interface as well as diffusion resistance in the electrolyte.

5. Aim of this thesis

The general purpose of the thesis is to develop well-designed and cost effective solid-state DSSCs to further enhance the energy conversion efficiency, along with an understanding of the relationship between the developed materials and the corresponding device performance. The major emphasis lies on the modification of the purely organic dye based on TAA of D- π -A configuration, designed with an electroactive monomer moiety with the aim to attach covalently the CP (HTM) to the dye so that the physical interface between dye and HTM in conventional ss-DSSCs would be removed.

Previous results showed that the covalent link between organic sensitizer and HTM is a promising approach to improve the performance of ss-DSSC. However, the stability of the formerly developed dyad by combining sensitizer and HTM through an ester link was found not sufficient enough to provide robust devices. Accordingly, changing the nature of the covalent link is a good starting point to provide support for the concept of bifunctional Dye-HTM, which is of high development potential.

References

- (1) Yugis, A. R.; Mansa, R. F.; Sipaut, C. S. Review on Metallic and Plastic Flexible Dye Sensitized Solar Cell. *IOP Conf. Ser. Mater. Sci. Eng.* **2015**, *78*, 012003. <https://doi.org/10.1088/1757-899X/78/1/012003>.
- (2) Sima, C.; Grigoriu, C.; Antohe, S. Comparison of the Dye-Sensitized Solar Cells Performances Based on Transparent Conductive ITO and FTO. *Thin Solid Films* **2010**, *519* (2), 595–597. <https://doi.org/10.1016/j.tsf.2010.07.002>.
- (3) O'Regan, B.; Grätzel, M. A Low-Cost, High-Efficiency Solar Cell Based on Dye-Sensitized Colloidal TiO₂ Films. *Nature* **1991**, *353* (6346), 737–740. <https://doi.org/10.1038/353737a0>.
- (4) Nazeeruddin, M. K.; Kay, A.; Rodicio, I.; Humphry-Baker, R.; Mueller, E.; Liska, P.; Vlachopoulos, N.; Graetzel, M. Conversion of Light to Electricity by Cis-X₂bis(2,2'-Bipyridyl-4,4'-Dicarboxylate)Ruthenium(II) Charge-Transfer Sensitizers (X = Cl-, Br-, I-, CN-, and SCN-) on Nanocrystalline Titanium Dioxide Electrodes. *J. Am. Chem. Soc.* **1993**, *115* (14), 6382–6390. <https://doi.org/10.1021/ja00067a063>.
- (5) Cavallo, C.; Di Pascasio, F.; Latini, A.; Bonomo, M.; Dini, D. Nanostructured Semiconductor Materials for Dye-Sensitized Solar Cells. *J. Nanomater.* **2017**, *2017*, 1–31. <https://doi.org/10.1155/2017/5323164>.
- (6) Hagfeldt, A.; Grätzel, M. Molecular Photovoltaics. *Acc. Chem. Res.* **2000**, *33* (5), 269–277. <https://doi.org/10.1021/ar980112j>.
- (7) Beltrán, A.; Gracia, L.; Andrés, J. Density Functional Theory Study of the Brookite Surfaces and Phase Transitions between Natural Titania Polymorphs. *J. Phys. Chem. B* **2006**, *110* (46), 23417–23423. <https://doi.org/10.1021/jp0643000>.
- (8) Dacurrrr, F. PRESSURE-TEMPERATURE STUDIES OF ANATASE, BROOKITE, RUTILE AND TiO₂-II. 11.
- (9) Dache, F.; Simons, P. Y.; Roy, R. Pressure-Temperature Studies of Anatase, Brookite, Rutile and TiO₂-II. *Am. Mineral.* **1968**, *53* (11–12), 1929–1939.
- (10) Xu, C.; Shin, P. H.; Cao, L.; Wu, J.; Gao, D. Ordered TiO₂ Nanotube Arrays on Transparent Conductive Oxide for Dye-Sensitized Solar Cells. *Chem. Mater.* **2010**, *22* (1), 143–148. <https://doi.org/10.1021/cm9027513>.
- (11) Zeng, W.; Cao, Y.; Bai, Y.; Wang, Y.; Shi, Y.; Zhang, M.; Wang, F.; Pan, C.; Wang, P. Efficient Dye-Sensitized Solar Cells with an Organic Photosensitizer Featuring Orderly Conjugated Ethylenedioxythiophene and Dithienosilole Blocks. *Chem. Mater.* **2010**, *22* (5), 1915–1925. <https://doi.org/10.1021/cm9036988>.

- (12) Nazeeruddin, M. K.; De Angelis, F.; Fantacci, S.; Selloni, A.; Viscardi, G.; Liska, P.; Ito, S.; Takeru, B.; Grätzel, M. Combined Experimental and DFT-TDDFT Computational Study of Photoelectrochemical Cell Ruthenium Sensitizers. *J. Am. Chem. Soc.* **2005**, *127* (48), 16835–16847. <https://doi.org/10.1021/ja052467l>.
- (13) Wu, J.; Lan, Z.; Lin, J.; Huang, M.; Huang, Y.; Fan, L.; Luo, G. Electrolytes in Dye-Sensitized Solar Cells. *Chem. Rev.* **2015**, *115* (5), 2136–2173. <https://doi.org/10.1021/cr400675m>.
- (14) Miettunen, K.; Etula, J.; Saukkonen, T.; Jouttijärvi, S.; Halme, J.; Romu, J.; Lund, P. Insights into Corrosion in Dye Solar Cells. *Prog. Photovolt. Res. Appl.* **2015**, *23* (8), 1045–1056. <https://doi.org/10.1002/pip.2534>.
- (15) Miettunen, K.; Halme, J.; Toivola, M.; Lund, P. Initial Performance of Dye Solar Cells on Stainless Steel Substrates. *J. Phys. Chem. C* **2008**, *112* (10), 4011–4017. <https://doi.org/10.1021/jp7112957>.
- (16) Wu, J.; Lan, Z.; Hao, S.; Li, P.; Lin, J.; Huang, M.; Fang, L.; Huang, Y. Progress on the Electrolytes for Dye-Sensitized Solar Cells. *Pure Appl. Chem.* **2008**, *80* (11), 2241–2258. <https://doi.org/10.1351/pac200880112241>.
- (17) Miettunen, K.; Ruan, X.; Saukkonen, T.; Halme, J.; Toivola, M.; Guangsheng, H.; Lund, P. Stability of Dye Solar Cells with Photoelectrode on Metal Substrates. *J. Electrochem. Soc.* **2010**, *157* (6), B814–B819. <https://doi.org/10.1149/1.3374645>.
- (18) Apostolopoulou, A.; Vlasiou, M.; Tziouris, P. A.; Tsiafoulis, C.; Tsipis, A. C.; Rehder, D.; Kabanos, T. A.; Keramidis, A. D.; Stathatos, E. Oxidovanadium(IV/V) Complexes as New Redox Mediators in Dye-Sensitized Solar Cells: A Combined Experimental and Theoretical Study. *Inorg. Chem.* **2015**, *54* (8), 3979–3988. <https://doi.org/10.1021/acs.inorgchem.5b00159>.
- (19) Nusbaumer, H.; Moser, J.-E.; Zakeeruddin, S. M.; Nazeeruddin, M. K.; Grätzel, M. Co^{II} (Dbbip)₂²⁺ Complex Rivals Tri-Iodide/Iodide Redox Mediator in Dye-Sensitized Photovoltaic Cells. *J. Phys. Chem. B* **2001**, *105* (43), 10461–10464. <https://doi.org/10.1021/jp012075a>.
- (20) Wang, Z.-S.; Sayama, K.; Sugihara, H. Efficient Eosin Y Dye-Sensitized Solar Cell Containing Br⁻/Br₃⁻ Electrolyte. *J. Phys. Chem. B* **2005**, *109* (47), 22449–22455. <https://doi.org/10.1021/jp053260h>.
- (21) Daeneke, T.; Kwon, T.-H.; Holmes, A. B.; Duffy, N. W.; Bach, U.; Spiccia, L. High-Efficiency Dye-Sensitized Solar Cells with Ferrocene-Based Electrolytes. *Nat. Chem.* **2011**, *3* (3), 211–215. <https://doi.org/10.1038/nchem.966>.
- (22) Wang, P.; Zakeeruddin, S. M.; Moser, J.-E.; Humphry-Baker, R.; Grätzel, M. A Solvent-Free, SeCN⁻/(SeCN)₃⁻ Based Ionic Liquid Electrolyte for High-Efficiency Dye-Sensitized

- Nanocrystalline Solar Cells. *J. Am. Chem. Soc.* **2004**, *126* (23), 7164–7165. <https://doi.org/10.1021/ja048472r>.
- (23) Mehmood, U.; Al-Ahmed, A.; Al-Sulaiman, F. A.; Malik, M. I.; Shehzad, F.; Khan, A. U. H. Effect of Temperature on the Photovoltaic Performance and Stability of Solid-State Dye-Sensitized Solar Cells: A Review. *Renew. Sustain. Energy Rev.* **2017**, *79*, 946–959. <https://doi.org/10.1016/j.rser.2017.05.114>.
- (24) Hagen, J.; Schaffrath, W.; Otschik, P.; Fink, R.; Bacher, A.; Schmidt, H.-W.; Haarer, D. Novel Hybrid Solar Cells Consisting of Inorganic Nanoparticles and an Organic Hole Transport Material. *Synth. Met.* **1997**, *89* (3), 215–220. [https://doi.org/10.1016/S0379-6779\(97\)81221-0](https://doi.org/10.1016/S0379-6779(97)81221-0).
- (25) Bach, U.; Lupo, D.; Comte, P.; Moser, J. E.; Weissörtel, F.; Salbeck, J.; Spreitzer, H.; Grätzel, M. Solid-State Dye-Sensitized Mesoporous TiO₂ Solar Cells with High Photon-to-Electron Conversion Efficiencies. *Nature* **1998**, *395* (6702), 583–585. <https://doi.org/10.1038/26936>.
- (26) Krüger, J.; Plass, R.; Cevey, L.; Piccirelli, M.; Grätzel, M.; Bach, U. High Efficiency Solid-State Photovoltaic Device Due to Inhibition of Interface Charge Recombination. *Appl. Phys. Lett.* **2001**, *79* (13), 2085–2087. <https://doi.org/10.1063/1.1406148>.
- (27) Snaith, H. J.; Moule, A. J.; Klein, C.; Meerholz, K.; Friend, R. H.; Grätzel, M. Efficiency Enhancements in Solid-State Hybrid Solar Cells via Reduced Charge Recombination and Increased Light Capture. *Nano Lett.* **2007**, *7* (11), 3372–3376. <https://doi.org/10.1021/nl071656u>.
- (28) Wang, M.; Moon, S.-J.; Xu, M.; Chittibabu, K.; Wang, P.; Cevey-Ha, N.-L.; Humphry-Baker, R.; Zakeeruddin, S. M.; Grätzel, M. Efficient and Stable Solid-State Dye-Sensitized Solar Cells Based on a High-Molar-Extinction-Coefficient Sensitizer. *Small* **2010**, *6* (2), 319–324. <https://doi.org/10.1002/sml.200901317>.
- (29) Cai, N.; Moon, S.-J.; Cevey-Ha, L.; Moehl, T.; Humphry-Baker, R.; Wang, P.; Zakeeruddin, S. M.; Grätzel, M. An Organic D- π -A Dye for Record Efficiency Solid-State Sensitized Heterojunction Solar Cells. *Nano Lett.* **2011**, *11* (4), 1452–1456. <https://doi.org/10.1021/nl104034e>.
- (30) Burschka, J.; Dualeh, A.; Kessler, F.; Baranoff, E.; Cevey-Ha, N.-L.; Yi, C.; Nazeeruddin, M. K.; Grätzel, M. Tris(2-(1 *H*-Pyrazol-1-Yl)Pyridine)Cobalt(III) as p-Type Dopant for Organic Semiconductors and Its Application in Highly Efficient Solid-State Dye-Sensitized Solar Cells. *J. Am. Chem. Soc.* **2011**, *133* (45), 18042–18045. <https://doi.org/10.1021/ja207367t>.
- (31) Murakoshi, K.; Kogure, R.; Wada, Y.; Yanagida, S. Solid State Dye-Sensitized TiO₂ Solar Cell with Polypyrrole as Hole Transport Layer. *Chem. Lett.* **1997**, *26* (5), 471–472. <https://doi.org/10.1246/cl.1997.471>.

- (32) KitamuraTakayuki; MaitaniMasato; MatsudaMizuho; WadaYuji; YanagidaShozo. Improved Solid-State Dye Solar Cells with Polypyrrole Using a Carbon-Based Counter Electrode. *Chem. Lett.* **2003**. <https://doi.org/10.1246/cl.2001.1054>.
- (33) Murakoshi, K.; Kogure, R.; Wada, Y.; Yanagida, S. Fabrication of Solid-State Dye-Sensitized TiO₂ Solar Cells Combined with Polypyrrole. *Sol. Energy Mater. Sol. Cells* **1998**, *13*.
- (34) Improved Solid-State Dye Solar Cells with Polypyrrole using a Carbon-Based Counter Electrode | Chemistry Letters | CSJ Journals <https://www.journal.csj.jp/doi/pdf/10.1246/cl.2001.1054> (accessed Sep 9, 2019).
- (35) Tan, S. X.; Zhai, J.; Wan, M. X.; Jiang, L.; Zhu, D. B. Polyaniline as Hole Transport Material to Prepare Solid Solar Cells. *Synth. Met.* **2003**, *137* (1–3), 1511–1512. [https://doi.org/10.1016/S0379-6779\(02\)01207-9](https://doi.org/10.1016/S0379-6779(02)01207-9).
- (36) Tan, S.; Zhai, J.; Xue, B.; Wan, M.; Meng, Q.; Li, Y.; Jiang, L.; Zhu, D. Property Influence of Polyanilines on Photovoltaic Behaviors of Dye-Sensitized Solar Cells. *Langmuir* **2004**, *20* (7), 2934–2937. <https://doi.org/10.1021/la036260m>.
- (37) Lancelle-Beltran, E.; Prené, P.; Boscher, C.; Belleville, P.; Buvat, P.; Sanchez, C. All-Solid-State Dye-Sensitized Nanoporous TiO₂ Hybrid Solar Cells with High Energy-Conversion Efficiency. *Adv. Mater.* **2006**, *18* (19), 2579–2582. <https://doi.org/10.1002/adma.200502023>.
- (38) Coakley, K. M.; Liu, Y.; McGehee, M. D.; Frindell, K. L.; Stucky, G. D. Infiltrating Semiconducting Polymers into Self-Assembled Mesoporous Titania Films for Photovoltaic Applications. *Adv. Funct. Mater.* **2003**, *13* (4), 301–306. <https://doi.org/10.1002/adfm.200304361>.
- (39) Coakley, K. M.; McGehee, M. D. Photovoltaic Cells Made from Conjugated Polymers Infiltrated into Mesoporous Titania. *Appl. Phys. Lett.* **2003**, *83* (16), 3380–3382. <https://doi.org/10.1063/1.1616197>.
- (40) Jiang, K.-J.; Manseki, K.; Yu, Y.-H.; Masaki, N.; Suzuki, K.; Song, Y.; Yanagida, S. Photovoltaics Based on Hybridization of Effective Dye-Sensitized Titanium Oxide and Hole-Conductive Polymer P3HT. *Adv. Funct. Mater.* **2009**, *19* (15), 2481–2485. <https://doi.org/10.1002/adfm.200900283>.
- (41) Lancelle-Beltran, E.; Prené, P.; Boscher, C.; Belleville, P.; Buvat, P.; Lambert, S.; Guillet, F.; Marcel, C.; Sanchez, C. Solid-State Organic/Inorganic Hybrid Solar Cells Based on Poly(Octylthiophene) and Dye-Sensitized Nanobrookite and Nanoanatase TiO₂ Electrodes. *Eur. J. Inorg. Chem.* **2008**, *2008* (6), 903–910. <https://doi.org/10.1002/ejic.200701033>.

- (42) Song, L.; Wang, W.; Körstgens, V.; González, D. M.; Yao, Y.; Minar, N. K.; Feckl, J. M.; Peters, K.; Bein, T.; Fattakhova-Rohlfing, D.; Santoro, G.; Roth, S. V.; Müller-Buschbaum, P. Spray Deposition of Titania Films with Incorporated Crystalline Nanoparticles for All-Solid-State Dye-Sensitized Solar Cells Using P3HT. *Adv. Funct. Mater.* **2016**, *26* (10), 1498–1506. <https://doi.org/10.1002/adfm.201504498>.
- (43) Mor, G. K.; Kim, S.; Paulose, M.; Varghese, O. K.; Shankar, K.; Basham, J.; Grimes, C. A. Visible to Near-Infrared Light Harvesting in TiO₂ Nanotube Array–P3HT Based Heterojunction Solar Cells. *Nano Lett.* **2009**, *9* (12), 4250–4257. <https://doi.org/10.1021/nl9024853>.
- (44) Chevrier, M.; Hawashin, H.; Richeter, S.; Mehdi, A.; Surin, M.; Lazzaroni, R.; Dubois, P.; Ratier, B.; Bouclé, J.; Clément, S. Well-Designed Poly(3-Hexylthiophene) as Hole Transporting Material: A New Opportunity for Solid-State Dye-Sensitized Solar Cells. *Synth. Met.* **2017**, *226*, 157–163. <https://doi.org/10.1016/j.synthmet.2017.02.015>.
- (45) Zafer, C.; Karapire, C.; Serdar Sariciftci, N.; Icli, S. Characterization of N, N'-Bis-2-(1-Hydroxy-4-Methylpentyl)-3, 4, 9, 10-Perylene Bis (Dicarboximide) Sensitized Nanocrystalline TiO₂ Solar Cells with Polythiophene Hole Conductors. *Sol. Energy Mater. Sol. Cells* **2005**, *88* (1), 11–21. <https://doi.org/10.1016/j.solmat.2004.09.009>.
- (46) Kudo, N.; Honda, S.; Shimazaki, Y.; Ohkita, H.; Ito, S.; Benten, H. Improvement of Charge Injection Efficiency in Organic-Inorganic Hybrid Solar Cells by Chemical Modification of Metal Oxides with Organic Molecules. *Appl. Phys. Lett.* **2007**, *90* (18), 183513. <https://doi.org/10.1063/1.2736192>.
- (47) Smestad, G. P.; Spiekermann, S.; Kowalik, J.; Grant, C. D.; Schwartzberg, A. M.; Zhang, J.; Tolbert, L. M.; Moons, E. A Technique to Compare Polythiophene Solid-State Dye Sensitized TiO₂ Solar Cells to Liquid Junction Devices. *Sol. Energy Mater. Sol. Cells* **2003**, *76* (1), 85–105. [https://doi.org/10.1016/S0927-0248\(02\)00252-0](https://doi.org/10.1016/S0927-0248(02)00252-0).
- (48) Yanagida, S.; Yu, Y.; Manseki, K. Iodine/Iodide-Free Dye-Sensitized Solar Cells. *Acc. Chem. Res.* **2009**, *42* (11), 1827–1838. <https://doi.org/10.1021/ar900069p>.
- (49) Kroeze, J. E.; Hirata, N.; Schmidt-Mende, L.; Orizu, C.; Ogier, S. D.; Carr, K.; Grätzel, M.; Durrant, J. R. Parameters Influencing Charge Separation in Solid-State Dye-Sensitized Solar Cells Using Novel Hole Conductors. *Adv. Funct. Mater.* **2006**, *16* (14), 1832–1838. <https://doi.org/10.1002/adfm.200500748>.
- (50) Groenendaal, L. ^aBert^o; Jonas, F.; Freitag, D.; Pielartzik, H.; Reynolds, J. R. Poly(3,4-Ethylenedioxythiophene) and Its Derivatives: Past, Present, and Future. 14.

- (51) Wang, M.; Grätzel, C.; Zakeeruddin, S. M.; Grätzel, M. Recent Developments in Redox Electrolytes for Dye-Sensitized Solar Cells. *Energy Environ. Sci.* **2012**, *5* (11), 9394. <https://doi.org/10.1039/c2ee23081j>.
- (52) Hu, L.; Hecht, D. S.; Grüner, G. Infrared Transparent Carbon Nanotube Thin Films. *Appl. Phys. Lett.* **2009**, *94* (8), 081103. <https://doi.org/10.1063/1.3075067>.
- (53) Saito, Y.; Kitamura, T.; Wada, Y.; Yanagida, S. Poly(3,4-Ethylenedioxythiophene) as a Hole Conductor in Solid State Dye Sensitized Solar Cells. *Synth. Met.* **2002**, *131* (1–3), 185–187. [https://doi.org/10.1016/S0379-6779\(02\)00198-4](https://doi.org/10.1016/S0379-6779(02)00198-4).
- (54) Saito, Y. Solid State Dye Sensitized Solar Cells Using in Situ Polymerized PEDOTs as Hole Conductor. *Electrochem. Commun.* **2004**, *6* (1), 71–74. <https://doi.org/10.1016/j.elecom.2003.10.016>.
- (55) Xia, J.; Masaki, N.; Lira-Cantu, M.; Kim, Y.; Jiang, K.; Yanagida, S. Influence of Doped Anions on Poly(3,4-Ethylenedioxythiophene) as Hole Conductors for Iodine-Free Solid-State Dye-Sensitized Solar Cells. *J. Am. Chem. Soc.* **2008**, *130* (4), 1258–1263. <https://doi.org/10.1021/ja075704o>.
- (56) Xia, J.; Masaki, N.; Lira-Cantu, M.; Kim, Y.; Jiang, K.; Yanagida, S. Effect of Doping Anions' Structures on Poly(3,4-Ethylenedioxythiophene) as Hole Conductors in Solid-State Dye-Sensitized Solar Cells. *J. Phys. Chem. C* **2008**, *112* (30), 11569–11574. <https://doi.org/10.1021/jp801878a>.
- (57) Liu, X.; Zhang, W.; Uchida, S.; Cai, L.; Liu, B.; Ramakrishna, S. An Efficient Organic-Dye-Sensitized Solar Cell with in Situ Polymerized Poly(3,4-Ethylenedioxythiophene) as a Hole-Transporting Material. *Adv. Mater.* **2010**, *22* (20), E150–E155. <https://doi.org/10.1002/adma.200904168>.
- (58) Kim, J.; Koh, J. K.; Kim, B.; Ahn, S. H.; Ahn, H.; Ryu, D. Y.; Kim, J. H.; Kim, E. Enhanced Performance of I₂-Free Solid-State Dye-Sensitized Solar Cells with Conductive Polymer up to 6.8%. *Adv. Funct. Mater.* **2011**, *21* (24), 4633–4639. <https://doi.org/10.1002/adfm.201101520>.
- (59) Liu, X.; Cheng, Y.; Wang, L.; Cai, L.; Liu, B. Light Controlled Assembling of Iodine-Free Dye-Sensitized Solar Cells with Poly(3,4-Ethylenedioxythiophene) as a Hole Conductor Reaching 7.1% Efficiency. *Phys. Chem. Chem. Phys.* **2012**, *14* (19), 7098. <https://doi.org/10.1039/c2cp40882a>.
- (60) Zhang, J.; Vlachopoulos, N.; Jouini, M.; Johansson, M. B.; Zhang, X.; Nazeeruddin, M. K.; Boschloo, G.; Johansson, E. M. J.; Hagfeldt, A. Efficient Solid-State Dye Sensitized Solar Cells: The Influence of Dye Molecular Structures for the in-Situ Photoelectrochemically

- Polymerized PEDOT as Hole Transporting Material. *Nano Energy* **2016**, *19*, 455–470. <https://doi.org/10.1016/j.nanoen.2015.09.010>.
- (61) Hauch, A.; Georg, A. Diffusion in the Electrolyte and Charge-Transfer Reaction at the Platinum Electrode in Dye-Sensitized Solar Cells. *Electrochimica Acta* **2001**, *46* (22), 3457–3466. [https://doi.org/10.1016/S0013-4686\(01\)00540-0](https://doi.org/10.1016/S0013-4686(01)00540-0).
- (62) Thomas, S.; Deepak, T. G.; Anjusree, G. S.; Arun, T. A.; Nair, S. V.; Nair, A. S. A Review on Counter Electrode Materials in Dye-Sensitized Solar Cells. *J Mater Chem A* **2014**, *2* (13), 4474–4490. <https://doi.org/10.1039/C3TA13374E>.
- (63) Liu, Q.; Li, C.; Jiang, K.; Song, Y.; Pei, J. A High-Efficiency Solid-State Dye-Sensitized Solar Cell with P3HT Polymer as a Hole Conductor and an Assistant Sensitizer. *Particuology* **2014**, *15*, 71–76. <https://doi.org/10.1016/j.partic.2012.12.005>.
- (64) *Molecular Devices for Solar Energy Conversion and Storage*; Tian, H., Boschloo, G., Hagfeldt, A., Eds.; Green Chemistry and Sustainable Technology; Springer Singapore, 2018. <https://doi.org/10.1007/978-981-10-5924-7>.
- (65) Ardo, S.; Meyer, G. J. Photodriven Heterogeneous Charge Transfer with Transition-Metal Compounds Anchored to TiO₂ Semiconductor Surfaces. *Chem Soc Rev* **2009**, *38* (1), 115–164. <https://doi.org/10.1039/B804321N>.
- (66) Anderson, N. A.; Lian, T. ULTRAFast ELECTRON TRANSFER AT THE MOLECULE-SEMICONDUCTOR NANOPARTICLE INTERFACE. *Annu. Rev. Phys. Chem.* **2005**, *56* (1), 491–519. <https://doi.org/10.1146/annurev.physchem.55.091602.094347>.
- (67) Nissfolk, J.; Fredin, K.; Hagfeldt, A.; Boschloo, G. Recombination and Transport Processes in Dye-Sensitized Solar Cells Investigated under Working Conditions. *J. Phys. Chem. B* **2006**, *110* (36), 17715–17718. <https://doi.org/10.1021/jp064046b>.
- (68) O'Regan, B. C.; Durrant, J. R. Kinetic and Energetic Paradigms for Dye-Sensitized Solar Cells: Moving from the Ideal to the Real. *Acc. Chem. Res.* **2009**, *42* (11), 1799–1808. <https://doi.org/10.1021/ar900145z>.
- (69) Hagfeldt, Anders.; Graetzel, Michael. Light-Induced Redox Reactions in Nanocrystalline Systems. *Chem. Rev.* **1995**, *95* (1), 49–68. <https://doi.org/10.1021/cr00033a003>.
- (70) *Handbook of Photovoltaic Science and Engineering*; Luque, A., Hegedus, S., Eds.; Wiley: Hoboken, NJ, 2003.
- (71) Calogero, G.; Bartolotta, A.; Marco, G. D.; Carlo, A. D.; Bonaccorso, F. Vegetable-Based Dye-Sensitized Solar Cells. *Chem. Soc. Rev.* **2015**, *44* (10), 3244–3294. <https://doi.org/10.1039/C4CS00309H>.

- (72) Chapin, D. M.; Fuller, C. S.; Pearson, G. L. A New Silicon P-n Junction Photocell for Converting Solar Radiation into Electrical Power. *J. Appl. Phys.* **1954**, *25* (5), 676–677. <https://doi.org/10.1063/1.1721711>.
- (73) Calogero, G.; Yum, J.-H.; Sinopoli, A.; Di Marco, G.; Grätzel, M.; Nazeeruddin, M. K. Anthocyanins and Betalains as Light-Harvesting Pigments for Dye-Sensitized Solar Cells. *Sol. Energy* **2012**, *86* (5), 1563–1575. <https://doi.org/10.1016/j.solener.2012.02.018>.

Chapter 3. Principle sensitizers in DSSCs and new design of sensitizers

In the DSSCs, light is absorbed by the dye anchored on the semi-conducting surface (TiO_2 , ZnO , etc...). After absorption process, it is then expected that the electrons from the excited state of the dye are injected in the conduction band (CB) of the semiconductor generating an electric current while the ground state of the dye is regenerated by the redox mediator (conducting polymer in the case for ss-DSSCs). The redox mediator is then regenerated in turn by the reduction reaction at the counter electrode. The circuit is completed via electron migration through the external load. Therefore, the dye or sensitizer is of crucial importance in the performance of the photovoltaic cell and to fulfill the previous requirement it must necessarily possess the following properties:

- (i) It should absorb in a very broad region of the UV-Vis spectrum with a high molar extinction coefficient (ϵ). Both characteristics enable efficient light harvesting when dye is deposited as thinner film on the semi-conducting surface (TiO_2 nanoparticles)
- (ii) The dye should show appropriate steric properties to suppress charge recombination at the TiO_2 interface and dye aggregation for their adverse effect on the photocurrent and photovoltage.
- (iii) The lowest unoccupied molecular orbital (LUMO) of the dye should be more negative (more stable) than the conduction band of TiO_2 (-0.5 V vs. NHE) in order to provide an efficient driving force for electron injection.
- (iv) The highest occupied molecular orbital (HOMO) of the dye should be more positive than the energy level of the redox mediator, i.e., polymer, to provide sufficient driving force for the regeneration of the oxidized dye.
- (v) The dye should have an anchoring group for grafting on the TiO_2 surface and to ascertain strong electronic coupling between the excited state wavefunction of the dye and the conduction band manifold of the semiconductor, typically of acidic nature, such as carboxylic acid, phosphoric acid, benzoic acid
- (vi) The photostability of the dye should be as high as possible to ensure the long lifetime of the photovoltaic cell.

Based on these requirements, numerous photosensitizers including metals complexes and organic compounds, have been developed aiming to improve the DSSC performance. Usually,

the sensitizers are divided into three main classes, Ru-based complexes, metal porphyrins derivatives and metal-free dyes.

As a fundamental trend, the development of dye belonging to the last classes of compounds, i.e., metal-free organic dye, is a very active field of research. Indeed, organic dyes are particularly attractive owing to their high molar absorption coefficient and the infinity of possible molecular structures.

In this chapter, we will present the different classes of dyes described in the literature to date. As the number of synthesized dyes is huge, this chapter will not be exhaustive, and we will focus on main families of compounds. For each family, strategies for improving optical properties or photovoltaic performance will be described. In addition, the advantages and disadvantages of different families of dyes based on metal complexes or purely organic will be discussed. The presentation of this state of the art of dye will allow us to define the main objectives of this thesis as well as the choice of the adopted dye structure.

1. Ru complexes

Despite their generally rather poor red/near-infrared light absorption, Ruthenium complexes, especially complexes based on bipyridyl dyes, have attracted increased interest as the most efficient sensitizer dyes reported so far for dye sensitized solar energy conversion. Ruthenium complexes have many advantageous features for applications as sensitizers for DSCs. Such complexes have strong metal-to-ligand charge-transfer (MLCT) absorption bands, covering a wide spectral range from near UV to visible. The photoexcited states and oxidized form of the complexes are chemically stable therefore long-lived and have appropriate redox potentials for electron injection to TiO_2 and for accepting electrons from the I^-/I_3^- redox couple in the electrolyte. However, high price and the limited resources of ruthenium will be a critical issue.

Ru complexes with carboxylated bipyridine ligands were used for sensitization since 1979¹. In 1991, O'Regan and Grätzel reported the manufacture of the first DSSC based on an optically transparent film of titanium dioxide particles, coated with a monolayer of a Ru trinuclear complex synthesized in 1990 to sensitize the film². The device, known as the Grätzel's cell, harvests a high proportion of the incident solar energy flux (46%) and shows exceptionally high efficiencies for the conversion of incident photons to electrical current (more than 80%) thanks to the high surface area of the semiconductor film and the ideal spectral characteristics of the dye. The overall light-to-electric energy conversion yield is 7.1-7.9% in simulated solar light and 12% in diffuse daylight. This breakthrough initiated intensive synthetic efforts of Ru

complexes to obtain better conversion efficiency. In 1993, Grätzel *et al.* published a series of bipyridyl Ru(II) complexes of general formula *cis*-X₂bis(2,2'-bipyridyl-4,4'-dicarboxylate)-Ru(II) where X = Cl, Br, I, CN, and SCN (Fig 3.1). The derivative containing two groups of isocyanate ligand (the thiocyanato derivative), *cis*-bis(isothiocyanato)-bis(2,2'-bipyridyl-4,4'-dicarboxylate)ruthenium(II), named **N3**, showed outstanding photovoltaics properties like long excited state life-time, strong adsorption on the semiconductor surface due to binding with up to four carboxyl groups, and the use of two thiocyanate groups instead of other ligands produced a redshift in the spectral response up to 800 nm, increasing the J_{SC} up to 17 mA.cm⁻² and achieving a competitive solar-to-electric energy conversion efficiency of 10%³.

The protonation effect on the DSSC performance of **N3** was investigated in 1999. It was found that the doubly protonated form with TBA⁺ (tetrabutylammonium) instead of H⁺ at two carboxyl groups, (Bu₄N)₂[Ru(dcbpyH)₂(NCS)₂], coded as **N719**, exhibited an improved power conversion efficiency due to the increased cell voltage⁴.

A different approach to optimize sensitizer is to extend the light absorption since the major drawback of **N3** dye is its lack of absorption in the red region of the visible spectrum (Fig 3.2). The trithiocyanato-ruthenium (II) terpyridyl complex, known as **N749** or black dye demonstrated that the thiocyanate groups were able to extend the light absorption further into the NIR part of the spectrum, thereby converting more photons to electrons. It is also called the black dye, for many years it was considered to be the dye with the widest light-harvesting ability, whose electric current generation is almost 100% over the wavelength range from 400 to 700 nm with light-harvesting capability extending up to 920 nm⁵.

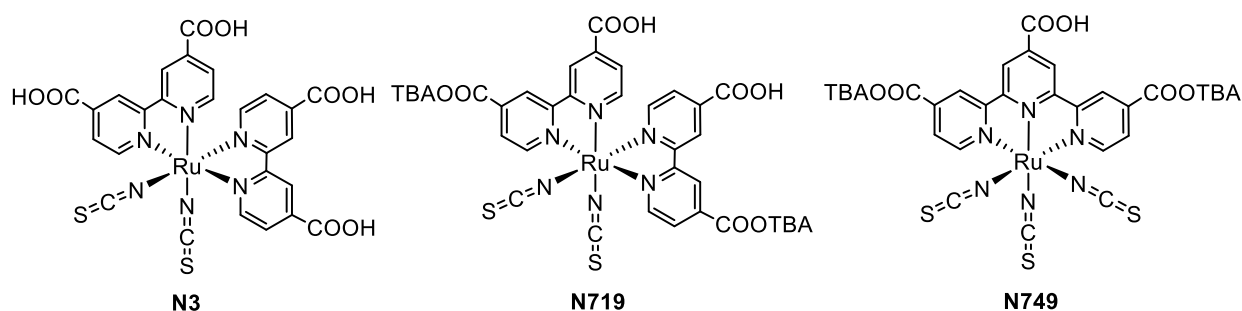


Figure 3.1 Molecular structure of **N3**, **N19**, **N749**.

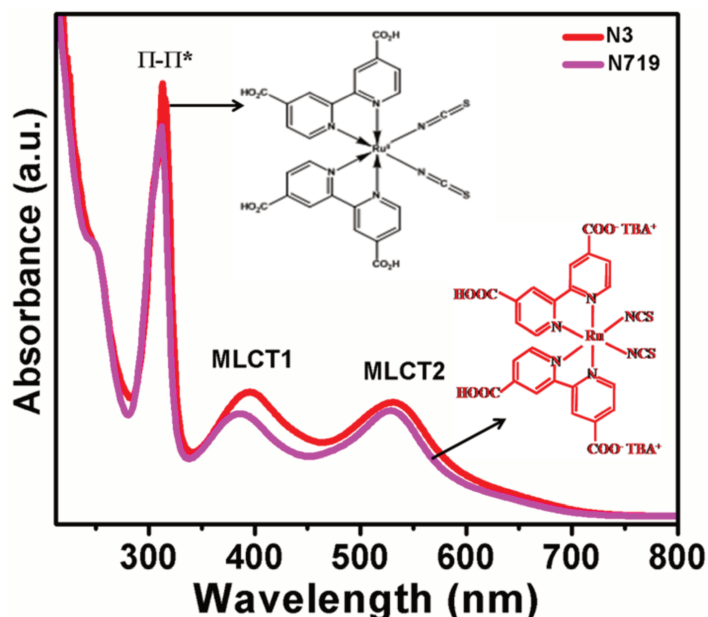


Figure 3.2 Absorption spectra of the N719 and N3 dye sensitizers in ethanol medium.⁶

With the aim to enhance the long-term stability of the dyes toward water-induced desorption from the TiO₂ surface in the operation of the device, new Ru-based photosensitizers carrying hydrophobic groups in the ancillary ligands were investigated (Fig 3.3). In 2003, a heteroleptic amphiphilic Ru(II) complex named **Z907** was reported exhibiting prominent thermal stability with about 7.8% power conversion efficiency⁷. The hydrophobic alkyl chains attached to one of the bipyridine ligands formed a hydrophobic layer keeping water molecules away from the chemical bonds between the dye and TiO₂ layer, which hinders the desorption process of the dye by residual water and meanwhile generates an insulating barrier between the electrolyte and the semiconductor, thus reduces the dark current. **Z907** sensitized DSSCs passed 1000 h at 80 °C in darkness and at 55 °C under illumination without any degradation. Moreover, in combination with decylphosphonic acid as co-absorber on the TiO₂ NPs, the hydrophobicity of the surface could be even enhanced, and stable cells have been demonstrated.

Although the amphiphilic sensitizers improved stability of DSSCs, its disadvantage of low molar extinction coefficients led to the development of new amphiphilic sensitizers with π -conjugated system of the bipyridine groups. The increase in the conjugation length resulted in promoted red shift of the MLCT and higher molar extinction coefficients, thus enhanced harvesting of solar light while maintaining the long-term stability. In 2004, the molecule nominated as **Z910**, (cis-dithiocyanato-(2,2'-bipyridyl-4,4'-dicarboxylate)-[4,4'-bis(3-methoxystyryl)-2,2'-bipyridyl]-Ru(II), containing both hydrophobic and conjugated moieties was reported. A red shift of 20 nm compared with **Z907** was obtained as well as a higher molar

extinction coefficient than **N719**. The achievement of 10.2% of **Z910** based DSSC demonstrated that enhancing the molar extinction coefficient of sensitizers is a good strategy to improve the photovoltaic performance of Ru-based dyes⁸. Another similar complex **K19** was published in 2005 with 4,4'-bis(*p*-hexyloxystyryl)-2,2'-bipyridyl moieties instead of the 4,4'-bis(3-methoxystyryl)-2,2'-bipyridyl groups coordinated to **Z910**⁹. The molar extinction coefficient $18.2 \times 10^3 \text{ M}^{-1} \text{ cm}^{-1}$ was reported, which is higher than that of **Z910** ($17.3 \times 10^3 \text{ M}^{-1} \text{ cm}^{-1}$). The **K19** dye exhibited a power conversion efficiency of only around 7%; however, the **K77** dye, obtained by replacing the *p*-hexyloxystyryl unit of **K19** by 3-*tert*-butyloxyphenyl(ethenyl) led to an efficiency of 9.5%¹⁰.

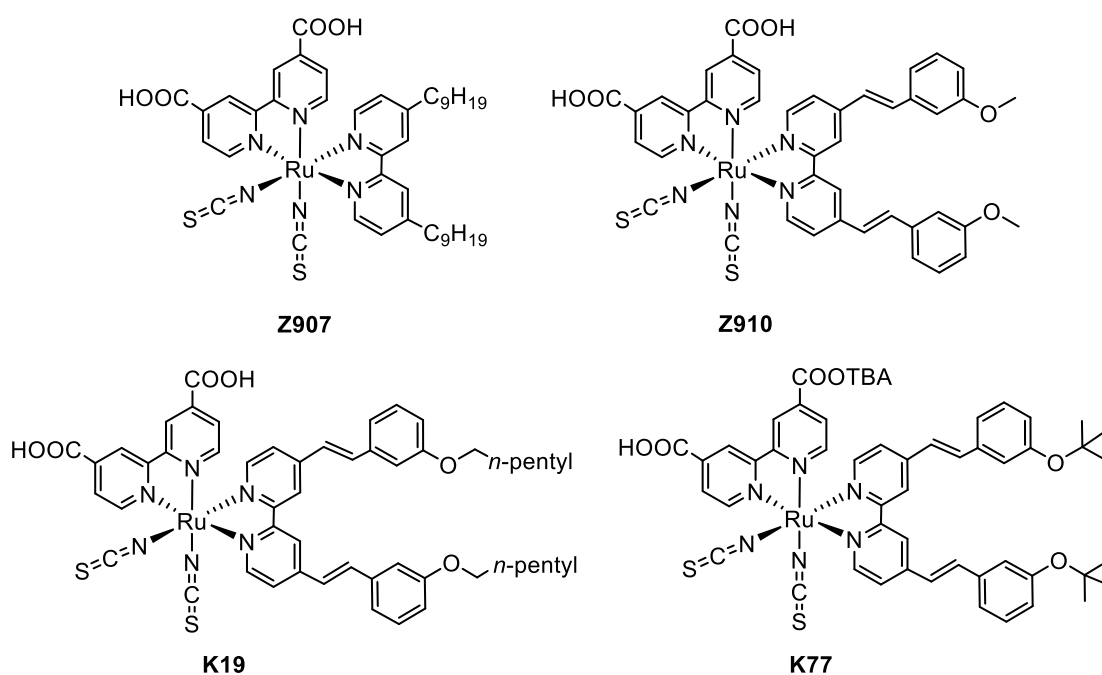


Figure 3.3 Molecular structure of **Z907**, **Z910**, **K19**, **K77**.

The use of thiophene instead of phenylene antenna on the ancillary ligands opens new opportunities for heteroleptic ruthenium complexes (Fig 3.4). A polythiophene may be viewed as a *cis*-polyacetylene chain bridged with sulfur atoms, the bridging sulfur atoms can provide excellent aromatic stability to the polyacetylene chain while preserving properties like high charge transport. Moreover, the incorporation of thiophene as a more electron-rich moiety onto bipyridine ligands can enhance the light-harvesting capacity of these complexes by increasing the molar absorptivity and red-shifting their spectral response. It is also important to note that the facile functionalization of thiophene could help to modify the properties of complexes, such as polarity, solubility, and bandgap tuning. Further, an alkyl group on the thiophene ring can

prevent water-induced desorption. **C101**¹¹, **C106**¹², **CYC-B1** and **CYC-B11**¹³, are representative examples of this new generation photosensitizers.

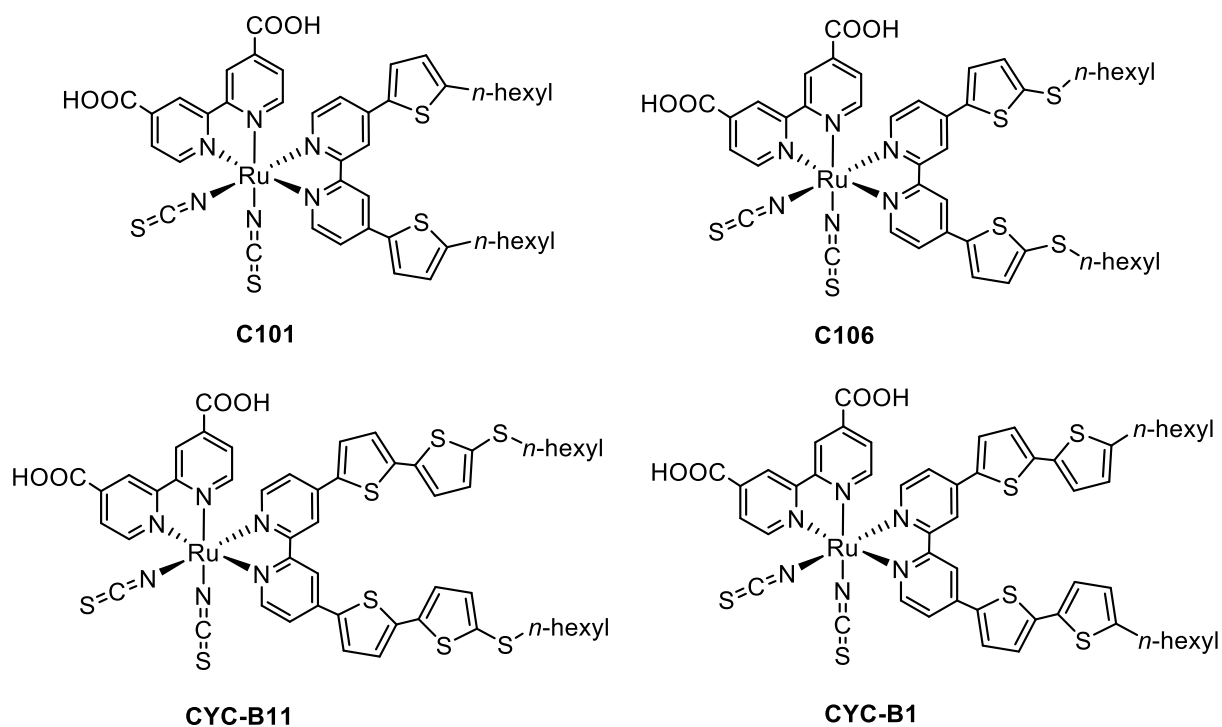


Figure 3.4 Molecular structure of **C101**, **C106**, **CYC-B11**, **CYC-B1**.

The MLCT transition absorptions of **C101** arise at ~ 407 and 547 nm, which are 23 nm red-shifted compared to that of **Z907** or its analogues¹¹. With the introduction of the alkyl-bis-thiophene moiety, **CYC-B1** has a strong new band centered at around 312 nm. The molar extinction coefficients of the low-energy MLCT absorption bands for **C101** is $17.5 \times 10^3 \text{ M}^{-1} \text{ cm}^{-1}$ and $21.2 \times 10^3 \text{ M}^{-1} \text{ cm}^{-1}$ for **CYC-B1**, which are significantly higher than the corresponding values for the standard **Z907**⁷ ($12.2 \times 10^3 \text{ M}^{-1} \text{ cm}^{-1}$), **N3**³ ($14.5 \times 10^3 \text{ M}^{-1} \text{ cm}^{-1}$) and **N719** ($14.2 \times 10^3 \text{ M}^{-1} \text{ cm}^{-1}$) sensitizers. The exceptional efficiency is 11% for **C101**¹¹ and 14% for **CYC-B1** proving that the thiophene moieties attached to the ancillary bipyridine ligand can enhance the light-harvesting capacity of these complexes by stepping up their molar absorptivity and red-shifting their spectral response, which leads to the improvement of the overall efficiency. Introducing a sulfur atom between the alkyl substituent and the thiophene ring might lead to an increase of the molar extinction coefficients and a shift of the absorption spectra to the NIR, as well as an enhanced electronic transition dipole momentum, yielding an increase in the absorption coefficient of the MLCT band. This is the case for **C106** compared to **C101**, and also for **CYC-B11** compared to **CYC-B1**. The ϵ values of **C106** and **CYC-B11**

increased by 19% and 14% respectively higher than the corresponding value of **C101** and **CYC-B1**. Promisingly, **CYC-B11** achieved a power conversion efficiency of 11.5%, 3% higher than that of **CYC-B1** and the cell η value of **C106** also augmented up to 11.4% compared to its analogue.

Thiocyanate (SCN) ligands have been employed as an electron-donating groups in the most efficient DSSCs since 1993³. However, many attempts have been made to prepare the thiocyanate-free Ru-based sensitizers on the grounds that the SCN groups are thought to be the weakest part of Ru complexes from a point of view of chemical stability. Replacement of the thiocyanate group with cyclometalated group was taken into consideration (Fig 3.5).

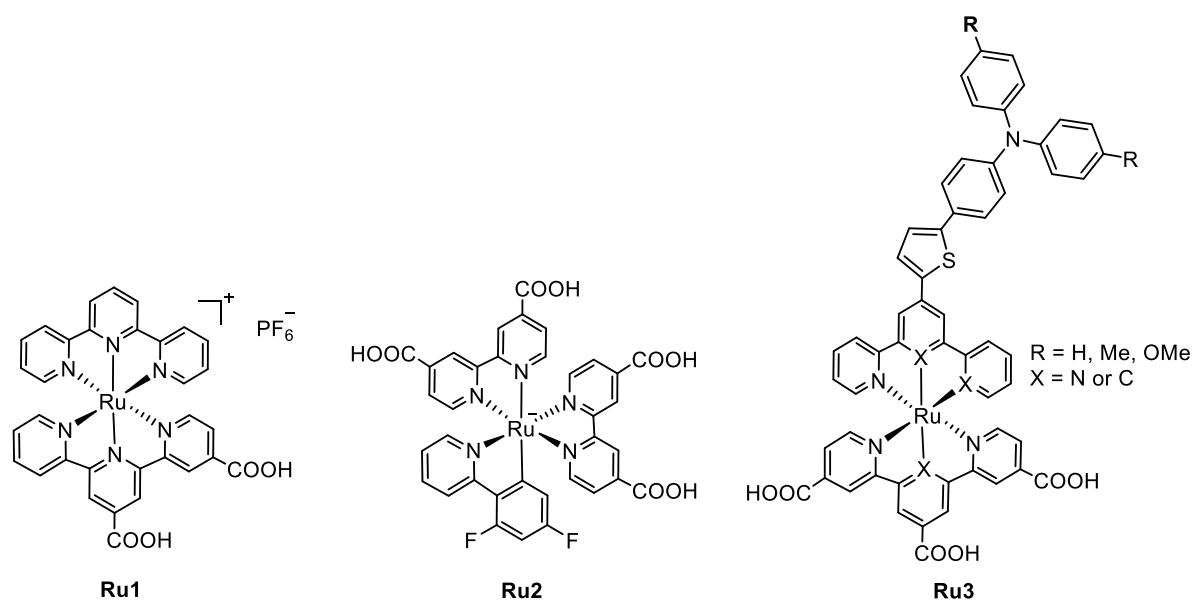


Figure 3.5 Molecular structure of **Ru1**, **Ru2**, **Ru3**.

Wadman *et al.* reported a new class of molecular sensitizers (**Ru1**), [Ru(C^{^N^N})-(N^{^N^N})] type, as a result of their broad and red-shifted visible absorption in comparison to the analogous [Ru(N^{^N^N})₂] type coordinative complexes¹⁴. Another example of thiocyanate-free Ru sensitizer was reported by Grätzel and coworkers in 2009, Bis(4,4'-dicarboxy-2,2'-bipyridine) 2-(2,4-Difluorophenyl)pyridine Ruthenium(II) (**Ru2**), it exhibited a remarkable IPCE value of 83% and gave rise to a device with 10.1% efficiency¹⁵. A series of asymmetrical bis-tridentate-cyclometalated Ru(II) complexes (**Ru3**) bearing terminal triphenylamine substituents was reported in 2011 by Robson and co-workers. The devices provided an efficiency of up to 8% using one of this class of complexes¹⁶.

2. Porphyrin based dyes

In spite of the high efficiencies provided by DSSCs based on Ru sensitizers, their applications are limited as Ru is an expensive and rare metal. Therefore, low cost and environmentally friendly sensitizers were investigated, in particular, the porphyrin-based sensitizers. The use of porphyrins in DSSCs presents several advantages, such as versatile modifications of the core, tunable redox potentials, appropriate LUMO and HOMO energy levels, very intense absorption bands. The nature of the frontier orbitals (i.e., HOMO and LUMO) in porphyrin macrocycles has been investigated in numerous studies. The absorption spectra of porphyrin derivatives show two characteristic π - π^* absorption regions, the weak Q band (transition to the first excited state (LUMO)) in the 550–700 nm range and the intense Soret band (transition to the second excited state (LUMO + 1)) in the 400–450 nm range (Fig 3.6)¹⁷. The porphyrins generally possess two a_{1u} and a_{2u} orbitals as the HOMO and HOMO-1¹⁸. The electron density in the a_{1u} type orbital is essentially localized on the C_α and C_β atoms of the pyrrole rings, while in the a_{2u} orbital it is mainly confined on the pyrrole nitrogens and on the meso-carbons. The LUMO levels are similar and two nearly degenerate $e_{2g}(\pi^*)$ orbitals are essentially centered on the porphyrin macrocycle.

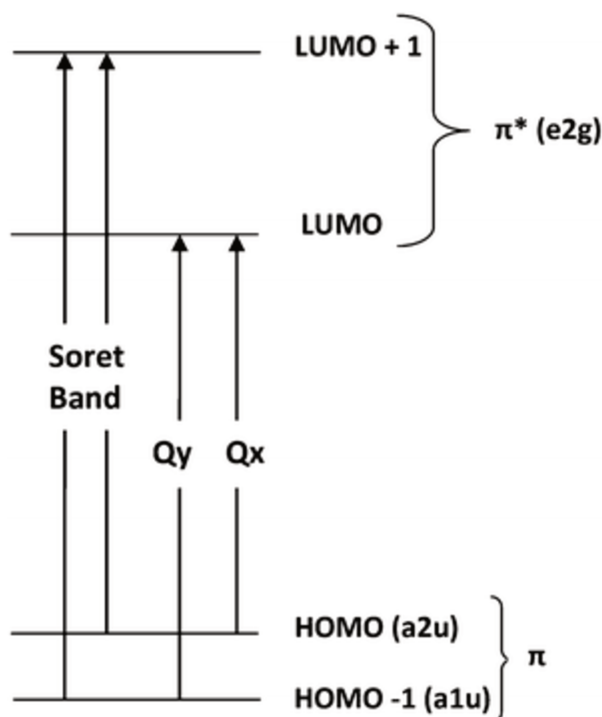


Figure 3.6 Schematic of π - π^* transitions responsible for the Soret and Q band of porphyrins

In 1993, A. Kay and M. Grätzel published their pioneering work on the design of a new copper meso porphyrin dye sensitizer, **mesoporphyrin IX** dye with an overall efficiency of 2.6%¹⁹. The IPCE value is 83% at Soret peak around 400 nm, which correspond to nearly unity quantum efficiency of charge separation when light reflection losses were taken into account. The authors also pointed out that the use of co-absorber, for example, cholanic acids was found to significantly prevent unfavorable dye aggregation.

In 2000, Durrant and co-workers compared different electron injection and charge recombination properties of dye **N3**, **TCPP** (tetrakis(4-carboxyphenyl)porphyrin) and **ZnTCPP** (tetrakis(4-carboxyphenyl) porphyrinato]zinc(II)) (Fig 3.7)²⁰. These three dyes were selected since they exhibit large differences in their oxidation potentials and photophysics, while retaining similar carboxylate groups for binding to the TiO₂ surface. It was found that the large differences mentioned above have rather little influence upon the interfacial electron transfer kinetics observed following adsorption of these dyes to the nanocrystalline TiO₂ films. The kinetics of electron injection into the TiO₂ conduction band are found to be ultrafast for all three sensitizer dyes, while similarly the recombination kinetics were only weakly sensitive to the identity of the sensitizer dye. The paper demonstrated that the kinetics of charge injection and recombination of porphyrin-based dyes are very similar to those of Ru polypyridyl complexes, paving the way for the design and study of various numerous porphyrin-based molecules as sensitizers for DSSC.

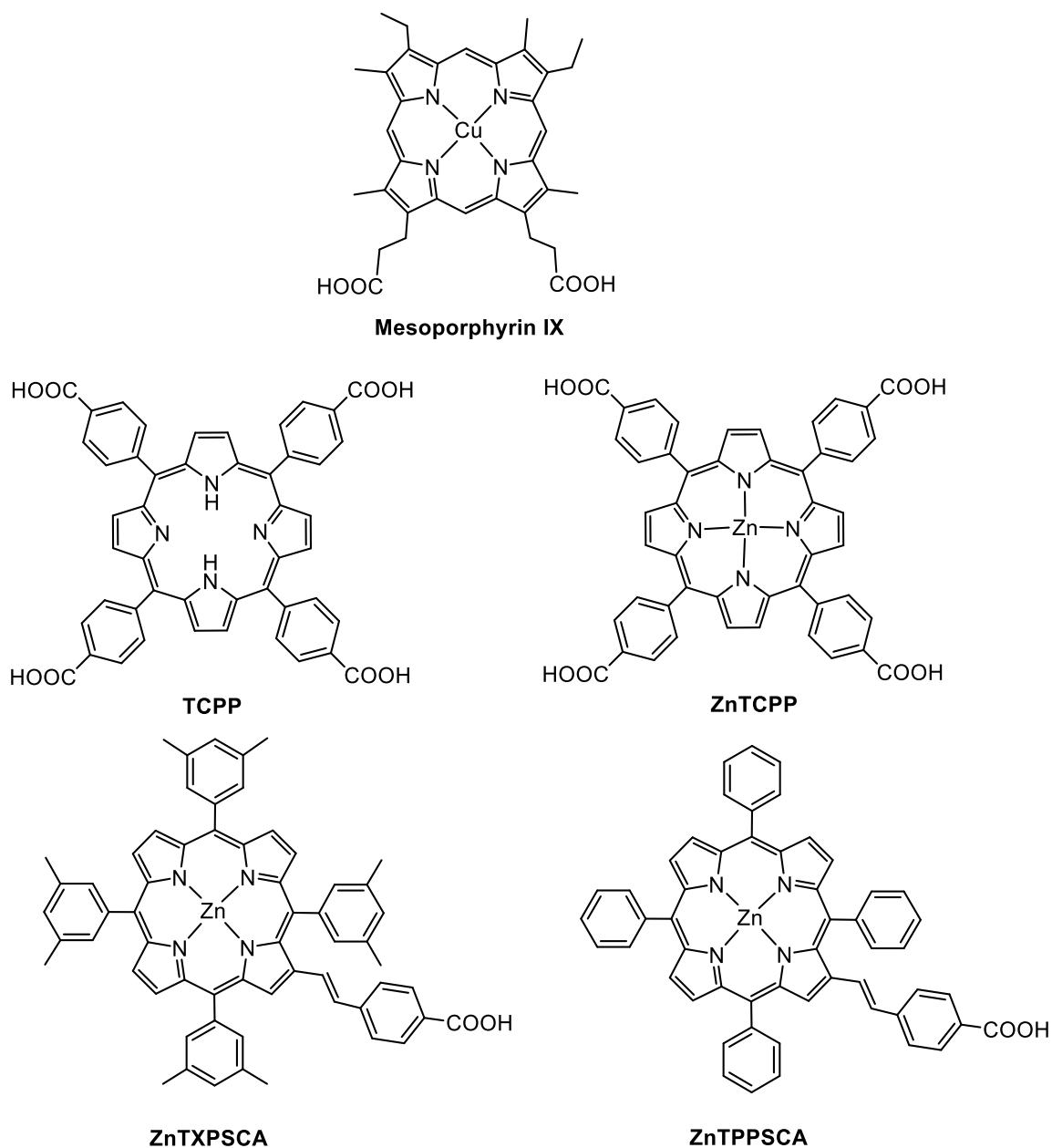


Figure 3.7 Molecular structure of **Mesoporphyrin IX**, **TCPP**, **ZnTCPP**, **ZnTXPSCA**, **ZnTPPSCA**.

In 2004, a series of porphyrin dyes with different central metal ions (Cu(II) or Zn(II)) and different anchoring groups (-COOH or -PO₃H₂) was reported by Nazeeruddin *et al.*²¹. The study demonstrated that Zn containing diamagnetic porphyrin sensitizers showed much higher IPCE values than those observed for the Cu containing paramagnetic metalloporphyrins for porphyrin sensitizers with carboxylic anchoring groups. In addition, the devices based on a carboxylate anchoring group showed higher efficiencies than those with a phosphonic acid. **ZnTXPSCA** has the highest conversion efficiency of 4.8%.

A possible strategy to enhance the performances of porphyrins-based sensitizers proposed at the same time is to functionalize the porphyrin macrocycle at the meso- and β - positions. In 2004, Jolley and co-workers published another variety of β -carboxylic substituted porphyrin monomers and multi-porphyrin arrays to evaluate their performance in the dye-sensitized TiO₂ solar cell²². A β -substituted monoporphyrin carboxylic acid derivative with a conjugated linker, 4-*trans*-2'-(2''-(5'',10'',15'',20''-tetraphenylporphyrinato zinc(II))yl)ethen-1'-yl)-1-benzoic acid (named as **ZnTPPSCA**, Fig 3.7) showed significant advantage over any antenna-type of multi-porphyrin arrays giving IPCE_{max} = 80% and an overall efficiency of 4.2%. It should be mentioned that the dye **ZnTXPSCA** (4.8%) with xylyl group has a higher conversion efficiency than that of **ZnTPPSCA** (4.1%) with phenyl group proving again that preventing aggregation help improve the efficiency of the devices.

In 2005, a series of novel zinc metalloporphyrins was published by Grätzel and co-workers demonstrating that the performance of porphyrin-based cells can be greatly improved by choosing the right linker and binding group²³. The dye cyano-3-(2'-(5',10',15',20'-tetraphenylporphyrinato zinc(II))yl)-acrylic acid coded as **Zn-3**, a combination of a conjugated ethenyl or diethenyl linker in the β -pyrrolic position and a carboxylate binding group that gives cell efficiencies of up to 5.2%. Density functional theory (DFT) and time-dependent DFT (TDDFT) calculations revealed that the LUMOs (key molecular orbitals) of **Zn-3** was stabilized and extended out onto the substituent through π -conjugation, causing enhancement and red shift of visible transitions and increasing the possibility of electron transfer from the substituent. Later, Officer *et al.* reported synthesis, electronic, and photovoltaic properties of novel green porphyrin sensitizers, the efficiency of which are all over 5%.²⁴ The malonic acid was used as anchoring group and the peripheral functional groups were modified from phenyl to methylphenyl, ethylphenyl, butylphenyl, octylphenyl and dimethylphenyl groups. The sensitizers **DYE 2** with the 4-methylphenyl groups gave the best cell efficiency of 7.1%. Besides the choice of anchoring group, the study conducted by Bignozzi and co-workers indicated that the substitution position of anchoring groups influences IPCE, thus the overall efficiency of the devices as well.

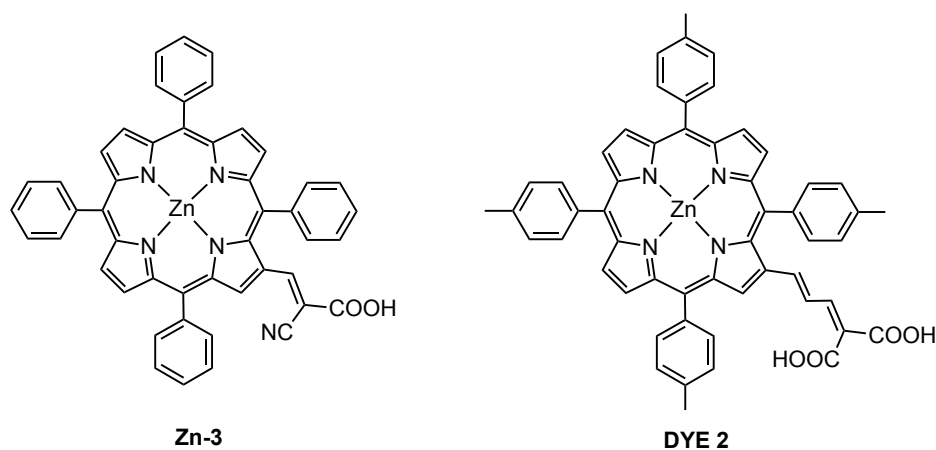


Figure 3.8 Molecular structure of **Zn-3** and **DYE 2**.

A series of acene-modified zinc porphyrins (benzene to pentacene, Fig 3.9) was prepared by C.-Y. Lin *et al.* to study the effect of introducing additional π -chromophore into the molecular backbone²⁵. It was demonstrated that porphyrin absorption spectra can be significantly affected by including acenes into the π -conjugation system. The broadening of the absorption bands by anthracene led to an effective minimization of the gap between B and Q bands of **LAC-3** giving the highest efficiency of 5.4%. The poor performance of **LAC-5** was due to the inefficient electron injection from **LAC-5** to TiO_2 resulting from rapid non-radiative relaxation of the molecule in the singlet excited state. As a continuous effort, the same group reported several new zinc porphyrin sensitizers modified by a series of cyclic aromatic hydrocarbon substituents on meso position, such as phenylethynyl, naphthalenylethynyl, anthracenylethynyl, phenanthrenylethynyl or pyrenylethynyl²⁶. A device based on pyrene-bearing zinc porphyrin, coded as **LD4** showed an improved photovoltaic performance, giving an overall efficiency of 10.1% due to the enhanced light harvesting ability broadly covering the entire visible region.

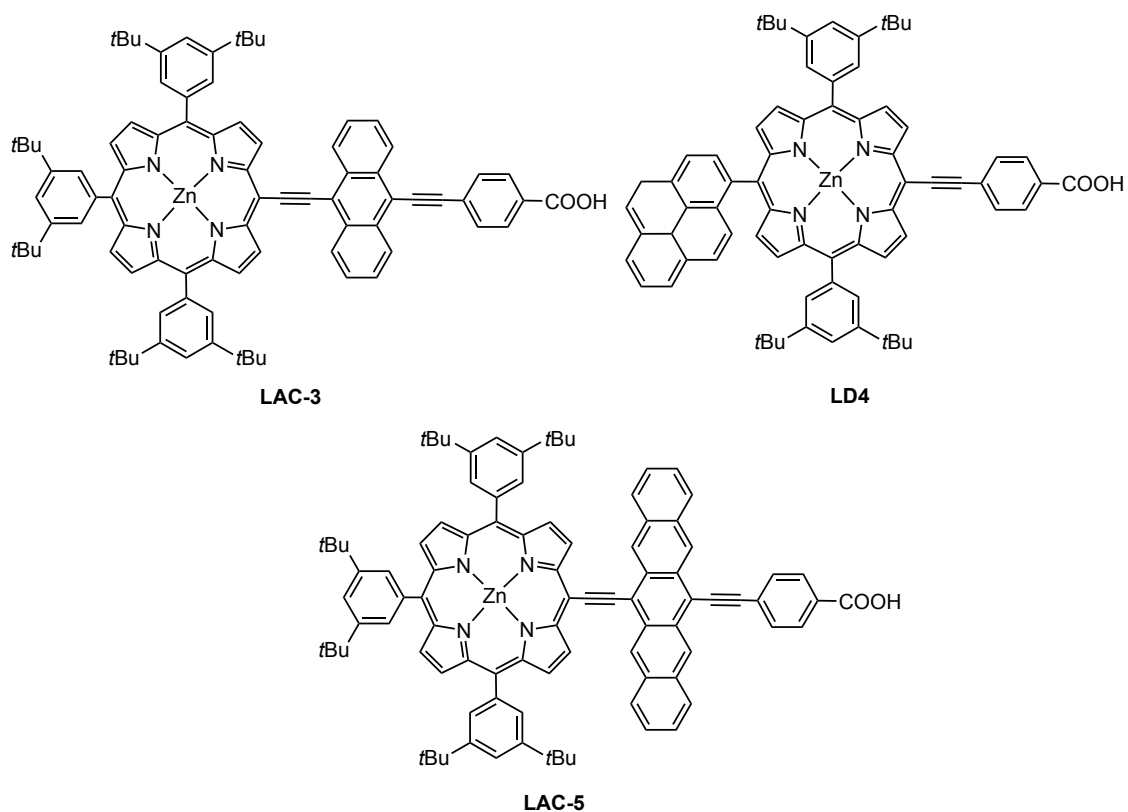


Figure 3.9 Molecular structure of **LAC-3**, **LD4**, **LAC-5**.

As the modification of the *meso*-position of porphyrin was proved to be an effective approach to improve the efficiency of DSSCs, Imahori and co-workers synthesized new porphyrin dyes with different π systems of 5-membered heteroaromatic rings, such as thienyl and furyl to evaluate the effect of spacers on the photovoltaic properties of the solar cells²⁷. Modifications including altering heteroelement of the bridge, in this case sulfur vs oxygen or switching the position of the anchoring group, 4- vs 5- position were found to have important effects on the dye adsorption behavior and saturated coverage on the TiO₂ surface. Particularly, dye **Zn-5S** (Fig 3.10) showed the highest IPCE of 65% and the highest efficiency of 3.1% due to the additional electron-transfer pathway through specific interaction between the sulfur atom inherent in the bridge and the TiO₂ surface. Continuously, they further developed two series of π -elongated dyes, naphthyl-fused porphyrins²⁸ and quinoxaline-fused porphyrins²⁹, which improved efficiencies to 5%.

In 2009, Tan and co-workers reported a novel series of thiophene-linked porphyrin derivatives with D- π -A structure, as the porphyrin plays the role of donor and cyanoacrylic acid acted as acceptor and anchoring group³⁰. In order to reduce aggregation between neighboring porphyrins on the TiO₂ surface by sterically hindering the porphyrin core, three methylphenyl

groups are introduced. The thiophene units were found capable to improve the light-harvesting property of porphyrin dyes, however the length of thiophene as well as the alkyl chain should be controlled because of their influence on electron transport efficiency. The device based on **P_{Zn}-hT** obtained a maximum power conversion efficiency of 5.1% and a maximum IPCE value of 72%.

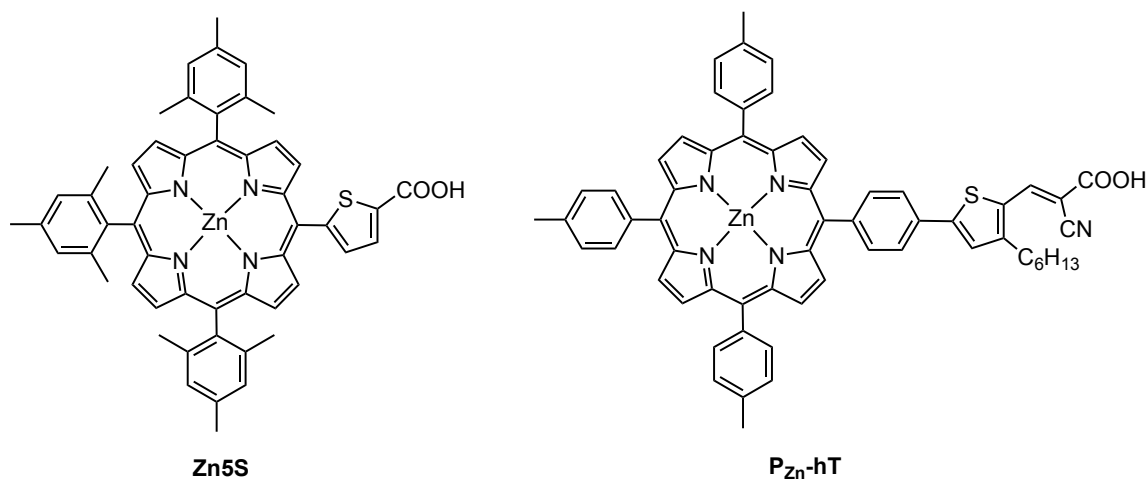


Figure 3.10 Molecular structure of **Zn5S** and **P_{Zn}-hT**.

A milestone in the field of porphyrin sensitizers for DSSCs is the concept of push-pull porphyrins. The macrocycle serves as π -spacer between an electron donor group and an electron acceptor group, which is beneficial to extend optical absorption and to harvest a larger fraction of solar photons. The Diao's group has done a lot of work on the development of push-pull porphyrins to further optimize the efficiency of the DSSC devices.³¹ An efficiency of 10.2% was obtained by one of the porphyrin sensitizers they designed in 201 coded as **LD14** (Fig 3.11), which possesses two phenyl groups at *meso*-positions of the macrocycle bearing two ortho-substituted long alkoxy chains. The authors believed that the functionalization the ortho position with long alkoxy-chains (four dodecoxyl chains of **LD14**) play a key role in wrapping the porphyrin core that prevents dye aggregation effectively and forms a blocking layer on the TiO₂ surface, as well as in delaying charge recombination in the electrolyte/TiO₂ interface.

A promising strategy to optimize the push-pull porphyrin dyes is the usage of diarylamino groups as strong electron donating units. In 2009, a series of Zn porphyrins sensitizers with an electron-donating diarylamino group attached at the meso position of the porphyrin ring phenylethynyl carboxyl anchoring group which also acts as acceptor to study the effect of diarylamino groups on dye aggregation and electron injection³². Compared to similar systems

without diarylamino groups, it was found that the diarylamino group can not only extend the absorption spectrally but also push the excited electrons spatially toward the TiO₂ film for an improved charge separation. An efficiency of 6.8% was achieved for the devices sensitized with **YD2** (Fig 3.11). Later, Grätzel and co-workers published an unprecedented efficiency of 11% using **YD2** as a result of device optimization³³. The introduction of various diarylamino groups in the porphyrin was also investigated by Imahori group to evaluate the effects of substituent number and position of the diarylamino groups on the optical, electrochemical, and photovoltaic properties of the porphyrins. The light harvesting properties were improved in the visible region by increasing the number of the diarylamino groups: the Soret band widens and slightly blue-shifts, while a new band appears at 450–500 nm and the Q band shifts toward longer wavelengths³⁴. The sensitizer **ZnPBAT** with ameliorated molecular structure exhibited an overall efficiency of 10% validating the author's idea that the molecular design concept based on the push–pull enhancement by the asymmetric substitution will be useful for further improving cell performance in DSSCs. One year later, Yeh and co-workers prepared several new novel porphyrin-based dyes by functionalizing the meso or β position by a carboxylic acid with different expanded π -system. The authors summarized three important points. Firstly, the introduction of tert-butyl groups onto phenyl rings help suppress the formation of dye aggregates on the TiO₂ surface. Secondly, the extension of π conjugation of the porphyrin ring led to broadening and red-shift the Soret and Q bands, and thus improved light-harvesting effect. Lastly, the introduction of an electron-donating group in the *meso*-position of the porphyrin ring could enhance the charge-separation capability. The device based on a diarylamino-substituted porphyrin sensitizer **DYE 5** exhibited an overall efficiency of 6%, the first sensitizer with a performance comparable to that of an N3-based DSSC³⁵.

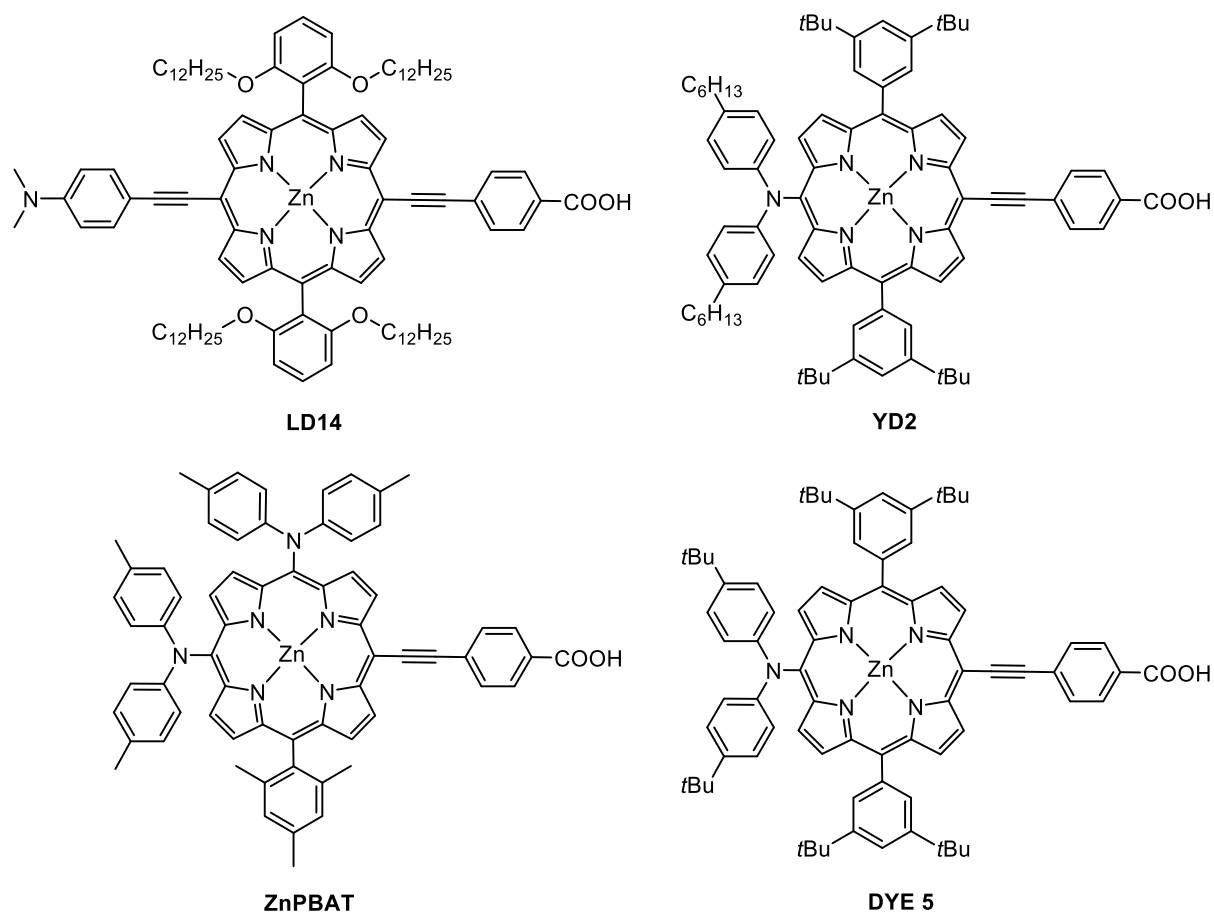


Figure 3.11 Molecular structure of **LD14**, **YD2**, **ZnPBAT**, **DYE 5**.

Despite high efficiencies of devices based on typical porphyrin D- π -A sensitizers comprising dialkylamine or diarylamine donors in conjunction with an ethynylbenzoic acid acceptor, the use of strong acceptor to further improve the performances of devices was barely investigated. In 2011, a dye (coded as **YD2-o-C8**, Fig 3.12) that combines many of previously studied concepts such as the functionalization with long alkoxy chain to prevent the aggregation of dyes, the design push-pull system by using diarylamino group was proposed by Yella *et al.*³⁶. Furthermore, energy losses between the energy of the dye HOMO and the electrolyte redox potential were minimized while maximizing the V_{OC} (0.965 V) by replacing the conventional redox couple I/I_3^- with $Co^{II/III}$ tris(bipyridyl) complex. A remarkable efficiency of 11.9% was obtained. In 2014, an impressive efficiency of 12.75% was achieved by a new porphyrin sensitizer named as **SM315** (Fig 3.12),³⁷ of which the structure is similar to **YD2-o-C8**, but with a benzothiadiazole (BTD) moiety incorporated as acceptor, also as part of the π -conjugated linker. Compared to the molecule without BTD, **SM315**'s Soret and A-Q-band absorbance has significantly broadened, increasing the light harvesting between 500-600 nm and up to 800 nm. The enhancement in light harvesting consequently resulted in an improved

J_{SC} ($18.1 \text{ mA}\cdot\text{cm}^{-2}$) an equivalent V_{OC} (0.91 V) in comparison with **YD2-o-C8**. A slight structural modification of **SM315**, by introduction of a phenyl group between the BTD and the carboxylic acid function, led to **GY50**, which afforded an efficiency of 13%³⁸.

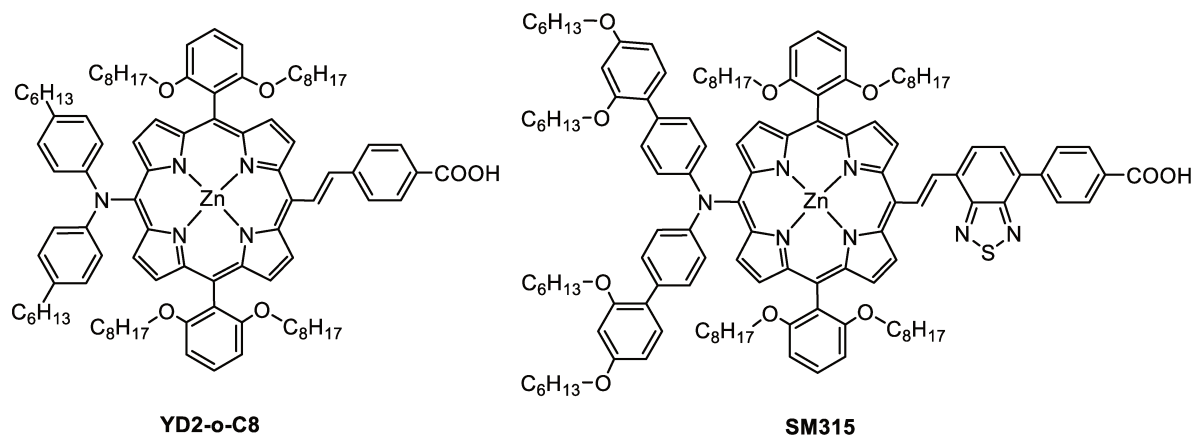


Figure 3.12 Molecular structure of **YD2-o-C8**, **SM 315**.

3. Metal-free sensitizers

Fully organic dyes are good alternative candidates as an alternative to the metal complexes, sensitizers since they exhibit many advantages: vast application potential due to possible large-scale production as a result of their low synthetic and purification cost; excellent extinction coefficients, usually one order of magnitude higher than those of metal complexes, making them an interesting option for thin film and solid-state DSSCs in combination with hole-transporting materials such as poly(3-hexylthiophene-2,5-diyl) (P3HT) or 2,2',7,7'-tetrakis(*N,N*-di-*p*-methoxyphenylamino)-9,9'-spirofluorene (spiro-MeOTAD)³⁹; tunable absorption spectra and energy levels are tunable via molecular structure tailing and basically without limitation of resources; their diverse molecular structures.

A number of organic dye sensitizers have so far been developed, and the relationship between their chemical structures and photovoltaic performances in DSSC has been examined. The prototypical structure of a metal-free sensitizer is generally constituted by Donor (D), π -bridge (π) and Acceptor (A) moieties, so-called D- π -A push-pull structure (Fig 3.13). This push-pull structure can induce an intramolecular charge transfer (ICT) from D to A through the π -bridge after the dye absorbs the incident light. Therefore, the push-pull structure should promote the charge transfer at the excited state through the π -bridge in order to favor the charge separation before electron injection into the semi-conductor. Considering the molecular orbitals, it is

generally observed that HOMO orbital is mainly localized in the donor part while the LUMO is mainly localized in the acceptor part.

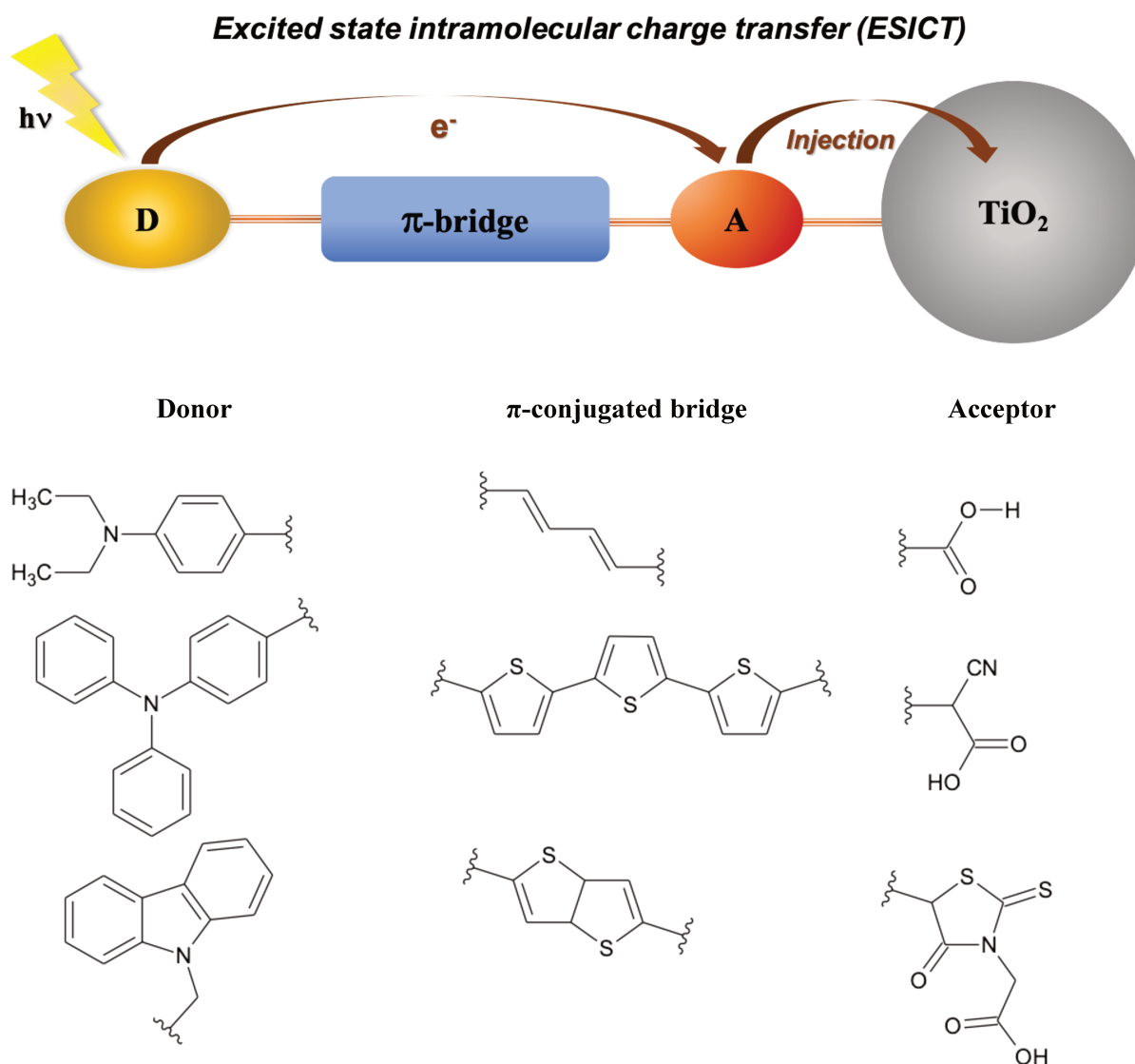


Figure 3.13 Design of organic sensitizers (top) and examples of building blocks (down)

After photoexcitation, a shift of electron density occurs subsequently from the donor part of the molecule toward the acceptor part. The sensitizer is connected to the TiO_2 surface thanks to the anchoring group, aiding the process of electron injection into the CB of TiO_2 . Numerous choices of sensitizers are available for various combinations. For instance, moieties like coumarin, indoline, and triarylamine (TAA) can act as an electron donor (D), while carboxylic acid, cyanoacrylic acid and rhodanine units can serve as electron acceptor (A), with polyene or oligothiophene as π spacers. Therefore, many D- π -A metal-free dyes with various donor moieties, such as coumarin^{40,41}, indoline⁴², phenothiazine⁴³, carbazole⁴⁴, and pyrrole⁴⁵, have been designed and used as efficient sensitizers for DSSC applications. The photon-to-current

conversion efficiency based on those sensitizers has achieved up to 10%. Herein, some representative metal-free sensitizers containing different electron donating group are briefly introduced, for example coumarin, and particularly triarylamine.

3.1. Coumarin

In 1996, a coumarin-based dye was firstly studied by Grätzel *et al.* to investigate the charge injection dynamics from the surface-bound dye to the conduction band of TiO₂. Although charge injection from the **C343** dye (Fig 3.14) to the CB of the TiO₂ occurs on a time scale of *ca.* 200 fs was demonstrated by ultrafast fluorescence dynamics due to strong electronic coupling between the dye and TiO₂ energy levels, lack of absorption in the visible region led to a lower conversion efficiency of the device. The Arakawa group made many efforts for the development of coumarin dyes. The absorption peak of **NKX-2398** is slightly red-shifted compared to that of **C343** as a methine unit and carboxyl group were introduced on the coumarin framework.

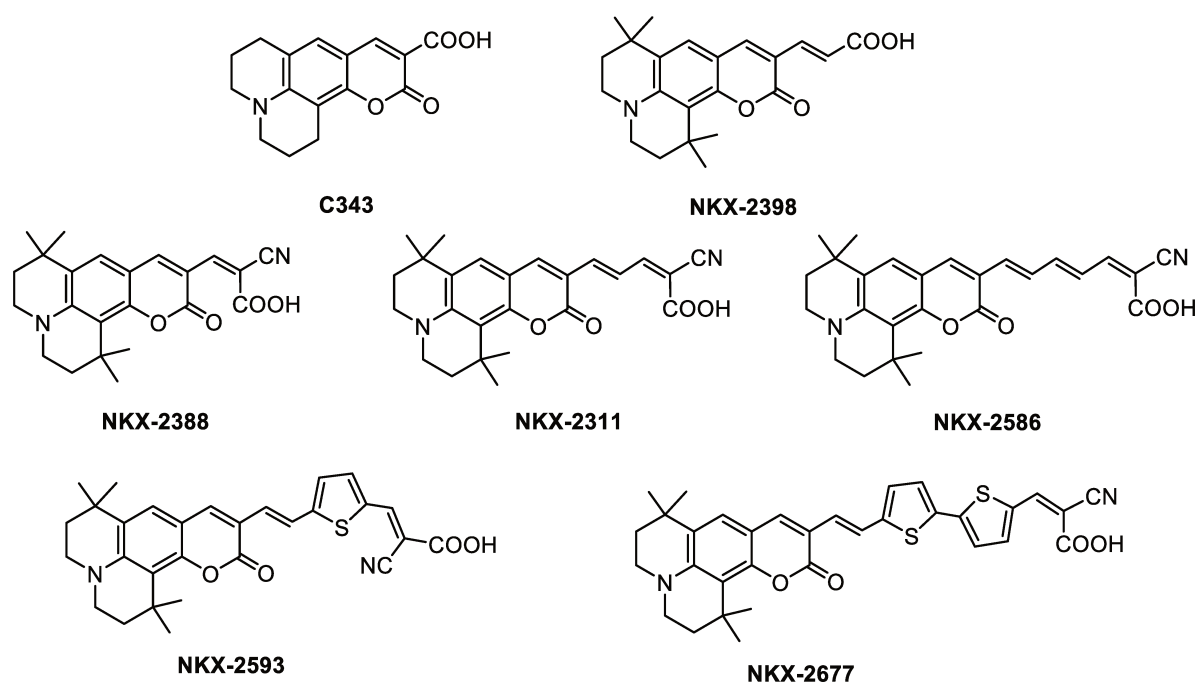


Figure 3.14 Molecular structure of **C343**, **NKX-2398**, **NKX-2388**, **NKX-2311**, **NKX-2586**, **NKX-2593**, **NKX-2677**.

A further redshift was observed by **NKX-2388** owing to the addition of a cyano (CN) group on **NKX-2398** on the grounds that the structure of a cyano group connected to the methine chain and the carboxyl group might be effective for electron injection due to its strong electron

acceptability. **NKX-2388**, **NKX-2311**, **NKX-2586** were synthesized to understand the effect of introducing vinylene units. **NKX-2311** gave the highest efficiency of 6% since the carboxyl group directly connected to the $-\text{CH}=\text{CH}-$ unit is advantageous for effective electron injection from the dye into the conduction band of TiO_2 . However, further increase in the number of vinylene units was found unfavorable for the performance of devices due to increase dye aggregation, and increased instability of the dye molecule because of the possibility of isomer formation, indicating that an optimal length was essential to improve the efficiency.

In addition, it would necessity the more complicated synthetic procedure through the introduction of π -conjugated ring moieties to expand π -conjugation and to improve the stability of dye molecule, for example a thiophene to provide **NKX-2677**. A η -value of 7.7% was achieved, confirming that thiophene moieties attributed to the broadening of absorption spectrum.

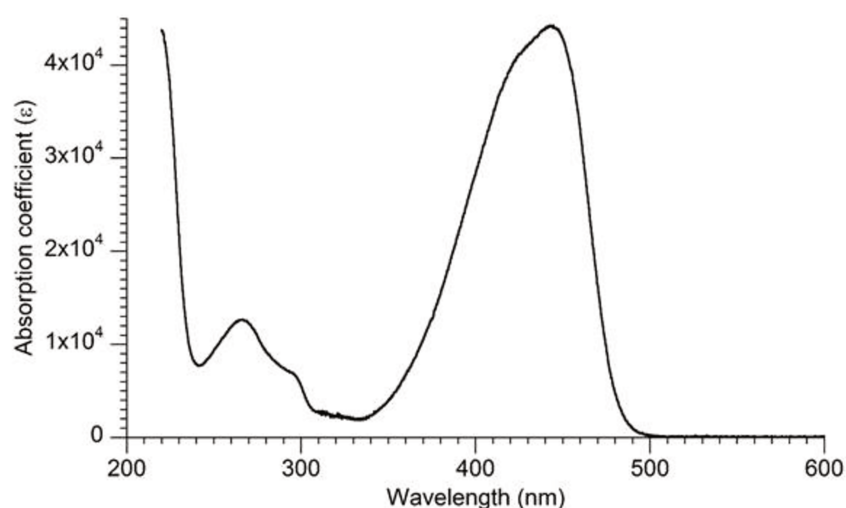


Figure 3.15 Absorption spectrum of C343 in ethanol from <http://www.photochemcad.com>

3.2. Triarylamine-based dyes

Since their first use as sensitizer in solar cells, triarylamine (TAA)-based dyes continue to stimulate a lot of research as demonstrated by the number of publications and citations containing this type of molecules in the title of articles (see Figure 3.16 below). The number of publications dealing with TAA-based dyes is growing exponentially for the last two decades. Encouraged with this particularly active field, we aim at developing TAA based dye for solid state dye solar cells (DSSCs).

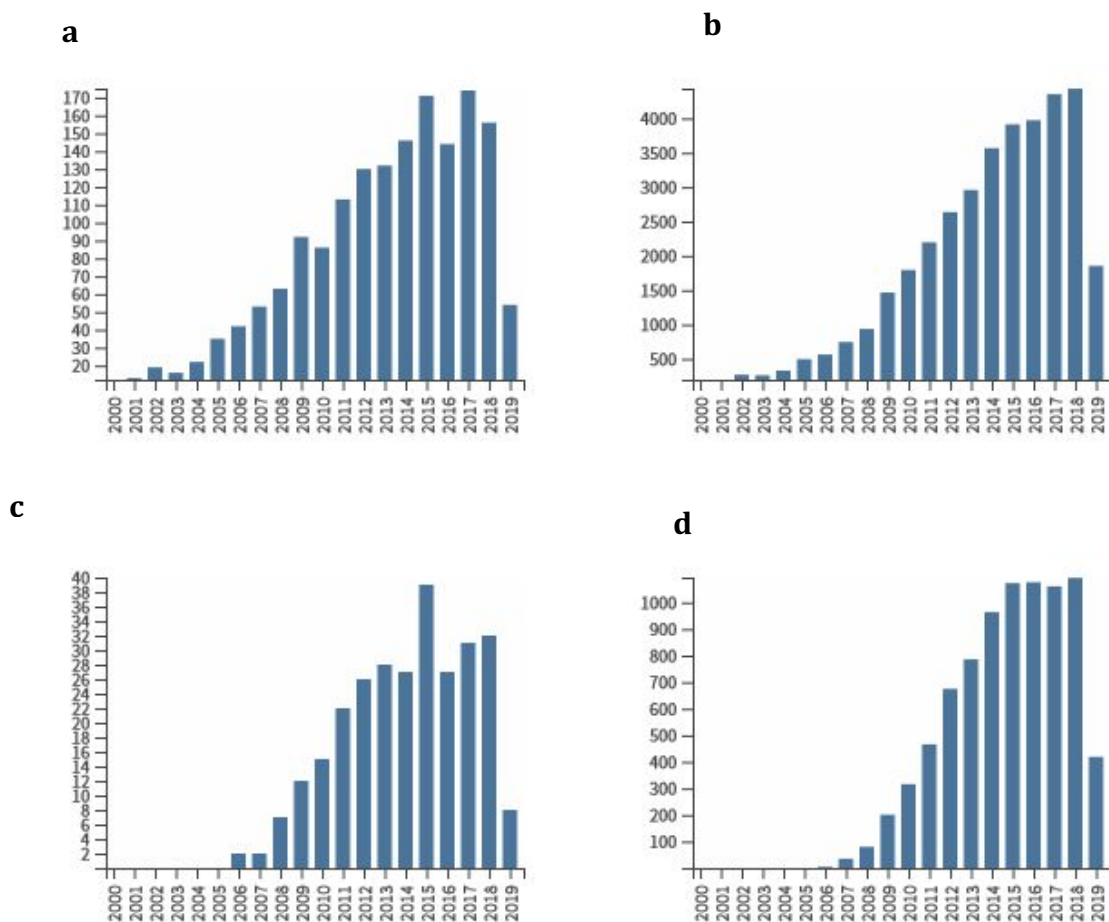


Figure 3.16 Number of publications containing in the title the word triphenylamine (a) the words triphenylamine and solar cells (c). Total of citations for papers containing in the title the word triphenylamine (b) the words triphenylamine and solar cells (d).

Among TAAs, the triphenylamine (TPA) has been widely used as an electron donor in the sensitizer since it offers a number of competitive advantages: the prominent electron donating ability, excellent hole transport capability which could be argued that TPA can form a stable radical cation after oxidation. Furthermore, TPA could locate and separate the cationic charge from TiO_2 surface leading to effective restriction of the recombination process between the injected electrons in TiO_2 and the excited dye (back electron transfer), thus achieving higher rates of charge separation and collection. Another important factor is its propeller starburst molecular structure with a non-planar configuration. As shown in the Figure 3.17 below the three benzene rings of the triphenylamine group are mutually twisted, and the triphenylamine and π -conjugated groups also have certain distortion angles. The non-planar structure of the

dye molecule effectively prevents intermolecular π - π aggregation, which is beneficial since the aggregation would cause electron transfer between the molecules leading to loss of energy and therefore affects the PCE of DSSCs⁴⁶⁻⁵⁴. Generally, the molecular structures of TAA-based sensitizers are in the form of donor- π bridge-acceptor and each section can be optimized to improve the device performance.

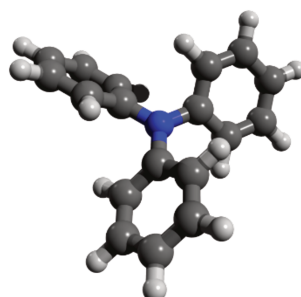


Figure 3.17 Tridimensional geometry of the triphenylamine unit

In 2004, Yanagida and co-workers published a series of novel oligoene dyes with different lengths of methine units, cyano groups and/or carboxylic groups as the electron acceptor units, and amino groups as the electron donor units, which are firstly TAP-based organic dyes applied in DSSCs. The most basic dye **e1** (Fig 3.20) exhibited a promising PCE value of 3.3%⁵⁵.

One option is to modify the TAA core by introducing electron-donating groups such as alkoxy substituents. The increase of electron donating ability of TPA results in up shift of the HOMO energy levels while slightly affects the LUMO, thus lower bandgap and better light harvesting capacity of the dye will have. Additionally, the long chain can form aliphatic network preventing the adverse charge combination between photo-injected electrons and electrolyte with longer distance between TiO_2 surface and the electrolyte. Compared with dye **e5**, dye **f1** with hexyloxy chains showed significantly red shifted absorption maximums (415 nm vs. 506 nm) and higher PCE (4.1 % vs. 5.8%) validating beneficial hypothesis of introduction of alkoxy groups on the TAA core^{56,57}.

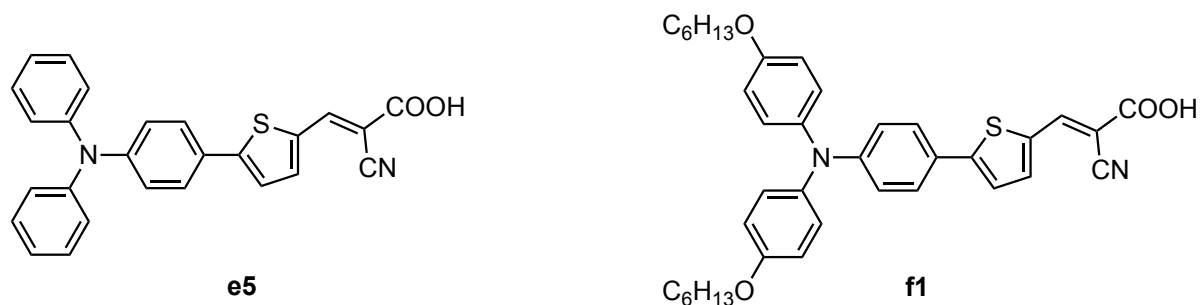


Figure 3.18 Molecular structure of **e5**, **f1**.

Li and co-workers also found that introduction of a $\text{CH}_2=\text{CH}$ - group into the TPA unit exhibited better photovoltaic performance by comparing the performance of DSSCs based on **TPAR4** (5.84%) and **TPAR1** (4.32%), due to the increase of the electron-density donor moiety (Fig 3.19)⁵⁸.

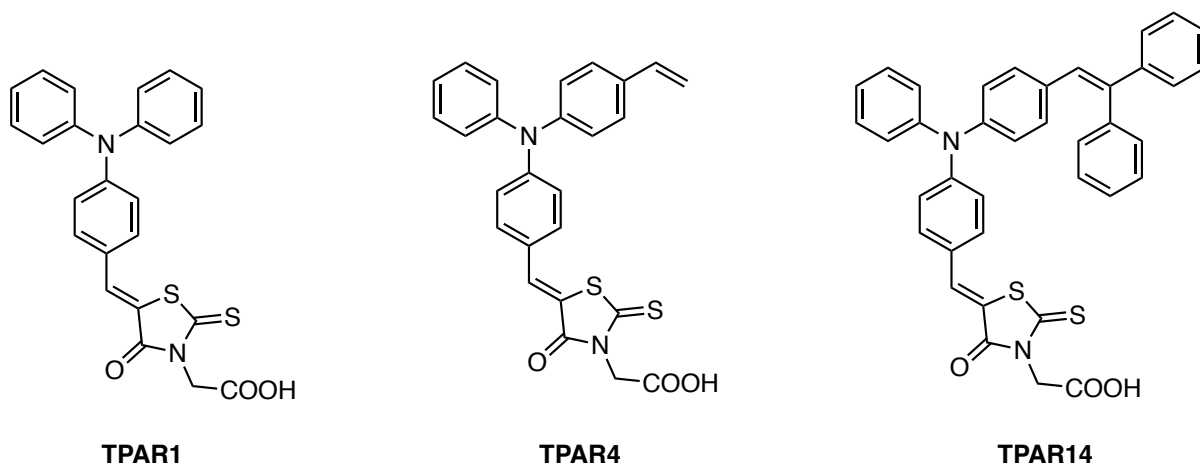


Figure 3.19 Molecular structure of **TPAR1**, **TPAR4**, **TPAR14**.

It has been shown that a bathochromic shift and broadening of the absorption range as well as enhanced absorptivity and high thermal stability can be obtained by incorporating additional electron rich units to form D-D- π -A configurations⁵⁹ Moreover, the introduction of the secondary electron transfer function is a possible alternative to retard the interfacial charge-recombination dynamics and to retain efficient light-induced charge separation, as demonstrated by the improved performance of DSSCs based on **TPAR14** (6.27%, Fig 3.19) than that of **TPAR1** (4.32%)⁶⁰.

Adjustments can also be performed in the π bridge part including extension and substitution of the π spacer (Fig 3.20). The expansion of the π -conjugation between donor and acceptor moieties can contribute to the improvement of PCE. Indeed, the intramolecular charge transfer is strongly dependent on the ability of density of charge to be shifted from the donor to the

acceptor group. This property can be greatly induced by conjugation that allows a large delocalization of the charge. A better conjugation leads consequently to a bathochromic shift of the maximum absorption as well as an increase in the J_{SC} which is related to the electron injection efficiency and to the light harvesting efficiency. Following this idea, great effort was dedicated to enlarging the effective conjugation of the dye. In comparison with **e1** (386 nm)⁵⁵, **e5**⁶¹ (415 nm) and **e6** (473 nm)⁶² with thiophene and bithiophene showed significantly red-shifted absorption maximums, and both dyes exhibited also better overall efficiencies with IPCE values of 4.1% and 6.2%, respectively. Triple bond-, 3,4-ethylenedioxythiophene-, benzotriazole-, cyclopentadithiophen-based sensitizers were also studied.

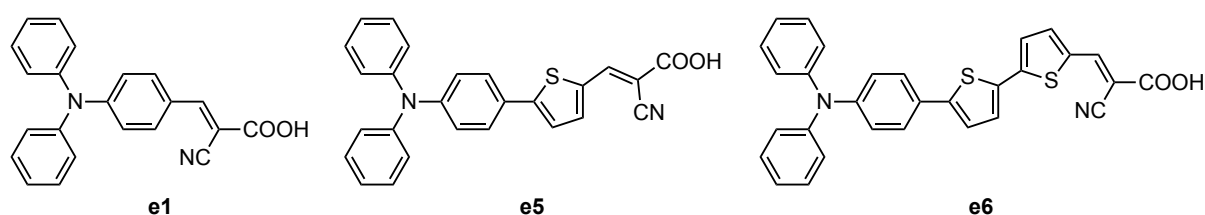


Figure 3.20 Molecular structure of **e1**, **e5**, **e6**.

Substituent effect on the π -linkers in triphenylamine sensitizers have been investigated. Significant differences in the redox potential in these dyes resulted from small structure changes are observed (Fig 3.21). Although bathochromic shift of absorption spectra was obtained, the decreasing molar extinction coefficients (ϵ) of the dyes with substitutes on the phenylene subunit could cause the dissatisfactory light harvesting efficiency, which leads to lower photocurrent. Furthermore, the electron-withdrawing substitutes on the phenylene subunit may be the barrier of the electron injection into TiO_2 CB and thus show a lower η value. **TPC1** showed the highest solar-to-electricity conversion efficiency (5.33%). Therefore, the substituted phenylene with electron-withdrawing units in dyes affords a negative effect on the DSSCs performances. In contrast, the PCE was improved by 0.5% when an electron-donating group, the methoxy group was introduced, as reported by Kim and co-workers.

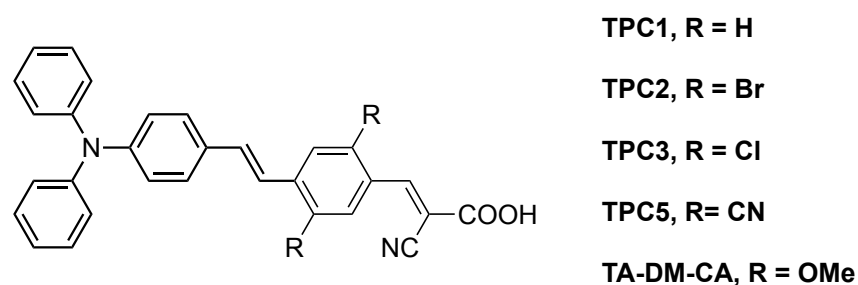


Figure 3.21 Molecular structure of **TPC1**, **TPC2**, **TPC3**, **TPC5**, **TA-DM-CA**.

For the purpose of restricting the recombination between the injected electrons in TiO_2 and cations in the electrolyte, a series of sensitizers were published in 2015 by Lin and co-workers including **NPT2** and **NPT5** (Fig 3.22)⁶³. **NPT5** exhibited an exceptional efficiency of 7.9% better than that of **NPT2**, mainly for two reasons. **NPT5** has broader and longer wavelength absorptions and the most effective dark-current suppression. Obviously, the incorporation of the hexyl substituent on the thiophene ring is beneficial to dark-current suppression.

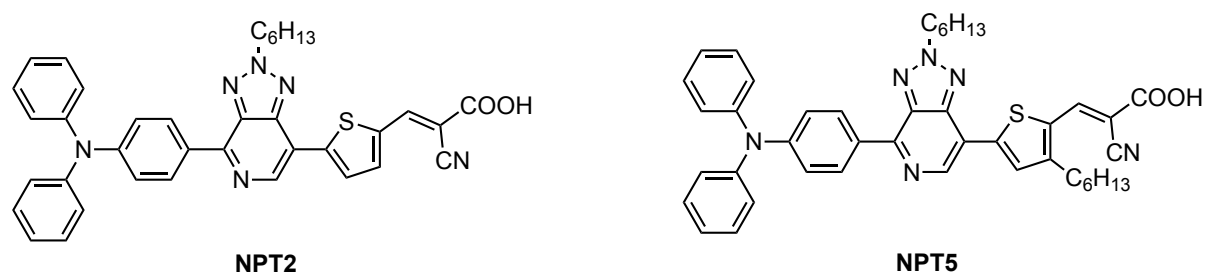


Figure 3.22 Molecular structure of **NPT2**, **NPT5**.

Although it is particularly interesting to increase the π -conjugation which shifts the maximum absorption and thus increases the J_{SC} , there is not a clear relationship between these two parameters. A large study conducted on more than 100 TPA dyes reveals that the dyes showing a redshifted maximum absorption are interesting to obtain high J_{SC} , but the relationship is far to be linear (Fig 3.23)⁶⁴.

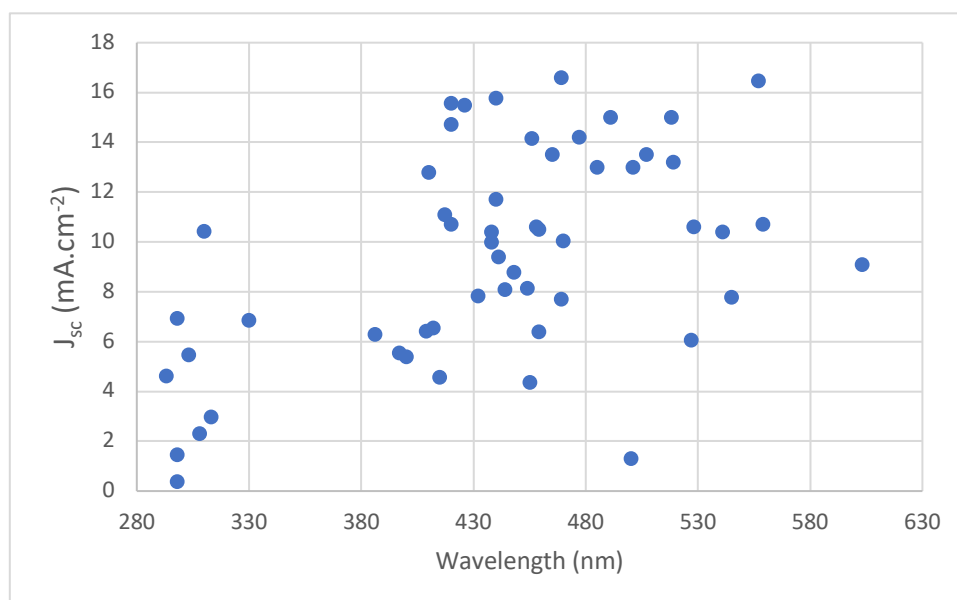


Figure 3.23 Non-correlation between J_{sc} and the maximum absorption wavelength for several TPA-based dyes.

In the interest of the injection of electrons from the dye into the conduction band of the metal oxide, it is crucial to immobilize the dye molecules on to the surface of semiconducting metal

oxide nanoparticle, which is usually achieved by an anchoring group. There are several mechanisms to assemble the dyes onto a metal oxide substrate surface, such as covalent attachment, electrostatic interaction, hydrogen bonding, hydrophobic interaction, van der Waals forces, or physical entrapment. Covalent bonding has been employed in an exclusive way for DSSCs to ensure strong coupling and stability. Other interactions involve weaker bonds which render adsorption quasi-reversible thus unstable. Zhang and Cole published a review on the anchoring groups for DSSCs⁶⁵, including pyridine, dicarboxylic acid anhydride, 2-hydroxybenzotrile, 8-hydroxyquinoline, pyridine-*N*-oxide, hydroxypyridium, catechol, hydroxamate, sulfonic acid, acetylacetate, boronic acid, nitro, tetrazole, rhodanine, and salicylic acid substituents. Additionally, these anchoring groups act as electron acceptors as well, therefore the LUMO is essentially located in anchoring groups. Cyanoacrylic acid is applied in most organic D- π -A dyes for its excellent electron withdrawing ability which promotes intramolecular charge transfer from the donor region of the dye to the region in the vicinity of the TiO₂ substrate. The close contact that CN can forge with the TiO₂ surface affords the necessary electron-withdrawing group, while the carboxylate group functions as the anchor.

Organic di-branched structures of D-(π -A)₂ type, each ending with a carboxylic was firstly reported by Abotto et al.⁶⁶ This architecture conferred enhanced stability, performances and optical properties to the dyes, increasing the photocurrent and broadening the absorption spectrum compared to its mono-branched analogue. The presence of more than one anchoring group in the case of Ruthenium-based sensitizers has already been proved to have a positive effect on the stability and electron injection.⁶⁷

From the analysis of previous results, it seems that general guideline principles to improve the performance of the dyes in the context of DSSC are difficult to extract as many interdependent factors are involved in the photovoltaic process.

4. Design of new metal-free sensitizers: a multifunctional system

As mentioned earlier (see I.4), *in-situ* PhotoElectroPolymerization (PEP) of a monomer beforehand grafted to a modified TPA is a powerful method to significantly increase the performance of a DSSC. In such device, the dye is adsorbed on the nanoporous TiO₂ and the *in-situ* PEP ensures that the conducting polymer, which is obtained from the electropolymerization and used as HTM, is in close contact with the sensitizer. Our group has recently published a device based on covalently linked dye/HTM.⁶⁸ In this s-DSSC device, the

dye ADCBZ was covalently linked to the HTM through an ester group (Figure 4.1). When *in situ* photopolymerization is carried out using this dye, the photocurrent measured was high, indicating a good electron transfer process from the dye to the TiO₂ nanoporous material. However, the efficiency of the cell using this dye is not as high as expected, and the low efficiency of the generated photocurrent was attributed to the electron back transfer from the TiO₂ nanoporous materials to the dye *via* the oxygen atoms of the two ester groups, that were suggested to be probably located close to the TiO₂ surface. This configuration generates other supplementary binding sites to the TiO₂ surface and results in an important back electron transfer process at the dye/TiO₂ interface.

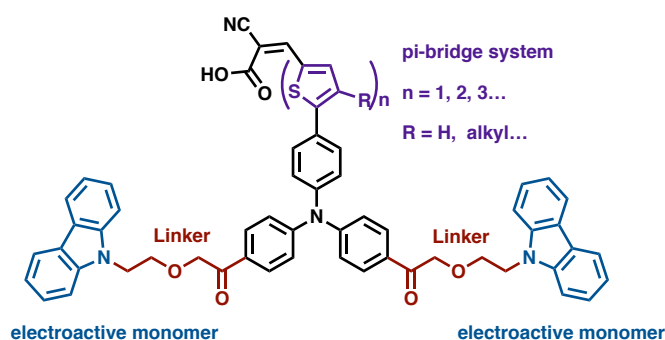


Figure 3.24 Schematic representation of dye ADCBZ.

As such, in order limit the back-electron transfer generated by the ester group and to improve the efficiency of ss-DSSC, we aim at synthesizing new compounds in this work that contain the sensitizer and the redox unit linked together with all-carbon covalent bonds to increase the regeneration of the dye after the injection of the electrons into the semi-conductor. Following this idea, we plan to develop two dyes based on the L1 core on which a carbazole unit is grafted as a precursor for the redox polymer. We are aware that the absorption properties do not fill the requirement for light harvesting in the near infrared region since the L1 compound absorbs at 430 nm. However, our aim is to demonstrate that the covalent bond linking the sensitizer and the redox mediator allows us to develop DSSCs that show reasonable performance (PCE or IPCE). With this proof of concept, it could be possible to tune the absorption spectrum as well as the HOMO and LUMO levels of the dye by variation using substitution of the donor, π -bridge and acceptor moieties leading to improved light harvesting properties.

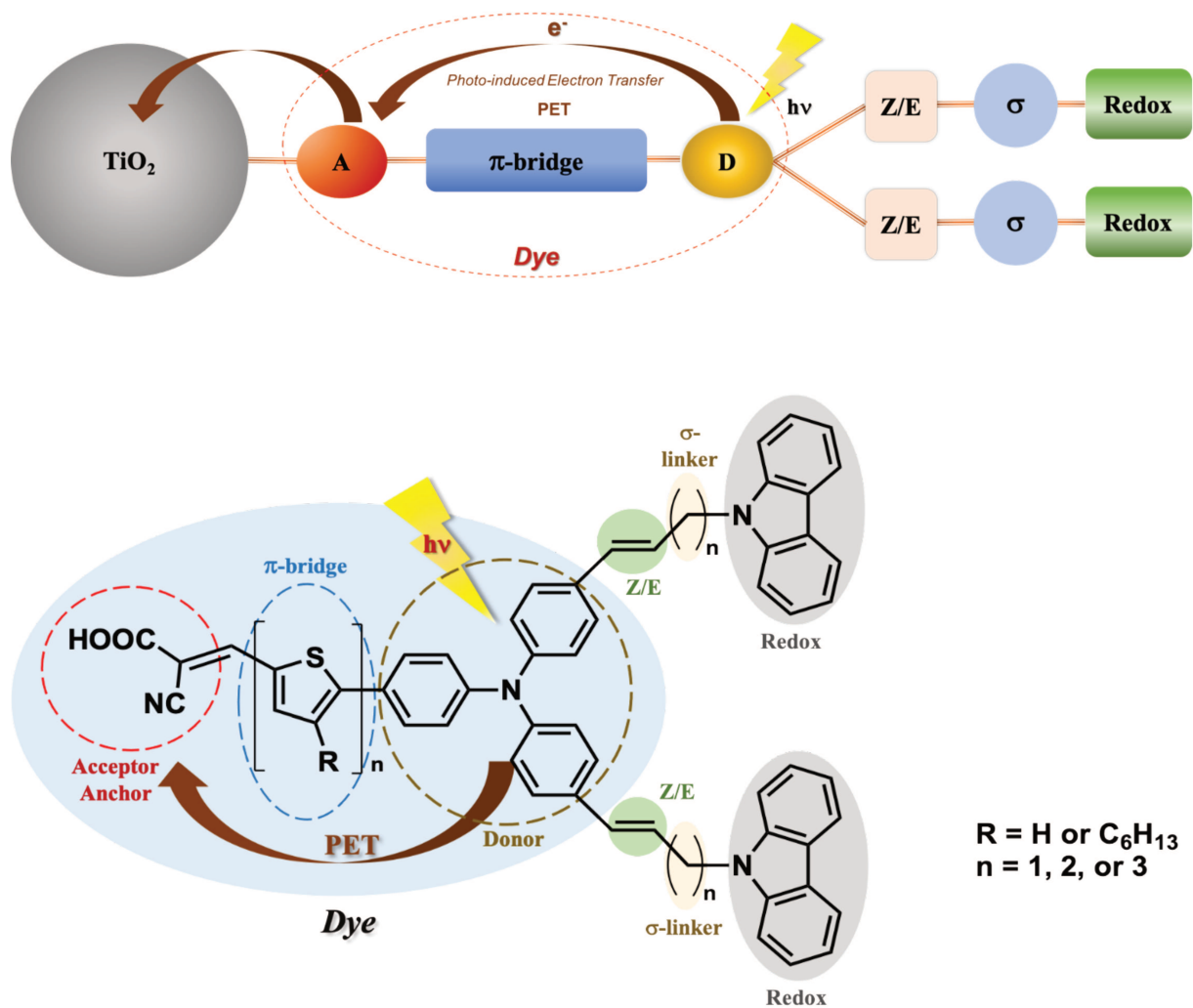
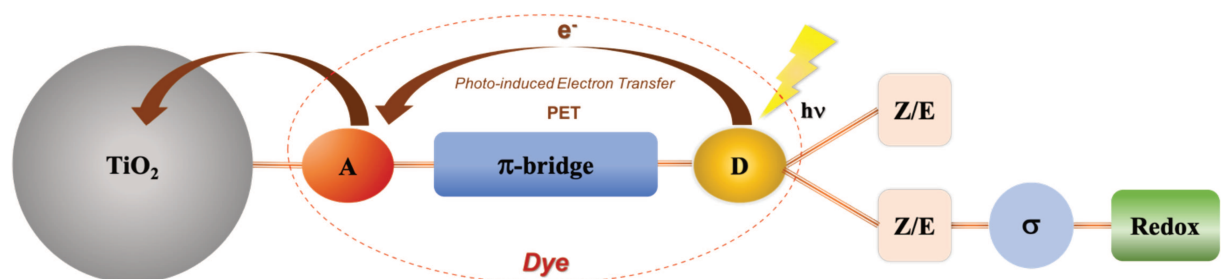


Figure 3.25 Schematic presentation of firstly designed sensitizers.

However, for reasons of synthesis difficulties, these dyes could not be obtained as explained in the following section. Consequently, the work was directed towards the elaboration of asymmetric dyes for which a synthesis route was successfully developed.



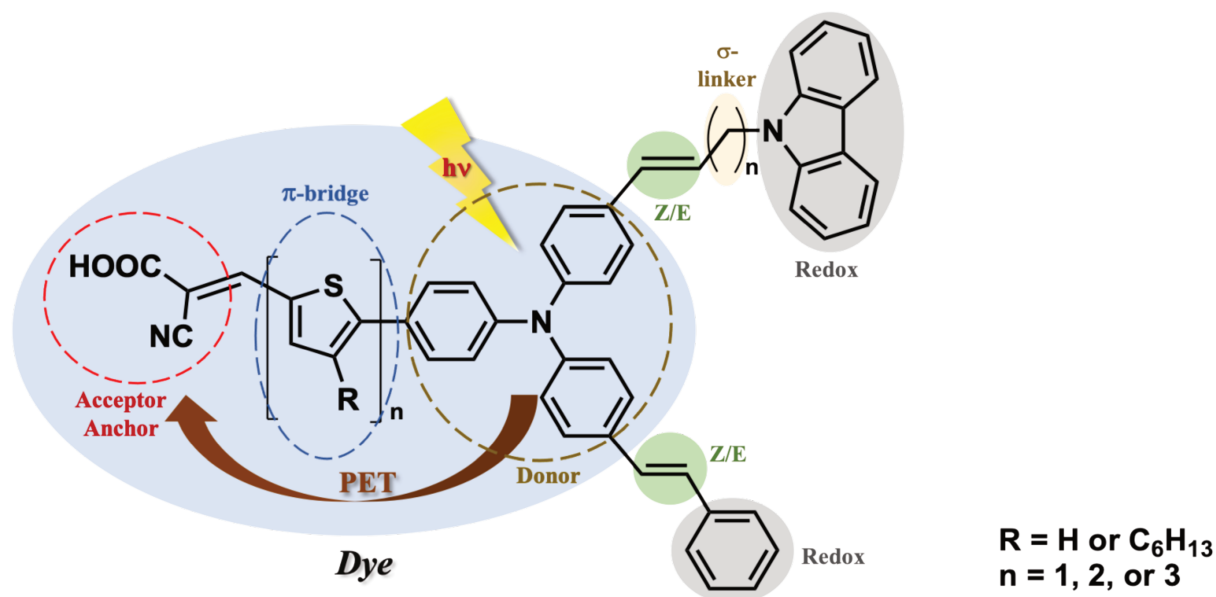


Figure 3.26 Schematic presentation of studied sensitizers.

The **L1** dye has been studied before and is used as reference dye in this work. Its structure is also taken as a model configuration for further modification on the chemical structure of dye molecules. The structure of **L1** can be resolved as three basic components: TPA as donor, thiophene as linker, and cyanoacrylic acid as acceptor.

The new dyes (Figure 3.27), 3-[5-[[4-(2-phenylethenyl)phenyl][5-(9H-carbazol-9-yl)pentenyl]aminophenyl]-2-thienyl]-2-cyano-2-propenoic acid, denoted as **ZJX4015** ($R = H$, $n=1$), and 3-[5-[[4-(2-phenylethenyl)phenyl][5-(9H-carbazol-9-yl)pentenyl]aminophenyl]-2-(4-hexyl-2-thienyl)]-2-cyano-2-propenoic acid, denoted as **ZJX4041** ($R = C_6H_{13}$, $n=1$) are both designed in D- π -A configuration based on the electron-rich TPA moiety similarly to the **L1** dye.

In the structures of new dyes, the TPA building block holds a thiophene as π -spacer with a cyanoacrylic acid anchoring group as electron acceptor, and one of the two remaining phenyl groups is *para*-substituted with a carbazole group (denoted **CBZ**). However, the proton at third (3) position on the thiophene ring in **ZJX4015** structure is replaced by an *n*-hexyl alkyl chain in **ZJX4041** structure. This substituent is generally used to hinder the phenyl rings of the dye from the TiO₂ nanomaterial in order to avoid the back electron transfer.^{69,70} Moreover, in comparison with the molecular structure of **L1**, one phenyl ring is substituted by a 1-pentenyl chain linking to the N atom of the carbazole unit, whereas the second phenyl ring is substituted by phenyl vinyl group on both new dyes. The latter is not electroactive in the potential domain

of electro-oxidation of the carbazole unit. This will lead to one covalent link per dye unit and the produced polymer (see the schematic representation in Figure 4.4).

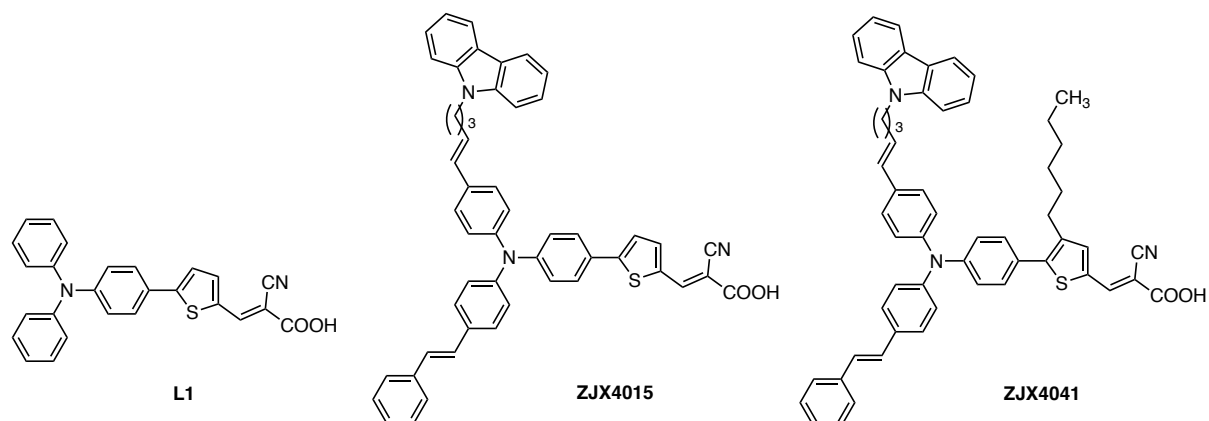


Figure 3.27 Molecular structures of the **ZJX4015** and **ZJX4041** organic D- π -A dyes covalently linked to the carbazole monomer. The structure of **L1** is displayed for comparison.

The electroactive group, the carbazole unit which undergoes copolymerization with monomer precursor in solution, here bis-EDOT, solubilized in organic electrolyte after adsorption of each of new dyes on the TiO₂ semiconductor. This approach should produce, inside the TiO₂ nanopores, a copolymer of bis-EDOT and carbazole unit covalently linked to the dye. The carbazole monomer acts evidently as electropolymerizable linker to the poly-bisEDOT used as HTM. The carbazole moiety has the advantages (i) to be an economical material, (ii) to have an excellent electron donating character, (iii) in which the nitrogen group can be easily substituted, (iv) where different substituents can be introduced, (v) to exhibit high thermal and photochemical stability, and (vi) can be easily electropolymerized. The oxidation of carbazoles results in the generation of relatively stable radical cations providing the poly(3,6-carbazole), where the repeat units in the polymer chain are linked at the 3- and 6-positions of the ring (see Figure 4.5). However, the resulting polymer is generally a dimer due to the stability of the biscarbazylum radical cations. Therefore, different approaches have been proposed to get a polymer of higher molecular weight. In this work, a co-polymerization of carbazole with bis-EDOT has been performed. This combination can give rise to a co-polymer possessing interesting properties with respect to the corresponding homopolymers as reported by the Sotzing group.⁷¹ The *N*-substituent linking the TPA moiety to the monomer is an unsaturated alkyl chain. This configuration is used with the interest of maintaining the electronic properties of the dye and of the electroactive group which is demonstrated by Houarner-Rassin and co-workers.⁷²

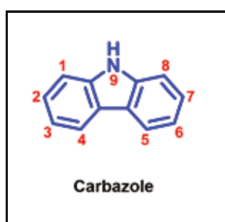


Figure 3.28 Structure of the carbazole monomers.

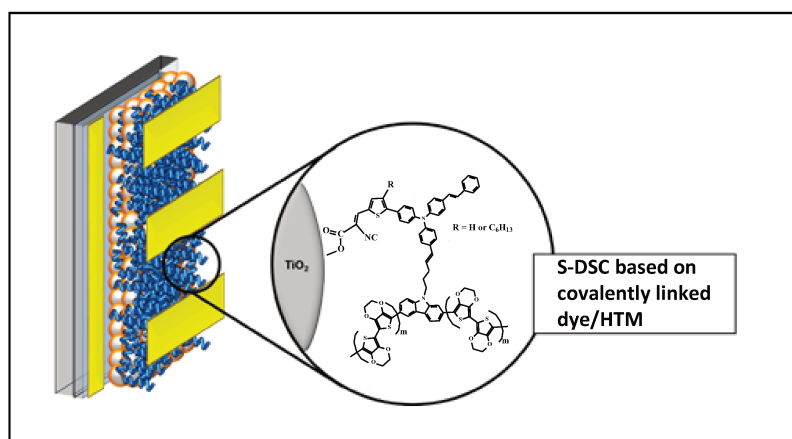
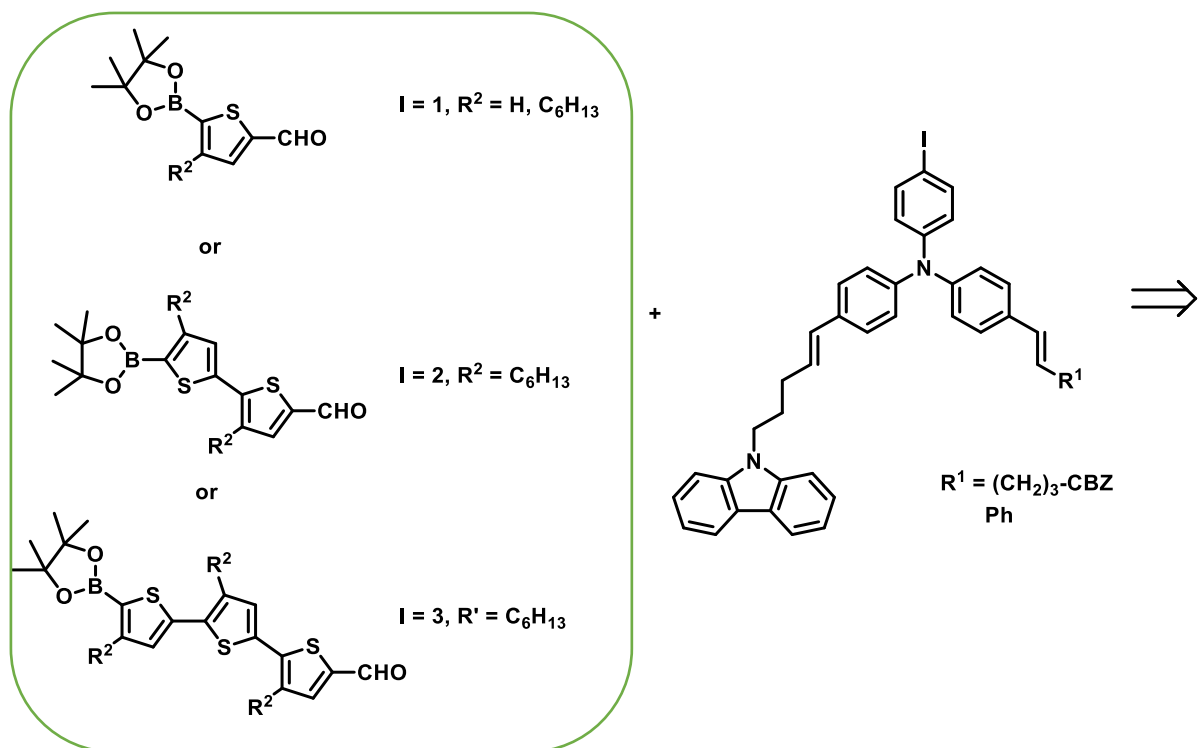
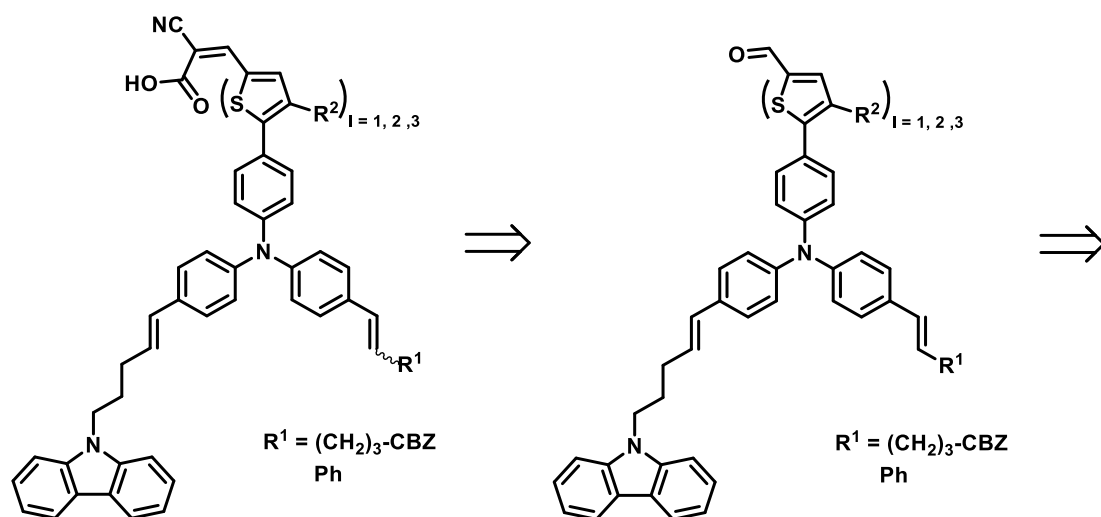
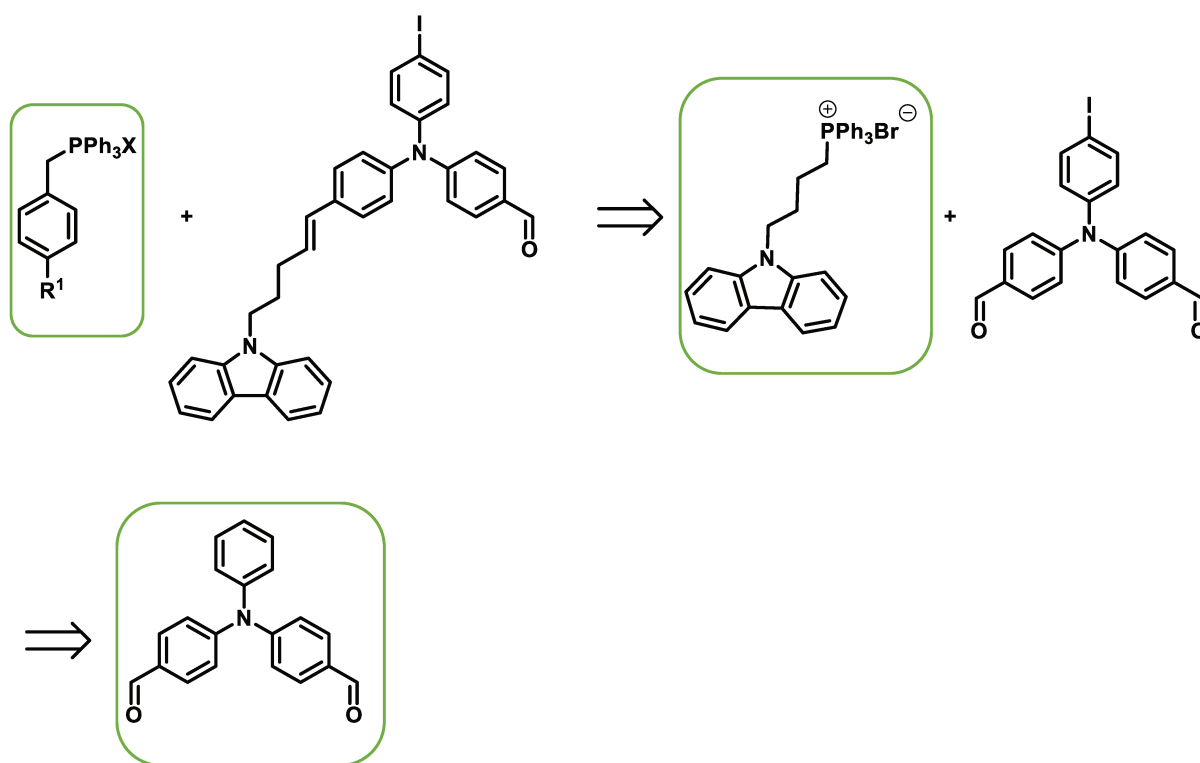


Figure 3.29 Schematic representation of a s-DSSC based on covalently linked HTM to the new dye (**ZJX4041** or **ZJX4015**).

5. Retrosynthetic analysis

The desired dyes could be obtained from the aldehyde by aldolization followed by crotonisation in an acidic medium. In order to prepare the target dyes, it was necessary to elaborate the synthesis of the different building blocks: phosphonium salts for the Wittig reactions, as well as the thiophenes-based pinacolboranes for the Suzuki coupling reaction, as outlined below.



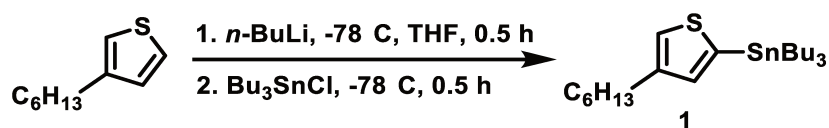


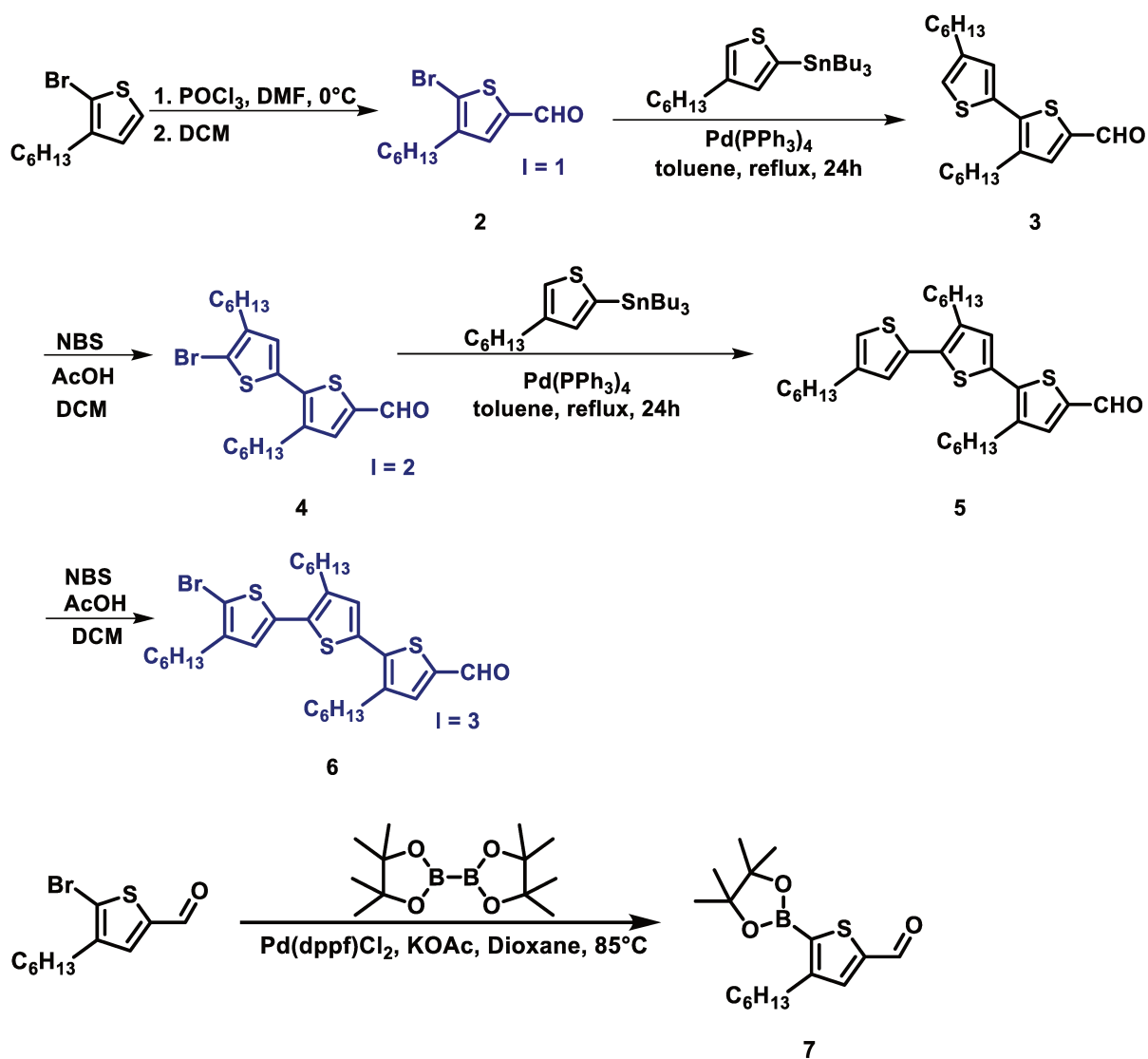
Scheme 3.1 Retrosynthesis.

6. The synthesis of thiophenes

The commercial reagent 3-hexylthiophene was firstly deprotonated by *n*-BuLi, and the carbanion formed reacted with Bu₃SnCl by nucleophilic substitution. The product **1** obtained quantitatively was used without further purification in the next step as described¹.

The compound **2** was synthesized from 2-bromo-3-hexylthiophene using the Vilsmeier-Haack reaction. 4-hexyl-2-tributylstannylthiophene **1** reacts with **2** to give **3** with a yield of 90% under the condition of the Stille reaction by using Pd(PPh₃) (0.1 eq) as catalyst, and K₂CO₃ as base. Thereafter, compound **3** was brominated with NBS giving **4** with the yield of 70%. Compound **5** was prepared in the same way as **3**, followed by bromination to achieve final product **6**. The compound **2** was then submitted to the conditions of borylation and the borate **7** was prepared in 56% yield.

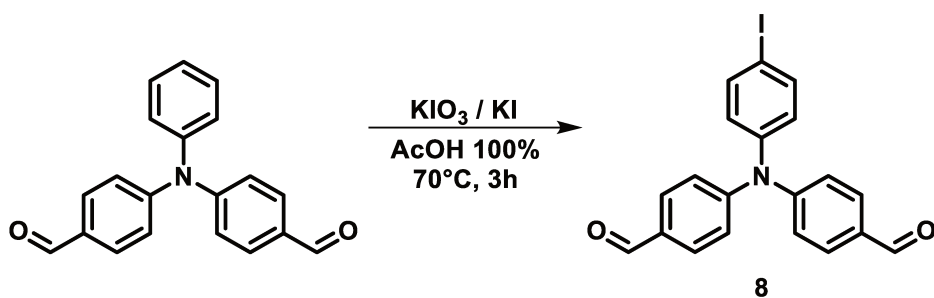




Scheme 3.2 Synthesis of thiophene-based pinacolborane.

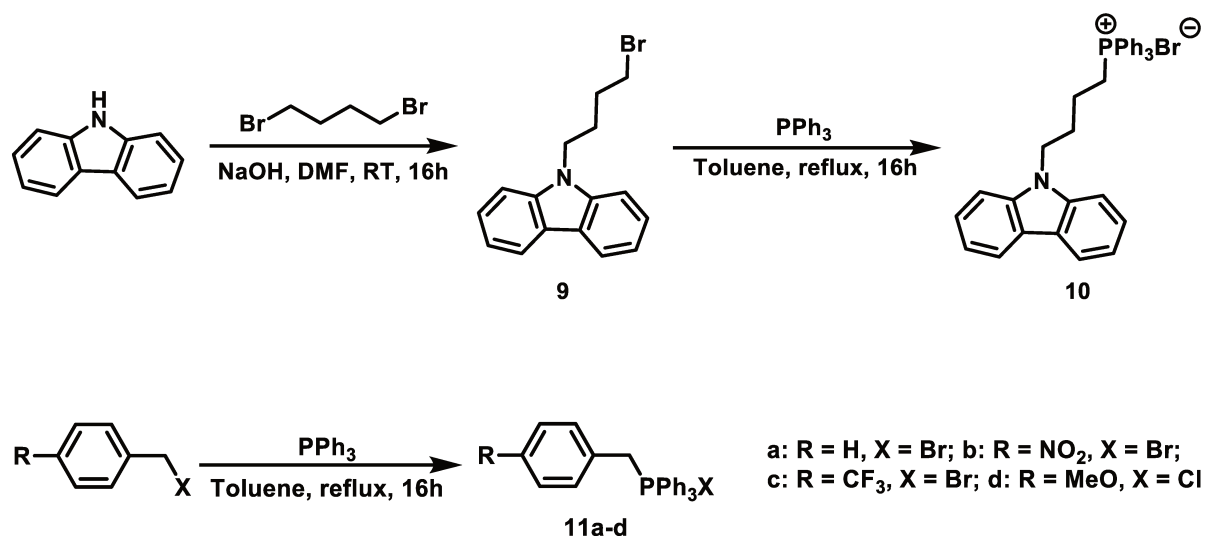
7. The step of Wittig reaction

7.1. Precursors for Wittig reaction



Scheme 3.3 Synthesis of compound 8.

As the key intermediate, 4,4'-(4-iodophenylazanediyl)dibenzaldehyde was furnished by iodation of 4,4'-diformyltriphenylamine, commercially available, to give 83% in yield following the procedure described by Li Z. *et al.*⁷³.



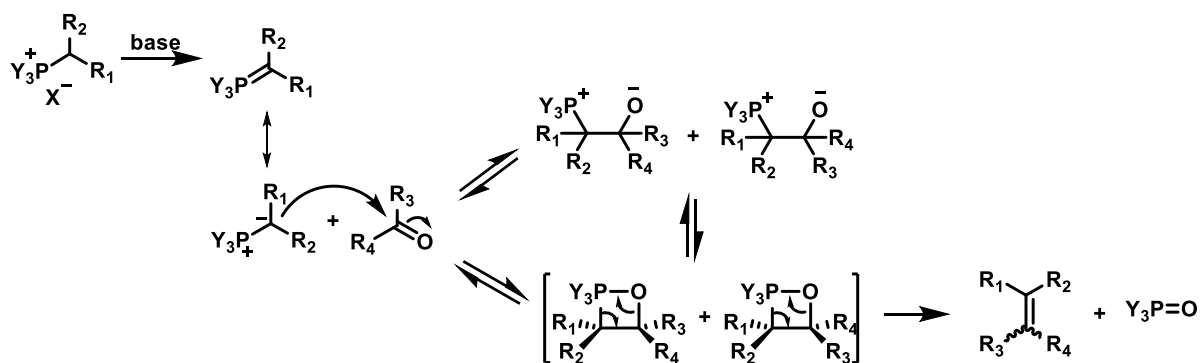
Scheme 3.4 Synthesis of precursors for Wittig reactions.

Starting from carbazole, the phosphonium bromide **10** was easily obtained in two steps. The first step consisted of the alkylation of carbazole by 1,4-dibromobutane in the presence of sodium hydroxide at room temperature and this reaction gave the compound **9** in 81% yield. The latter was heated to reflux with three equivalents of triphenylphosphine overnight to supply the target compound **10** as white solid in 95% yield. Similarly, the phosphonium bromide **11a-d** were prepared from the corresponding benzyl halides and triphenylphosphine in 40-93% yields.

7.2. The Wittig reaction

General procedure and reverse procedure

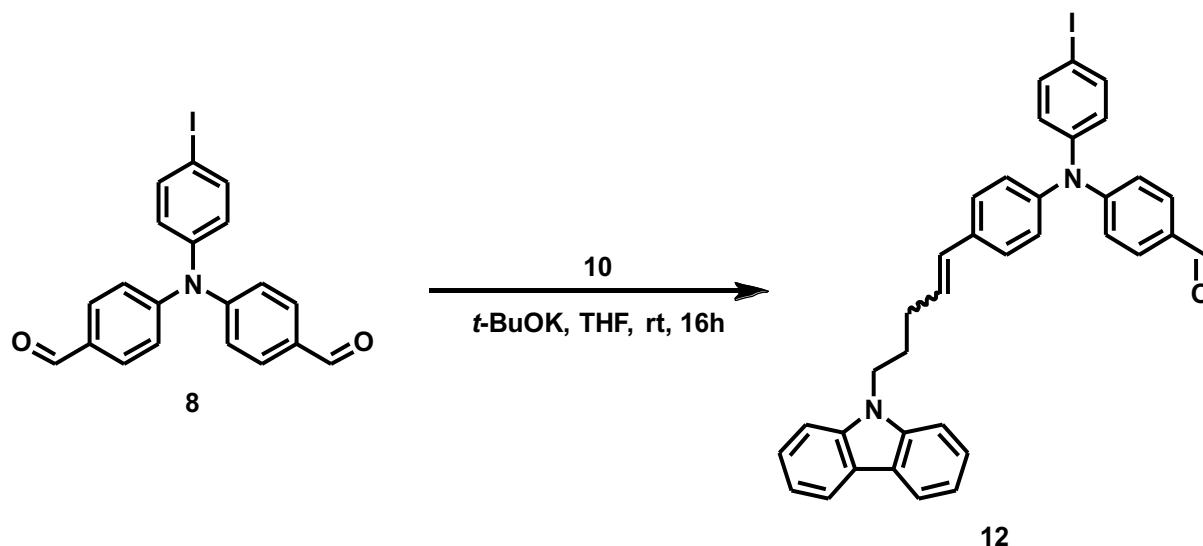
Normally, the first step of a Wittig reaction is to deprotonate the phosphonium salt with a base. The formed ylide then attacks the electrophilic carbonyl carbon to give the betaine, a species with a positive charge on phosphorous and a negative charge on oxygen. The resulting oxygen attacks at phosphorous to form an oxaphosphetane. The four-membered ring subsequently rearranges then generates the olefin product and release a triphenylphosphine oxide by-product, *via* the formation of a strong bond P=O as the driving force of this reaction. Experimentally, the phosphonium salts are firstly mixed with base, and the aldehyde is added at last.



Scheme 3.5 Mechanism of Wittig reaction under general conditions.

However, there are certain problems with the usual experimental method according to previous work by Dr. Annette Delices. The reaction was firstly tested by varying solvents and bases, but the starting material aldehyde was still present in all cases. It can thus be suggested that formation of ylide is not completed. In consequence, the reaction between the phosphonium salts and one chosen base, *t*-BuOK was exclusively studied. The NMR spectrum of phosphorous shows that no trace of desired product, the ylide, leading to the conclusion that an elimination reaction takes place in preference to the olefination in this case by applying the usual experimental method. Therefore, the reverse procedure is put into practice; the aldehyde and the phosphonium salts were firstly mixed together, and the base was added at last.

Preparation of homo-Wittig and hetero-Wittig products



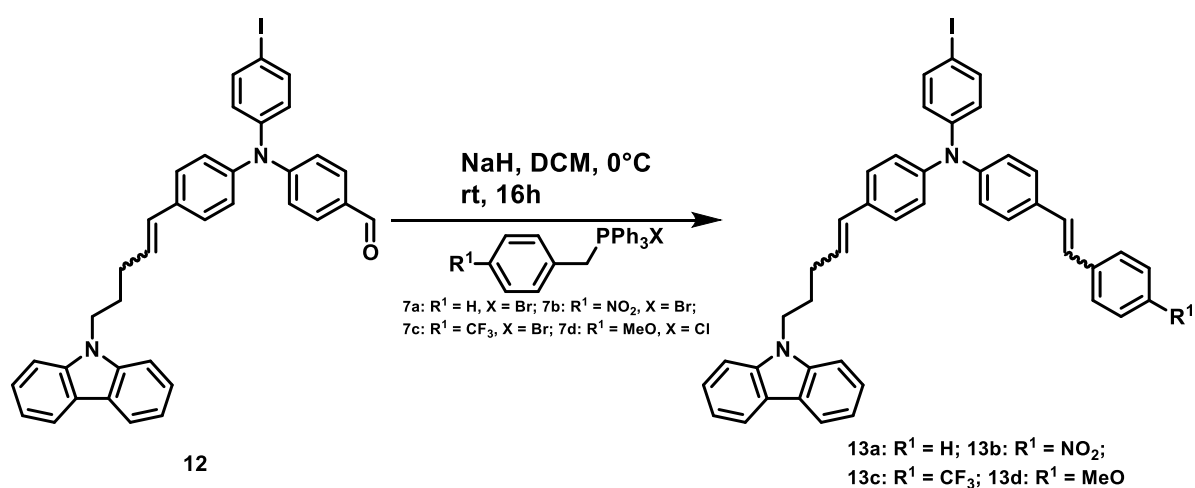
Scheme 3.6 Synthesis of mono-Wittig Product.

One aldehyde of 4,4'-(4-iodophenylazanediyl)dibenzaldehyde was easily olefinated through Wittig reaction to give mono-Wittig product (compound **12**) in 70% yield. According to the

NMR spectrum, both the geometric isomers of **12** were obtained in a ratio of about 3/7. However, the other one was stable enough even if the corresponding ylide was used in excess (2.4 equivalents). Indeed, the double olefination, very interesting to us by itself, has never occurred under different test conditions shown below.

Table 3.1 Screening various condition of homo-Wittig product.

Base	Solvent	Temperature
<i>t</i> -BuOK	DCM	Room temperature
<i>t</i> -BuOK	DCM	Reflux ($\approx 40\text{ }^{\circ}\text{C}$)
<i>t</i> -BuOK	THF	Room temperature
<i>t</i> -BuOK	THF	Reflux ($\approx 66\text{ }^{\circ}\text{C}$)
NaH	DCM	Room temperature
NaH	DCM	Reflux ($\approx 40\text{ }^{\circ}\text{C}$)
NaH	THF	Room temperature
NaH	THF	Reflux ($\approx 66\text{ }^{\circ}\text{C}$)

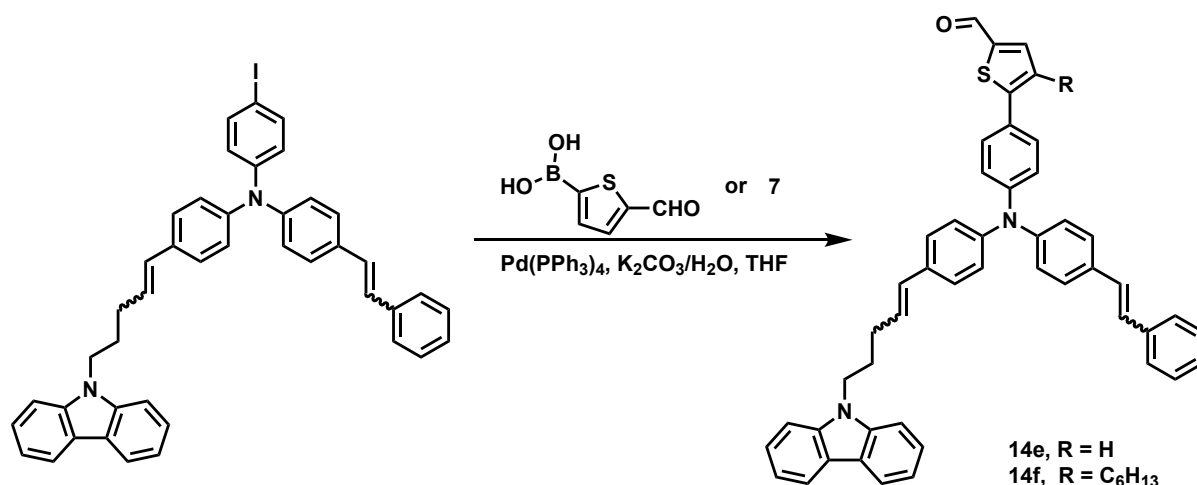


Scheme 3.7 Synthesis of bis-Wittig product.

We next studied the reactivity of the second aldehyde function towards a different ylide. To our amazing surprise, the compound **13a** was isolated in 94% yield. This indicated that the second aldehyde function was not inert towards all types of ylides. Encouraged by this observation, a new Wittig olefination was tested with the compounds **2** and **7** in the same conditions as for the formation of **13a**. Unfortunately, no reaction has taken place at all. Other

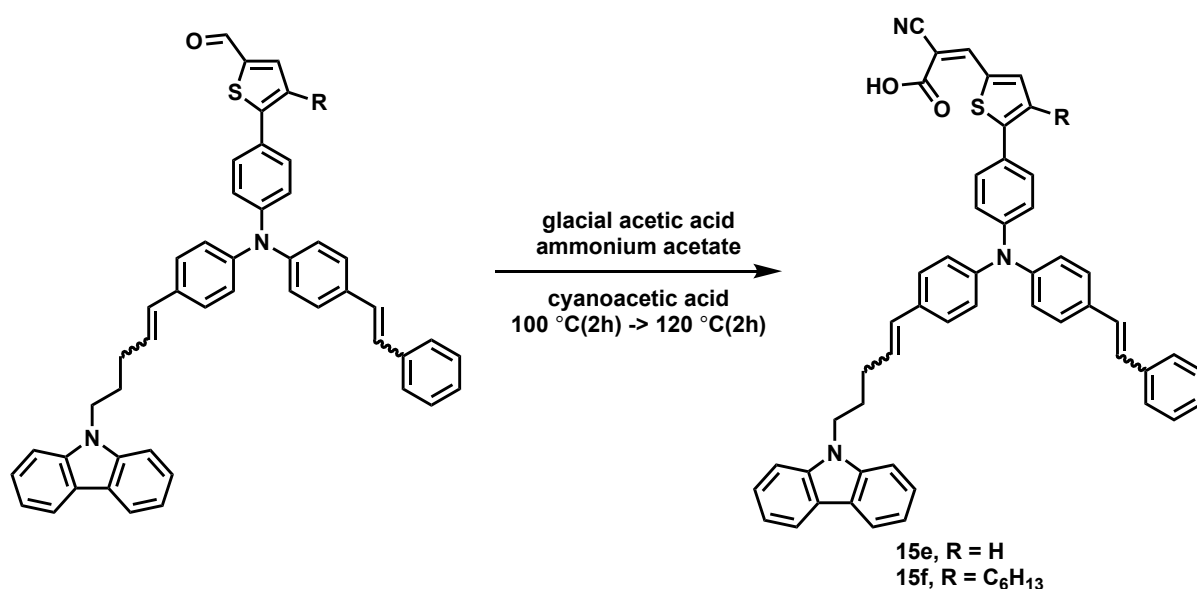
ylides with various substituted benzyl groups were submitted to this ylide-selective Wittig olefination and the compounds **13b-d** were formed with no surprise, in 46-100% yield. The intriguing reactivity of the second aldehyde opens opportunities for new design of dyes with interesting functional groups acting as attractor, or donor, or anchoring group.

Final steps



Scheme 3.8 Suzuki-Miyaura coupling to form 14e-f.

Only the compound **13a** was engaged in the following preparation of the dyes **14e-f**. It was coupled to commercial 5-formylthiophene-2-boronic acid or **7** under Suzuki's conditions and the compounds **14e-f** were isolated in 69% and 76% yields respectively.



Scheme 3.9 Aldolization to form 15e-f.

The last step of the synthesis pathway corresponds to a condensation between **14e-f** and cyanoacetic acid, followed by dehydration to furnish the target dyes **15e-f** in 74% and 77% yields.

References

- (1) Anderson, S.; Constable, E. C.; Dare-Edwards, M. P.; Goodenough, J. B.; Hamnett, A.; Seddon, K. R.; Wright, R. D. Chemical Modification of a Titanium (IV) Oxide Electrode to Give Stable Dye Sensitisation without a Supersensitiser. *Nature* **1979**, *280* (5723), 571–573. <https://doi.org/10.1038/280571a0>.
- (2) O'Regan, B.; Grätzel, M. A Low-Cost, High-Efficiency Solar Cell Based on Dye-Sensitized Colloidal TiO₂ Films. *Nature* **1991**, *353* (6346), 737–740. <https://doi.org/10.1038/353737a0>.
- (3) Nazeeruddin, M. K.; Kay, A.; Rodicio, I.; Humphry-Baker, R.; Mueller, E.; Liska, P.; Vlachopoulos, N.; Graetzel, M. Conversion of Light to Electricity by Cis-X₂bis(2,2'-Bipyridyl-4,4'-Dicarboxylate)Ruthenium(II) Charge-Transfer Sensitizers (X = Cl-, Br-, I-, CN-, and SCN-) on Nanocrystalline Titanium Dioxide Electrodes. *J. Am. Chem. Soc.* **1993**, *115* (14), 6382–6390. <https://doi.org/10.1021/ja00067a063>.
- (4) Nazeeruddin, Md. K.; Zakeeruddin, S. M.; Humphry-Baker, R.; Jirousek, M.; Liska, P.; Vlachopoulos, N.; Shklover, V.; Fischer, C.-H.; Grätzel, M. Acid–Base Equilibria of (2,2'-Bipyridyl-4,4'-Dicarboxylic Acid)Ruthenium(II) Complexes and the Effect of Protonation on Charge-Transfer Sensitization of Nanocrystalline Titania. *Inorg. Chem.* **1999**, *38* (26), 6298–6305. <https://doi.org/10.1021/ic990916a>.
- (5) Nazeeruddin, M. K.; Péchy, P.; Renouard, T.; Zakeeruddin, S. M.; Humphry-Baker, R.; Comte, P.; Liska, P.; Cevey, L.; Costa, E.; Shklover, V.; Spiccia, L.; Deacon, G. B.; Bignozzi, C. A.; Grätzel, M. Engineering of Efficient Panchromatic Sensitizers for Nanocrystalline TiO₂ - Based Solar Cells. *J. Am. Chem. Soc.* **2001**, *123* (8), 1613–1624. <https://doi.org/10.1021/ja003299u>.
- (6) Das, P. P.; Roy, A.; Agarkar, S.; Devi, P. S. Hydrothermally Synthesized Fluorescent Zn₂SnO₄ Nanoparticles for Dye Sensitized Solar Cells. *Dyes Pigments* **2018**, *154*, 303–313. <https://doi.org/10.1016/j.dyepig.2017.12.066>.
- (7) Wang, P.; Zakeeruddin, S. M.; Comte, P.; Charvet, R.; Humphry-Baker, R.; Grätzel, M. Enhance the Performance of Dye-Sensitized Solar Cells by Co-Grafting Amphiphilic Sensitizer and Hexadecylmalonic Acid on TiO₂ Nanocrystals. *J. Phys. Chem. B* **2003**, *107* (51), 14336–14341. <https://doi.org/10.1021/jp0365965>.
- (8) Wang, P.; Zakeeruddin, S. M.; Moser, J. E.; Humphry-Baker, R.; Comte, P.; Aranyos, V.; Hagfeldt, A.; Nazeeruddin, M. K.; Grätzel, M. Stable New Sensitizer with Improved Light Harvesting for Nanocrystalline Dye-Sensitized Solar Cells. *Adv. Mater.* **2004**, *16* (20), 1806–1811. <https://doi.org/10.1002/adma.200400039>.

- (9) Wang, P.; Klein, C.; Humphry-Baker, R.; Zakeeruddin, S. M.; Grätzel, M. A High Molar Extinction Coefficient Sensitizer for Stable Dye-Sensitized Solar Cells. *J. Am. Chem. Soc.* **2005**, *127* (3), 808–809. <https://doi.org/10.1021/ja0436190>.
- (10) Kuang, D.; Klein, C.; Ito, S.; Moser, J.-E.; Humphry-Baker, R.; Evans, N.; Durrant, J. R.; Grätzel, M.; Zakeeruddin, S. M.; Grätzel, M. High-Efficiency and Stable Mesoscopic Dye-Sensitized Solar Cells Based on a High Molar Extinction Coefficient Ruthenium Sensitizer and Nonvolatile Electrolyte. *Adv. Mater.* **2007**, *19* (8), 1133–1137. <https://doi.org/10.1002/adma.200602172>.
- (11) Sauvage, F.; Decoppet, J.-D.; Zhang, M.; Zakeeruddin, S. M.; Comte, P.; Nazeeruddin, M.; Wang, P.; Grätzel, M. Effect of Sensitizer Adsorption Temperature on the Performance of Dye-Sensitized Solar Cells. *J. Am. Chem. Soc.* **2011**, *133* (24), 9304–9310. <https://doi.org/10.1021/ja110541t>.
- (12) Cao, Y.; Bai, Y.; Yu, Q.; Cheng, Y.; Liu, S.; Shi, D.; Gao, F.; Wang, P. Dye-Sensitized Solar Cells with a High Absorptivity Ruthenium Sensitizer Featuring a 2-(Hexylthio)Thiophene Conjugated Bipyridine. *J. Phys. Chem. C* **2009**, *113* (15), 6290–6297. <https://doi.org/10.1021/jp9006872>.
- (13) Chen, C.-Y.; Wang, M.; Li, J.-Y.; Pootrakulchote, N.; Alibabaei, L.; Ngoc-le, C.; Decoppet, J.-D.; Tsai, J.-H.; Grätzel, C.; Wu, C.-G.; Zakeeruddin, S. M.; Grätzel, M. Highly Efficient Light-Harvesting Ruthenium Sensitizer for Thin-Film Dye-Sensitized Solar Cells. *ACS Nano* **2009**, *3* (10), 3103–3109. <https://doi.org/10.1021/nn900756s>.
- (14) Wadman, S. H.; Kroon, J. M.; Bakker, K.; Lutz, M.; Spek, A. L.; van Klink, G. P. M.; van Koten, G. Cyclometalated Ruthenium Complexes for Sensitizing Nanocrystalline TiO₂ Solar Cells. *Chem. Commun.* **2007**, No. 19, 1907. <https://doi.org/10.1039/b703636a>.
- (15) Bessho, T.; Yoneda, E.; Yum, J.-H.; Guglielmi, M.; Tavernelli, I.; Imai, H.; Rothlisberger, U.; Nazeeruddin, M. K.; Grätzel, M. New Paradigm in Molecular Engineering of Sensitizers for Solar Cell Applications. *J. Am. Chem. Soc.* **2009**, *131* (16), 5930–5934. <https://doi.org/10.1021/ja9002684>.
- (16) Robson, K. C. D.; Koivisto, B. D.; Yella, A.; Spornova, B.; Nazeeruddin, M. K.; Baumgartner, T.; Grätzel, M.; Berlinguette, C. P. Design and Development of Functionalized Cyclometalated Ruthenium Chromophores for Light-Harvesting Applications. *Inorg. Chem.* **2011**, *50* (12), 5494–5508. <https://doi.org/10.1021/ic200011m>.
- (17) Calogero, G.; Di Marco, G.; Caramori, S.; Cazzanti, S.; Argazzi, R.; Bignozzi, C. A. Natural Dye Sensitizers for Photoelectrochemical Cells. *Energy Environ. Sci.* **2009**, *2* (11), 1162. <https://doi.org/10.1039/b913248c>.

- (18) Solomon, E. I.; Lever, A. B. P. *Inorganic Electronic Structure and Spectroscopy, : Applications and Case Studies*, Volume II edition.; Wiley-Interscience: Hoboken, N.J, 2006.
- (19) Kay, A.; Graetzel, M. Artificial Photosynthesis. 1. Photosensitization of Titania Solar Cells with Chlorophyll Derivatives and Related Natural Porphyrins. *J. Phys. Chem.* **1993**, *97* (23), 6272–6277. <https://doi.org/10.1021/j100125a029>.
- (20) Tachibana, Y.; Haque, S. A.; Mercer, I. P.; Durrant, J. R.; Klug, D. R. Electron Injection and Recombination in Dye Sensitized Nanocrystalline Titanium Dioxide Films: A Comparison of Ruthenium Bipyridyl and Porphyrin Sensitizer Dyes. *J. Phys. Chem. B* **2000**, *104* (6), 1198–1205. <https://doi.org/10.1021/jp992774b>.
- (21) Nazeeruddin, Md. K.; Humphry-Baker, R.; Officer, D. L.; Campbell, W. M.; Burrell, A. K.; Grätzel, M. Application of Metalloporphyrins in Nanocrystalline Dye-Sensitized Solar Cells for Conversion of Sunlight into Electricity. *Langmuir* **2004**, *20* (15), 6514–6517. <https://doi.org/10.1021/la0496082>.
- (22) Campbell, W. M.; Burrell, A. K.; Officer, D. L.; Jolley, K. W. Porphyrins as Light Harvesters in the Dye-Sensitized TiO₂ Solar Cell. *Coord. Chem. Rev.* **2004**, *248* (13–14), 1363–1379. <https://doi.org/10.1016/j.ccr.2004.01.007>.
- (23) Wang, Q.; Campbell, W. M.; Bonfantani, E. E.; Jolley, K. W.; Officer, D. L.; Walsh, P. J.; Gordon, K.; Humphry-Baker, R.; Nazeeruddin, M. K.; Grätzel, M. Efficient Light Harvesting by Using Green Zn-Porphyrin-Sensitized Nanocrystalline TiO₂ Films. *J. Phys. Chem. B* **2005**, *109* (32), 15397–15409. <https://doi.org/10.1021/jp052877w>.
- (24) Campbell, W. M.; Jolley, K. W.; Wagner, P.; Wagner, K.; Walsh, P. J.; Gordon, K. C.; Schmidt-Mende, L.; Nazeeruddin, M. K.; Wang, Q.; Grätzel, M.; Officer, D. L. Highly Efficient Porphyrin Sensitizers for Dye-Sensitized Solar Cells. *J. Phys. Chem. C* **2007**, *111* (32), 11760–11762. <https://doi.org/10.1021/jp0750598>.
- (25) Lin, C.-Y.; Wang, Y.-C.; Hsu, S.-J.; Lo, C.-F.; Diao, E. W.-G. Preparation and Spectral, Electrochemical, and Photovoltaic Properties of Acene-Modified Zinc Porphyrins. *J. Phys. Chem. C* **2010**, *114* (1), 687–693. <https://doi.org/10.1021/jp909232b>.
- (26) Wang, C.-L.; Chang, Y.-C.; Lan, C.-M.; Lo, C.-F.; Wei-Guang Diao, E.; Lin, C.-Y. Enhanced Light Harvesting with π -Conjugated Cyclic Aromatic Hydrocarbons for Porphyrin-Sensitized Solar Cells. *Energy Environ. Sci.* **2011**, *4* (5), 1788. <https://doi.org/10.1039/c0ee00767f>.
- (27) Eu, S.; Hayashi, S.; Umeyama, T.; Oguro, A.; Kawasaki, M.; Kadota, N.; Matano, Y.; Imahori, H. Effects of 5-Membered Heteroaromatic Spacers on Structures of Porphyrin Films and Photovoltaic Properties of Porphyrin-Sensitized TiO₂ Cells. *J. Phys. Chem. C* **2007**, *111* (8), 3528–3537. <https://doi.org/10.1021/jp067290b>.

- (28) Hayashi, S.; Tanaka, M.; Hayashi, H.; Eu, S.; Umeyama, T.; Matano, Y.; Araki, Y.; Imahori, H. Naphthyl-Fused π -Elongated Porphyrins for Dye-Sensitized TiO₂ Cells. *J. Phys. Chem. C* **2008**, *112* (39), 15576–15585. <https://doi.org/10.1021/jp805122z>.
- (29) Eu, S.; Hayashi, S.; Umeyama, T.; Matano, Y.; Araki, Y.; Imahori, H. Quinoxaline-Fused Porphyrins for Dye-Sensitized Solar Cells. *J. Phys. Chem. C* **2008**, *112* (11), 4396–4405. <https://doi.org/10.1021/jp710400p>.
- (30) Liu, Y.; Xiang, N.; Feng, X.; Shen, P.; Zhou, W.; Weng, C.; Zhao, B.; Tan, S. Thiophene-Linked Porphyrin Derivatives for Dye-Sensitized Solar Cells. *Chem. Commun.* **2009**, No. 18, 2499. <https://doi.org/10.1039/b821985k>.
- (31) Chang, Y.-C.; Wang, C.-L.; Pan, T.-Y.; Hong, S.-H.; Lan, C.-M.; Kuo, H.-H.; Lo, C.-F.; Hsu, H.-Y.; Lin, C.-Y.; Diau, E. W.-G. A Strategy to Design Highly Efficient Porphyrin Sensitizers for Dye-Sensitized Solar Cells. *Chem. Commun.* **2011**, *47* (31), 8910. <https://doi.org/10.1039/c1cc12764k>.
- (32) Lu, H.-P.; Tsai, C.-Y.; Yen, W.-N.; Hsieh, C.-P.; Lee, C.-W.; Yeh, C.-Y.; Diau, E. W.-G. Control of Dye Aggregation and Electron Injection for Highly Efficient Porphyrin Sensitizers Adsorbed on Semiconductor Films with Varying Ratios of Coadsorbate. *J. Phys. Chem. C* **2009**, *113* (49), 20990–20997. <https://doi.org/10.1021/jp908100v>.
- (33) Bessho, T.; Zakeeruddin, S. M.; Yeh, C.-Y.; Diau, E. W.-G.; Grätzel, M. Highly Efficient Mesoscopic Dye-Sensitized Solar Cells Based on Donor–Acceptor-Substituted Porphyrins. *Angew. Chem. Int. Ed.* **2010**, *49* (37), 6646–6649. <https://doi.org/10.1002/anie.201002118>.
- (34) Kurotobi, K.; Toude, Y.; Kawamoto, K.; Fujimori, Y.; Ito, S.; Chabera, P.; Sundström, V.; Imahori, H. Highly Asymmetrical Porphyrins with Enhanced Push-Pull Character for Dye-Sensitized Solar Cells. *Chem. - Eur. J.* **2013**, *19* (50), 17075–17081. <https://doi.org/10.1002/chem.201303460>.
- (35) Lee, C.-W.; Lu, H.-P.; Lan, C.-M.; Huang, Y.-L.; Liang, Y.-R.; Yen, W.-N.; Liu, Y.-C.; Lin, Y.-S.; Diau, E. W.-G.; Yeh, C.-Y. Novel Zinc Porphyrin Sensitizers for Dye-Sensitized Solar Cells: Synthesis and Spectral, Electrochemical, and Photovoltaic Properties. *Chem. – Eur. J.* **2009**, *15* (6), 1403–1412. <https://doi.org/10.1002/chem.200801572>.
- (36) Yella, A.; Lee, H.-W.; Tsao, H. N.; Yi, C.; Chandiran, A. K.; Nazeeruddin, M. K.; Diau, E. W.-G.; Yeh, C.-Y.; Zakeeruddin, S. M.; Gratzel, M. Porphyrin-Sensitized Solar Cells with Cobalt (II/III)-Based Redox Electrolyte Exceed 12 Percent Efficiency. *Science* **2011**, *334* (6056), 629–634. <https://doi.org/10.1126/science.1209688>.
- (37) Mathew, S.; Yella, A.; Gao, P.; Humphry-Baker, R.; Curchod, B. F. E.; Ashari-Astani, N.; Tavernelli, I.; Rothlisberger, U.; Nazeeruddin, Md. K.; Grätzel, M. Dye-Sensitized Solar Cells

- with 13% Efficiency Achieved through the Molecular Engineering of Porphyrin Sensitizers. *Nat. Chem.* **2014**, *6* (3), 242–247. <https://doi.org/10.1038/nchem.1861>.
- (38) Yella, A.; Mai, C.-L.; Zakeeruddin, S. M.; Chang, S.-N.; Hsieh, C.-H.; Yeh, C.-Y.; Grätzel, M. Molecular Engineering of Push-Pull Porphyrin Dyes for Highly Efficient Dye-Sensitized Solar Cells: The Role of Benzene Spacers. *Angew. Chem. Int. Ed.* **2014**, *53* (11), 2973–2977. <https://doi.org/10.1002/anie.201309343>.
- (39) Urnikaite, S.; Daskeviciene, M.; Send, R.; Wonneberger, H.; Sackus, A.; Bruder, I.; Getautis, V. Organic Dyes Containing a Hydrazone Moiety as Auxiliary Donor for Solid-State DSSC Applications. *Dyes Pigments* **2015**, *114*, 175–183. <https://doi.org/10.1016/j.dyepig.2014.11.012>.
- (40) Wang, Z.-S.; Cui, Y.; Dan-oh, Y.; Kasada, C.; Shinpo, A.; Hara, K. Thiophene-Functionalized Coumarin Dye for Efficient Dye-Sensitized Solar Cells: Electron Lifetime Improved by Coadsorption of Deoxycholic Acid. *J. Phys. Chem. C* **2007**, *111* (19), 7224–7230. <https://doi.org/10.1021/jp067872t>.
- (41) Wang, Z.-S.; Cui, Y.; Dan-oh, Y.; Kasada, C.; Shinpo, A.; Hara, K. Molecular Design of Coumarin Dyes for Stable and Efficient Organic Dye-Sensitized Solar Cells. *J. Phys. Chem. C* **2008**, *112* (43), 17011–17017. <https://doi.org/10.1021/jp806927b>.
- (42) Kim, J. Y.; Kim, Y. H.; Kim, Y. S. Indoline Dyes with Various Acceptors for Dye-Sensitized Solar Cells. *Curr. Appl. Phys.* **2011**, *11* (1), S117–S121. <https://doi.org/10.1016/j.cap.2010.11.098>.
- (43) Tian, H.; Yang, X.; Chen, R.; Pan, Y.; Li, L.; Hagfeldt, A.; Sun, L. Phenothiazine Derivatives for Efficient Organic Dye-Sensitized Solar Cells. *Chem. Commun.* **2007**, No. 36, 3741. <https://doi.org/10.1039/b707485a>.
- (44) Koumura, N.; Wang, Z.-S.; Mori, S.; Miyashita, M.; Suzuki, E.; Hara, K. Alkyl-Functionalized Organic Dyes for Efficient Molecular Photovoltaics. *J. Am. Chem. Soc.* **2006**, *128* (44), 14256–14257. <https://doi.org/10.1021/ja0645640>.
- (45) Qin, P.; Yang, X.; Chen, R.; Sun, L.; Marinado, T.; Edvinsson, T.; Boschloo, G.; Hagfeldt, A. Influence of π -Conjugation Units in Organic Dyes for Dye-Sensitized Solar Cells. *J. Phys. Chem. C* **2007**, *111* (4), 1853–1860. <https://doi.org/10.1021/jp065550j>.
- (46) Zhang, Y.; Lai, S.-L.; Tong, Q.-X.; Lo, M.-F.; Ng, T.-W.; Chan, M.-Y.; Wen, Z.-C.; He, J.; Jeff, K.-S.; Tang, X.-L.; Liu, W.-M.; Ko, C.-C.; Wang, P.-F.; Lee, C.-S. High Efficiency Nondoped Deep-Blue Organic Light Emitting Devices Based on Imidazole- π -Triphenylamine Derivatives. *Chem. Mater.* **2012**, *24* (1), 61–70. <https://doi.org/10.1021/cm201789u>.

- (47) Singh, S. P.; Roy, M. S.; Thomas, K. R. J.; Balaiah, S.; Bhanuprakash, K.; Sharma, G. D. New Triphenylamine-Based Organic Dyes with Different Numbers of Anchoring Groups for Dye-Sensitized Solar Cells. *J. Phys. Chem. C* **2012**, *116* (9), 5941–5950. <https://doi.org/10.1021/jp210971u>.
- (48) Yang, X.; Huang, H.; Pan, B.; Aldred, M. P.; Zhuang, S.; Wang, L.; Chen, J.; Ma, D. Modified 4,4',4''-Tri(*N* -Carbazolyl)Triphenylamine as a Versatile Bipolar Host for Highly Efficient Blue, Orange, and White Organic Light-Emitting Diodes. *J. Phys. Chem. C* **2012**, *116* (28), 15041–15047. <https://doi.org/10.1021/jp3034566>.
- (49) Fang, Y.-K.; Liu, C.-L.; Yang, G.-Y.; Chen, P.-C.; Chen, W.-C. New Donor–Acceptor Random Copolymers with Pendent Triphenylamine and 1,3,4-Oxadiazole for High-Performance Memory Device Applications. *Macromolecules* **2011**, *44* (8), 2604–2612. <https://doi.org/10.1021/ma200187e>.
- (50) Tsuchiya, K.; Sakakura, T.; Ogino, K. Synthesis of Triphenylamine Copolymers and Effect of Their Chemical Structures on Physical Properties. *Macromolecules* **2011**, *44* (13), 5200–5208. <https://doi.org/10.1021/ma200940v>.
- (51) Leliège, A.; Blanchard, P.; Rousseau, T.; Roncali, J. Triphenylamine/Tetracyanobutadiene-Based D-A-D π -Conjugated Systems as Molecular Donors for Organic Solar Cells. *Org. Lett.* **2011**, *13* (12), 3098–3101. <https://doi.org/10.1021/ol201002j>.
- (52) Gómez Esteban, S.; de la Cruz, P.; Aljarilla, A.; Arellano, L. M.; Langa, F. Panchromatic Push–Pull Chromophores Based on Triphenylamine as Donors for Molecular Solar Cells. *Org. Lett.* **2011**, *13* (19), 5362–5365. <https://doi.org/10.1021/ol202242j>.
- (53) Polander, L. E.; Yella, A.; Teuscher, J.; Humphry-Baker, R.; Curchod, B. F. E.; Ashari Astani, N.; Gao, P.; Moser, J.-E.; Tavernelli, I.; Rothlisberger, U.; Grätzel, M.; Nazeeruddin, Md. K.; Frey, J. Unravelling the Potential for Dithienopyrrole Sensitizers in Dye-Sensitized Solar Cells. *Chem. Mater.* **2013**, *25* (13), 2642–2648. <https://doi.org/10.1021/cm401144j>.
- (54) Yang, L.; Xu, B.; Bi, D.; Tian, H.; Boschloo, G.; Sun, L.; Hagfeldt, A.; Johansson, E. M. J. Initial Light Soaking Treatment Enables Hole Transport Material to Outperform Spiro-OMeTAD in Solid-State Dye-Sensitized Solar Cells. *J. Am. Chem. Soc.* **2013**, *135* (19), 7378–7385. <https://doi.org/10.1021/ja403344s>.
- (55) Kitamura, T.; Ikeda, M.; Shigaki, K.; Inoue, T.; Anderson, N. A.; Ai, X.; Lian, T.; Yanagida, S. Phenyl-Conjugated Oligoene Sensitizers for TiO₂ Solar Cells. *Chem. Mater.* **2004**, *16* (9), 1806–1812. <https://doi.org/10.1021/cm0349708>.
- (56) Li, R.; Lv, X.; Shi, D.; Zhou, D.; Cheng, Y.; Zhang, G.; Wang, P. Dye-Sensitized Solar Cells Based on Organic Sensitizers with Different Conjugated Linkers: Furan, Bifuran, Thiophene,

- Bithiophene, Selenophene, and Biselenophene. *J. Phys. Chem. C* **2009**, *113* (17), 7469–7479. <https://doi.org/10.1021/jp900972v>.
- (57) Liu, J.; Li, R.; Si, X.; Zhou, D.; Shi, Y.; Wang, Y.; Jing, X.; Wang, P. Oligothiophene Dye-Sensitized Solar Cells. *Energy Environ. Sci.* **2010**, *3* (12), 1924. <https://doi.org/10.1039/c0ee00304b>.
- (58) Liang, M.; Xu, W.; Cai, F.; Chen, P.; Peng, B.; Chen, J.; Li, Z. New Triphenylamine-Based Organic Dyes for Efficient Dye-Sensitized Solar Cells. *J. Phys. Chem. C* **2007**, *111* (11), 4465–4472. <https://doi.org/10.1021/jp067930a>.
- (59) Mishra, A.; Fischer, M. K. R.; Bäuerle, P. Metal-Free Organic Dyes for Dye-Sensitized Solar Cells: From Structure: Property Relationships to Design Rules. *Angew. Chem. Int. Ed.* **2009**, *48* (14), 2474–2499. <https://doi.org/10.1002/anie.200804709>.
- (60) Pei, J.; Peng, S.; Shi, J.; Liang, Y.; Tao, Z.; Liang, J.; Chen, J. Triphenylamine-Based Organic Dye Containing the Diphenylvinyl and Rhodanine-3-Acetic Acid Moieties for Efficient Dye-Sensitized Solar Cells. *J. Power Sources* **2009**, *187* (2), 620–626. <https://doi.org/10.1016/j.jpowsour.2008.11.028>.
- (61) Tang, J.; Hua, J.; Wu, W.; Li, J.; Jin, Z.; Long, Y.; Tian, H. New Starburst Sensitizer with Carbazole Antennas for Efficient and Stable Dye-Sensitized Solar Cells. *Energy Environ. Sci.* **2010**, *3* (11), 1736. <https://doi.org/10.1039/c0ee00008f>.
- (62) Justin Thomas, K. R.; Hsu, Y.-C.; Lin, J. T.; Lee, K.-M.; Ho, K.-C.; Lai, C.-H.; Cheng, Y.-M.; Chou, P.-T. 2,3-Disubstituted Thiophene-Based Organic Dyes for Solar Cells. *Chem. Mater.* **2008**, *20* (5), 1830–1840. <https://doi.org/10.1021/cm702631r>.
- (63) Chaurasia, S.; Ni, J.-S.; Hung, W.-I.; Lin, J. T. 2 H-[1,2,3]Triazolo[4,5- c]Pyridine Cored Organic Dyes Achieving a High Efficiency: A Systematic Study of the Effect of Different Donors and π Spacers. *ACS Appl. Mater. Interfaces* **2015**, *7* (39), 22046–22057. <https://doi.org/10.1021/acsami.5b07205>.
- (64) Mahmood, A. Triphenylamine Based Dyes for Dye Sensitized Solar Cells: A Review. *Sol. Energy* **2016**, *123*, 127–144. <https://doi.org/10.1016/j.solener.2015.11.015>.
- (65) Zhang, L.; Cole, J. M. Anchoring Groups for Dye-Sensitized Solar Cells. *ACS Appl. Mater. Interfaces* **2015**, *7* (6), 3427–3455. <https://doi.org/10.1021/am507334m>.
- (66) Abbotto, A.; Manfredi, N.; Marini, C.; De Angelis, F.; Mosconi, E.; Yum, J.-H.; Xianxi, Z.; Nazeeruddin, M. K.; Grätzel, M. Di-Branched Di-Anchoring Organic Dyes for Dye-Sensitized Solar Cells. *Energy Environ. Sci.* **2009**, *2* (10), 1094. <https://doi.org/10.1039/b910654e>.

- (67) De Angelis, F.; Fantacci, S.; Selloni, A.; Grätzel, M.; Nazeeruddin, M. K. Influence of the Sensitizer Adsorption Mode on the Open-Circuit Potential of Dye-Sensitized Solar Cells. *Nano Lett.* **2007**, *7* (10), 3189–3195. <https://doi.org/10.1021/nl071835b>.
- (68) Delices, A. Organized Organic Dye / Hole Transporting Materials for TiO₂- and ZnO- Based Solid-State Dye-Sensitized Solar Cells (s-DSSCs). These de doctorat, Sorbonne Paris Cité, 2017.
- (69) Kroeze, J. E.; Hirata, N.; Koops, S.; Nazeeruddin, Md. K.; Schmidt-Mende, L.; Grätzel, M.; Durrant, J. R. Alkyl Chain Barriers for Kinetic Optimization in Dye-Sensitized Solar Cells. *J. Am. Chem. Soc.* **2006**, *128* (50), 16376–16383. <https://doi.org/10.1021/ja065653f>.
- (70) Wu, Z.; Li, X.; Li, J.; Ågren, H.; Hua, J.; Tian, H. Effect of Bridging Group Configuration on Photophysical and Photovoltaic Performance in Dye-Sensitized Solar Cells. *J. Mater. Chem. A* **2015**, *3* (27), 14325–14333. <https://doi.org/10.1039/C5TA02120K>.
- (71) Sotzing, G. A.; Reddinger, J. L.; Katritzky, A. R.; Soloducho, J.; Musgrave, R.; Reynolds, J. R.; Steel, P. J. Multiply Colored Electrochromic Carbazole-Based Polymers. *Chem. Mater.* **1997**, *9* (7), 1578–1587. <https://doi.org/10.1021/cm960630t>.
- (72) Houarner-Rassin, C.; Blart, E.; Buvat, P.; Odobel, F. Improved Efficiency of a Thiophene Linked Ruthenium Polypyridine Complex for Dry Dye-Sensitized Solar Cells. *J. Photochem. Photobiol. Chem.* **2007**, *186* (2–3), 135–142. <https://doi.org/10.1016/j.jphotochem.2006.07.022>.
- (73) Li, Z.; Ye, T.; Tang, S.; Wang, C.; Ma, D.; Li, Z. Triphenylamine-Based π -Conjugated Dendrimers: Convenient Synthesis, Easy Solution Processability, and Good Hole-Transporting Properties. *J. Mater. Chem. C* **2015**, *3* (9), 2016–2023. <https://doi.org/10.1039/C4TC01923G>.

Chapter 4. Alkyl linked Dye-HTM: effect of linker nature on ss-DSSC performances

I. Introduction

This chapter focuses on the fabrication and study of the solid-state DSSCs based on the two dyes the synthesis of which is presented in the previous chapter. The main feature of these two dyes is the electropolymerizable unit which they hold, being able to give rise to an HTM interface. More specifically, we are focusing on the charge transfer occurring at dye/HTM interface, after the electron injection in the TiO_2 , for a better dye regeneration process in ss-DSSCs.¹ For this purpose, the original idea is to completely remove this interface and to set new ss-DSSCs based on covalently linked dye to the CP used as HTM.

1.1. Optimization of the Interfacial Charge Transfer

The interfacial charge transfer processes play key roles in impacting the photovoltaic performances of an ss-DSSC. After the electron injection from the photo-excited dye into the CB of the TiO_2 , the resulting oxidized dye returns to ground state through the injection of a hole in the HTM. The dye regeneration process must be faster than each of the following two back electron transfer processes (Figure 4.1): ① from TiO_2 to the oxidized dye in order to achieve a high photocurrent density of the device; and ② from TiO_2 to the HTM in order to have a high photovoltage of the device.

In ss-DSSCs with CP produced by *in-situ* PEP as HTM, the dye regeneration process is faster than that in conventional DSSCs based on liquid electrolyte. This is attributed to the fast charge transport within the CP and hence to the direct electron transfer into the oxidized dye. Indeed, a charge transport hopping mechanism between HTM and oxidized dye is expected in solid-state DSSC, whereas this process can only occur by diffusion mechanism to the electrode for DSSC used liquid electrolyte.

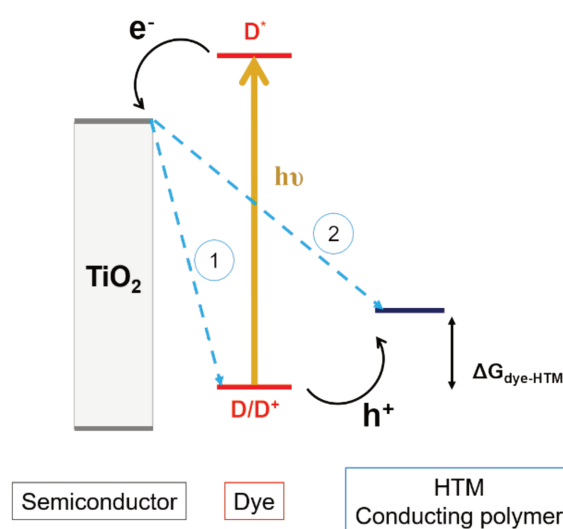


Figure 4.1 Schematic diagram of charge transfer processes occurring in ss-DSSC.

1.2. In-situ PEP

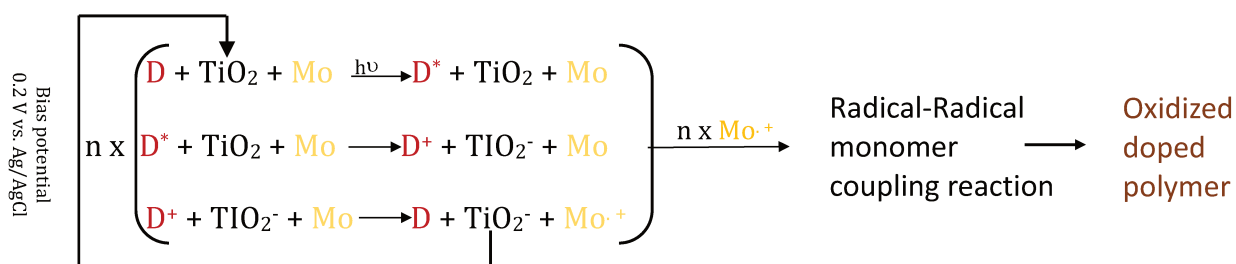


Figure 4.2 Schematic representation of in-situ PEP process

As demonstrated above in the Figure 4.2, the photoelectrochemical polymerization is initiated by the photoexcitation of the dye on the TiO_2 under visible light irradiation. The injection of electrons creates holes at HOMO level of dyes leaving the dye in its oxidized state. As an active site, the oxidized dye is reduced by the transform of the monomer (bis-EDOT) into the radical cationic form. The dye is again photo-excited and the cycle is reproduced. The oxidized bis-EDOT undergo the coupling reaction to give rise to oligomer or polymer. An external potential of 0.2 - 0.3 V is applied with the purpose of draining the electrons to TiO_2 reported by Yanagida and co-workers.²

The dye molecule, the dopant and light irradiation intensity are main parameters that influence the *in-situ* PEP. Xia *et al.* reported the effect of dopant anions on PEDOT in ss-DSSCs,^{3,4} bistrifluoromethanesulfonylimide (TFSI^- or $\text{N}(\text{CF}_2\text{SO}_2)_2^-$) was found more suitable than commonly used ClO_4^- as dopant anions in the conversion efficiency of PEDOT-based ss-DSSC for its excellent charge transfer between PEDOT/ TFSI^- and TiO_2 /dye for the unidirectional electron flow required in an iodine-free ss-DSSC. In 2013, Park and coworkers investigated dye-sensitized solar cells (DSSCs) based on PEDOT prepared by photo-electrochemical polymer deposition under light of different intensities.⁵ In comparison with solar cells under 0.3 sun, ss-DSSCs based on 0.1 sun exhibits higher efficiencies. It was concluded that both conductivity and mobility were higher for the solar cell with PEDOT prepared under low light intensity. This result was used to explain the faster charge transport and longer lifetime of the charges compared to the solar cells with PEDOT prepared at higher light intensity. Therefore, 0.1 sun is applied in this work to obtain higher conductive PEDOT.

2. Experimental details

2.1. Dye synthesis

For details, see the synthetic strategy and results described in chapter 2.

2.2. Techniques used for the characterization of dye structures and Dye-sensitized TiO₂ substrates

The chemical structures of the new dyes are elucidated by:

¹H NMR measured on a Bruker AVANCE III 400 MHz NMR spectrometer using CDCl₃ or DMSO as solvent and chemical shifts were reported as δ (ppm) values.

High resolution mass spectrum (HRMS) was measured with Waters LCT Premier Mass Spectrometer in the Small Molecule Mass Spectrometry platform of ICSN.

The optical properties of dyes were investigated by fluorescence spectroscopy in acetonitrile ($C=4 \times 10^{-6}$ M), by UV-Vis spectroscopy in DCM ($C=2 \times 10^{-5}$ M). These experimental results were compared to the theoretical results obtained using the DFT.

The electrochemical properties of **ZJX4015**, **ZJX4041**, and **L1** dyes are investigated by cyclic voltammetry (CV) in acetonitrile containing 0.1 M LiClO₄. The measurements were carried out using a Biologic P150 potentiostat/galvostat. To measure UV-Vis-NIR absorption spectra in solid state, dye-sensitized TiO₂ electrodes, with and without PEDOT are prepared. The measurements were performed on a Cary 5000 UV-Vis-NIR spectrophotometer (VARIAN, photometric accuracy is ≤ 0.00025 Abs., photometric range is 8 Abs.). The TiO₂/FTO substrate signal was used as calibration background.

The *in-situ* PEP process was carried out by chronoamperometry (see the experimental section below) in organic medium using bis-EDOT as monomer precursor. ss-DSSCs are assembled following the procedure detailed in the following. The photovoltaic performances of ss-DSSCs are determined from the I-V curves and from Electrochemical Impedance Spectroscopy (EIS) measurements.

2.3. Cell assembly (Fabrication process of ss-DSSCs)

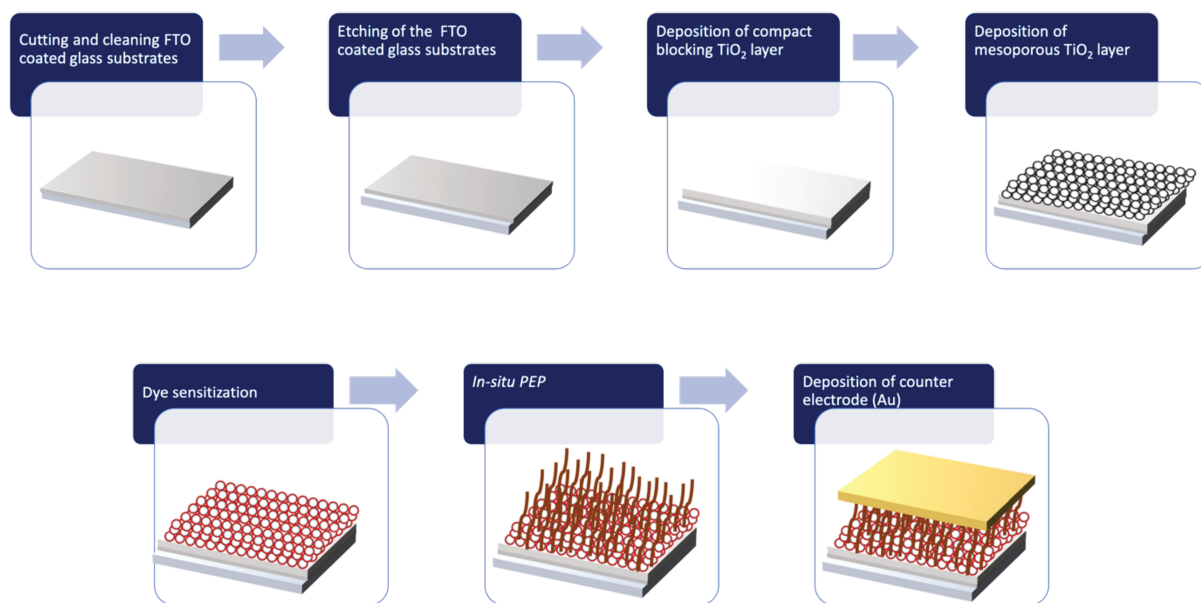


Figure 4.3 ss-DSSC fabrication process demonstration.

The commercially available FTO coated glass substrates (15W/sq) were cut into appropriate shape and size and then etched to form electrodes with desired pattern.

The compact TiO₂ blocking layer was prepared by spray pyrolysis with a solution that contains TiO₂ precursors: 0.2 M of titanium isopropoxide and 2 M of acetylacetonate in isopropanol. The thickness of blocking layer measured by profilometer is around 100 nm, which is in agreement with results revealed by SEM. The conductivity of these substrates was studied by CV proving the blocking character of this compact layer deposited.

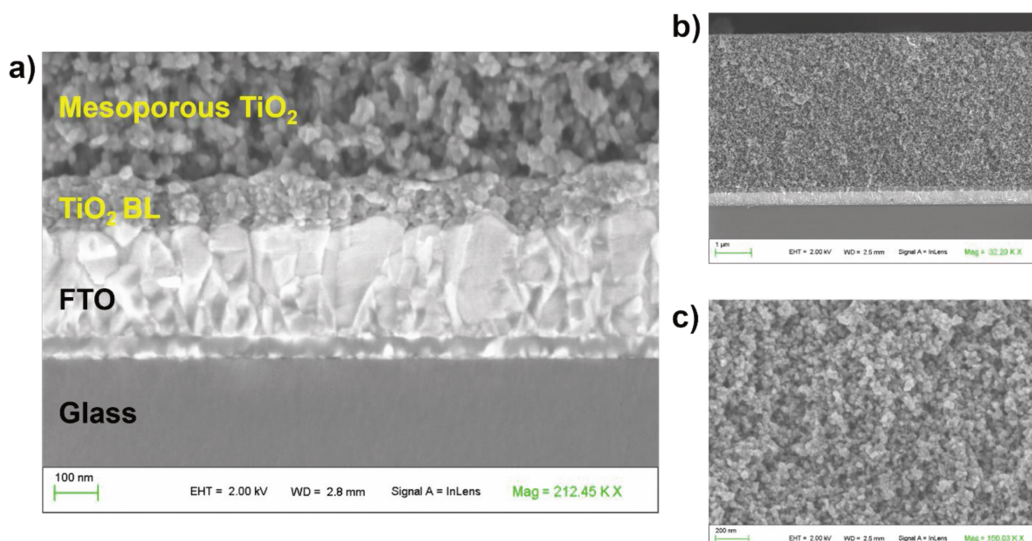


Figure 4.4 Cross sectional SEM views of TiO₂ (blocking layer + mesoporous layer) deposited on the FTO substrate (a) with 100 μm scale bar (b) with 1 μm scale bar. And (c) top-view of the mesoporous TiO₂ layer.

Figure was adapted from reference 3.

The mesoporous layer of TiO₂ was prepared by doctor blade technique with a colloidal paste of TiO₂. The film is made up of TiO₂ nanoparticles of 20 nm in diameter with the thickness of 6-7 nm, characterized by profilometer, SEM, and XRD (Figure 4.4).⁶

The TiO₂ electrodes were firstly cleaned with acetone, dried, then heated up to 350°C and kept at 350 °C for 10 minutes before left cooling down to 50 °C. Immersed in the dye solution of 0.2 mM in DCM overnight, the electrodes were rinsed with DCM and acetonitrile in order to remove the excess of dye molecules physically adsorbed and dried by a gentle flow of nitrogen.

With dye sensitized TiO₂ electrode as working electrode, Ag/AgCl (3.0 M KCl) as the reference electrode and stainless-steel grid as the counter electrode, the polymer was fabricated under *in-situ* PEP in an electrochemical cell. The potentiostatic approach is applied in a solution of 10 mM bis-EDOT and 0.1 M LiTFSI in acetonitrile with 0.2 V (vs. Ag/AgCl). The back side of the working electrode was exposed to white light of 0.1 sun until the total charge of photoelectrochemical polymerization achieves 20 mC.cm⁻². The dye sensitized TiO₂ electrodes with co-polymer were then washed with acetonitrile and dried with nitrogen flow with care.

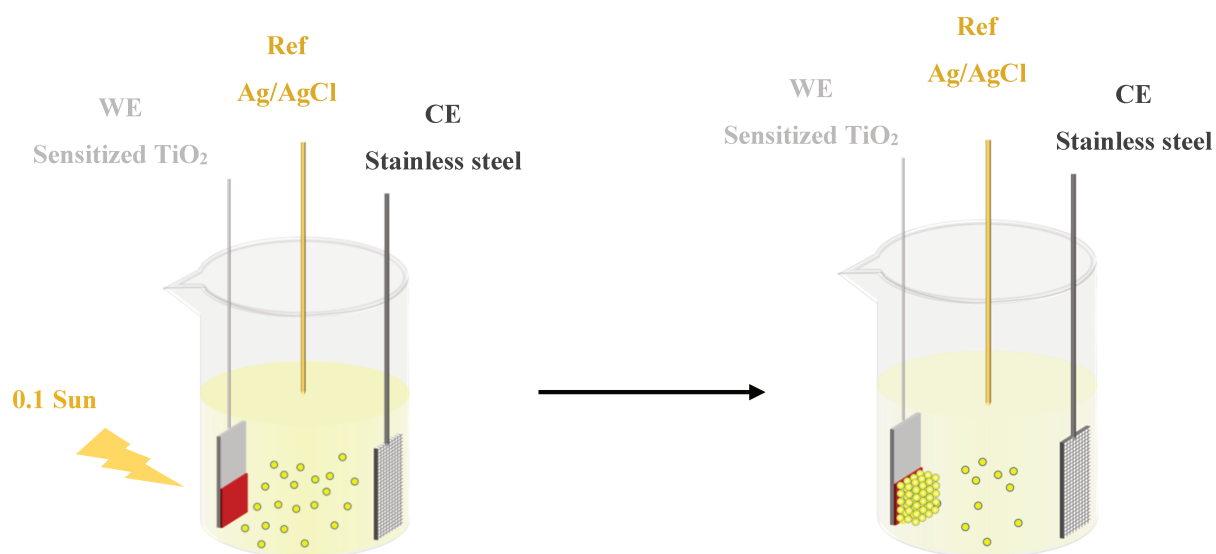


Figure 4.5 Demonstration of the working principle of in-situ PEP process.

The TiO₂ electrode was spin coated with an ionic liquid additive composed of *t*BP:LiTFSI (5:1) in acetonitrile. On top of the PEDOT layer, a gold counter electrode of 200 nm was deposited by thermal evaporation under the pressure around 10⁻⁷ mbar with controlled coating rate in a vacuum chamber.

3. Results and Discussion

3.1. Optical Properties of the dyes

The UV-Vis absorption spectra of dyes in Figure 4.6 were measured in DCM ($c = 2 \times 10^{-5} \text{M}$ for both dyes) over a range of 250 to 600 nm. Generally, the absorption bands of dyes in the UV region are assigned to the $\pi\text{-}\pi^*$ transition of the conjugated system, whereas the absorption bands in the visible region are attributed to the intramolecular charge transfer (ICT) in D- π -A systems⁷⁻¹⁰. The visible spectrum of **L1** shows a maximum absorption band at $\lambda = 430 \text{ nm}$ ($\epsilon = 23300 \text{ M}^{-1}\cdot\text{cm}^{-1}$), which is assigned to intramolecular charge transfer (ICT) from the TPA to the cyanoacrylic acid acceptor. The same ICT absorption band for **ZJX4015** is observed at $\lambda = 443 \text{ nm}$ ($\epsilon = 13450 \text{ M}^{-1}\cdot\text{cm}^{-1}$), whereas it is observed at about $\lambda = 477 \text{ nm}$ ($\epsilon = 11900 \text{ M}^{-1}\cdot\text{cm}^{-1}$) for **ZJX4041** with the comparable molecular absorption coefficients for both dyes. In near UV region, **ZJX4015** dye shows an absorption maximum at $\lambda = 370 \text{ nm}$ with $\epsilon = 14660 \text{ M}^{-1}\cdot\text{cm}^{-1}$; whereas **ZJX4041** dye shows an absorption maximum at $\lambda = 372 \text{ nm}$ with $\epsilon = 27230 \text{ M}^{-1}\cdot\text{cm}^{-1}$ twice that of the first dye. This will result in more light harvesting effect and an

efficient PEP process for **ZJX4041** dye than for **ZJX4015** dye and probably more light conversion efficiency in DSSCs.

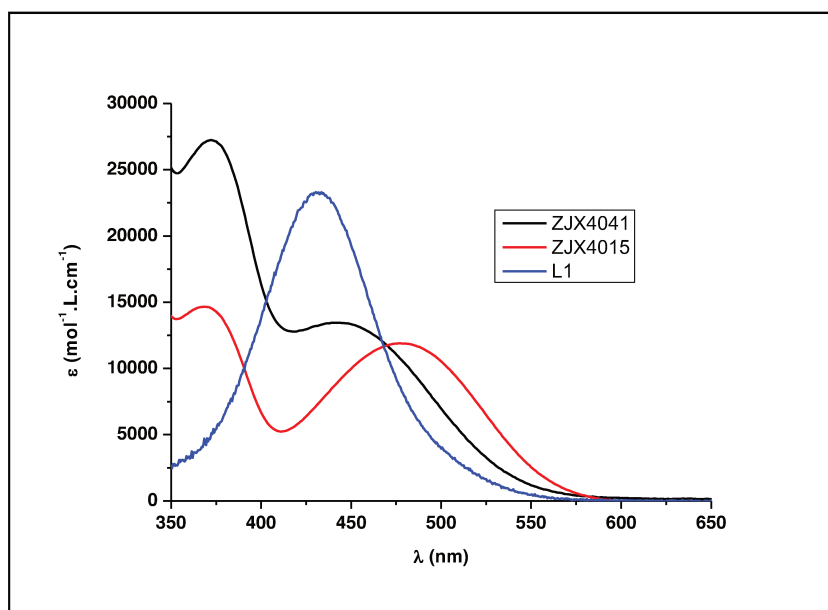


Figure 4.6 UV-Vis spectra of **ZJX4015** and **ZJX4041** dyes compared to the UV-Vis spectrum of L1 dye and carried out at $C = 2 \times 10^{-5} \text{M}$ in DCM.

3.2. Fluorescence spectra of the dyes

The excitation and emission spectra were recorded in the polar solvent dichloromethane (DCM) at $C = 4 \times 10^{-6} \text{M}$. Figure 4.7 shows the obtained spectra for the three dyes. These measurements provide information on E_{0-0} which corresponds to the HOMO-LUMO frontier orbital bandgaps of the dyes. For each dye, the bandgap is determined from the intercept (λ_{int}) of the dye excitation and emission spectra and is calculated as follows.

$$E_{0-0} (eV) = \frac{1240}{\lambda_{int}}$$

The HOMO is determined through electrochemical measurements on dye in solution, from the potential value at the current onset of the oxidation wave of the dye,¹¹⁻¹⁴

$$E_{HOMO} = -(E_{ref}^{SHE} + E_{abs}^{SHE} + E_{onset,ox vs.ref})$$

where E_{ref}^{SHE} is the potential of the reference electrode (in V) with respect to the reference electrode, $E_{Ag/AgCl}^{SHE} = 0.21 \text{V}$ with Ag/AgCl as reference; E_{abs}^{SHE} is the absolute potential (in eV) of the standard hydrogen electrode at 298K and $E_{abs}^{SHE} = 4.44 \text{eV}$ according to Trasatti;¹⁵ and $E_{onset,ox vs.ref}$ is the onset oxidation potential (in V) with respect to the reference electrode.

As a consequence, the LUMO level is calculated from following equation:

$$E_{LUMO} = E_{HOMO} - E_{0-0}$$

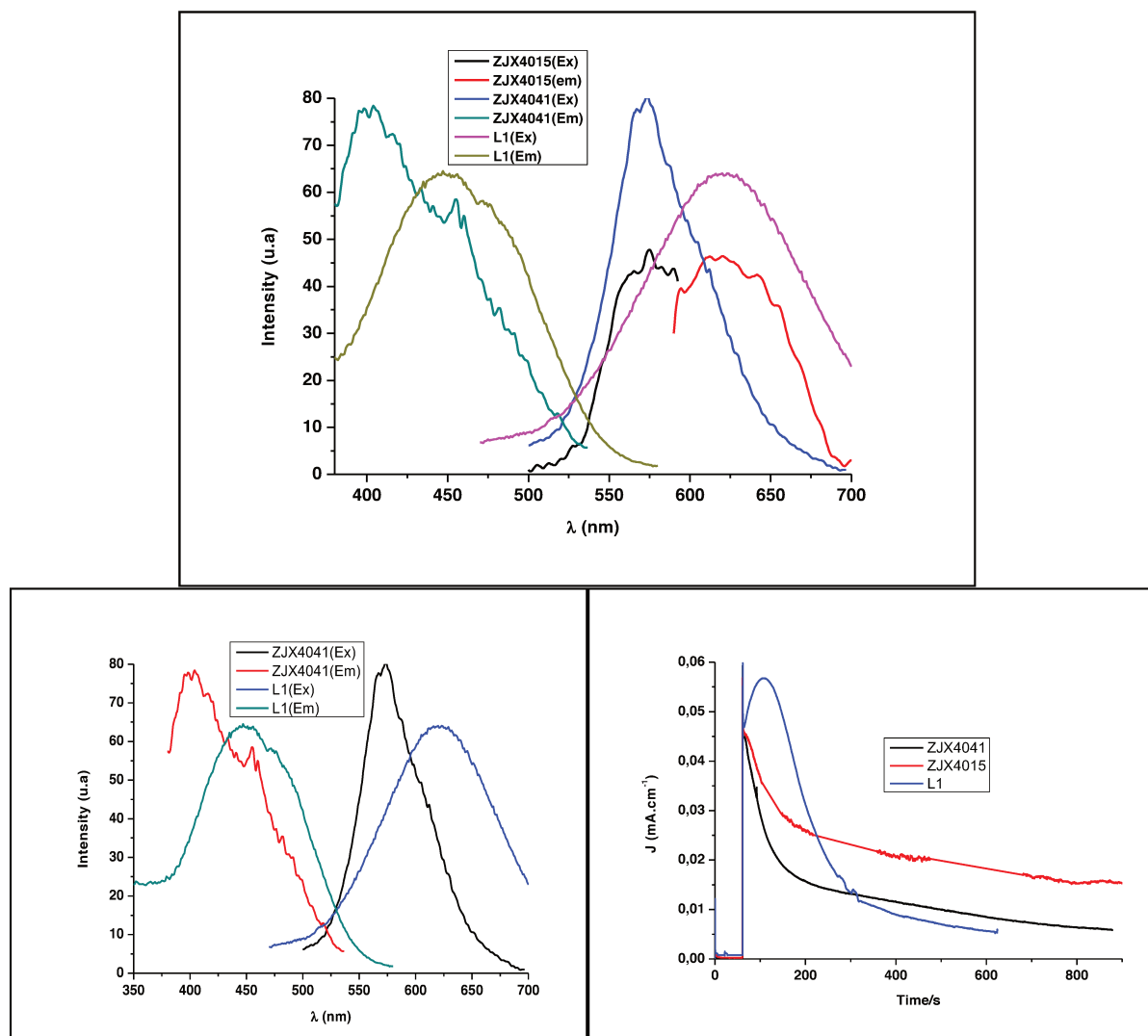


Figure 4.7 Excitation and fluorescence curves obtained from DCM solution of the dyes at 4×10^{-6} M.

3.3. Electrochemical properties of the dyes

The cyclic voltammetry curves carried out on dye sensitized TiO_2 electrodes are presented in Figure 4.8 compared to the CV carried out on TiO_2 electrode without adsorbed dye (blank) and also to the CV carried in organic bis-EDOT solution on TiO_2 electrode without blocking layer. Depending on the stability of the radical cation produced after the electron transfer when the dye oxidation occurs, the CVs may display reversible or irreversible redox behavior of each dye. The CVs show a reversible behavior of **L1** which corresponds to the oxidation and the reduction of the TPA moiety when only the thiophene linker and cyanoacrylic acid acceptor are present on this TPA moiety. The CVs of both dyes **ZJX4041** and **ZJX4015** show an

oxidation wave with a very small current for the reduction wave. This indicates that the carbazole moiety in both dyes undergoes irreversible oxidation reaction which is suitable for *in-situ* photopolymerization. The small reduction current probably corresponds to the reversible redox reaction of the TPA core.

Besides, since the HOMO energy is determined from the onset of the oxidation potential ($E_{\text{onset,ox}}$),^{11,13,14} the CVs show an $E_{\text{onset,ox}}$ at 0.830 V vs. Ag/AgCl for **L1** dye, which is the highest onset oxidation potential with a corresponding HOMO energy of $E_{\text{HOMO,L1}} = -5.29$ eV. The $E_{\text{onset,ox}}$ is located at 0.800 V vs. Ag/AgCl for **ZJX4015** and at 0.720 V vs. Ag/AgCl for **ZJX4041** corresponding to $E_{\text{HOMO}} = -5.27$ eV for **ZJX4015** and to $E_{\text{HOMO}} = -5.24$ eV for **ZJX4041**. These low values highlight the importance of the carbazole donor substituent on the TPA core in decreasing $E_{\text{onset,ox}}$ of both dyes **ZJX4015** and **ZJX4041**. It is necessary to outline that, to achieve correct PEP process on dye TiO₂ modified electrodes, the $E_{\text{onset,ox}}$ values of the dyes must be higher than the bis-EDOT monomer oxidation potential in order to allow its oxidation. Both CVs show that this is still the case for both dyes in organic solvent with $E_{\text{onset,ox}}$ (bis-EDOT) = 0.57 V.

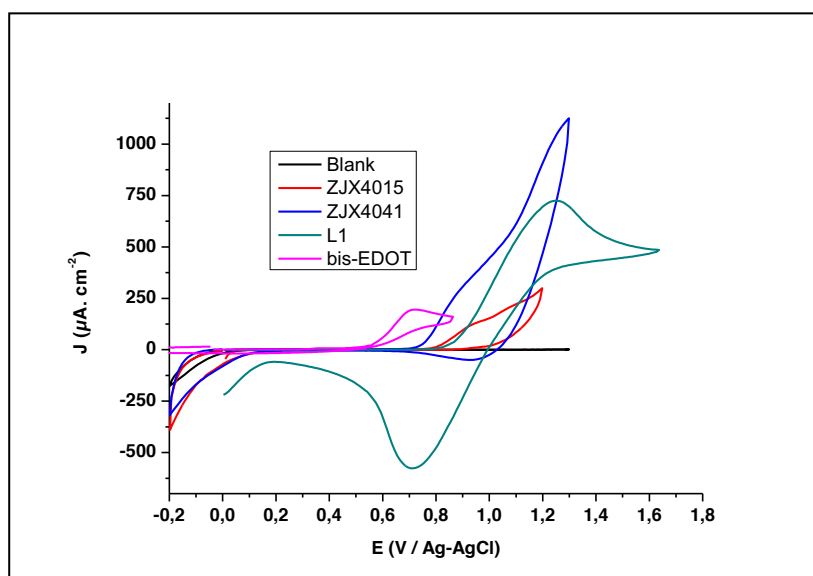


Figure 4.8 Cyclic voltammograms of dye sensitized TiO₂ electrodes carried out in acetonitrile.

Table of photophysical properties

The corresponding absorption and emission data, as well as thermodynamic parameters obtained from electrochemical measurements, are listed in Table 4.1:

Table 4.1 photo physical parameters of new dyes compared to the parameters of **L1** dye.

Dye	$\lambda_{\text{max, abs}}$ (nm)	ϵ_{max} ($\text{M}^{-1} \cdot \text{cm}^{-1}$)	$E_{\text{onset ox}}$ (V vs. Ag/AgCl)	HOMO (eV)	LUMO (eV)	E_{0-0} (eV)	λ_{int} (nm)
L1	432	23300	0,830	-5,29	-2,95	2,34	530
ZJX4015	370	14660	0,800	-5,27	-3,18	2,09	593
	443	31400					
ZJX4041	372	27230	0,720	-5,24	-2,86	2,38	520
	477	25000					

3.4. *In-situ* PEP deposition of PEDOT on the Dye Sensitized TiO₂ Photoanodes

Figure 4.9 presents the chrono-amperograms (CAs) obtained from PEP processes carried on dye-modified TiO₂ working electrodes. The CAs clearly show light-induced current. Indeed, when the light is off, the curves show zero current, whereas a high current is observed when light is on.

All the CAs show a high transient current at first followed by a plateau and the transient current of **L1** is higher than that observed for both **ZJX4015** and **ZJX4041** dyes. This may be due to:

- i) the high amount of dye adsorbed on TiO₂ nanomaterial which very often results in high transient current. The **L1** dye may lead to stacked molecules at the TPA core when adsorbed on TiO₂ nanomaterial surface, since there is no side chain which hinder this phenomenon,
- ii) and the higher onset oxidation potential of the **L1** dye compared to the onset oxidation potential of both **ZJX4015** and **ZJX4041** dyes.

The current plateau during PEP represents the regular polymer formation process after nucleation on the electrode surface. The current plateau decreases from **ZJX4015** which represents the highest plateau to **ZJX4041** and to **L1**, which shows the lowest current plateau. This indicates that the polymer formed is more regular for **ZJX4015** and less regular from **ZJX4041** to **L1**. It must be outlined that, when electropolymerization of organic monomers is carried out in organic solution on conducting surfaces, a low transient current and a more regular plateau generally leads to more conductive films. Since a high transient current is equivalent to high oxidation potential leading to over-oxidation of the polymer film, even though the working electrode potential is fixed at 0.2 V vs Ag/AgCl, and the driving force for the PEP process is the potential supplied by the dye. The fact that the plateau is higher for **ZJX4015** than for **ZJX4041** may result from a more important amount of **ZJX4015** dye than the amount of **ZJX4041** dye adsorbed on the surface of TiO₂. This is coherent with the hexyl side chain on **ZJX4041** which may hinder the stack of the dye and results in less dye amount adsorbed.

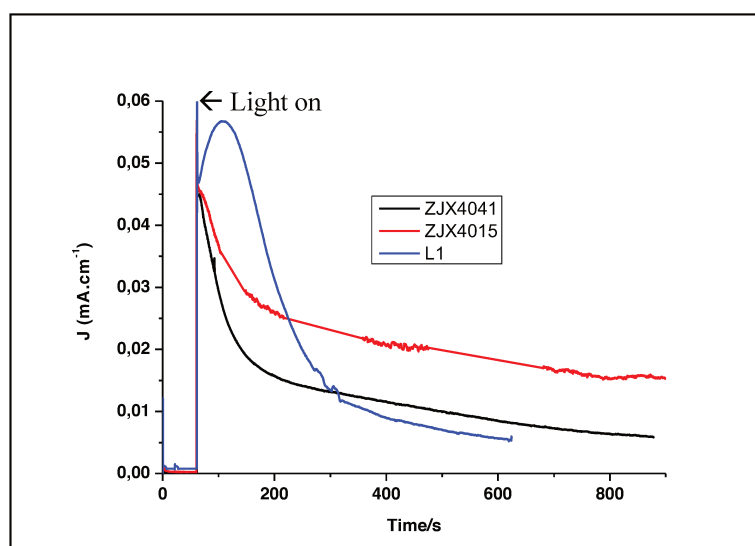


Figure 4.9 chrono-amperograms (CAs) obtained from PEP processes carried on dye-modified TiO₂ working electrodes with bis-EDOT in CAN containing 0.1 M LiTFSi in dark and then under 0.1 sun under a potential of 0.20 V vs. Ag/AgCl.

4. DSSCs devices

4.1. Photovoltaic Parameters

The photovoltaic performances of FTO/TiO₂/Dye/PEDOT/Au cells obtained for each dye are listed in Table 4.2.

A minimum of 3 cells have been performed using each dye and the table presents the results of cells that show the highest performances. To support the pertinence of the claim concerning

each dye, the average of the performances of the cells based on each dye is also listed in the same table. This average value depends on several parameters, which are not related to the dye structures but depend on the cell's fabrication process. Indeed, in order to minimize these differences, all the cells were performed using a unique starting FTO modified glass wafer. The process consists to deposit TiO₂ blocking layer and TiO₂ nano porous material using the same conditions as well as the dye soaking time for adsorption and the same thickness of deposited polymer layer. Nevertheless, some differences between the obtained photo-electrodes inevitably remain even if the process applied is the same.

The results in Table 4.2 show very interesting results obtained with ss-DSSCs using each of the dyes. Indeed, one important result is that under the same conditions, the efficiency of the ss-DSSCs based on each dye is largely higher than efficiency of ss-DSSCs based on **L1** dye. These results already allow to claim clearly and easily that the strategy proposed to remove the physical interface by establishing a covalent bond between the dye and the HTM in order to decrease the energy barrier of charge transfer between both components is even more topical.¹⁶⁻
¹⁸ This has been already demonstrated by the work described in the PhD thesis of Annette Délices from the laboratory,⁶ and our results confirm this statement. Furthermore, we can also state obviously that changing the ester group by an alkyl chain in the two new synthesized metal-free organic dyes leads to a better result in ss-DSSCs efficiency. Indeed, the efficiency obtained in previous results of the group when the dye and the HTM are linked by an ester group,⁶ is lower than those obtained in our case where the linker corresponds to an alkyl chain. The highest efficiency obtained using each of the new dyes containing alkyl chain, is undoubtedly due to the less electron back transfer from the TiO₂ nanoporous materials to the dye which occurs via the oxygen atoms when the ester groups is present in the starting dye molecule.

Another interesting result must be outlined which corresponds to the efficiency differences between the ss-DSSCs based on the new dyes. In fact, the efficiency obtained for ss-DSSCs based on **ZJX4041** dye are a little higher than those obtained for ss-DSSCs based on **ZJX4015** dye. This efficiency improvement is only due to the structure difference between the two dyes since all the devices elaboration procedure is identical except this molecular structure difference corresponding to the replacement of the hydrogen atom in the third position of the thiophene ring in the structure of **ZJX4015** dye by one hexyl side chain in **ZJX4041** dye. This idea has already been proposed by several authors.¹⁹ For example, Ito and co-workers developed an efficient indoline dye with a rhodanine framework substituted with *n*-octyl to

suppress the dye π -stacked aggregation on the semiconductor surface and obtained a 9.5% efficiency.²⁰ Moreover, endowing the sensitizer with an octyl chain can effectively suppress electron recombination between electrons in the conduction band of TiO₂ and electrolyte, resulting in higher open-circuit voltage and short-circuit current.²¹ Dyes in Figure 4.10 are two examples of the molecular optimization with alkyl chains.²² The introduction of long alkyl chains into thiophene π -bridge of dyes in Figure 4.10 can enhance the tolerance toward water in the electrolytes. A 139-based DSC with volatile electrolyte yielded an overall conversion efficiency of 8.6%, whereas the conversion efficiency of the same sensitizer-based DSC with a solvent-free ionic-liquid electrolyte was 7% under AM 1.5 G. Remarkably, the solar cells based on these dyes fabricated using a solvent-free ionic-liquid electrolyte exhibited an excellent stability under light soaking at 60 °C for 1000 h. Also, the introduction of long alkyl chains into dimethylfluorenylamino units can improve the photovoltaic performance and stability of the organic dyes.²³ This strategy is valid with structures of new dyes even though the resulting conducting polymer (used as HTM) is linked to the dye.

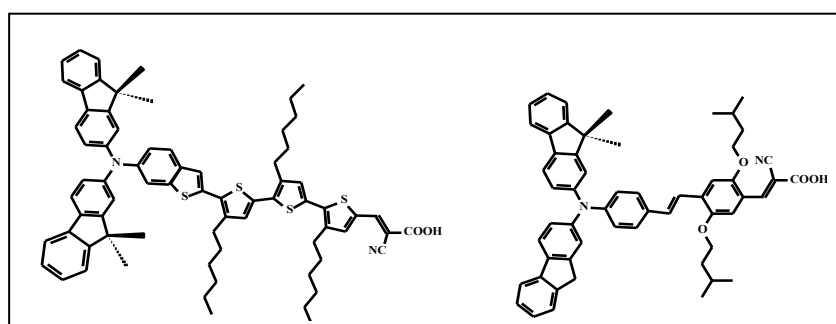


Figure 4.10 Molecular structure of dyes with alkyl chains **JK-45** and **JK-46**.

The data obtained just after cells preparation and results obtained three months later on the same cells are presented in Table 4.2. We can observe that the efficiency of the cells obtained 3 months later is much higher than those obtained just after cells preparation. This is a very interesting result, since aging of DSSCs is a very important issue and for example in cells based on I₃⁻/I⁻ as HTM, which suffer from electrolyte leakage problems, efficiency decreases very quickly with aging. Considering our DSSCs based on conducting polymers used as HTM, the improvement of the efficiency with aging could be due to the solvent evaporation over time. Indeed, when the polymer photo-deposition is carried out, the polymer layer contains enough solvent to enhance charge transfer in both directions at the two interfaces polymer/ dye and dye / TiO₂. This probably results in high electron back transfer from the TiO₂ nanoporous materials to the dye and to the polymer. As time goes by, solvent evaporation occurs in the HTM material

resulting in the decrease in charges transfer in both directions at the same interfaces. It is plausible that this solvent evaporation process is more favorable to prevent electron back transfer from the TiO₂ nanoporous materials to the dye and to the polymer, thus yielding higher efficiency in aged DSSCs.

We must outline that preliminary cells seem to be very stable, since after 6 years of age they show the same current and the same efficiency. The aging process of our ss-DSSCs is under study; because of efficiency improvement with aging is a good and happy surprise in DSSCs, but more time is necessary.

Table 4.2 Photovoltaic Parameters of ss-DSSCs based PEDOT produced in organic medium from bis-PEDOT illuminated 100 mW cm⁻² (AM 1.5G). For **L1** based ss-DSSCs, the results are from the previous study.⁶
Parameters measured a) 3 days after preparation. b) 3 months after preparation.

	ZJX4041			ZJX4015			L1
	Average		Maximum	Average		Maximum	
	a	b	selected	a	b	selected	b
V _{oc} (mV)	353	530	540	547	470	441	430
J _{sc} (mA/cm ²)	330	1554	1928	605	1660	1856	3.7
Fill Factor	36%	50.5%	46%	34%	40%	48%	57%
Efficiency η _c (%)	0.45%	4.07%	4.77%	1.12	3.09%	3.96%	0.91%

4.2. Electrochemical Impedance Spectroscopy

The electron-transfer processes at TiO₂/dye/HTM and HTM/counter electrode interfaces in the ss-DSSCs base on dyes **ZJX4015** and **ZJX4041** were analyzed by electrochemical impedance spectroscopy (EIS). The experiments were carried out under dark conditions and set at the V_{oc} of the cells: at -530 mV for **ZJX4041**-based device and at -440 mV for **ZJX4015**-based one.

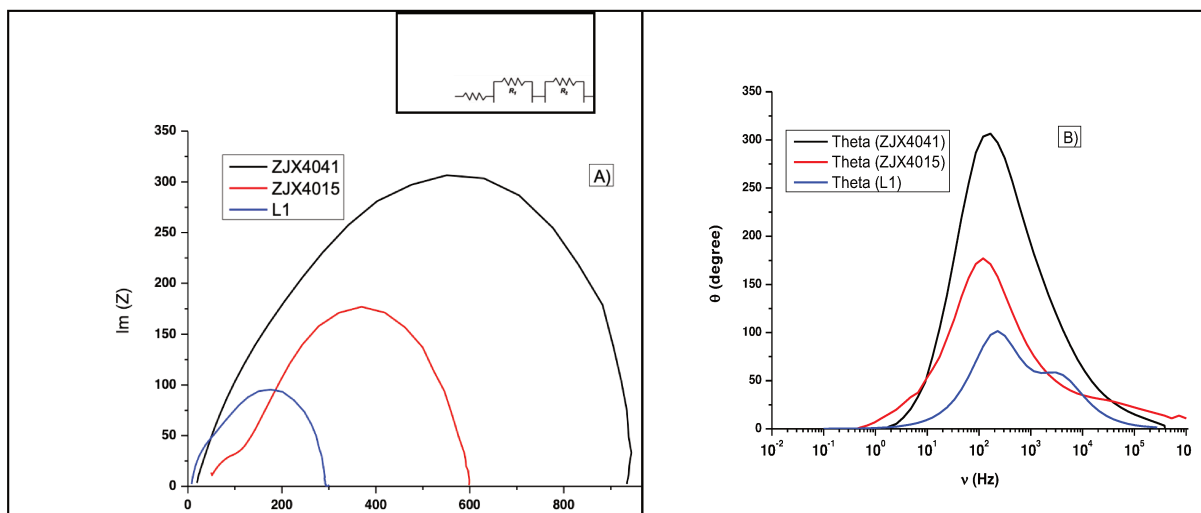


Figure 4.11 Electrochemical impedance spectra of L1 dye based ss-DSSC and of the new dyes based ss-DSSCs. (a) Nyquist plots; (b) Fitted Bode phase plots.

Figure 4.11 (a) shows the Nyquist plot and (b) shows the fitted Bode phase angle for **L1** and the new dyes-based devices. The equivalent circuit used to fit the experimental impedance spectra of both devices consists of two RC circuits connected in series with a resistance also in series, and their corresponding fitting data are summarized in Table 4.3. R_0 , which refers to the intercept of the curve with the real axis in the high-frequency region, describes the resistance of the TiO_2 blocking layer.^{24,25} In the devices based on the new dyes, R_0 is a little higher than that obtained for **L1**-based device.

These differences are attributed to the difference in TiO_2 layer thickness in the handmade devices. What we can conclude is that the device based on **ZJX4041** is thicker than the one based on **ZJX4015** dye which is thicker than that based on **L1** dye. The semicircles observed in the operating frequency ranging from 0.1 Hz to 300 kHz for all the devices are very different (Figure 4.11). Indeed, the semicircle of **ZJX4041**-based device is larger than that of **L1**-based one which is larger than that of **ZJX4015**-based ss-DSSC. The first semicircle at higher frequencies (10^3 - 3×10^5 Hz) is described by the charge-transfer resistance (R_1) attributed to charge-transfer processes occurring at the Au/HTM interface, and the second semicircle (R_2) in frequency region 1- 10^3 Hz refers to the charge-transfer process at FTO- TiO_2 /dye/HTM interface.

For **ZJX4015** and **ZJX4041**, the obtained hole transporting material (PEDOT) corresponds to a bis-PEDOT/carbazole copolymer. In these two devices, a little better conducting PEDOT is observed corresponding to a little low resistances R_1 . Indeed, in Figure 4.9 both new dyes show a high starting current followed by a relatively slow decrease. If one can agree that the overall

resistances values obtained for the two dyes are comparable, the resistance value R1 for the **ZJX4041** based device showed in table 4.3 is a little higher than that of **ZJX4015** based device as showed in table 4.3, this was expected since the current decrease (Figure 4.9) is more important when **ZJX4041** dye is used which indicates that a more resistive film is obtained with this dye in PEP process. Nevertheless, the fact that the resistance value R1 is a little higher for **ZJX4041**-based device than that obtained for **ZJX4015** dye based one is intriguing. Indeed, the PCE of the latter device is lower (3.96%) than the PCE for the **ZJX4015**-based device (4.77%). These contradictory results may be explained by the luminescence results which indicate that the excited state of dye **ZJX4015** may decrease through non-radiative decay. This non-radiative decay is harmful for the device light conversion efficiency when it is a possible decay, and it is equivalent to a back electron transfer from the TiO₂ to the excited dye. This reduces relatively the efficiency of the device based on this dye.

The results obtained in the frequency region 1 to 10³ Hz correspond to the measured resistance R₂ value attributed to FTO-TiO₂/dye/HTM interface, and the R₂ value for devices based on the new dyes are a little different and correspond to (518 Ω) for **ZJX4015** and (715 Ω) for **ZJX4041**. These results indicate that the charge transfer at the FTO-TiO₂/dye/HTM interface is a little efficient in the device based on **ZJX4041** dye than that based on **ZJX4015** dye. Again, we can think that the aggregation phenomenon of **ZJX4015** dye may lead to a relative decrease of the resistance of the device based on this dye when compared to that of the device based on **ZJX4041** dye. But this aggregation increases the back electron transfer and may decrease the photo-conversion efficiency of the ss-DSSC based on **ZJX4015** dye.

Table 4.3 Parameters Obtained by Fitting the Impedance Spectra of PEDOT/DSCs Shown in Figure 4.11 Using the Equivalent Circuit

Dye	R ₀ Ohm	R ₁ Ohm	C ₁ /F	R ₂ Ohm	C ₂ /F
L1	9	192	3.90 x 10 ⁻⁶	93	0.45 x 10 ⁻⁶
ZJX4041	26	156	0.280 x 10 ⁻⁶	715	1.143 x 10 ⁻⁶
ZJX4015	55	101	0.165 10 ⁻⁶	428	3.181 x 10 ⁻⁶

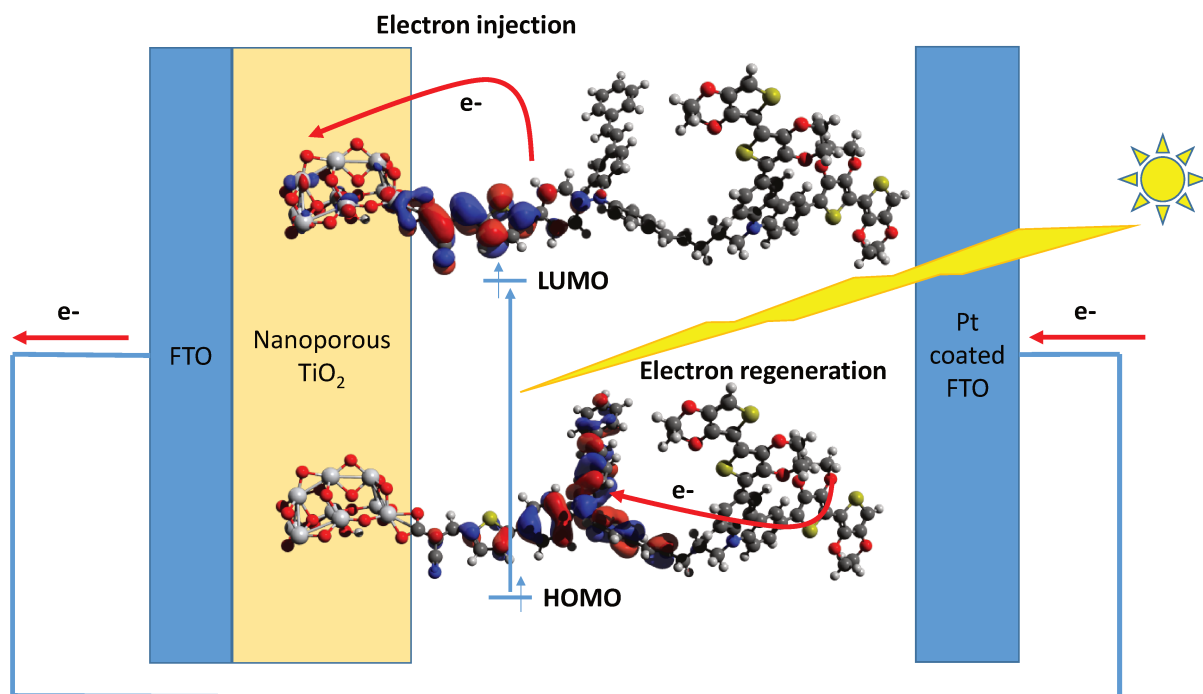
References

- (1) Zhang, J.; Vlachopoulos, N.; Jouini, M.; Johansson, M. B.; Zhang, X.; Nazeeruddin, M. K.; Boschloo, G.; Johansson, E. M. J.; Hagfeldt, A. Efficient Solid-State Dye Sensitized Solar Cells: The Influence of Dye Molecular Structures for the in-Situ Photoelectrochemically Polymerized PEDOT as Hole Transporting Material. *Nano Energy* **2016**, *19*, 455–470. <https://doi.org/10.1016/j.nanoen.2015.09.010>.
- (2) Saito, Y. Solid State Dye Sensitized Solar Cells Using in Situ Polymerized PEDOTs as Hole Conductor. *Electrochem. Commun.* **2004**, *6* (1), 71–74. <https://doi.org/10.1016/j.elecom.2003.10.016>.
- (3) Xia, J.; Masaki, N.; Lira-Cantu, M.; Kim, Y.; Jiang, K.; Yanagida, S. Effect of Doping Anions' Structures on Poly(3,4-Ethylenedioxythiophene) as Hole Conductors in Solid-State Dye-Sensitized Solar Cells. *J. Phys. Chem. C* **2008**, *112* (30), 11569–11574. <https://doi.org/10.1021/jp801878a>.
- (4) Xia, J.; Masaki, N.; Lira-Cantu, M.; Kim, Y.; Jiang, K.; Yanagida, S. Influence of Doped Anions on Poly(3,4-Ethylenedioxythiophene) as Hole Conductors for Iodine-Free Solid-State Dye-Sensitized Solar Cells. *J. Am. Chem. Soc.* **2008**, *130* (4), 1258–1263. <https://doi.org/10.1021/ja075704o>.
- (5) Park, B.; Yang, L.; Johansson, E. M. J.; Vlachopoulos, N.; Chams, A.; Perruchot, C.; Jouini, M.; Boschloo, G.; Hagfeldt, A. Neutral, Polaron, and Bipolaron States in PEDOT Prepared by Photoelectrochemical Polymerization and the Effect on Charge Generation Mechanism in the Solid-State Dye-Sensitized Solar Cell. *J. Phys. Chem. C* **2013**, *117* (44), 22484–22491. <https://doi.org/10.1021/jp406493v>.
- (6) Delices, A. Organized Organic Dye / Hole Transporting Materials for TiO₂- and ZnO- Based Solid-State Dye-Sensitized Solar Cells (s-DSSCs). These de doctorat, Sorbonne Paris Cité, 2017.
- (7) Lee, M.-W.; Kim, J.-Y.; Son, H. J.; Kim, J. Y.; Kim, B.; Kim, H.; Lee, D.-K.; Kim, K.; Lee, D.-H.; Ko, M. J. Tailoring of Energy Levels in D- π -A Organic Dyes via Fluorination of Acceptor Units for Efficient Dye-Sensitized Solar Cells. *Sci. Rep.* **2015**, *5* (1), 7711. <https://doi.org/10.1038/srep07711>.
- (8) Prachumrak, N.; Sudyoasuk, T.; Thangthong, A.; Nalaoh, P.; Jungsuttiwong, S.; Daengngern, R.; Namuangruk, S.; Pattanasattayavong, P.; Promarak, V. Improvement of D- π -A Organic Dye-Based Dye-Sensitized Solar Cell Performance by Simple Triphenylamine Donor Substitutions on the π -Linker of the Dye. *Mater. Chem. Front.* **2017**, *1* (6), 1059–1072. <https://doi.org/10.1039/C6QM00271D>.
- (9) Park, K.-W.; Serrano, L. A.; Ahn, S.; Baek, M. H.; Wiles, A. A.; Cooke, G.; Hong, J. An Investigation of the Role the Donor Moiety Plays in Modulating the Efficiency of 'Donor- π -Acceptor- π -Acceptor' Organic DSSCs. *Tetrahedron* **2017**, *73* (8), 1098–1104. <https://doi.org/10.1016/j.tet.2016.12.061>.

- (10) Duvva, N.; Kanaparthi, R. K.; Kandhadi, J.; Marotta, G.; Salvatori, P.; De Angelis, F.; Giribabu, L. Carbazole-Based Sensitizers for Potential Application to Dye Sensitized Solar Cells. *J. Chem. Sci.* **2015**, *127* (3), 383–394. <https://doi.org/10.1007/s12039-015-0794-1>.
- (11) Smestad, G. P.; Spiekermann, S.; Kowalik, J.; Grant, C. D.; Schwartzberg, A. M.; Zhang, J.; Tolbert, L. M.; Moons, E. A Technique to Compare Polythiophene Solid-State Dye Sensitized TiO₂ Solar Cells to Liquid Junction Devices. *Sol. Energy Mater. Sol. Cells* **2003**, *76* (1), 85–105. [https://doi.org/10.1016/S0927-0248\(02\)00252-0](https://doi.org/10.1016/S0927-0248(02)00252-0).
- (12) Cardona, C. M.; Li, W.; Kaifer, A. E.; Stockdale, D.; Bazan, G. C. Electrochemical Considerations for Determining Absolute Frontier Orbital Energy Levels of Conjugated Polymers for Solar Cell Applications. *Adv. Mater.* **2011**, *23* (20), 2367–2371. <https://doi.org/10.1002/adma.201004554>.
- (13) Kumara, N. T. R. N.; Ekanayake, P.; Lim, A.; Iskandar, M.; Ming, L. C. Study of the Enhancement of Cell Performance of Dye Sensitized Solar Cells Sensitized With Nephelium Lappaceum (F: Sapindaceae). *J. Sol. Energy Eng.* **2013**, *135* (3). <https://doi.org/10.1115/1.4023877>.
- (14) Leonat, L.; Sbarcea, G.; Branzoi, I. V. Cyclic Voltammetry for Energy Levels Estimation of Organic Materials. *UPB Sci Bull Ser. B* **2013**, *75* (3), 111–118.
- (15) Trasatti, S. The Absolute Electrode Potential: An Explanatory Note. In *IUPAC Standards Online*; De Gruyter: Berlin, Boston, 2016.
- (16) Houarner, C.; Blart, E.; Buvat, P.; Odobel, F. Ruthenium Bis-Terpyridine Complexes Connected to an Oligothiophene Unit for Dry Dye-Sensitised Solar Cells. *Photochem. Photobiol. Sci.* **2005**, *4* (2), 200. <https://doi.org/10.1039/b414031a>.
- (17) Houarner-Rassin, C.; Blart, E.; Buvat, P.; Odobel, F. Solid-State Dye-Sensitized TiO₂ Solar Cells Based on a Sensitizer Covalently Wired to a Hole Conducting Polymer. *Photochem. Photobiol. Sci.* **2008**, *7* (7), 789. <https://doi.org/10.1039/b715013j>.
- (18) Delices, A.; Zhang, J.; Santoni, M.-P.; Dong, C.-Z.; Maurel, F.; Vlachopoulos, N.; Hagfeldt, A.; Jouini, M. New Covalently Bonded Dye/Hole Transporting Material for Better Charge Transfer in Solid-State Dye-Sensitized Solar Cells. *Electrochimica Acta* **2018**, *269*, 163–171. <https://doi.org/10.1016/j.electacta.2018.02.119>.
- (19) Kroeze, J. E.; Hirata, N.; Koops, S.; Nazeeruddin, Md. K.; Schmidt-Mende, L.; Grätzel, M.; Durrant, J. R. Alkyl Chain Barriers for Kinetic Optimization in Dye-Sensitized Solar Cells. *J. Am. Chem. Soc.* **2006**, *128* (50), 16376–16383. <https://doi.org/10.1021/ja065653f>.

- (20) Ito, S.; Miura, H.; Uchida, S.; Takata, M.; Sumioka, K.; Liska, P.; Comte, P.; Péchy, P.; Grätzel, M. High-Conversion-Efficiency Organic Dye-Sensitized Solar Cells with a Novel Indoline Dye. *Chem. Commun.* **2008**, No. 41, 5194. <https://doi.org/10.1039/b809093a>.
- (21) Kuang, D.; Uchida, S.; Humphry-Baker, R.; Zakeeruddin, S. M.; Grätzel, M. Organic Dye-Sensitized Ionic Liquid Based Solar Cells: Remarkable Enhancement in Performance through Molecular Design of Indoline Sensitizers. *Angew. Chem. Int. Ed.* **2008**, *47* (10), 1923–1927. <https://doi.org/10.1002/anie.200705225>.
- (22) Choi, H.; Baik, C.; Kang, S. O.; Ko, J.; Kang, M.-S.; Nazeeruddin, Md. K.; Grätzel, M. Highly Efficient and Thermally Stable Organic Sensitizers for Solvent-Free Dye-Sensitized Solar Cells. *Angew. Chem. Int. Ed.* **2008**, *47* (2), 327–330. <https://doi.org/10.1002/anie.200703852>.
- (23) Kim, S.; Kim, D.; Choi, H.; Kang, M.-S.; Song, K.; Kang, S. O.; Ko, J. Enhanced Photovoltaic Performance and Long-Term Stability of Quasi-Solid-State Dye-Sensitized Solar Cells via Molecular Engineering. *Chem. Commun.* **2008**, No. 40, 4951. <https://doi.org/10.1039/b811401c>.
- (24) Han, L.; Koide, N.; Chiba, Y.; Mitate, T. Modeling of an Equivalent Circuit for Dye-Sensitized Solar Cells. *Appl. Phys. Lett.* **2004**, *84* (13), 2433–2435. <https://doi.org/10.1063/1.1690495>.
- (25) Yanagida, S.; Yu, Y.; Manseki, K. Iodine/Iodide-Free Dye-Sensitized Solar Cells. *Acc. Chem. Res.* **2009**, *42* (11), 1827–1838. <https://doi.org/10.1021/ar900069p>.
- (26) Zhang, J.; Ellis, H.; Yang, L.; Johansson, E. M. J.; Boschloo, G.; Vlachopoulos, N.; Hagfeldt, A.; Bergquist, J.; Shevchenko, D. Matrix-Assisted Laser Desorption/Ionization Mass Spectrometric Analysis of Poly(3,4-Ethylenedioxythiophene) in Solid-State Dye-Sensitized Solar Cells: Comparison of In Situ Photoelectrochemical Polymerization in Aqueous Micellar and Organic Media. *Anal. Chem.* **2015**, *87* (7), 3942–3948. <https://doi.org/10.1021/ac504851f>.

Chapter 5. Theoretical study of the organic TAA-based dyes: ZJX4015 and ZJX4041.



This chapter is concerned with the characterization of the two dyes **ZJX4015** and **ZJX4041** (see Figure 5.1). These two molecular systems are based on the triphenylamine unit carrying three groups with a well-defined role. The cyanoacrylic acid unit acts as an anchoring group on the semiconductor and the thiophene unit provides an additional conjugation to shift the absorption of triphenylamine in the visible region. The styryl group also adds an additional conjugation to shift the absorption of the triphenylamine core to the red region of the spectrum. Finally, the carbazole group linked to TPA via an alkyl chain is an active and polymerizable redox unit which serves as the precursor of the hole transporting moiety to regenerate the dye. It should be noted that the alkyl chain connecting the carbazole unit to the core of the dye has three carbons, which gives it a certain flexibility and enables different positions of the carbazole unit in space to be envisaged. This point will be analyzed and illustrated in the theoretical part. The properties of these two original dyes will be compared with those of the reference compound **L1**.

Along the experimental studies detailed in chapter 4, it appears that a fine understanding about the electronic structures and properties of the molecular dyes studied in the thesis of great importance to establish a structure-property relationship. For that purpose, theoretical calculations, especially quantum calculations based on the density functional theory (DFT) are useful to study the geometries, electronic structure, absorption and emission spectra and photovoltaic performances for organic dyes. The quantum chemical methods are become well used in the context of DSSCs can provide semi-quantitative information about the efficiency of sensitizers. Compared to experiment effort, computational chemistry methods are inexpensive alternative of synthesis methods. In this chapter we reported results obtained on the newly synthesized dyes using DFT and time dependent density functional theory (TD-DFT). Computational details are reported in supplementary materials.

As already explained in Chapter 2, the working principle of the DSSCs is based on light absorption in a dye anchored on TiO₂ anatase nanoparticles, followed by transfer of the photoelectron from the dye to the wide-bandgap semiconductor and through the transparent conducting oxide to the external load; at the counter electrode, the redox polymer should facilitate the transport of the electron back to the dye and the regeneration of the sensitizer, through reduction of the polymer at the counter electrode, followed by oxidation of the polymer by the dye. The efficiency of the photovoltaic device depends strongly upon the dye and the HTM in use.

Regarding the dye, the basic structure of most of the organic dye used in DSSCs is made of donor (D), bridge (a π spacer) and an acceptor (A) moieties. All these units are combined together through covalent bonds to ensure the overlap of π orbitals in the D- π -A configuration and to promote a photoinduced intra-molecular charge transfer (ICT). Therefore, the important factors that influence the sensitization of the photovoltaic cell are:

- i. A high harvesting ability of the dye to get a substantial photocurrent response, which is in connection with an intense absorption in the visible part of the spectrum.
- ii. The conjugation across the donor and acceptor determines the charge transfer (CT) character of the electronic transition in the visible region.
- iii. The excited state redox potential of the dye should match the energy of the conduction band (CB) edge of the semi-conductor.
- iv. The highest occupied molecular orbital (HOMO) must fit the HTM redox potential, and the lowest unoccupied orbital (LUMO) has to be higher in energy than the conduction band edge of the semiconductor.
- v. The electronic coupling strength between dye's LUMO and semiconductor CB is also a key property for an efficient electron injection from the dye onto the semiconductor surface. A strong adsorption to the semiconductor surface through anchoring groups is necessary. Furthermore, a fast charge transfer from the dye to the substrate, with low loss of photoelectrons is required.

In this context, quantum chemistry molecular techniques offer a competitive and alternative way for the understanding of the properties of the molecules. Density Functional Theory (DFT) is recognized as a well-established method of choice to study the electronic structure of organic dye while for UV/Vis calculations, the most popular approach employed remains the time-dependent Density functional Theory (TD-DFT) which provide accurate results with a reasonable computational effort. Furthermore, in the last years, considerable progress has been made to predict the excited state energy of large molecules with reasonable accuracies of a few tenths of an eV, allowing for the description not only of the absorption spectrum of the dye, but also of the more complex system consisting of the dye and the TiO₂ cluster. In this part we illustrate the applicability of the DFT and TD-DFT methods to study the synthesized dyes as free molecules and also ones adsorbed on TiO₂ clusters. The results will be compared to the reference **L1** dye for which similar DFT and TD-DFT calculations have been done. The structure of **L1** can be divided into the three basic components: TPA as donor, thiophene as linker and cyanoacrylic acid as acceptor. In both new dyes, the thiophene linker and

cianoacrylic acid acceptor groups of **L1** are maintained but the proton at 3-position on the thiophene ring is replaced by a hexadecyl alkyl chain in the structure of **ZJX4041** structure. Moreover, the TPA donor part is strongly modified with 1-pentene chain terminating by a carbazole and styryl group is added on the second phenyl group.

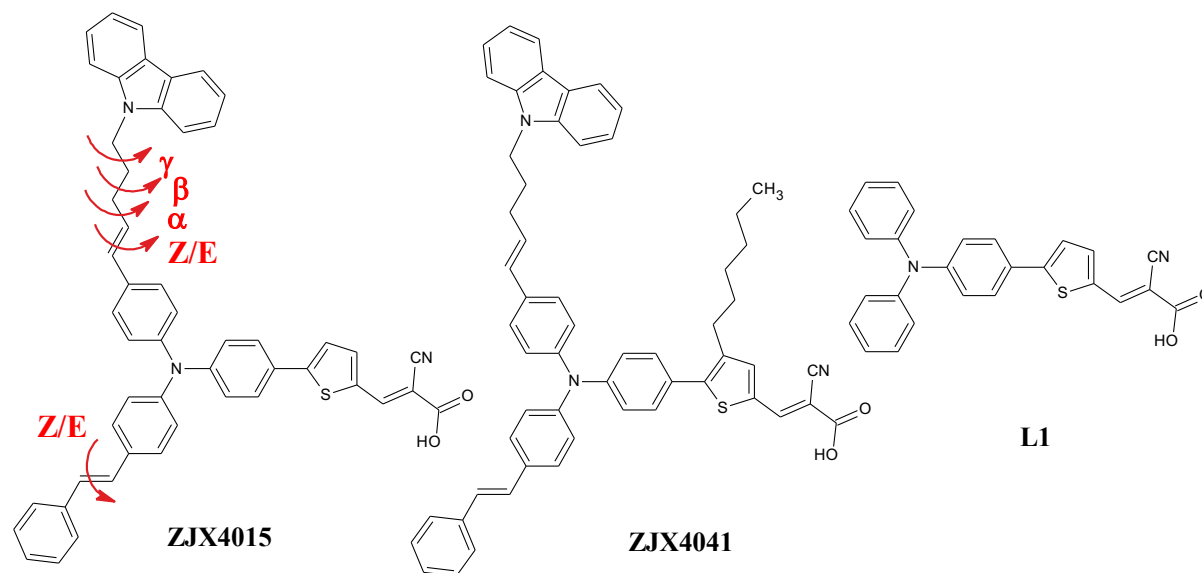


Figure 5.1 Structures of compounds **ZJX4015** and **ZJX4041** studied in this chapter.

The compound **ZJX4041** differs from **ZJX4015** by the addition of a 6-carbon alkyl chain to thiophene, which is an important structural element in preventing aggregation between dyes and thus limiting unwanted radiative de-excitation processes. Indeed, some research groups have demonstrated the interest of adding alkyl chain to improve the performance of organic cells¹⁻⁷.

I. Free Dyes **ZJX4015** and **ZJX4041**

In this part we aim at studying the geometric properties and electronic structures of the new synthesized compounds **ZJX4015** and **ZJX4041**. The well-known **L1** dye will also be discussed for comparison.

The new developed dyes **ZJX4015** and **ZJX4041** hold an important complexity related both to the stereochemistry and to the conformational flexibility. Indeed, each of the two ethylene bonds can be in E or Z configuration, leading to a number of 4 isomers hereafter noted EE, EZ, ZE or ZZ. The first letter indicates the configuration of the ethylene bond connecting the TPA with the carbazole moiety while the second is related to the styryl group. The alkyl chain

linking the TPA core and the carbazole unit is highly flexible due to three single bonds that leads to numerous stable conformations, each of it noted by the dihedral angle α , β and γ (see **Figure 5.2**).

1.1. Conformational properties of the C3 alkyl chain. Study of the ZJX4015 compound.

The **ZJX4015** compound is relatively flexible since it possesses three rotatable bonds between the carbazole and TPA groups (see the dihedral angles α , β , γ , in **Figure 5.1**). Considering the flexibility of the alkyl chain, numerous conformations are expected. However, a systematic conformational search represents a considerable task at the DFT level of calculations. Therefore, in order to inquire about conformational flexibility semi-empirical calculations using AM1 Hamiltonian were performed by varying the dihedral angles step by step. Seven conformers noted from A to G were found and then optimized at the highest DFT level of calculations. This study has been performed starting from the EE isomer of the **ZJX4015**.

The relative energies (in $\text{kJ}\cdot\text{mol}^{-1}$) as well as the values of the dihedral angles of the optimized conformers are listed in the **Table 5.1**. The optimized geometries calculated at the DFT level are displayed in **Figure 5.2**.

Table 5.1 Calculated conformer of the **ZJX4015** compound at the DFT level. Relative energies, E_{rel} , are given in $\text{kJ}\cdot\text{mol}^{-1}$ and dihedral angles are in degree.

Conformer	E_{rel}	Geometry (dihedral angles α , β et γ)		
		α	β	γ
1 A	25.7	-118.3	-178.4	179.7
2 B	11.4	-124.4	63.1	57.8
3 C	0.0	-62.3	-71.1	57.7
4 D	22.0	-118.9	-179.1	60.1
5 E	11.0	-124.5	-61.4	52.7
6 F	20.6	-93.0	-51.4	-46.5
7 G	20.9	-113.8	67.4	-173.7

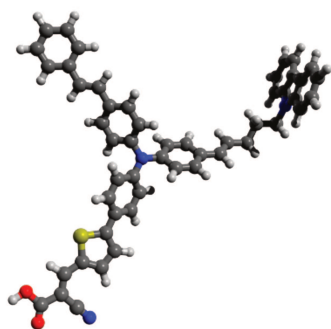
The seven conformations are ranging within 25 kJ.mol⁻¹ scale of energy suggesting that the dihedral angle in the different conformer is always different from 180 indicating the alkyl chain cannot adopt a completely *trans* arrangement.

In the most stable conformation, the carbazole unit is found above a phenyl of the TPA group with a separating distance of 3.4 Å. Such a distance is in agreement with π - π interaction between the aromatic rings.

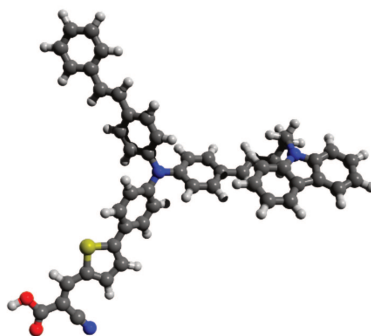
In the conformation the β and γ are always close to 180°, 120° or 60° which reflect a *trans* or *gauche* conformation.

Seven different conformations with relative energies ranging from 0 to more than 25.0 kJ.mol⁻¹ are obtained. For all these conformations, the dihedral angle α is between -62.3° and -124.4° which means that the carbazole-bearing moiety is not in the plane of the double bond. It can be seen that the most stable conformer has a folded structure with the carbazole unit above the phenyl group as shown in the figure below (Conformation C). The carbazole unit is approximately 3.4 Å above the phenyl of the TPA which is compatible with electron cloud interaction. The greatest stability of this conformer can therefore be interpreted as the establishment of a non-covalent interaction between the two. This interaction is sufficiently important to compensate for the destabilization induced by the *gauche* interactions on the links of the alkyl chain ($\alpha = -62,3^\circ$; $\beta = -71,1^\circ$ et $\gamma = 57,7^\circ$). The fully unfolded conformation, 1A (β and γ are close to 180°) is the most unstable of all conformations found, the other conformations differing by the orientation of the carbazole unit in space.

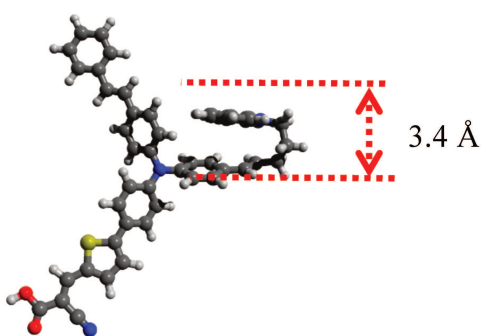
1A



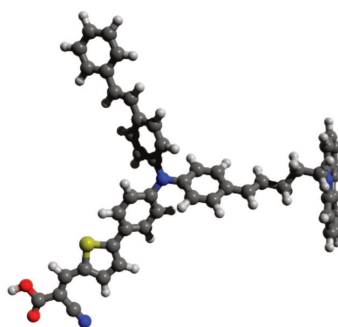
2B



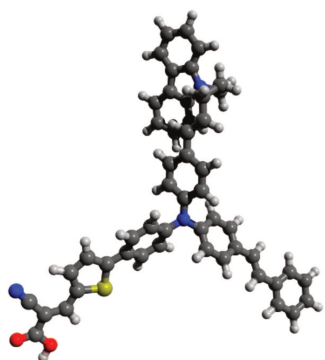
3C



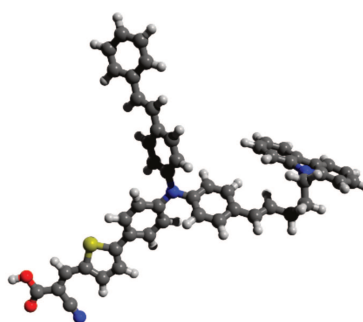
4D



5E



6F



7G

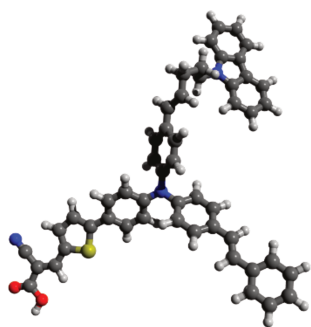


Figure 5.2 Optimized geometries of the conformers of ZJX4015 (EE configuration)

In order to study the impact of the flexibility of the alkyl chain on the electronic, optical and photovoltaic properties of the **ZJX4015** compound, we will focus on the conformer 1A and 3C in our following work, hereafter noted extended and folded, respectively.

1.2. Energies and geometries of the isomer of ZJX4015 and ZJX4041

The E to Z reaction can be obtained upon irradiation and it is well known that the photo-induced twisting around a double carbon-carbon bond is a fundamental photochemical process can be regarded as a typical motion in molecular machines. Our molecules, e.g., **ZJX4015** and **ZJX4041** holds two carbon-carbon double bond where E-Z reaction can occur: the stilbene moiety and the carbon-carbon double bond that link the phenyl group and the alkyl chain terminated by the carbazole unit. Therefore, it can be anticipated that four isomeric states can exist. It will be named with two letters (Z or E): the first letter indicates the configuration of the double bond of the stilbene part while the other letter refers to the other double bond, as mentioned above.

Energies

The previous study conducted on all the configuration isomeric conformers (EE, EZ, ZE and ZZ isomers) would be too long to carry out on the 3 other theoretically possible isomers (EZ, ZE and ZZ isomers). Therefore, in order to study all 4 stereoisomers and to compare them, we have limited the study to two borderline conformations by considering the extended arrangement of the C3 chain (extended noted conformation) and a folded arrangement (folded conformation).

The calculated energies of the stereoisomers are gathered in **Table 5.2**. The most stable stereoisomer is found to be EE while the less stable is ZZ. The relative energies of ZE and EZ isomers lie between those of EE and ZZ, with EZ being more stable in folded conformation while the reverse situation is found for the extended structure. It can be concluded that the E to Z isomerization induces a strong penalty of energy and only the EE isomer can be found at the room temperature and in ground state.

Therefore, considering the possibility to obtain a trans–cis photoisomerization, we studied the different isomers of the **ZJX4015** and **ZJX4041**. We restricted our study to the conformer A and C of each of these compounds. **Table 5.2**. Calculated relative energies (E_{rel} in $\text{kJ}\cdot\text{mol}^{-1}$) of the isomers of **ZJX4015** and **ZJX4041** compounds.

Table 5.2 Calculated relative energies (E_{rel} in $\text{kJ}\cdot\text{mol}^{-1}$) of the isomers of **ZJX4015** and **ZJX4041** compounds.

	Isomer	$\Delta E_{\text{rel}}(\text{kJ/mol})$	$\mu_{\text{S0}}(\text{Debye})$	HOMO (eV)	LUMO (eV)	$\mu_{\text{S1}}(\text{Debye})$
ZJX4015						
extended	EE	25.7	7.8	-5.655	-2.091	21.1
	ZZ	44.7	7.8	-5.735	-2.221	21.4
	EZ	38.0	9.4	-5.699	-2.210	22.7
	ZE	32.8	8.3	-5.684	-2.227	21.2
	DHP	165.7	7.8	-6.677	-1.052	
folded	EE	0.0	11.0	-5.662	-2.073	24.7
	ZZ	26.8	12.5	-5.658	-2.087	25.5
	EZ	6.6	11.7	-5.711	-2.053	25.3
	ZE	13.8	12.6	-5.614	-2.083	25.7
	Isomer	$\Delta E_{\text{rel}}(\text{kJ/mol})$	$\mu_{\text{S0}}(\text{Debye})$	HOMO (eV)	LUMO (eV)	$\mu_{\text{S1}}(\text{Debye})$

ZJX4041						
extended	EE	20.7	7.9	-5.665	-2.021	19.8
	ZZ	39.6	7.8	-5.754	-2.017	19.6
	EZ	33.0	9.5	-5.711	-2.017	21.4
	ZE	27.7	7.5	-5.741	-2.010	19.3
folded	EE	0		-5.648	-2.015	
	ZZ	25.7		-5.672	-2.025	
	EZ	7.3		-5.723	-1.997	
	ZE	13.4		-5.623	-2.025	

Note that in addition to the E/Z isomerization process, it has been showed in recent studies that photoisomerization of stilbene unit ca occur upon UV irradiation. Indeed, several studies undertaken on stilbene molecule showed that an excited electronic state with very short lifetime (nano-second) is created after *trans*-stilbene excitation. The deactivation of this excited state is due to crossing of a barrier along a reaction coordinate which is dominated by twisting around the ethylenic double bond. After the barrier, at about 90°twist angle is reached, a fast internal conversion leads to a mixture of *trans*- and *cis*-stilbene in the ground state with comparable yields. It could be noted that about 10% of the excited population rather forms 4a,4b-dihydrophenanthrene (DHP) where the two phenyl rings are linked⁸⁻¹¹ (known as the Mallory reaction). Furthermore, DHP can dehydrogenate to produce phenanthrene (PT) upon photoexcitation^{9,12-15}. We also calculated the dihydrophenanthrene (DHP) and phenanthrene (PT) products for the **ZJX4015**. The very high relative energy found for the DHP product ruled out its presence even after irradiation.

Table 5.3 Calculated geometries and relative energies (E_{rel} in kJ.mol⁻¹) of the isomers of ZJX4015 and ZJX4041 compounds. Results on L1 are also given for comparison.

Isomer	E _{rel}	φ ₁	φ ₂	φ ₃	φ ₄	φ ₅	d ₁	d ₂	d ₃	d ₄	d ₅
L1		-43.9	-31.1	-34.2	27.0	-2.9	1.465	1.381	1.406	1.384	1.432
ZJX4015											
extended											
EE	25.7	-46.0	-43.3	-33.6	29.0	-1.5	1.465	1.381	1.407	1.384	1.432
ZZ	44.7	-45.8	-44.2	-33.5	28.0	-1.7	1.465	1.382	1.406	1.384	1.432
EZ	38.0	-44.4	-45.0	-33.7	28.5	-1.4	1.465	1.381	1.406	1.384	1.431
ZE	32.8	-46.0	-43.3	-33.0	28.8	-1.3	1.465	1.381	1.407	1.384	1.432
folded											
EE	0.0	-54.6	-48.3	-30.9	25.2	-2.9	1.464	1.381	1.406	1.384	1.431
ZZ	26.8	-51.5	-34.7	-29.7	29.1	-0.3	1.465	1.381	1.406	1.384	1.432
EZ	6.6	-54.9	-53.9	-19.0	26.5	-3.2	1.464	1.382	1.406	1.385	1.431
ZE	13.8	-48.8	-40.9	-30.2	27.5	-3.1	1.465	1.381	1.407	1.384	1.431
ZJX4041											
extended											
EE	20.7	-44.9	-43.7	-35.6	51.6	-1.3	1.473	1.387	1.412	1.383	1.432
ZZ	39.6	-45.4	-44.2	-34.0	51.2	-1.7	1.473	1.387	1.412	1.383	1.432
EZ	33.0	-44.4	-45.3	-34.1	51.4	-1.1	1.473	1.387	1.412	1.383	1.432
ZE	27.7	-46.2	-42.3	-34.0	51.4	-1.2	1.473	1.387	1.412	1.383	1.432
folded											
EE	0.0	-54.5	-42.5	-36.0	48.3	-3.9	1.472	1.384	1.415	1.381	1.433

ZZ	25.7	-55.0	-31.9	-31.2	46.2	-1.9	1.472	1.384	1.415	1.381	1.433
EZ	7.3	-52.2	-58.0	-20.5	45.0	-4.1	1.471	1.385	1.414	1.381	1.432
ZE	13.4	-50.0	-38.1	-31.7	45.8	-3.3	1.471	1.384	1.415	1.381	1.433

Geometries

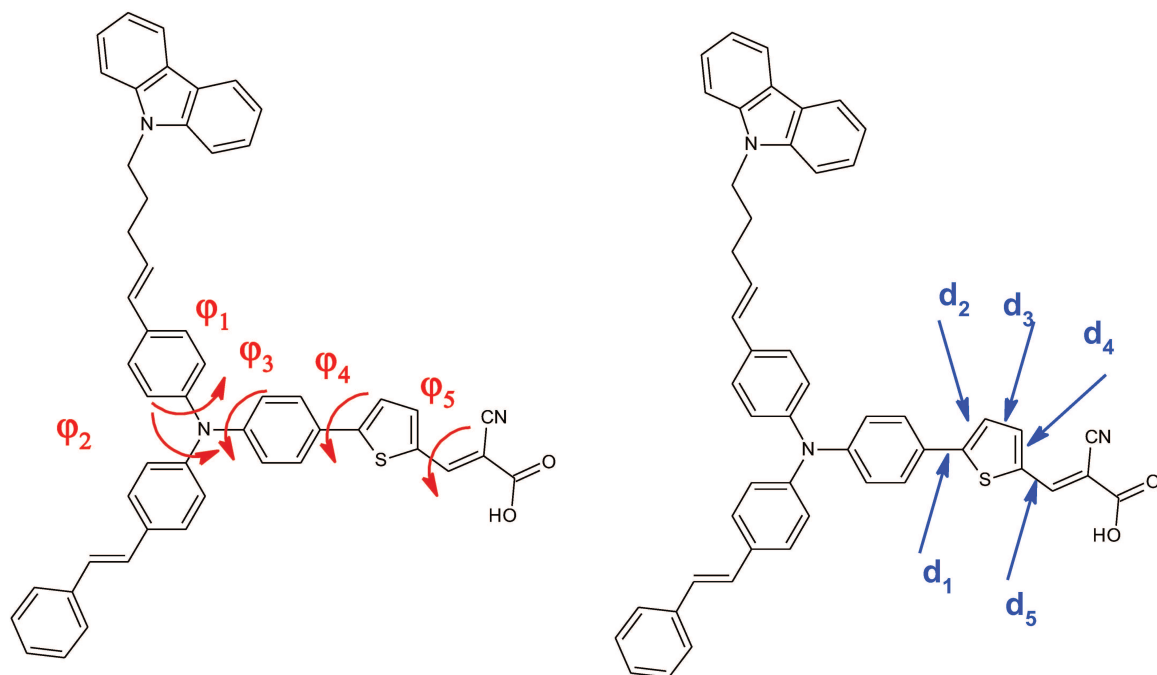


Figure 5.3 **ZJX4015** structure, with the selected d_1 to d_5 bond lengths, and the dihedral angles φ_1 , φ_2 , φ_3 , φ_4 and φ_5 .

a)



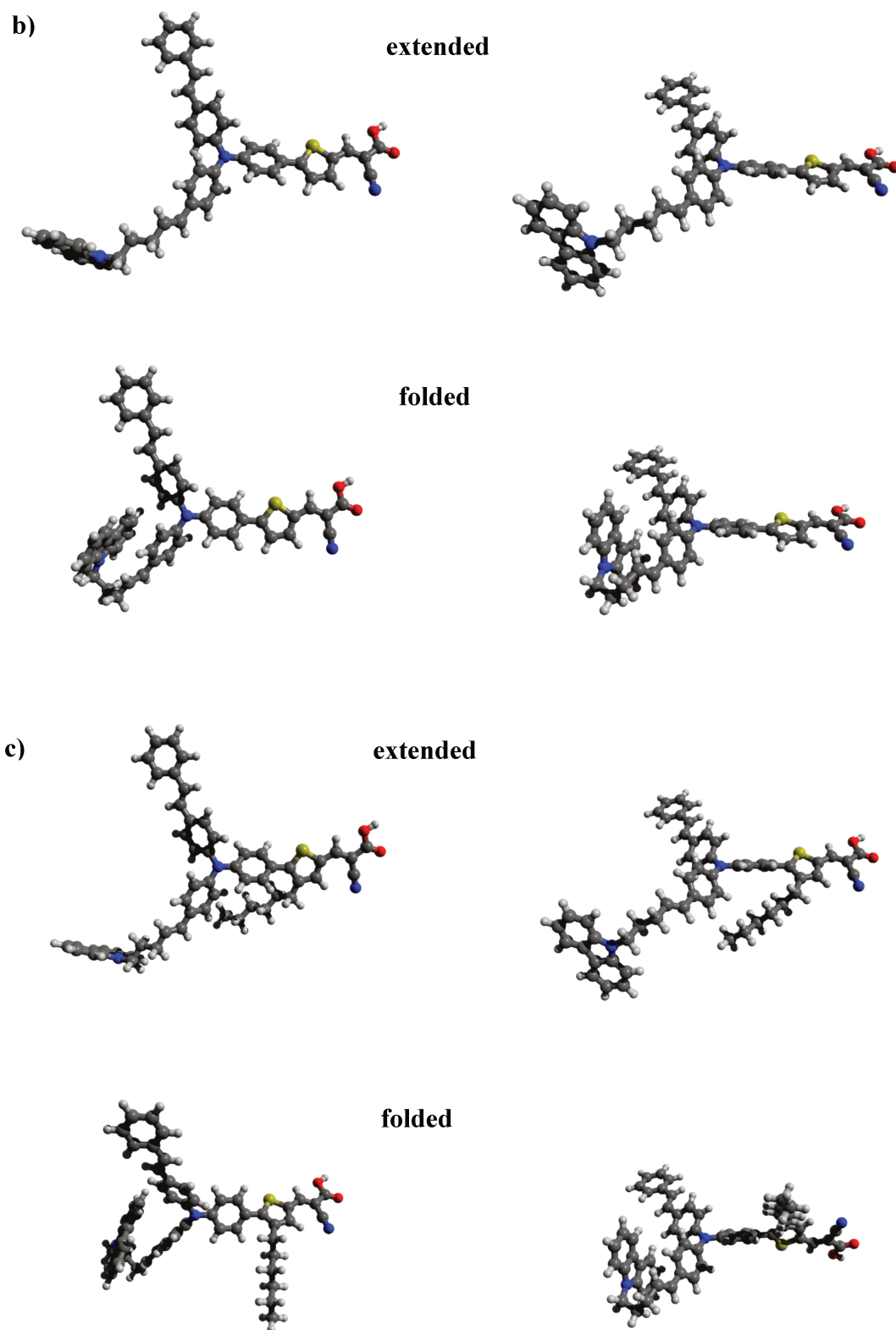


Figure 5.4 Optimized geometries of the dyes a) L1, b) ZJX4015 and c) ZJX4041. Front view on left and side view on right

The optimized structures are shown in **Figure 5.4**. The structure of the D- π -A part of the molecules are found similar in the three molecules.

The conjugation degree is an important parameter that affects importantly the absorption property of the dyes. We thus studied the ground state structures of dyes optimized using DFT calculations in chloroform solvent, and the selected parameters (the C-C bond lengths, d_i $i=1-5$ which participate in π -electrons transfer process between electron-donor and electron-acceptor parts, and dihedral angles φ_i $i=1-5$) are listed in **Table 5.3**.

The calculated C=C bond lengths (d_1), linking the phenyl ring of TPA to thiophene ring, are found equal ≈ 1.46 Å, which is in between single and double bonds ($d(\text{C}=\text{C}) = 1.339$ Å and $d(\text{C}-\text{C}) = 1.530$ Å)¹⁶. This implies that strong resonance structures are exist through the C-C bond length chain, linking the donor TPA and π -linker thiophene moieties for all dyes. In the same way, the d_5 bond length linking the thiophene π -linker to the cyanoacrylic acid is found 1.432 Å a lower value compared to d_1 . This result indicates a high degree of conjugation between thiophene π -linker to the cyanoacrylic acid moiety than between the phenyl ring of donor TPA and the adjacent thiophene π -linker, which was clearly shown by the more coplanar structure presented between the thiophene π -linker and the acceptor acrylic acid ($\varphi_5 \approx -2^\circ$). Overall, all the C-C bond lengths are similar in all three dyes which suggest that the conjugation pathway between the donor and acceptor almost efficient as for **L1**. However, the resonance can be reduced due to steric reasons leading to the distortion of conjugated pathway.

The dihedral angles between the TPA and the thiophene π -linker, and φ_4 is found in the range 25.2-29.1° (not very close to zero) for the isomers of **ZJX4015**. As φ_5 is found close to zero the π -bridge is nearly coplanar to the donor as well as to the acceptor moiety, which favors the intramolecular charge transfer. By contrast φ_4 in the isomers of **ZJX4041** are found in the range 45.0-51.6° all values that reduce the conjugation and decrease the effectiveness of the charge transfer. Hence, the introduction of alkyl chain on thiophene ring most probably inhibits π -aggregation between dyes but decreases the conjugation degree due to the slightly higher dihedral angle (φ_4).

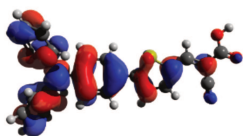
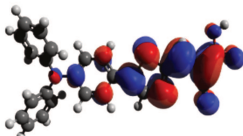
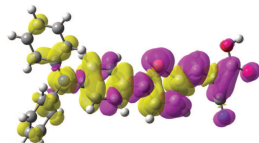
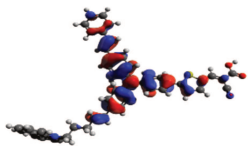
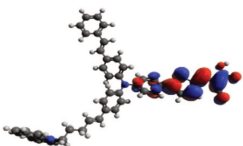
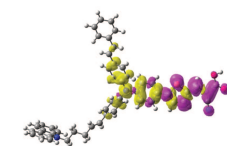
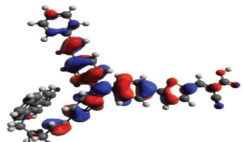
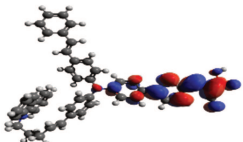
1.3. Electronic structures of ZJX4015 and ZJX4041

Electronic structures: frontier orbitals HOMO LUMO

In most of the organic dyes the electronic maximum absorption in the visible region is due to a promotion of an electron from the HOMO to the LUMO. Therefore, these orbitals should

have spatial distribution that promote the charge separation in excited state. The dyes studied in this work inject electron into the CB of TiO₂, indicating that the HOMO and LUMO should be localized on the donor and acceptor (anchoring) group, respectively.

The HOMO and LUMO orbitals of the **L1**, **ZJX4015** and **ZJX4015** dyes are displayed in **Figure 5.5**. As general trend, the electron distribution of the HOMO orbital is delocalized over the π -system with the highest electron density centered on the nitrogen atom of the TPA unit. In **ZJX4015** and **ZJX4015** the HOMO extends to the styryl unit suggesting a participation in the conjugation. By contrast the LUMO orbitals have larger compositions on the terminal thiophene and cyanoacrylic groups compared with the HOMO. Therefore, the HOMO \rightarrow LUMO excitation induced by light irradiation could shift the electron distribution from the middle of the molecule to the anchoring moieties, thus favoring electron injection from dye to TiO₂. Such a feature is characteristic of a push-pull behavior.

	HOMO	LUMO	EDDM
L1	-5.855 eV	-2.079 eV	
			
ZJX4015			
Extended	-6.753 eV	-1.054 eV	
			
Folded	-5.662 eV	-2.073 eV	
			

ZJX4041

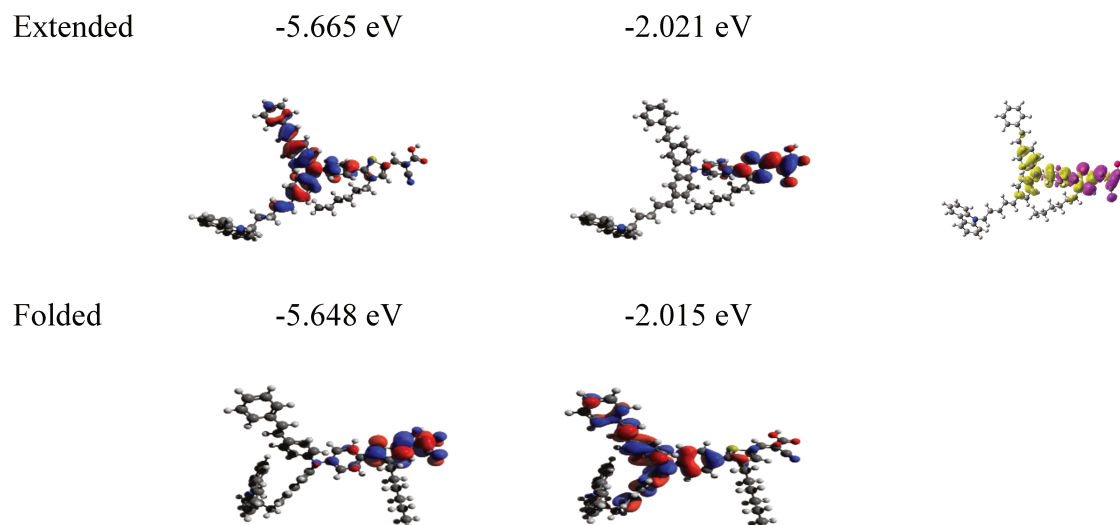


Figure 5.5 Plot of the frontiers orbitals, HOMO, LUMO and electron density differences maps (EDDM) between the first excited and ground states of L1, ZJX4015 and ZJX4041 (isovalue: 0.02 au). Yellow (purple) areas correspond to a loss (gain) of electronic density.

The HOMO/LUMO energy levels and energy gap for **L1**, **ZJX4015** and **ZJX4041** are shown in Figure 5.5. It has been well established that the dye LUMO should be higher than the TiO₂ CB (-4.00 eV) to allow for an adequate driving force for efficient electron injection, at the same time, the dye HOMO should be lower than the HTM redox potential (-4.53 eV) to facilitate dye regeneration.

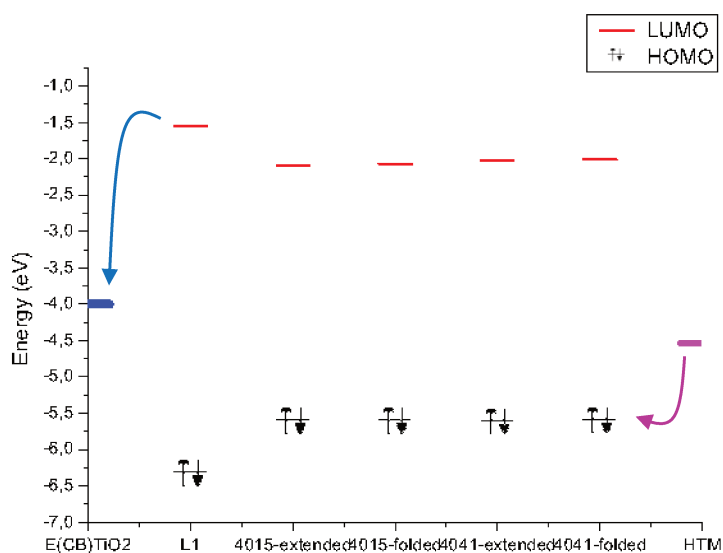


Figure 5.6 Calculated energy levels and HOMO/LUMO gaps for **L1**, **ZJX4015** and **ZJX4041** dyes.

The absolute energies of the HOMOs are -6.38 , -5.66 , and -5.66 eV, while the absolute energy of the LUMOs is -1.55 , -2.09 , and -2.02 eV for **L1**, **ZJX4015** and **ZJX4041** in extended conformation, respectively. Therefore, DFT calculations suggest there is a reasonable position of the energy of the LUMO of all the dyes with respect to band edge of TiO_2 to facilitate charge injection. The extension of the conjugation by adding the styryl unit to **L1** results in an increase of the HOMO and significant decrease in the LUMO energies. These opposite evolutions explain a decrease of the HOMO-LUMO gap: the calculated HOMO-LUMO gaps are 4.83, 3.64, and 3.56 eV for **L1**, **ZJX4041** and **ZJX4015** dyes, respectively, and this agrees well with the trends in absorption maxima of the dyes in solution.

A quantitative composition of the frontier orbitals on the functional group of the dye can be conducted and the results are gathered in **Table 5.4**. The percent contributions from the donor, the π -linker, styryl, carbazole-alkyl chain and cyanoacrylic acid groups in the frontier orbitals are listed in Table 5.X. and give a quantitative analysis on their spatial distribution. A high contribution ranging from 73 to 87% from the donor is found to the HOMO. The HOMO of 4015 and 4015 is delocalized on TAA (more than 73% major contribution) and on the styryl unit (12% minor contribution). Comparing the contributions among the three dyes, it is clear that the contributions of the donor to the HOMOs decrease with increasing the conjugation. Accordingly, the contribution HOMO of **L1** has a largest composition from the donor. The LUMOs show delocalization over the π -linker and the cyanoacrylic acid anchoring groups and the contribution of these two groups, almost constant for the three dyes, is close to 90% (36% of π -linker and 54-58% of cyanoacrylic).

Therefore, it can be expected that the photoexcited electrons would transfer from the TAA moiety to the acceptor group during the excitation process, which is of benefit to the injection of the photoexcited electrons to the CB of the semiconductor. In support of the assertion of charge transfer character, **Figure 5.5** shows the electron density maps (EDDM) between the first excited and ground states of **L1**, **ZJX4015** and **ZJX4041** with yellow regions representing a depletion of density and purple regions denoting an accumulation of density upon excitation. The density depletion zones are mostly located on the TAA and conjugation spacer segments, while the regions of density enhancement are mainly localized on the acceptor moiety which is indicative of ICT when the transition occurs.

Table 5.4 Percentage (%) molecular orbital contribution of the HOMO and LUMO (BMK/6-31G(d)// ωB97XD/6-31G(d) level of calculation).

MO	Donor (TAA)	Thiophene π -linker	styryl	Carbazole-C3-chain-C=C	cyanoacrylic acid
L1					
HOMO	87	9			4
LUMO	10	36			54
4015					
extended					
HOMO	74	5	12	7	2
LUMO	10	36		0	56
folded					
HOMO	73	7	11	7	3
LUMO	10	36	0	0	53
4041					
extended					
HOMO	76	3	13	7	1
LUMO	6	37	0	0	56
folded					
HOMO	75	3	14	7	1
LUMO	6	36	0	0	58

Charge transfer analysis

The intra-molecular charge transfer is the initial process resulting from photo-excitation after light harvesting. In order to quantify the extent of intra-molecular charge transfer, several

charge transfer indexes, such as Δr_{ICT} , Q_{ICT} , and t , are discussed in this section. The calculation of these indexes depends on the charge density difference between the ground and excited states ($\Delta\rho$). The formulation of the three parameters are well established and can be found in several previous studies¹⁷ (see explanation in supporting information). Specifically, Δr_{ICT} directly gives the effective charge transfer distance; Q_{ICT} estimates the amount of charge transfer, and t characterizes the extent of charge separation. Larger t indicates more overlap between the electron density increment and depletion, which usually leads to incomplete charge separation. Table 5.5 lists the charge transfer indexes for the dyes. In the first excited state, Δr_{ICT} increases in the following order: **L1** (5.34 Å) < **ZJX4015** (5.64 Å) < **ZJX4041** (5.88 Å and 5.912 Å depending on the conformation). Q_{ICT} are roughly equal for **L1** and **ZJX4015**, while slightly larger for **ZJX4041**. **L1** and **ZJX4015** have similar t values, which are smaller than that of **ZJX4041**. **ZJX4041** presents the largest degree of charge transfer since it transfers the electron about 1.028e and 1.041e, in extended and folded conformations over 5.884 and 5.912 Å, respectively. Although **L1** and **ZJX4015** exhibit strong charge transfer its efficiency is found weaker than in **ZJX4041**.

Δr_{ICT} increases in the following order: **L1** (5.34 Å) < **ZJX4015** (5.643 Å) < **ZJX4041** (5.884 Å). Q_{ICT} increases in the same order: **L1** (0.820 e) < **ZJX4015** (0.883 e) < **ZJX4041** (1.028 e). The computed values for t follow the same trend. All these three indexes show a clear increase in the charge transfer going from **L1** to **ZJX4041** dye. The **ZJX4041** presents the largest degree of charge transfer while **L1** has the lowest ICT character.

Table 5.5 Computed energies of HOMO, LUMO (BMK/6-31G(d)// ωB97XD/6-31G(d) level of calculation) HOMO-LUMO energy gap, Δ_{H-L} (in eV), calculated dipole moment in ground and first excited states (in Debye) and charge transfer distance (in Å) of the studied dyes.

	HOMO	LUMO	Δ_{H-L}	μ_g	μ_e	Δr_{ICT}	Q_{ICT}	t
L1	-6.38	-1.55	4.83	10.6	32.1	5.34	0.820	0.913
4015								
extended	-5.655	-2.091	3.56	11.77	35.47	5.643	0.883	0.965
folded	-5.662	-2.073	3.59	11.77	36.06	5.643	0.883	0.965
4041								

extended	-5.665	-2.021	3.64	8.2616	36.8941	5.884	1.028	1.041
folded	-5.648	-2.015	3.63	11.2038	39.9806	5.912	1.041	1.504

1.4. Optical properties

An important requirement for a dye used in ss-DSSCs is to exhibit an absorption spectrum matching, as much as possible, the solar irradiation spectrum. In this part we thus calculated the UV-Vis simulated absorption spectra of **L1**, **ZJX4015** and **ZJX4041** by TD-DFT method in dichloromethane.

Validation of the method

In order to produce a highly reliable computational data, the first step of a theoretical study is to test the performance of the computational methodology, especially to predict the absorption spectra. Based on numerous UV/Vis experimental data that are available for TPA-based dyes, we calculated the maximum absorption spectra for 15 compounds for which the substitution is characterized with an increase of the conjugation pathway to check the accuracy of the computational approach (see supplementary document for the structures).

The different compounds studied are depicted in the Figure 5.6. For most of the studied compounds, the calculated UV/Vis spectra displayed to allowed excited states characterized by large transition probability (see Figure SX in supplementary materials). This is in agreement with the experimental findings since an intense first absorption band is found in the 400-600 nm region while a second absorption band of high intensity is found in the 300-400 nm region. Since the lowest transition excitation shows a large intramolecular charge transfer (ICT) character from the donor the acceptor group of the molecule, a strong prerequisite for photovoltaic efficiency, we will focus only on this band in the following.

The **Table 5.7** gathered the maximum absorption wavelength calculated with the BMK functional compared with the experimental values. The results of calculations using CAM-B3LYP functional are presented in supplementary materials. From the results of table, we can conclude that the BMK functionals is a method of choice for the UV/Vis spectra calculation since the mean average error is only 4.1 nm (0.02 eV). Comparing to another functional well adapted to the charge transfer state such as CAM-B3LYP, it can be seen that BMK offers the highest accuracy in the prediction of the maximum absorption of these compounds.

Table 5.6 Experimental and calculated maximum absorption wavelengths $\lambda_{\max}(\text{nm})$ and corresponding vertical excitation energies E_{ex} (eV) (in parentheses), molar extinction coefficient ϵ ($10^4 \text{ M}^{-1} \text{ cm}^{-1}$), oscillator strengths f and light harvesting efficiency (LHE) for different triphenylamine derivative dyes.

	Exptl	theoretical				
		BMK				
	$\lambda_{\max}^{\text{exptl}}$	$\lambda_{\max}^{\text{calc}}$	$\Delta\lambda(\text{nm})^{\text{i}}$	$\Delta\lambda(\text{eV})$	ϵ^{ii}	f^{iii}
e1	386	408	22	-0.17	4.92	1.21
e3	476	507	31	-0.16	6.53	1.61
e5=L1	430	465	35	-0.20	5.18	1.28
e6	473	482	9	-0.05	5.93	1.46
e7	480	497	17	-0.09	7.26	1.79
e14	426	467	41	-0.26	5.06	1.25
e16	486	532	46	-0.22	3.00	0.74
e9	478	467	-11	0.06	4.97	0.95
e17	491	505	14	-0.07	4.00	0.96
24	438	462	24	-0.15	6.37	1.57
RK1	478	461	-17	0.10	4.47	0.95
4015	477	477	0	0.00	5.09	1.24
ADCBZ	444	427	-17	0.11	5.52	1.35
ADCBZ-A	444	442	-2	0.01	6.13	1.51
ADCBZ-B	444	434	-10	0.06	5.62	1.39
ADCBZ-C	444	437	-7	0.04	5.25	1.30

ADSNS	440	429	-11	0.07	5.56	1.36
ADSNS-A	440	438	-2	0.01	6.00	1.48
ADSNS-2	470	472	2	-0.01	5.15	1.27
ADSNS-2-A	470	468	-2	0.01	5.99	1.48
ADCBZ-2-A	477	453	-24	0.14	5.87	1.48
ADCBZ-2-B	477	456	-21	0.12	5.99	1.45
BA741	431	466	-35	0.22		0.93
BA504	512	538	-26	0.12		1.15
MAE ^{iv}			3.25	-0.01		

ⁱ $\Delta\lambda = \Delta(\lambda_{\max}^{\text{calc}} - \lambda_{\max}^{\text{exptl}})(\text{nm})$

ⁱⁱ extinction coefficient

ⁱⁱⁱ oscillator strength

^{iv} Mean average error

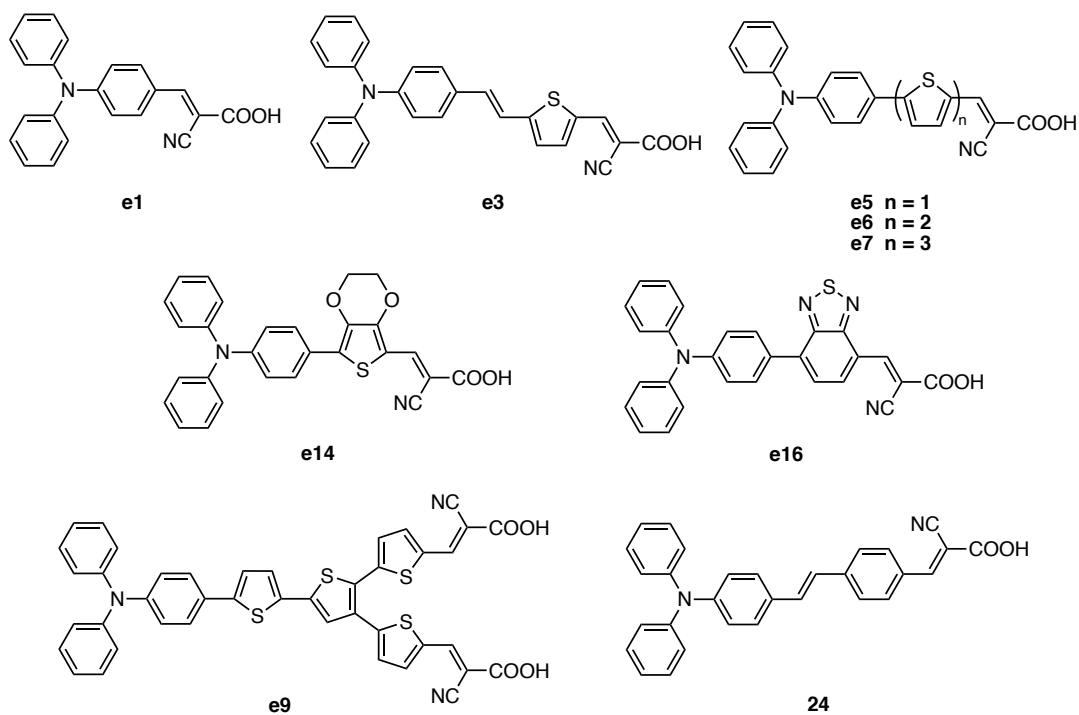


Figure 5.7 Structures of the dyes used to validate the TD-DFT calculations.

The mean average error obtained on this large number of TPA-dye (3.25 nm or 0.02 eV) indicates a small discrepancy between theory and experiment when using the BMK functional. This result confirms the accuracy of the employed computational levels for predicting the absorption spectra using TD-DFT method.

Optical properties of ZJX4015 and ZJX4041

Transition energies and oscillator strengths of the main excited states in **ZJX4015** and **ZJX4041** are listed in **Table 5.7**.

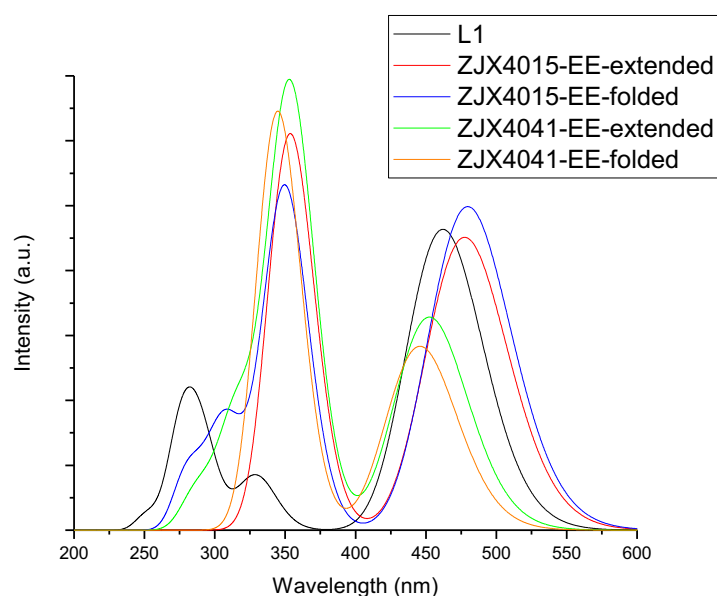


Figure 5.8 Simulated TD-DFT absorption spectra of the **L1**, **ZJX4015** and **ZJX4041** dyes.

The calculated first three excitation energies for **L1**, **ZJX4015** and **ZJX4041** dyes are compared with the experimental values in Table 5.7 and the simulated spectra are displayed in **Figure 5.8**. The simulated spectra are consistent with the experimental results and previous experimental studies. The TAA based dyes exhibit two major absorption bands¹⁸ which include the intramolecular charge transfer (ICT) band and a π - π^* transition within the visible to near-UV region.

The lowest energy electronic transition arises from a HOMO to LUMO transition. Considering the topologies of these two orbitals discussed previously, this band is attributed to a charge transfer transition. The second absorption is attributed a π to π^* electron transition within the entire organic skeleton. The calculated maximum absorption of **L1** ($S_0 \rightarrow S_1, f=1.279$) is found at 462 nm, 32 nm red-shifted as compared to the experimental value (430 nm). This difference

between experimental and TD-DFT calculations is not rare and calculations often underestimate the energy of a charge transfer excitation. The second absorption band $S_0 \rightarrow S_1$ is calculated at 329 nm ($f=0.2327$) in better agreement with experiment (324 nm).

ZJX4015 in extended conformation contains the similar conjugated pathway from the donor to the cyanoacrylic group as for **L1** but also presents an additional large, conjugated region originating from the styryl group. This enhanced π -conjugation leads to a red-shift of the maximum absorption relative to **L1** ($\lambda_{\max}(\text{calc})=477$ nm and $\lambda_{\text{exptl}}(\text{calc})=443$ nm). This redshift is also in agreement with the decrease of the HOMO-LUMO band gap going from **L1** to **ZJX4015**. Interestingly the second absorption is found at 356 nm (experimentally 370 nm) with a strong increase in oscillator strength of about 5.7-fold ($f=1.3113$) as compare to **L1**. The folded conformation shows almost similar maximum absorption energy ($\lambda_{\max}(\text{calc})=480$ nm) while the second absorption is slightly blue shifted due to the π - π interaction between styryl and carbazole units that causes a decrease of the HOMO energy (see Table 5.3).

Similar to **ZJX40415**, **ZJX4041** exhibits two strongest band in the visible calculated at 452 nm and 356 nm for extended conformation (446 and 345 nm for the folded conformation). The first transition is blue-shifted by 25 nm in extended conformation (30 nm for folded) when compared to the ICT of **ZJX4015**. This can be explained by the geometric distortion along the conjugation pathway caused by the alkyl chain carried by the thiophene group.

Table 5.7 Main electronic transition in the 300-550 nm region of **L1**, EE isomers of **ZJX4015** and **ZJX4041**. Calculated absorption maximum wavelength (λ^{calc} in nm), oscillator strength and assignment (H = HOMO, H-1 = HOMO -1 and L = LUMO) with percentage of configuration.

transition	λ^{calc}	λ^{exptl}	f^*	Composition of the transition
L1				
$S_0 \rightarrow S_1$	462	430	1.2795	HOMO \rightarrow LUMO (90%)
$S_0 \rightarrow S_2$	329		0.2327	HOMO-1 \rightarrow L (88%)
$S_0 \rightarrow S_3$	292		0.2466	HOMO \rightarrow L+1 (65%)
4015				
extended				
$S_0 \rightarrow S_1$	477	477	1.2454	HOMO \rightarrow LUMO (87%)

	$S_0 \rightarrow S_2$	356	370	1.3113	HOMO \rightarrow L+1 (84%)
	$S_0 \rightarrow S_3$	347		0.4231	H-4 \rightarrow LUMO (45%)
folded					
	$S_0 \rightarrow S_1$	480		1.3761	HOMO \rightarrow LUMO (87%)
	$S_0 \rightarrow S_2$	352		1.0707	HOMO \rightarrow L+1 (76%)
	$S_0 \rightarrow S_3$	345		0.3906	H-4 \rightarrow LUMO (37%)
<hr/>					
4041					
extended					
	$S_0 \rightarrow S_1$	452	443	0.9062	HOMO \rightarrow LUMO (87%)
	$S_0 \rightarrow S_2$	356	372	1.3603	HOMO \rightarrow L+1 (88%)
	$S_0 \rightarrow S_3$	346		0.6105	H-4 \rightarrow LUMO (58%)
folded					
	$S_0 \rightarrow S_1$	446		0.782	HOMO \rightarrow LUMO (89%)
	$S_0 \rightarrow S_2$	348		1.2413	HOMO \rightarrow L+1 (85%)
	$S_0 \rightarrow S_3$	338		0.6127	H-4 \rightarrow LUMO (56%)

* Oscillator strength

The maximum absorption wavelength, λ_{\max} , is related to the $S_0 \rightarrow S_1$ transition and, as expected for the D- π -A dyes structures, is sensitive to the electron withdrawing units between the donor and acceptor groups (**Table 2**). The wavelength at maximum absorption for L1 is calculated at 462 nm vs 432 nm experimentally.

1.5. Calculated Photovoltaic Performances using DFT

Theoretical calculations are applied to predict key parameters controlling the photovoltaic performances such as, the short-circuit current density (J_{sc}), the light harvesting efficiency at a given wavelength LHE (λ); the injection driving force ($\Delta G_{\text{inject.}}$), the reorganization energy (λ_{reorg}); the extent of the regeneration of the dye by the HTM after electron injection into the

semiconductor (ΔG_{reg}). In this part, we will evaluate these parameters for the studied dyes **L1**, **ZJX4015** and **ZJX4041** using DFT calculations. All these theoretical data have been successfully used to evaluate the performance of the dyes used in DSSCs^{19–26}. (see details in computational details).

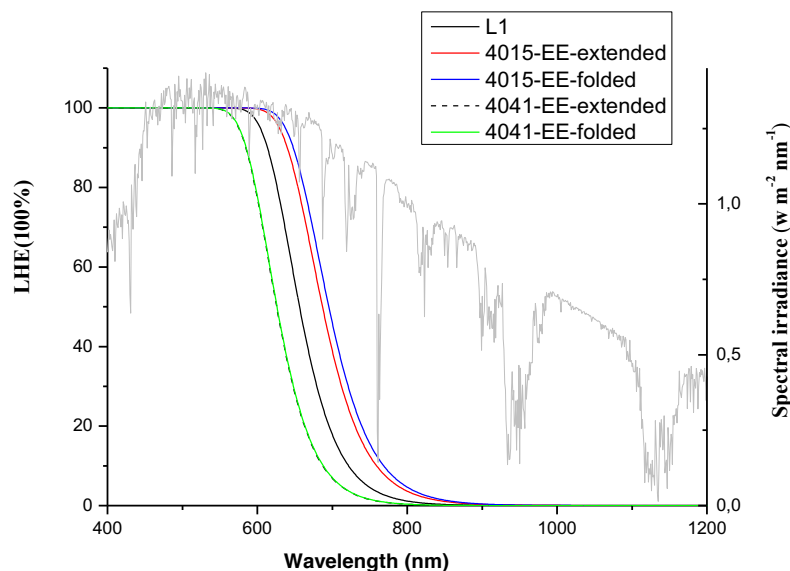


Figure 5.9 Calculated LHE as function of the wavelength for the **L1**, **ZJX4015** and **ZJX4041** dyes.

A sensitizer with $LHE(\lambda)$ covering a wide range from visible to infrared regions could guarantee a better photocurrent response, subsequently a more efficient photovoltaic performance, the LHE value of sensitizers may be higher, close to the unity. The LHE at the maximum absorption wavelength values (**Table 5.8**) of **L1** and **ZJX4015** are near the unity indicating a good power conversion efficiency. The LHE for **ZJX4041** is only 0.834 and 0.876 depending on the conformation and suggest a less effective capability to absorb the light. The $LHE(\lambda)$ spectra in **Figure 5.9** provide additional information and indicate some differences between **L1**, **ZJX4015** and **ZJX4041**. **L1** shows a good light harvesting abilities in the region of 200–600 nm region with $LHE(\lambda)$ value close to 100%. When comparing with **L1**, **ZJX4015** and **ZJX4041** show opposite behavior for the $LHE(\lambda)$ evolution. **ZJX4041** presents an $LHE(\lambda)$ value to be close to 100% in a narrower region from 200 to 570 nm while **ZJX4015** has wider coverage than the other dyes showing an $LHE(\lambda)$ value to be close to 100% in the 200 – 630 nm region.

The calculated $LHE(\lambda)$ curves indicate that the extent of the conjugation through a styryl group would cause a decrease in $\Delta_{\text{H-L}}$, thus result in broadening the absorption band and improving

the light harvesting abilities of dye. On the contrary the addition of an alkyl chain on the thiophene linker increase Δ_{H-L} , and thus reduces the light harvesting abilities of the dye.

The simulated J_{SC}^{max} (see Eq. 2 in computational details) are about 3.29, 3.66, 3.76, 2.90 and 2.91 mA cm⁻² for **L1**, **ZJX4015-extended**, **ZJX4015-folded**, **ZJX4041-extended** and **ZJX4041-folded** (see **Table 5.8**). This indicates that **ZJX4015** would exhibit the best photocurrent performance and that extension of π -spacer significantly affects the $LHE(\lambda)$ curve by improving the J_{SC}^{max} . Indeed, **Table 5.8** shows that the J_{SC}^{max} values obtained with **ZJX4015** with respect to those obtained with **L1** is the highest, mainly due to its red-shifted absorption spectrum. However, as shown in Eq. 2, the photocurrent can be affected by ϕ_{inject} which is related to the ΔG_{inject} . The ΔG_{inject} of all studied dyes have been calculated using Eq. 7 and are listed in **Table 5.8**. The negative values of ΔG_{inject} imply spontaneous electron injection. ΔG_{inject} negatively decreases with increasing length of acyclic linker mainly because of the lowering of the energy of the LUMO. **Table 5.8** shows that the calculated ΔG_{inject} are more negative for **ZJX4015** and **ZJX4041** than for **L1**. The free energy change ΔG_{inject} decreases in the order **L1** (-0.303) > **ZJX4015-folded** (-0.921) > **ZJX4015-extended** (-0.944) > **ZJX4041-extended** (-1.078) > **ZJX4041-folded** (-1.123) from -0.303 to -1.123 eV, indicating that the driving force of the electron injection from the excited state of the dye increases in this order. From the data provided by the calculation it can be said that both J_{SC}^{max} and ΔG_{inject} factors contribute to the increase of J_{sc} from **L1** to **ZJX4015** as observed experimentally (see **Table 7**: J_{sc} (**L1**) = 3.1 mA/cm² and J_{sc} (**ZJX4015**) = 5.6 mA/cm²) while they play in an opposite way when comparing **ZJX4041**. Hence although **ZJX4041** has the highest ability for electron injection, its lowest calculated J_{SC}^{max} disfavors the J_{sc} .

The other key parameters influencing the PCE of ss-DSSCs are calculated and listed in **Table 5.8**, and show for all the dyes, that the absolute values of ΔG_{inject} and ΔG_{reg} are larger than 0.3 eV. This latter value could guarantee the effective interface charge injection and fast dye regeneration^{27,28}.

Table 5.8 Calculated driving force for electron injection (ΔG_{inject} in eV), driving force for dye regeneration (ΔG_{reg} in eV), maximum of short-circuit current density (J_{sc}^{max} in mA/cm²), excited lifetime (τ) and light harvesting efficiency (LHE, calculated at the maximum absorption wavelength) of the studied dyes

Dyes	ΔG_{inject}	ΔG_{reg}	τ (10 ⁻⁹ s)	LHE	J_{SC}^{max} (mA/cm ²)
L1	-0.303	1.850	2.500	0.947	3.29

ZJX4015					
extended	-0.944	1.125	2.739	0.943	3.66
folded	-0.921	1.132	2.510	0.958	3.76
ZJX4041					
extended	-1.078	1.135	3.380	0.876	2.90
folded	-1.123	1.118	3.813	0.834	2.91

The excited state lifetime of was computed using the Eq. 11 gathered in **Table 5.8** and was found in the nanosecond order for all the dyes. The cell performance is related to the lifetime of the excited state of the dye and to the lifetime of the electron injection from the LUMO to the CB of the semiconductor. A long-excited state lifetime associated to a high rate for injection increases the cell performance. The injection of electrons to semiconductor is often measured in the picoseconds order²⁹. Therefore, our results suggest that the excited state decay cannot compete with the electron injection reaction. The excited lifetime of **ZJX4015** and **L1** are similar, and **ZJX4041** the longer.

Table 5.9 Calculated hole (λ_{hole}), electron ($\lambda_{\text{electron}}$) and total (λ_{total}) reorganization energies calculated in eV.

	λ_1	λ_2	λ_{hole}	λ_3	λ_4	$\lambda_{\text{electron}}$	λ_{reorg}
L1	0.126	0.104	0.230	0.315	0.329	0.644	0.874
4015							
extended	0.144	0.123	0.267	0.323	0.351	0.674	0.941
folded	0.136	0.191	0.327	0.328	0.362	0.690	1.017
4041							
extended	0.162	0.150	0.312	0.296	0.357	0.653	0.965
folded	0.138	0.159	0.297	0.331	0.314	0.645	0.942

From **Table 5.9**, it can be seen that the electron reorganization energies ($\lambda_{\text{electron}}$) of the four dyes are larger than their hole reorganization energies (λ_{hole}). These results confirm that the TAA based dyes are better hole transfer material than electron transfer one. The hole reorganization energies increase in the order: **L1** < **ZJX4015-extended** < **ZJX4041-folded** < **ZJX4041-extended** < **ZJX4015-folded**. This trend is difficult to explain and result from a subtle balance between the energy penalty to reach the geometry of the cation (λ_1) and the relaxation of the geometry of the cation (λ_2). However, the results show that **L1**, **ZJX4015** and **ZJX4041** have similar hole reorganization energies and this factor cannot explain the changes in photovoltaic efficiency between these dyes.

In summary, by combining various factors that influence the J_{sc} , *i.e.*, ΔG_{inj} and LHE, we can conclude that **ZJX4015** dye should be the more efficient LHE and the second best for electron injection and therefore should exhibit a favorable J_{sc} value. Concerning the **ZJX4041** dye although it shows the best electron injection behavior the LHE is the weaker of all the dye that contribute to a less good J_{sc} value. For the **ZJX4041** the good charge transfer properties attested by several index values do not guarantee an electron injection due to the less conjugated behavior between donor and acceptor group.

2. Conclusion

In this chapter we have studied the conformational and electronic properties of the new dyes synthesized by theoretical approach based on density functional theory. These dyes have been compared to the reference compound **L1**. We have shown that the existence of a C3 alkyl chain linking the carbazole unit to the core of the dye leads to a high conformational flexibility. In the most stable energy structure obtained, the carbazole is located above a phenyl group of the dye donor unit (TPA) establishing a π - π interaction. Concerning the conjugated system between the donor part of the dye (TPA) and the acceptor part, its geometry is perturbed by the presence of the alkyl chain carried by the thiophene group. In the absence of the six-carbon chain (compounds **L1** and **ZJX4015**), the conjugated system is practically coplanar from the donor to the acceptor part which is in interaction with the semiconductor.

The presence of the alkyl chain on the thiophene in **ZJX4041** deforms the conjugated system out of the plane which leads to energetic changes on the boundary molecular orbitals (the HOMO-LUMO gap is larger in **ZJX4041** than in **ZJX4015**) and on the optical properties (the absorption maximum of **ZJX4041** is shifted towards the blue with respect to that of **ZJX4015**). Regarding the optical properties, the newly developed dyes reveal the existence of a new

absorption band around 350 nm which is linked to the presence of the styryl group which brings an additional conjugation. The calculation of the photovoltaic properties shows contrasting conclusions depending on the evaluated parameter. Thus, the dye **ZJX4015** seems to be better concerning the J_{SC} , its ability to inject an electron into the semiconductor (ΔG_{inj}) or its greater photon collection (LHE). The compound **ZJX4041** shows much better charge transfer properties than **L1** and **ZJX4015**.

It should be noted that the calculations performed only ascribed to the photovoltaic performance of the isolated dyes, and the entire complexity of the system is not addressed in this approach. Thus, the interaction with the electrode is not taken into account as well as the influence of the polymer generated in situ within the cell. It is therefore difficult to decide on the performance of the dyes only from these calculations made on a simplistic model of the cell. Additional calculations must be carried out by integrating an electrode model, for example in the form of a TiO_2 cluster and a polymer model in the form of an oligomer of EDOT grafted to the carbazole unit.

Computational details

Electronic structure and excited states calculations

The molecular calculations of the studied dyes have been carried out with Gaussian 09 program package³⁰. The ground state geometries have been fully optimized with density functional theory (DFT) by employing the long-range corrected hybrid functional ω B97XD³¹ functional which includes empirical dispersion and minimizes the delocalization error^{22,32} basis set was used for all the calculations. A tight SCF convergence criterion (10^{-8} a.u.) and integration grid of 10^{-8} were used for all calculations.

Frequency calculations have been performed on the optimized geometries to verify the nature of the computed geometries and the lack of imaginary values in the wave numbers calculations confirmed the successful optimization as a minimum geometry.

For the excited state calculations we have employed time-dependent density functional theory (TD-DFT) and selected the Boese-Martin for Kinetics functional (BMK)³³ which showed the best performance for the lowest maximum absorption of the dyes. TD-DFT calculations were performed along with 6-31G(d) basis set. The conductor-like polarizable continuum model (C-PCM) has been employed for the simulation of UV-vis spectra. Solvent effect (dichloromethane) was undertaken using the Polarizable Continuum Model (PCM) using the integral equation formalism variant (IEFPCM)³⁴. Ground state optimized structures were used to compute absorption wavelength maxima (λ_{\max}), excitation energy (E_g) and oscillator strengths (f) for the 10 states.

Theoretical determination of the photovoltaic parameters

The efficiency of the DSSC can be affected by many different parameters. We present here the main of them that can be estimated through quantum chemical calculations. The overall performance of the DSSC can be evaluated based on sunlight-to-electric power conversion efficiency (η):

$$\eta = \frac{FF \times J_{sc} \times V_{oc}}{P_{in}} \quad \text{Eq. 1}$$

where J_{sc} , V_{oc} , P_{in} and FF are the short-circuit current density, open-circuit cell voltage, incident radiant power, and fill factor, respectively, the latter defined as the ratio of the maximal cell power to the product of open-circuit voltage and short-circuit current. In the equation (1) the product of J_{sc} and V_{oc} should be as high as possible to improve the performance of the cell. J_{sc} depends on the kinetics of the electron injection, dye regeneration, reorganization energy and light harvesting efficiency³⁵. J_{sc} can be determined as:

$$J_{SC} = e \int_{\lambda} LHE(\lambda) \phi_{inject} \eta_{reg} \eta_{coll} \varphi_{ph.AM1.5G} d\lambda \quad \text{Eq. 2}$$

where ϕ_{inject} , η_{coll} , η_{reg} are the electron injection efficiency, electron collection efficiency, dye regeneration efficiency, respectively. $\varphi_{ph.AM 1.5G}$ is the photon flux under AM1.5G solar irradiation spectra. $LHE(\lambda)$ is the light harvesting efficiency at a specified wavelength, which is directly related to the absorption intensity. $LHE(\lambda)$ and ϕ_{inject} are the two main influencing factors on J_{SC} . The high $LHE(\lambda)$ could enhance the J_{SC} and finally increase η of DSSCs according to equation (1).

$LHE(\lambda)$ can be determined by:

$$LHE(\lambda) = 1 - 10^{-\varepsilon(\lambda)bc} \quad \text{Eq. 3}$$

Where $\varepsilon(\lambda)$ is the molar absorption coefficient at the wavelength λ and b and c are the TiO_2 film thickness and dye concentration, respectively which are usually assigned with the experimental value of 10 μm and 300 mmol/L ^{36–38}. When considering: ϕ_{inject} , η_{coll} and η_{reg} as the constants and all equal to 1 in equation (2), the J_{SC}^{max} can be obtained. Note that in the equation (2) the product $LHE(\lambda)\phi_{inject}\eta_{coll}$ represents the incident photon conversion efficiency (IPCE)^{39,40}. In the equation (2) ϕ_{inject} is related to injection driving force ΔG_{inject} of electrons injecting from the excited dye molecule into the semiconductor substrate. ΔG_{inject} can be estimated as follows^{24,41,42}:

$$\Delta G_{inject} = E_{ox}^{dye*} - E_{CB}^{TiO2} \quad \text{Eq. 4}$$

In this expression E_{ox}^{dye*} is the oxidation potential of the excited dye and E_{CB}^{TiO2} is the reduction potential of the semiconductor conduction band. The E_{CB}^{TiO2} is difficult to be accurately determined since it is sensitive to the pH conditions and thus, we used the commonly adopted -4.0 eV value⁴³. The excited state oxidation potential of the dye, E_{ox}^{dye*} , can be estimated from the redox potential of the ground state E_{ox}^{dye} as⁴²:

$$E_{ox}^{dye*} = E_{ox}^{dye} - \lambda_{max}^{ICT} \quad \text{Eq. 5}$$

where λ_{max}^{ICT} is the energy of the intramolecular charge transfer transition. Based on Koopmans' theorem that states the first ionization energy of a molecular system can be estimated to the negative of the orbital energy of the HOMO, the ground state oxidation potential E_{ox}^{dye} can be estimated from negative energy of the HOMO. The E_{ox}^{dye*} can be written as:

$$E_{ox}^{dye*} = -E_{HOMO} - \lambda_{max}^{ICT} \quad \text{Eq. 6}$$

Finally, ΔG_{inject} can be approximated using the following formulae:

$$\Delta G_{inject} = -E_{HOMO} - \lambda_{max}^{ICT} - E_{CB}^{TiO_2} \quad \text{Eq. 7}$$

The ground state oxidation potential of the dye also determines the extent of the excited dye regeneration. ΔG_{reg} can be calculated by subtracting the oxidation potential of the dye from the oxidation potential of the hole transporting material (HTM). In this study the HTM used to build the ss-DSSC is PEDOT and its work function is reported to be at -5.2 eV⁴⁴. In a similar manner as for the dye, the oxidation potential of the HTM can also be estimated as the opposite energy of the HOMO of the polymer. To theoretically determine the HOMO of the polymer we used the oligomer approach and calculated the geometries and energies of the orbitals of several oligomers of (EDOT)_n for size ranging from n=2 to n=12. As shown in Figure A.1, the evolution of the energy of the HOMO as function of the inverse of the number of EDOT units nicely agree with a linear relation. Using this linear relation, we were able to determine the HOMO of the polymer as -4.53 eV.

$$\Delta G_{reg} = E_{ox}^{dye} - E_{ox}^{polymer} = -E_{HOMO} - 4.53 \quad \text{Eq. 8}$$

The charge carrier mobility in the organic studied dyes can be evaluated using the Marcus electron transfer theory⁴⁵. The rate constant for electron/hole transfer can be expressed with the following equation:

$$k_{ET} = V^2 / \hbar \sqrt{\pi / \lambda k_B T} \exp(-\lambda_{tot} / 4k_B T) \quad \text{Eq. 9}$$

Where λ_{tot} is the reorganization energy due to structural reorganization of the molecule upon an excess on a charge (hole or electron), \hbar is reduced Planck constant, k_B is the Boltzmann constant, T is the temperature. Therefore λ_{tot} acts as the barrier for the charge transport in molecular pathway. The total reorganization energy (λ), which is the sum of the hole and electron reorganization energies, could also enhance the J_{SC} . This implies that the smaller the λ value obtained the faster charge-carrier transport rates will be. The λ values of the isolated dyes can be computed according to the following formula:

$$\lambda_{tot} = \lambda_{hole} + \lambda_{elec} = \lambda_1 + \lambda_2 + \lambda_3 + \lambda_4$$

with $\lambda_{hole} = \lambda_1 + \lambda_2$ and $\lambda_{elec} = \lambda_3 + \lambda_4$ Eq. 10

λ_1 is the energy difference (in eV) of the positively charged molecule associated to the geometric relaxation from ground state geometry to optimized cationic state and λ_2 the energy required to reorganize from the neutral state at the cation geometry to the ground state upon re-

accepting an electron. In a similar manner, the anion reorganization energy is evaluated for electron transport (λ_3 and λ_4)

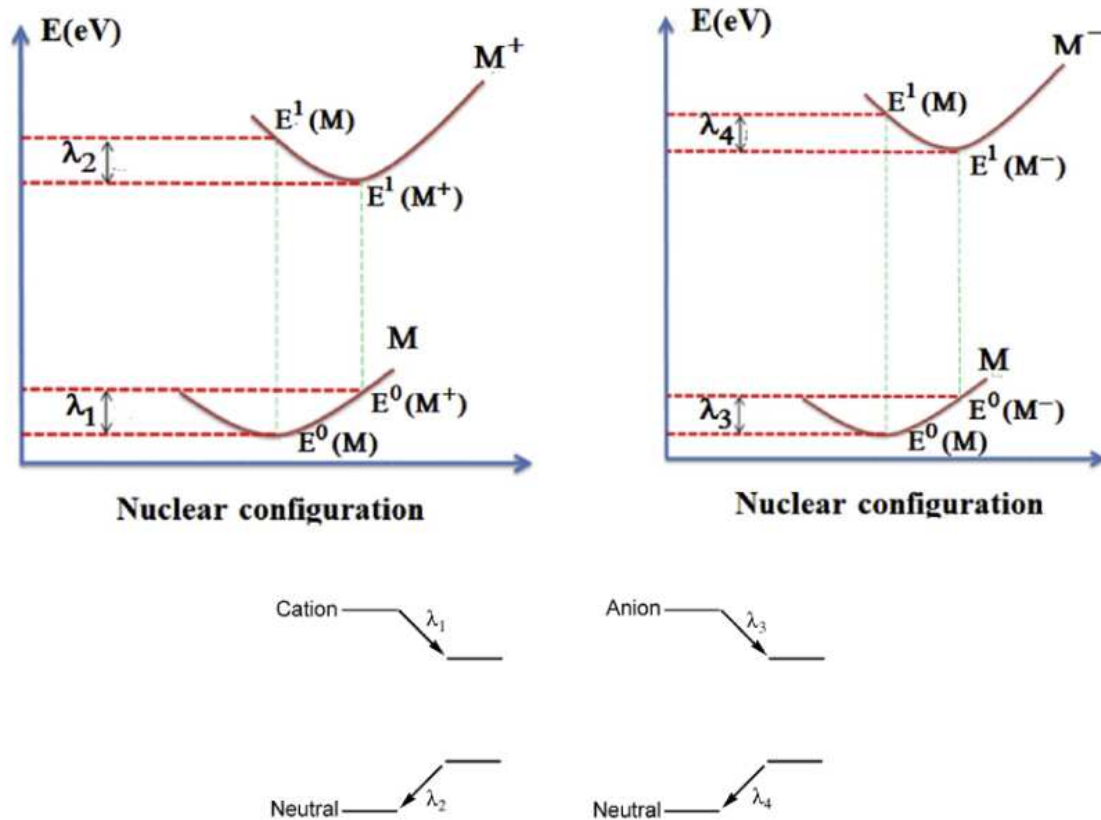


Figure 5.10 Jablonski diagram of the intermolecular transfer reaction between neutral molecule and cationic/anionic specie.

From the equation (9) it is clear that the reorganization energy should be low to have a large electron/hole transport. The smaller the total reorganization energy is, the slower recombination process will be due to the efficient separation of hole and electron in DSSC which leads to a higher rate of charge transfer and J_{SC} will be enhanced. Therefore J_{SC} has an inverse relationship with λ_{tot} .

The lifetime of the injected electron into the semiconductor is related to the degree of the charge recombination occurring in the device. In first approximation the lifetime of the injected electron can be the same as the first excited state lifetime τ , which can be expressed as:

$$\tau = 1.499 / E^2 f \quad \text{Eq. 11}$$

where E corresponds to the vertical excitation energy (cm^{-1}) and f the oscillator strength. A larger lifetime τ indicates a less charge recombination and can be related to a better V_{oc} .

Supplementary materials

Charge transfer analysis and calculated index

Charge transfer (CT) parameters have been developed⁴⁶ along with a code to perform the calculations⁴⁷. The developed code calculates the parameters from the ground state (GS) and the excited state (ES) densities produced by the Gaussian cubegen. The parameters include the CT distance (D^{CT}), transferred charge (q^{CT}), change in dipole moment ($\Delta\mu^{CT}$), H index and t index according to Eqs. (A.1)–(A.8) below⁴⁶.

The difference in densities between the ground and excited states ($\Delta\rho_i$) can be calculated according to Eq. (A.1). Note that $\Delta\rho_i^+$ and $\Delta\rho_i^-$ define the points in space where an increment or a depletion of the density is produced upon absorption.

$$\Delta\rho_i = \Delta\rho_i^{ES} - \Delta\rho_i^{GS} \begin{cases} \Delta\rho_i = \Delta\rho_i^{ES} - \Delta\rho_i^{GS} \\ = \Delta\rho_i^+ \quad (\text{if } \Delta\rho_i > 0) \\ = \Delta\rho_i^- \quad (\text{if } \Delta\rho_i < 0) \end{cases} \quad \text{Eq. (A.1)}$$

The transferred charge (q^{CT}) can be calculated via Eq. (2):

$$q^{CT} = \sum_i \rho_i^+ = \left| \sum_i \rho_i^- \right| \quad \text{Eq. (A.2)}$$

Barycenter's corresponding to the $\Delta\rho_i^+$ and $\Delta\rho_i^-$ can be represented by r^+ and r^- , respectively as:

$$\begin{cases} r^+ = (x^+, y^+, z^+) = \frac{\sum_i r_i \rho_i^+}{q^{CT}} \\ r^- = (x^-, y^-, z^-) = \frac{\sum_i r_i \rho_i^-}{q^{CT}} \end{cases} \quad \text{Eq. (A.3)}$$

The distance separating the two points is the CT distance, which is given by Eq. (A.4).

$$D^{CT} = |r^+ - r^-| \quad \text{Eq. (A.4)}$$

The change in dipolemoment of the molecule as a result of the electronic excitation is calculated using Eq. (A.5).

$$\Delta\mu^{CT} = D^{CT} q^{CT} \quad \text{Eq. (A.5)}$$

For a rod-like system in which the CT predominantly takes place along the x-axis, an index denoted as H is defined as:

$$H = \frac{|\sigma^{+x} - \sigma^{-x}|}{2} \quad \text{Eq. (A. 6)}$$

where $\sigma^{\pm x}$ is the root mean square derivation for the positive or negative components along the x-axis and can be calculated as:

$$\sigma^{\pm x} = \sqrt{\frac{\sum_i q_i^{\pm} (x_i - x^{\pm})^2}{q^{CT}}} \quad \text{Eq. (A. 7)}$$

Two centroids of the charges $C^{+}(r)$ and $C^{-}(r)$, associated to the positive and negative density regions, respectively were defined for visualization purposes. Finally, a descriptor giving the difference between the calculated D^{CT} and H denoted as the t-index is defined via Eq. (A.8). If t is larger than 1.6 Å, the used functional would not be to provide a correct description of the transition energy associated with a CT excitation⁴⁶. However, if t is lower than 1.6 Å, a good description of the transition energy can be obtained⁴⁶.

$$t = D^{CT} - H \quad \text{Eq. (A. 8)}$$

Reference

- (1) Beni, A. S.; Zarandi, M.; Madram, A. R.; Bayat, Y.; Chermahini, A. N.; Ghahary, R. Molecular Design of Carbazole-Based Dyes and the Influence of Alkyl Substituent on the Performance of Dye-Sensitized Solar Cells. *Mol. Cryst. Liq. Cryst.* **2016**, *629* (1), 29–43. <https://doi.org/10.1080/15421406.2015.1106895>.
- (2) Ezhumalai, Y.; Lee, B.; Fan, M.-S.; Harutyunyan, B.; Prabakaran, K.; Lee, C.-P.; Chang, S. H.; Ni, J.-S.; Vegiraju, S.; Priyanka, P.; Wu, Y.-W.; Liu, C.-W.; Yau, S.; Lin, J. T.; Wu, C.-G.; Bedzyk, M. J.; Chang, R. P. H.; Chen, M.-C.; Ho, K.-C.; Marks, T. J. Metal-Free Branched Alkyl Tetrathienoacene (TTAR)-Based Sensitizers for High-Performance Dye-Sensitized Solar Cells. *J. Mater. Chem. A* **2017**, *5* (24), 12310–12321. <https://doi.org/10.1039/C7TA01825H>.
- (3) Xue, X.; Zhang, W.; Zhang, N.; Ju, C.; Peng, X.; Yang, Y.; Liang, Y.; Feng, Y.; Zhang, B. Effect of the Length of the Alkyl Chains in Porphyrin Meso-Substituents on the Performance of Dye-Sensitized Solar Cells. *RSC Adv.* **2014**, *4* (17), 8894. <https://doi.org/10.1039/c3ra46212a>.
- (4) Koumura, N.; Wang, Z.-S.; Mori, S.; Miyashita, M.; Suzuki, E.; Hara, K. Alkyl-Functionalized Organic Dyes for Efficient Molecular Photovoltaics. *J. Am. Chem. Soc.* **2006**, *128* (44), 14256–14257. <https://doi.org/10.1021/ja0645640>.
- (5) Chen, H.; Lyu, G.; Yue, Y.; Wang, T.; Li, D.-P.; Shi, H.; Xing, J.; Shao, J.; Zhang, R.; Liu, J. Improving the Photovoltaic Performance by Employing Alkyl Chains Perpendicular to the π -Conjugated Plane of an Organic Dye in Dye-Sensitized Solar Cells. *J. Mater. Chem. C* **2019**, *7* (24), 7249–7258. <https://doi.org/10.1039/C9TC01520E>.
- (6) Kroeze, J. E.; Hirata, N.; Koops, S.; Nazeeruddin, Md. K.; Schmidt-Mende, L.; Grätzel, M.; Durrant, J. R. Alkyl Chain Barriers for Kinetic Optimization in Dye-Sensitized Solar Cells. *J. Am. Chem. Soc.* **2006**, *128* (50), 16376–16383. <https://doi.org/10.1021/ja065653f>.
- (7) Wu, Z.; Li, X.; Li, J.; Ågren, H.; Hua, J.; Tian, H. Effect of Bridging Group Configuration on Photophysical and Photovoltaic Performance in Dye-Sensitized Solar Cells. *J. Mater. Chem. A* **2015**, *3* (27), 14325–14333. <https://doi.org/10.1039/C5TA02120K>.
- (8) Petek, H.; Yoshihara, K.; Fujiwara, Y.; Frey, J. G. Isomerization of Cis-Stilbene in Rare-Gas Clusters: Direct Measurements of Trans-Stilbene Formation Rates on a Picosecond Time Scale. *JOSA B* **1990**, *7* (8), 1540–1544. <https://doi.org/10.1364/JOSAB.7.001540>.
- (9) Rodier, J. M.; Myers, A. B. Cis-Stilbene Photochemistry: Solvent Dependence of the Initial Dynamics and Quantum Yields. *J. Am. Chem. Soc.* **1993**, *115* (23), 10791–10795. <https://doi.org/10.1021/ja00076a041>.

- (10) Saltiel, J.; Waller, A. S.; Sears, D. F. Dynamics of Cis-Stilbene Photoisomerization: The Adiabatic Pathway to Excited Trans-Stilbene. *J. Photochem. Photobiol. Chem.* **1992**, *65* (1), 29–40. [https://doi.org/10.1016/1010-6030\(92\)85029-T](https://doi.org/10.1016/1010-6030(92)85029-T).
- (11) Repinec, S. T.; Sension, R. J.; Szarka, A. Z.; Hochstrasser, R. M. Femtosecond Laser Studies of the Cis-Stilbene Photoisomerization Reactions: The Cis-Stilbene to Dihydrophenanthrene Reaction. *J. Phys. Chem.* **1991**, *95* (25), 10380–10385. <https://doi.org/10.1021/j100178a026>.
- (12) Moore, W. M.; Morgan, D. D.; Stermitz, F. R. The Photochemical Conversion of Stilbene to Phenanthrene. The Nature of the Intermediate. *J. Am. Chem. Soc.* **1963**, *85* (6), 829–830. <https://doi.org/10.1021/ja00889a050>.
- (13) Irie, M. Diarylethenes for Memories and Switches. *Chem. Rev.* **2000**, *100* (5), 1685–1716. <https://doi.org/10.1021/cr980069d>.
- (14) Muszkat, K. A.; Fischer, E. Structure, Spectra, Photochemistry, and Thermal Reactions of the 4a,4b-Dihydrophenanthrenes. *J. Chem. Soc. B Phys. Org.* **1967**, No. 0, 662–678. <https://doi.org/10.1039/J29670000662>.
- (15) Gooden, R.; Brauman, J. I. Photodissociation of Stilbene Radical Cation. *J. Am. Chem. Soc.* **1982**, *104* (6), 1483–1486. <https://doi.org/10.1021/ja00370a006>.
- (16) Mo, Y.; Lin, Z.; Wu, W.; Zhang, Q. Bond-Distorted Orbitals and Effects of Hybridization and Resonance on C–C Bond Lengths. *J. Phys. Chem.* **1996**, *100* (28), 11569–11572. <https://doi.org/10.1021/jp953433a>.
- (17) Le Bahers, T.; Adamo, C.; Ciofini, I. A Qualitative Index of Spatial Extent in Charge-Transfer Excitations. *J. Chem. Theory Comput.* **2011**, *7* (8), 2498–2506. <https://doi.org/10.1021/ct200308m>.
- (18) Huang, S.-T.; Hsu, Y.-C.; Yen, Y.-S.; Chou, H. H.; Lin, J. T.; Chang, C.-W.; Hsu, C.-P.; Tsai, C.; Yin, D.-J. Organic Dyes Containing a Cyanovinyl Entity in the Spacer for Solar Cells Applications. *J. Phys. Chem. C* **2008**, *112* (49), 19739–19747. <https://doi.org/10.1021/jp806606h>.
- (19) Le Bahers, T.; Adamo, C.; Ciofini, I. A Qualitative Index of Spatial Extent in Charge-Transfer Excitations. *J. Chem. Theory Comput.* **2011**, *7* (8), 2498–2506. <https://doi.org/10.1021/ct200308m>.
- (20) Huang, S.-T.; Hsu, Y.-C.; Yen, Y.-S.; Chou, H. H.; Lin, J. T.; Chang, C.-W.; Hsu, C.-P.; Tsai, C.; Yin, D.-J. Organic Dyes Containing a Cyanovinyl Entity in the Spacer for Solar Cells Applications. *J. Phys. Chem. C* **2008**, *112* (49), 19739–19747. <https://doi.org/10.1021/jp806606h>.

- (21) Preat, J.; Jacquemin, D.; Perpète, E. A. Towards New Efficient Dye-Sensitized Solar Cells. *Energy Environ. Sci.* **2010**, *3* (7), 891–904. <https://doi.org/10.1039/C000474J>.
- (22) Zhang, J.; Li, H.-B.; Sun, S.-L.; Geng, Y.; Wu, Y.; Su, Z.-M. Density Functional Theory Characterization and Design of High-Performance Diarylamine-Fluorene Dyes with Different π Spacers for Dye-Sensitized Solar Cells. *J. Mater. Chem.* **2011**, *22* (2), 568–576. <https://doi.org/10.1039/C1JM13028E>.
- (23) Ji, Z.; Hai-Bin, L. I.; Yong, W. U.; Yun, G.; Yu-Ai, D.; Yi*, L.; Zhong-Min*, S. U. TD-DFT Studies on Phenothiazine-Based Dyes with Different Donor in Dye-Sensitized Solar Cells. *Chem. J. Chin. Univ.* **2011**, *32* (6), 1343.
- (24) Preat, J.; Jacquemin, D.; Michaux, C.; Perpète, E. A. Improvement of the Efficiency of Thiophene-Bridged Compounds for Dye-Sensitized Solar Cells. *Chem. Phys.* **2010**, *376* (1), 56–68. <https://doi.org/10.1016/j.chemphys.2010.08.001>.
- (25) Fan, W.; Tan, D.; Deng, W.-Q. Acene-Modified Triphenylamine Dyes for Dye-Sensitized Solar Cells: A Computational Study. *ChemPhysChem* **2012**, *13* (8), 2051–2060. <https://doi.org/10.1002/cphc.201200064>.
- (26) Chen, J.; Bai, F.-Q.; Wang, J.; Hao, L.; Xie, Z.-F.; Pan, Q.-J.; Zhang, H.-X. Theoretical Studies on Spectroscopic Properties of Ruthenium Sensitizers Absorbed to TiO₂ Film Surface with Connection Mode for DSSC. *Dyes Pigments* **2012**, *94* (3), 459–468. <https://doi.org/10.1016/j.dyepig.2012.01.018>.
- (27) Fujisawa, J.; Hanaya, M. Light Harvesting and Direct Electron Injection by Interfacial Charge-Transfer Transitions between TiO₂ and Carboxy-Anchored Dye LEG4 in Dye-Sensitized Solar Cells. *J. Phys. Chem. C* **2018**, *122* (1), 8–15. <https://doi.org/10.1021/acs.jpcc.7b04749>.
- (28) Meng, S.; Ren, J.; Kaxiras, E. Natural Dyes Adsorbed on TiO₂ Nanowire for Photovoltaic Applications: Enhanced Light Absorption and Ultrafast Electron Injection. *Nano Lett.* **2008**, *8* (10), 3266–3272. <https://doi.org/10.1021/nl801644d>.
- (29) Hagfeldt, Anders.; Graetzel, Michael. Light-Induced Redox Reactions in Nanocrystalline Systems. *Chem. Rev.* **1995**, *95* (1), 49–68. <https://doi.org/10.1021/cr00033a003>.
- (30) Gaussian 09, Revision A.02, M. J. Frisch, G. W. Trucks, H. B. Schlegel, G. E. Scuseria, M. A. Robb, J. R. Cheeseman, G. Scalmani, V. Barone, B. Mennucci, G. A. Petersson, H. Nakatsuji, M. Caricato, X. Li, H. P. Hratchian, A. F. Izmaylov, J. Bloino, G. Zheng, J. L. Sonnenberg, M. Hada, M. Ehara, K. Toyota, R. Fukuda, J. Hasegawa, M. Ishida, T. Nakajima, Y. Honda, O. Kitao, H. Nakai, T. Vreven, J. A. Montgomery, Jr., J. E. Peralta, F. Ogliaro, M. Bearpark, J. J. Heyd, E. Brothers, K. N. Kudin, V. N. Staroverov, R. Kobayashi, J. Normand, K. Raghavachari, A. Rendell, J. C. Burant, S. S. Iyengar, J. Tomasi, M. Cossi, N. Rega, J. M.

- Millam, M. Klene, J. E. Knox, J. B. Cross, V. Bakken, C. Adamo, J. Jaramillo, R. Gomperts, R. E. Stratmann, O. Yazyev, A. J. Austin, R. Cammi, C. Pomelli, J. W. Ochterski, R. L. Martin, K. Morokuma, V. G. Zakrzewski, G. A. Voth, P. Salvador, J. J. Dannenberg, S. Dapprich, A. D. Daniels, O. Farkas, J. B. Foresman, J. V. Ortiz, J. Cioslowski, and D. J. Fox, Gaussian, Inc., Wallingford CT, 2009.
- (31) Chai, J.-D.; Head-Gordon, M. Long-Range Corrected Hybrid Density Functionals with Damped Atom–Atom Dispersion Corrections. *Phys. Chem. Chem. Phys.* **2008**, *10* (44), 6615–6620. <https://doi.org/10.1039/B810189B>.
- (32) Do, K.; Saleem, Q.; Ravva, M. K.; Cruciani, F.; Kan, Z.; Wolf, J.; Hansen, M. R.; Beaujuge, P. M.; Brédas, J.-L. Impact of Fluorine Substituents on π -Conjugated Polymer Main-Chain Conformations, Packing, and Electronic Couplings. *Adv. Mater.* **2016**, *28* (37), 8197–8205. <https://doi.org/10.1002/adma.201601282>.
- (33) Boese, A. D.; Martin, J. M. L. Development of Density Functionals for Thermochemical Kinetics. *J. Chem. Phys.* **2004**, *121* (8), 3405–3416. <https://doi.org/10.1063/1.1774975>.
- (34) Tomasi, J.; Mennucci, B.; Cammi, R. Quantum Mechanical Continuum Solvation Models. *Chem. Rev.* **2005**, *105* (8), 2999–3094. <https://doi.org/10.1021/cr9904009>.
- (35) Chaitanya, K.; Ju, X.-H.; Heron, B. M. Can Elongation of the π -System in Triarylamine Derived Sensitizers with Either Benzothiadiazole and/or Ortho-Fluorophenyl Moieties Enrich Their Light Harvesting Efficiency? – A Theoretical Study. *RSC Adv.* **2015**, *5* (6), 3978–3998. <https://doi.org/10.1039/C4RA09914A>.
- (36) Jiao, Y.; Ma, W.; Meng, S. Quinoid Conjugated Dye Designed for Efficient Sensitizer in Dye Sensitized Solar Cells. *Chem. Phys. Lett.* **2013**, *586*, 97–99. <https://doi.org/10.1016/j.cplett.2013.09.008>.
- (37) Ma, W.; Jiao, Y.; Meng, S. Predicting Energy Conversion Efficiency of Dye Solar Cells from First Principles. *J. Phys. Chem. C* **2014**, *118* (30), 16447–16457. <https://doi.org/10.1021/jp410982e>.
- (38) Zhang, J.; Zhang, J.-Z.; Li, H.-B.; Wu, Y.; Geng, Y.; Su, Z.-M. Rational Modifications on Champion Porphyrin Dye SM315 Using Different Electron-Withdrawing Moieties toward High Performance Dye-Sensitized Solar Cells. *Phys. Chem. Chem. Phys.* **2014**, *16* (45), 24994–25003. <https://doi.org/10.1039/C4CP03355H>.
- (39) Deng, W. F. and W. Incorporation of Thiadiazole Derivatives as π -Spacer to Construct Efficient Metal-Free Organic Dye Sensitizers for Dye-Sensitized Solar Cells: A Theoretical Study. *Commun. Comput. Chem.* **2013**, *1* (2), 152–170. <https://doi.org/10.4208/cicc.2013.v1.n2.6>.

- (40) Wang, J.; Li, H.; Ma, N.-N.; Yan, L.-K.; Su, Z.-M. Theoretical Studies on Organoimido-Substituted Hexamolybdates Dyes for Dye-Sensitized Solar Cells (DSSC). *Dyes Pigments* **2013**, *99* (2), 440–446. <https://doi.org/10.1016/j.dyepig.2013.05.027>.
- (41) Zhang, J.; Kan, Y.-H.; Li, H.-B.; Geng, Y.; Wu, Y.; Su, Z.-M. How to Design Proper π -Spacer Order of the D- π -A Dyes for DSSCs? A Density Functional Response. *Dyes Pigments* **2012**, *95* (2), 313–321. <https://doi.org/10.1016/j.dyepig.2012.05.020>.
- (42) Feng, J.; Jiao, Y.; Ma, W.; Nazeeruddin, Md. K.; Grätzel, M.; Meng, S. First Principles Design of Dye Molecules with Ullazine Donor for Dye Sensitized Solar Cells. *J. Phys. Chem. C* **2013**, *117* (8), 3772–3778. <https://doi.org/10.1021/jp310504n>.
- (43) Asbury, J. B.; Wang, Y.-Q.; Hao, E.; Ghosh, H. N.; Lian, T. Evidences of Hot Excited State Electron Injection from Sensitizer Molecules to TiO₂ Nanocrystalline Thin Films. *Res. Chem. Intermed.* **2001**, *27* (4–5), 393–406. <https://doi.org/10.1163/156856701104202255>.
- (44) Docampo, P.; Guldin, S.; Leijtens, T.; Noel, N. K.; Steiner, U.; Snaith, H. J. Lessons Learned: From Dye-Sensitized Solar Cells to All-Solid-State Hybrid Devices. *Adv. Mater.* **2014**, *26* (24), 4013–4030. <https://doi.org/10.1002/adma.201400486>.
- (45) Marcus, R. A. Electron Transfer Reactions in Chemistry. Theory and Experiment. *Rev. Mod. Phys.* **1993**, *65* (3), 599–610. <https://doi.org/10.1103/RevModPhys.65.599>.
- (46) Le Bahers, T.; Brémond, E.; Ciofini, I.; Adamo, C. The Nature of Vertical Excited States of Dyes Containing Metals for DSSC Applications: Insights from TD-DFT and Density Based Indexes. *Phys. Chem. Chem. Phys.* **2014**, *16* (28), 14435. <https://doi.org/10.1039/c3cp55032j>.
- (47) Le Bahers, T.; Adamo, C.; Ciofini, I. A Qualitative Index of Spatial Extent in Charge-Transfer Excitations. *J. Chem. Theory Comput.* **2011**, *7* (8), 2498–2506. <https://doi.org/10.1021/ct200308m>.

General conclusions and perspectives

In this work, solid-state dye-sensitized solar cells based on purely organic sensitizers have been developed in order to further enhance the energy conversion efficiency, along with a better understanding of the relationship between the developed materials and the corresponding device performance. As such, this manuscript contains a general context of photovoltaic solar cells, the working principal, and parameters of DSSCs, the state-of-the-art concept of novel organic dyes by deeply understanding the nature of sensitizers, the experimental and theoretical results of DSSCs fabricated with originally designed sensitizer, respectively.

In chapter 2, the structure and different components of dye sensitized solar cell are firstly introduced, namely TCOs, the metal oxide semiconductor, the sensitizer, the redox mediator, and the counter electrode. Secondly, the operational principles and fundamental processes that take place in the device involving light absorption, electron injection and transport, dye regeneration by the redox mediator, and restoration of redox mediator are described, where also includes the thermodynamic and kinetic aspects. Thirdly, basic parameters to characterize DSSCs such as V_{OC} (the open circuit voltage), J_{SC} (the current density), FF (the fill factor), IPCE (the incident photon-to-electron conversion efficiency) and η (overall energy conversion efficiency) together with usual characterization techniques including I-V (current-voltage) and IPCE measurement and EIS (electrochemical impedance spectroscopy) are demonstrated. In the last part, the aim of the thesis is presented.

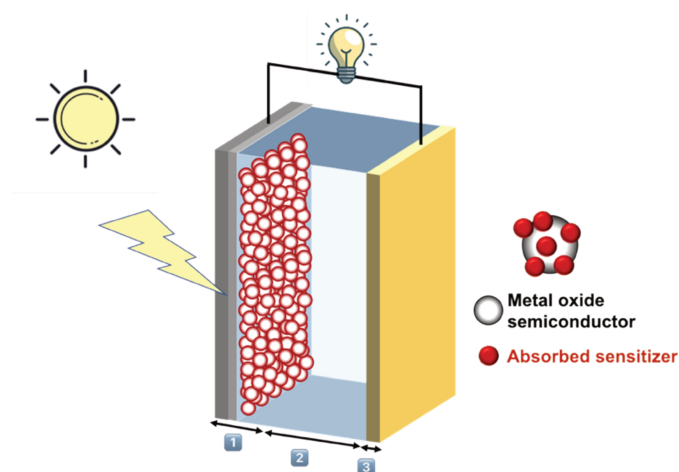


Figure 0.1 Schematic representation of a DSSC: transparent conductive oxide (light grey); transparent conductive glass (dark grey); semiconductor metal oxide covered with sensitizer (red); redox mediator (blue); and counter electrode (yellow).

Chapter 3 starts with the presentation of three main classes of sensitizers: Ru-based complexes, Zn-porphyrins, and metal-free sensitizers which are typically of D- π -A push-pull structure to induce an ICT (intramolecular charge transfer). Examples of different choices of donors, acceptors and π -spacers are listed. One branch of the metal-free sensitizers, TAA-based sensitizers are particularly stressed to point out its advantages, such as the prominent electron donating ability, excellent hole transport capability, its propeller starburst molecular structure with non-planar configuration which could prevent intermolecular π - π aggregation. The framework of design strategies is also established especially for the fully organic sensitizers in the process to tune the properties such as the absorption band shift by the extension of π -spacers, lowered recombination dynamics by the introduction of an alkyl chain. As such, new original sensitizers which could be covalently linked to the HTM are designed in the aim of eliminating the surface to improve the performance of ss-DSSCs. The retrosynthetic analysis towards simple precursors as well as the versatile synthesis to obtain target sensitizers IS then presented.

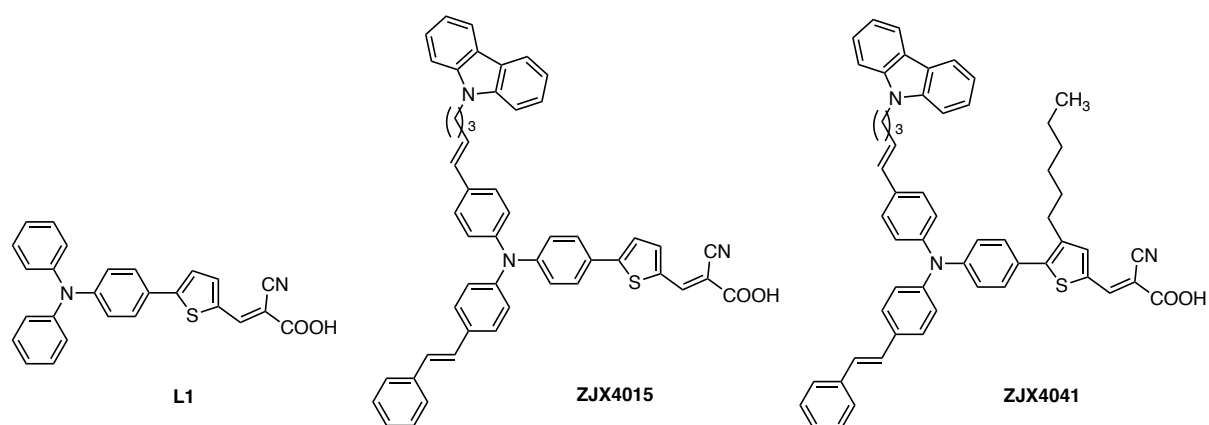


Figure 2 Molecular structures of the **ZJX4015** and **ZJX4041** organic D- π -A dyes covalently linked to the carbazole monomer. The structure of **L1** is displayed for comparison.

In Chapter 4, optimization of interfacial charge transfer was firstly mentioned which explains the purpose of the covalent link of HTM to the sensitizer, followed by explicit presentation of the *in-situ* PEP process which will produce directly the conducting co-polymer that serves as HTM. In the second part, each step of the fabrication process of solar cells is described in detail: the deposition of compact blocking TiO₂ layer, the deposition of mesoporous TiO₂, dye sensitization, *in-situ* PEP, and preparation of the counter electrode. Experimental results of properties of dyes and solar cells including improved performance were presented. Cyclic voltammetry (CV), ultraviolet-visible spectroscopy (UV-vis), fluorescence,

chronoamperometry (CA), and current-voltage measurements (I-V curves) and EIS were applied to characterize the physico-chemical properties of sensitizers, sensitizer-adsorbed TiO₂ photoanode, and DSSC. Overall energy conversion efficiencies of 4.0% and 4.8% were obtained for **ZJX4015**- and **ZJX4041**-based DSSCs, respectively.

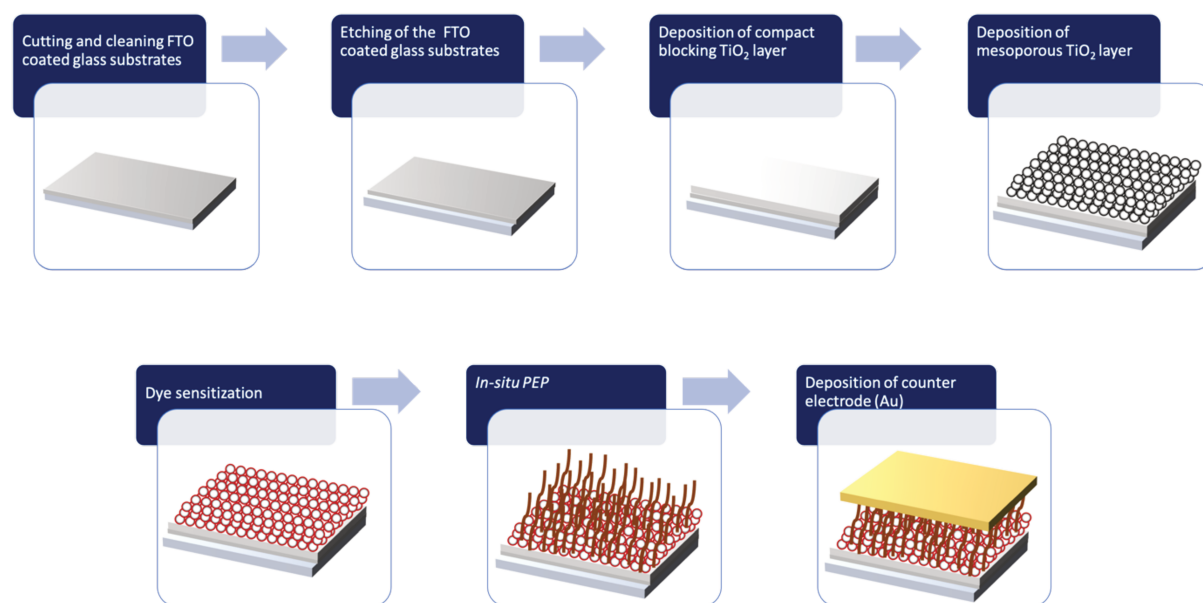


Figure 3 ss-DSSC fabrication process demonstration

Chapter 5 focuses on the investigation of sensitizers by means of quantum calculations based on DFT and TD-DFT for a fine understanding on the electronic structures and properties of the molecular dyes studied in the thesis, which is of great importance to establish a structure-property relationship. Conformational properties of the C3 alkyl chain linking the TPA core and the monomer carbazole are firstly discussed by studying the sensitizer **ZJX4015**. We obtained not only a clear electronic structure of sensitizers, but also satisfactory results in agreement with experimental results are presented, for example, optical properties, and energy levels. Moreover, in addition to the HOMO-LUMO gap and optical property differences which originate from the structural features of **ZJX4041** and **ZJX4015**, contrasting photovoltaic properties are also observed depending on the evaluated parameter.

The newly designed purely organic sensitizers with covalently linked HTM with interesting physicochemical properties are proved to be promising candidates for ss-DSSCs. Following investigations are proposed, either on sensitizers by (i) extension of p bridge with fabricated blocking block molecules to further enlarge absorption spectrum (ii) variation of electroactive monomer (iii) substitution on TPA donor; or on devices by systematically studying on the time-

dependent evolution of solar cells. Additional theoretical investigations could also be performed taking account of the electrodes and HTM to further understand the complexity of the system.

Appendix

Experimental methods and materials

^1H NMR and ^{13}C NMR spectra were recorded at 400 MHz, on Bruker Avance III 400 spectrometer at 298 K using CDCl_3 or DMSO as solvent. Chemical shifts are reported in ppm downfield from tetramethylsilane (TMS: $\delta = 0$ ppm) relative to the signal corresponding to the residual non-deuterated solvent (CD_3CN : δ 1.94 ppm; CDCl_3 : δ 7.26 ppm). Full assignments were made using COSY, HMBC and HMQC methods. The following abbreviations were used to describe the signals: s for singlet, d for doublet, t for triplet, m for multiplet. All chemicals and solvent purchased from Sigma-Aldrich, Fluka, TCI and VWR were analytical grade and were used without further purification. Thin layer chromatography (TLC) was carried out on plates coated with silica gel 40 F254 purchased from Aldrich. All reactions were conducted under dry oxygen free atmosphere using oven-dried glassware unless otherwise stated.

The optical properties of dyes were investigated by fluorescence spectroscopy in acetonitrile ($C = 4 \times 10^{-6}$ M), by UV-Vis spectroscopy in DCM ($C = 2 \times 10^{-5}$ M). These experimental results were compared to the theoretical results obtained using the DFT.

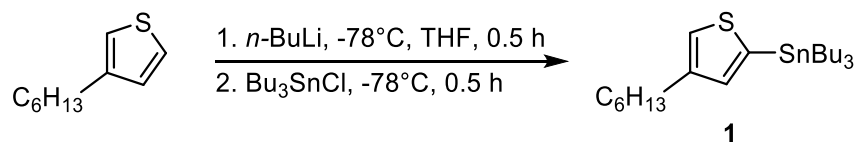
The electrochemical properties of **ZJX4015**, **ZJX4041**, and **L1** dyes are investigated by cyclic voltammetry (CV) in acetonitrile containing 0.1 M LiClO_4 . The measurements were carried out using a Biologic P150 potentiostat/galvostat. To measure UV-Vis-NIR absorption spectra in solid state, dye-sensitized TiO_2 electrodes, with and without PEDOT are prepared. The measurements were performed on a Cary 5000 UV-Vis-NIR spectrophotometer (VARIAN, photometric accuracy is ≤ 0.00025 Abs., photometric range is 8 Abs.). The TiO_2/FTO substrate signal was used as calibration background.

The *in-situ* PEP process was carried out by chronoamperometry (see the experimental section below) in organic medium using bis-EDOT as monomer precursor. ss-DSSCs are assembled following the procedure detailed in the following. The photovoltaic performances of ss-DSSCs are determined from the I-V curves and from Electrochemical Impedance Spectroscopy (EIS) measurements.

Synthesis and characterization data

Synthesis of thiophenes

4-Hexyl-2-(tributylstannyl)thiophene (1)

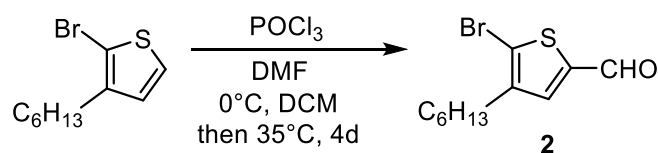


To a solution of 3-hexylthiophene (2.1 mL, 12 mmol) in THF (20 mL) under argon, *n*-BuLi (9.4 mL, 15 mmol) of 1.6 M, was added dropwise at -78°C . The solution was stirred at -78°C for 0.5 h then allowed to return to room temperature and stirred at room temperature for 0.5 h. The reaction mixture was again cooled to -78°C and Bu_3SnCl (4 mL, 15 mmol) was added. The solution was stirred at room temperature for 16 hours and then poured into ice water. After the extraction with DCM, the organic layer was dried over MgSO_4 . The solvent was removed by reduced pressure, giving the crude product **1** as yellow oil, which was used for next step without further purification.

$^1\text{H NMR}$ (400 MHz, CDCl_3) : δ 7,19 (s, 1H), 6,97 (s, 1H), 2,67-2,64 (t, 2H, $J = 3,7$ Hz), 1,65-1,53 (m, 6H), 1,39-1,30 (m, 8H), 1,15-1,05 (m, 12H), 1,00-0,87 (m, 12H)

$^{13}\text{C NMR}$ (101 MHz, CDCl_3) δ 144.58, 137.03, 136.47, 125.72, 31.92, 30.90, 30.21, 29.49, 29.18, 27.36, 22.77, 14.11, 13.66, 11.11.

2-Bromo-5-formyl-3-hexylthiophene (**2**)

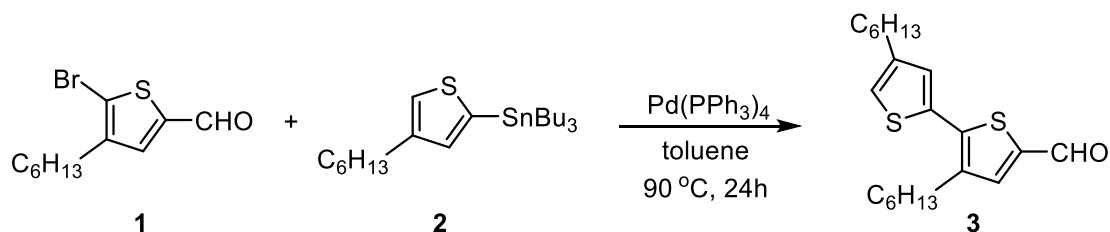


POCl_3 (31 mL, 33 mmol) was injected under argon dropwise into anhydrous DMF (35 mL, 45 mmol) at 0°C . The solution was stirred for one hour at 0°C , and then 2-bromo-3-hexylthiophene (4.5 g, 1.8 mmol) in anhydrous DCM (40 mL) was added dropwise at 0°C . After heating at 35°C for 4 days, the mixture was cooled to room temperature and then poured in ice water (600 mL). The NaOH was added into the solution in order to neutralize the medium. The mixture was extracted with DCM and washed with water. The organic layer was dried over MgSO_4 . After removal of the solvents under reduced pressure, the crude product was purified by column chromatography (ethyl acetate/petroleum ether 4:96) to give 2-bromo-5-formyl-3-hexylthiophene (**2**) as yellow oil (4.26 g, 85%).

$^1\text{H NMR}$ (400 MHz, CDCl_3) δ 9.72 (s, 1H), 7.44 (s, 1H), 2.56 (t, $J = 7.7$ Hz, 2H), 1.63 – 1.52 (m, 2H), 1.30 (m 6H), 0.92 – 0.82 (m, 3H).

^{13}C NMR (101 MHz, CDCl_3) δ 182.28, 143.23, 138.35, 111.34, 31.73, 29.71, 29.45, 29.02, 28.67, 22.67, 14.06.

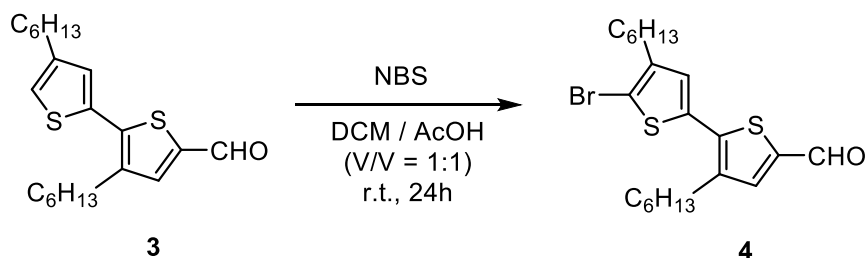
3,4'-Dihexyl-2,2'-dithiophene-5-carbaldehyde (3)



Under argon, a solution of 3-hexyl-5-tributylstannylthiophene (5.95 g, 13 mmol), 2-bromo-5-formyl-3-hexylthiophene (2.47 g, 13 mmol) and $\text{Pd}(\text{PPh}_3)_4$ (0.376 g, 0.325 mmol) in deaerated toluene was heated at 90°C for 24 hours. The solution was extracted with DCM and then washed with water. After drying the organic layer over MgSO_4 , the solvent was removed under reduced pressure. The mixture was purified by column chromatography (DCM/Petroleum ether 3:7) to give 3,4'-dihexyl-2,2'-dithiophene-5-carbaldehyde (**3**) as yellow oil (4.16 g, 88%).

^1H NMR (400 MHz, CDCl_3) δ 9.81 (s, 1H), 7.56 (s, 1H), 6.95 (s, 1H), 2.82 – 2.75 (m, 2H), 2.64 – 2.59 (m, 2H), 1.70 – 1.59 (m, 4H), 1.45 – 1.21 (m, 12H), 0.95 – 0.82 (m, 6H).

5'-Bromo-3,4'-dihexyl-(2,2'-dithiophene)-5-carbaldehyde (4)

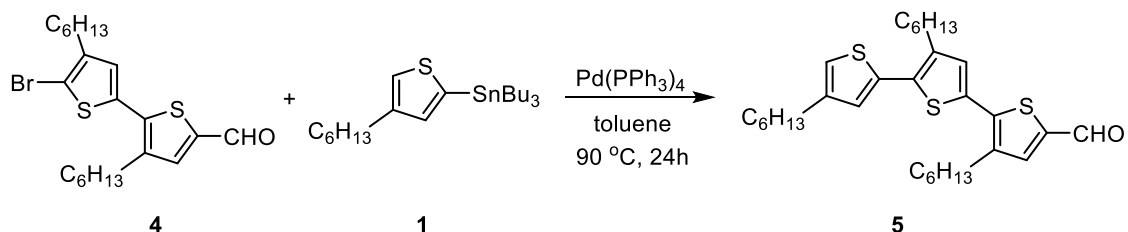


At 0°C , *N*-bromosuccinimide (0.982 g, 5.52 mmol) was added in small portions to a solution of compound 3,4'-dihexyl-2,2'-dithiophene-5-carbaldehyde (2.00 g, 5.52 mmol) in chloroform and acetic acid (30 ml / 30 ml, 1:1, v/v). After being stirred for 24 hours at room temperature, the reaction mixture was poured into water and extracted with DCM. The organic layer was thoroughly washed with water, aqueous sodium bicarbonate, and brine and again with water, and then dried over MgSO_4 . After removal of solvent, the crude product (2.34 g, 96%) was used for the next step without further purification.

^1H NMR (400 MHz, CDCl_3) δ 9.82 (s, 1H), 7.56 (s, 1H), 6.96 (s, 1H), 2.78 – 2.71 (m, 2H), 2.61 – 2.52 (m, 2H), 1.62 (m, 4H), 1.43 – 1.22 (m, 12H), 0.96 – 0.82 (m, 6H).

^{13}C NMR (101 MHz, CDCl_3) δ 182.23, 143.21, 141.12, 140.94, 140.50, 138.32, 134.74, 128.56, 111.32, 31.72, 31.68, 30.54, 30.44, 29.44, 29.20, 29.10, 29.01, 22.67, 22.66, 14.05, 14.02.

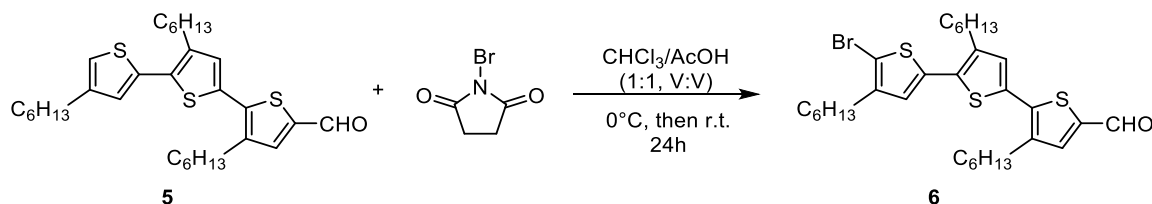
3,4',4''-trihexyl-2,2':5',2''-terthiophene-5-carbaldehyde (5)



Under argon, a solution of **1** (0.39 g, 0.85 mmol), **4** (0.15 g, 0.34 mmol) and $\text{Pd}(\text{PPh}_3)_4$ (10 mg, 8.49×10^{-6} mol) in deaerated toluene was heated at 90°C for 24 hours. The solution was extracted by DCM and then washed by water. After drying the organic layer over MgSO_4 , the solvent was removed under reduced pressure. The mixture was purified by column chromatography (DCM/Petroleum ether: 3:7) to give the product **5** as yellow oil (0.17 g, 94%).

^1H NMR (400 MHz, CDCl_3) δ 9.82 (s, 1H), 7.58 (s, 1H), 7.11 (s, 1H), 7.00 (d, $J = 1.4$ Hz, 1H), 6.94 (d, $J = 1.3$ Hz, 1H), 2.86 – 2.71 (m, 4H), 2.65 – 2.58 (m, 2H), 1.76 – 1.60 (m, 6H), 1.47 – 1.23 (m, 18H), 0.94 – 0.81 (m, 9H).

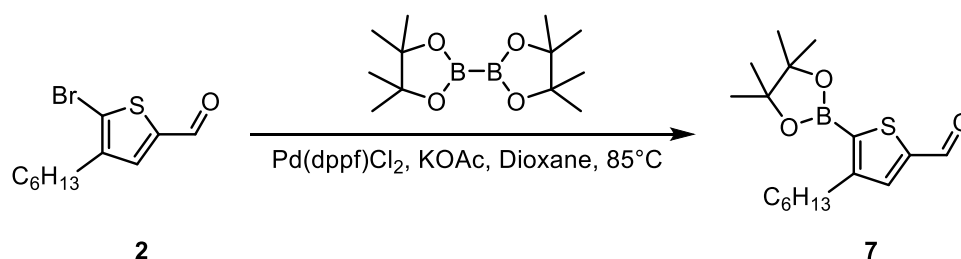
5''-Bromo-3,4',4''-trihexyl-(2,2':3',2''-terthiophene)-5-carbaldehyde (6)



At 0°C , *N*-bromosuccinimide (23 mg, 0.13 mmol) was added in small portions to a solution of **5** (80 mg, 0.13 mmol) in chloroform and acetic acid (0.7 ml / 0.7 ml, 1:1, v/v). After being stirred for 24 h at room temperature, the reaction mixture was poured into water and extracted with DCM. The organic layer was thoroughly washed with water, aqueous sodium bicarbonate, brine and again with water, and then dried over MgSO_4 . After removal of solvent, the crude product **6** was used for next step without further purification.

^1H NMR (400 MHz, CDCl_3) δ 9.82 (s, 1H), 7.58 (s, 1H), 7.09 (s, 1H), 6.85 (s, 1H), 2.85 – 2.77 (m, 2H), 2.75 – 2.69 (m, 2H), 2.61 – 2.54 (m, 2H), 1.73 – 1.56 (m, 6H), 1.47 – 1.23 (m, 18H), 0.92 – 0.80 (m, 9H).

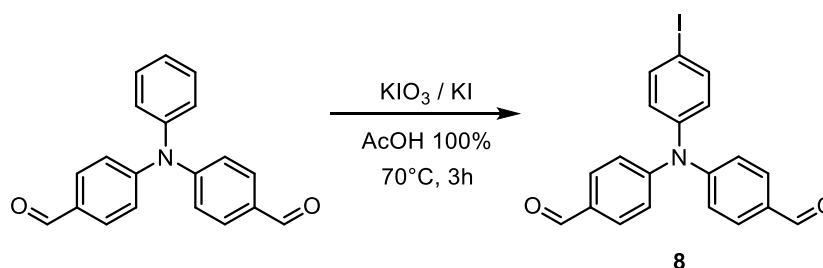
4-Hexyl-5-(4,4,5,5-tetramethyl-1,3,2-dioxaborolan-2-yl)-2-thiophenecarboxaldehyde (**7**)



To a degassed solution of **2** (2.72 g, 10 mmol, 1 eq.), bis(pinacolato)diboron (5.08 mg, 20 mmol, 2 eq.) and K_3PO_4 (6.4 g, 30 mmol, 3 eq.) in dioxane (10 mL), was added $Pd(dppf)Cl_2$ (860 mg, 1 mmol, 10 %). The reaction mixture was stirred under argon at 85 °C for 16 hours. After evaporation of the solvents, CH_2Cl_2 (20 mL) was added and the mixture was extracted with H_2O (2 x 20 mL). The combined organic layers were dried ($MgSO_4$). After evaporation of the solvents, the crude product was purified by column chromatography (SiO_2 , Petroleum Ether / DCM = 3/1 then 1/1), affording the desired product as a yellow oil in 56 % yield (1.8 g).

Preparations of Wittig reactions

4,4'-(4-iodophenylazanediyl)dibenzaldehyde (**8**)

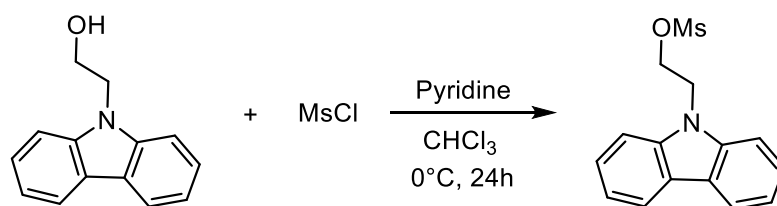


KI (2.9 g, 17.45 mmol) and KIO_3 (5.15 g, 24.2 mmol) was added in a solution of 4,4'-diformyltriphenylamine (5 g, 16.6 mmol) in glacial acetic acid (125 ml). The reaction mixture was heated to 70 °C and stirred for 3 hours. The solution was firstly filtered than extracted with DCM (100 ml) / H_2O (100 ml). The organic phase obtained was washed with a saturated solution of $NaHCO_3$ and was then dried over anhydrous Na_2SO_4 . After filtration and evaporation of the solvent under reduced pressure, the product **8** was obtained as yellow-greenish solid (6.43 g, 90 %).

1H NMR (400 MHz, $CDCl_3$) δ (ppm): 9.90 (s, 2H), 7.80 (d, $J = 8.7$ Hz, 4H), 7.70 (d, $J = 8.8$ Hz, 2H), 7.12 (d, $J = 8.6$ Hz, 4H), 6.93 (d, $J = 8.8$ Hz, 2H).

Carbazoles (2-4C chain)

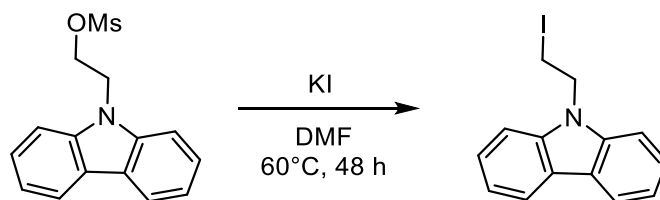
2-(9H-carbazol-9-yl)ethyl methanesulfonate



To a solution of 9H-carbazole-9-ethanol (3.00 g, 14 mmol) and pyridine (3.3 mL, 42 mmol) in CHCl₃ (60 mL) at 0°C, freshly distilled MsCl (1.8 mL, 23 mmol) was added dropwise. The reaction mixture was stirred for 24 hours. The solution was first washed with KHSO₄ and then with saturated NaHCO₃. The organic layer was dried over MgSO₄. After evaporation of the solvent under reduced pressure, the product was obtained as a white solid (6.00 g) and used directly for the next step without any further purification.

¹H NMR (400 MHz, CDCl₃) δ 8.10 (d, 2H, *J* = 3.9 Hz), 7.52-7.42 (m, 4H), 7.31-7.24 (m, 2H), 4.67 (t, 2H, *J* = 5.5 Hz), 4.59 (t, 2H, *J* = 5.5 Hz), 3.0 (s, 3H)

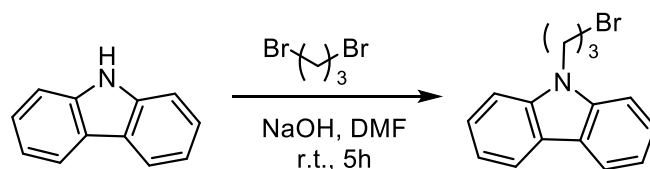
9-(2-iodoethyl)-9H-carbazole



The solution of 2-(9H-carbazol-9-yl)ethyl methanesulfonate and KI in dry DMF was stirred at 60°C for 48 hours. After the evaporation of DMF, the mixture was dissolved in DCM and water. The organic layer was washed with water then dried over MgSO₄. After removal of the solvent under reduced pressure, the crude product was purified by column chromatography (DCM/ Petroleum ether 1:9) to give 9-(2-iodoethyl)-9H-carbazole as white solid.

¹H NMR (400 MHz, CDCl₃) δ 8.10-8.08 (d, 2H, *J* = 3.9 Hz), 7.49-7.45 (t, 2H, *J* = 4.1 Hz), 7.41-7.39 (d, 2H, *J* = 4.1 Hz), 7.28-7.24 (t, 2H, *J* = 3.7 Hz), 4.70-4.66 (t, 2H, *J* = 4.0 Hz), 3.45-3.40 (t, 2H, *J* = 4.0 Hz)

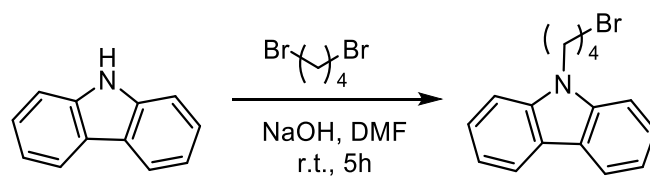
9-(3-bromopropyl)-9H-carbazole



To a mixture of carbazole (1.5 g, 9 mmol) and NaOH (520 mg, 13 mmol) in DMF (30 mL) at 0 °C was added 1,3-dibromopropane (5.4 g, 27 mmol, 3 eq). The reaction mixture was stirred at room temperature for 16 h. The DMF was evaporated under reduced pressure. The mixture was dissolved in DCM/H₂O, the organic phase obtained was dried over MgSO₄ and the solvent was removed under reduced pressure. The residue was purified by column chromatography (silica gel, petroleum ether: EtOAc = 5:1) to the corresponding product (2.0 g, 79 %) as white powder.

¹H NMR (400 MHz, CDCl₃) δ 8.12 (dt, *J* = 7.8, 1.0 Hz, 2H), 7.52 – 7.48 (m, 4H), 7.29 – 7.22 (m, 2H), 4.53 (t, *J* = 6.5 Hz, 2H), 3.41 (t, *J* = 6.5 Hz, 2H), 2.46 (m, 2H)

9-(4-Bromobutyl)-9*H*-carbazole (**9**)



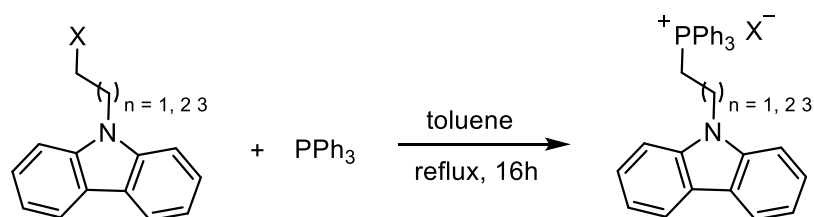
9

The same procedure as *9*-(3-bromopropyl)-9*H*-carbazole synthesis, while using 1,4-dibromopropane. Yield: 2.2 g, 81%.

¹H NMR (400 MHz, CDCl₃) δ 8.13 (dt, *J* = 7.7, 1.0 Hz, 2H), 7.50 (ddd, *J* = 8.2, 7.0, 1.0 Hz, 2H), 7.43 (dt, *J* = 8.2, 1.0 Hz, 2H), 7.32 – 7.19 (m, 2H), 4.38 (t, *J* = 7.0 Hz, 2H), 3.40 (t, *J* = 7.0 Hz, 2H), 2.19 – 2.03 (m, 2H), 2.00 – 1.86 (m, 2H).

¹³C NMR (101 MHz, CDCl₃) δ 140.41, 125.85, 123.03, 120.56, 119.09, 108.66, 42.29, 33.27, 30.38, 27.79.

General procedure for the phosphonium bromides CBZ-*n*C-PPh₃-X (*n* = 2,3,4)



Triphenylphosphine (15 mmol) was added to the solution of 9-(halogenoalkyl)-9H-carbazole (5 mmol) in toluene (80 ml). The mixture was stirred under reflux for 16 h. After cooling to room temperature, the salts were filtered off and washed with DCM. The combined organic phase was evaporated under reduced pressure. The residue was purified by silica gel column chromatography using 5% of MeOH in DCM to afford the compound as white solid.

CBZ-2C(ethyl)-PPh₃-X

¹H NMR (400 MHz, CDCl₃) δ 7,90-7,80 (d, 2H, $J = 3,7$ Hz), 7,70-7,50 (m, 9H), 7,47-7,44 (m, 6H), 7,23-7,20 (t, 2H, $J = 3,84$ Hz), 7,12-7,09 (t, 2H, $J = 3,7$ Hz), 7,00-6,98 (d, 2H, $J = 4,1$ Hz), 5,06-4,98 (dt, 2H, $J_1 = 9,7$ Hz, $J_2 = 6,1$ Hz), 4,60-4,54 (m, 2H)

CBZ-3C(propyl)-PPh₃-X

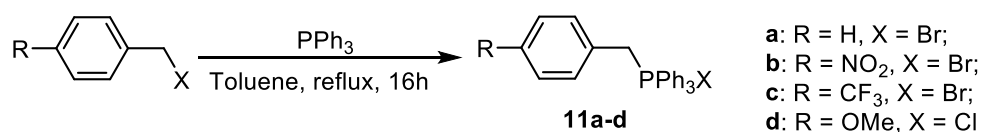
¹H NMR (400 MHz, CDCl₃) δ 8.03 (dt, $J = 7.8, 1.0$ Hz, 2H), 7.67 (m, 3H), 7.57 – 7.46 (m, 13H), 7.41 – 7.33 (m, 4H), 7.19 (ddd, $J = 7.9, 5.1, 3.0$ Hz, 2H), 4.48 (t, $J = 6.0$ Hz, 2H), 3.85 – 3.69 (m, 2H), 2.39 (p, $J = 6.7$ Hz, 2H).

CBZ-4C(butyl)-PPh₃-Br (10)

¹H NMR (400 MHz, CDCl₃) δ 8.03 (dt, $J = 7.8, 1.0$ Hz, 2H), 7.71 – 7.61 (m, 3H), 7.57 – 7.43 (m, 13H), 7.40 – 7.34 (m, 4H), 7.18 (ddd, $J = 7.9, 5.2, 2.8$ Hz, 2H), 4.47 (t, $J = 6.1$ Hz, 2H), 3.84 – 3.65 (m, 2H), 2.38 (p, $J = 6.7$ Hz, 2H), 1.46 (h, $J = 9.0$ Hz, 2H).

¹³C NMR (101 MHz, CDCl₃) δ 140.81, 134.92, 134.89, 133.82, 133.72, 130.52, 130.39, 125.97, 123.14, 120.32, 119.08, 109.43, 42.25, 29.51, 29.36, 20.57.

General procedure for the phosphonium bromides *Bz-PPh₃-X*



NaH (13 mg, 0.52 mmol) was added into a solution of the aldehyde **7** (0.10 g, 0.13 mmol) and the phosphonium **3a** (0.14 g, 0.32 mmol) in anhydrous DCM (10 mL) at 0°C under argon. The solution was stirred for 16 h at room temperature under argon, then washed with H₂O. The organic phase obtained was dried over MgSO₄ and the solvent was removed under reduced pressure. The residue was purified by column chromatography (DCM/EP = 2/8) to give the desired product, **8a** as pale-yellow solid in 94% yield.

¹H NMR (400 MHz, CDCl₃) δ 8.21 – 7.93 (m, 2H), 7.61 – 7.26 (m, 9H), 7.26 – 7.10 (m, 4H), 7.09 – 6.95 (m, 4H), 6.92 – 6.77 (m, 5H), 6.54 (qd, *J* = 12.3, 9.0 Hz, 1H), 6.43 – 6.27 (m, 1H), 6.10 (dt, *J* = 15.8, 6.7 Hz, 0.3 H), 5.63 (dtd, *J* = 11.5, 7.2, 5.7 Hz, 0.7 H), 4.36 (qd, *J* = 7.0, 4.3 Hz, 2H), 2.46 – 2.23 (m, 2H), 2.16 – 1.97 (m, 2H)

4-(5-(9H-carbazol-9-yl)pent-1-en-1-yl)-N-(4-iodophenyl)-N-(4-(4-nitrostyryl)phenyl)aniline (**8b**)

8b (0.25 g) was prepared from the phosphonium **3b** (0.18 g, 0.38 mmol) and the aldehyde **7** in quantitative yield.

¹H NMR (400 MHz, CDCl₃) δ 6.80-8.20 (m, 26H), 6.36 (m, 1H), 5.65 (m, 1H), 4.37 (q, *J* = 7.1 Hz, 2H), 2.40 (m, 1H), 2.30 (m, 1H), 2.10 (m, 2H).

4-(5-(9H-carbazol-9-yl)pent-1-en-1-yl)-N-(4-iodophenyl)-N-(4-(4-trifluoromethylstyryl)phenyl)-aniline (**8c**)

8c (0.11 g) was prepared from the phosphonium **3c** (0.19 g, 0.38 mmol) and the aldehyde **7** in 46% yield.

¹H NMR (400 MHz, CDCl₃) δ 6.80-8.20 (m, 26H), 6.60 (m, 1H), 6.35 (m, 1H), 4.40 (m, 2H), 2.40 (m, 1H), 2.30 (m, 1H), 2.10 (m, 2H).

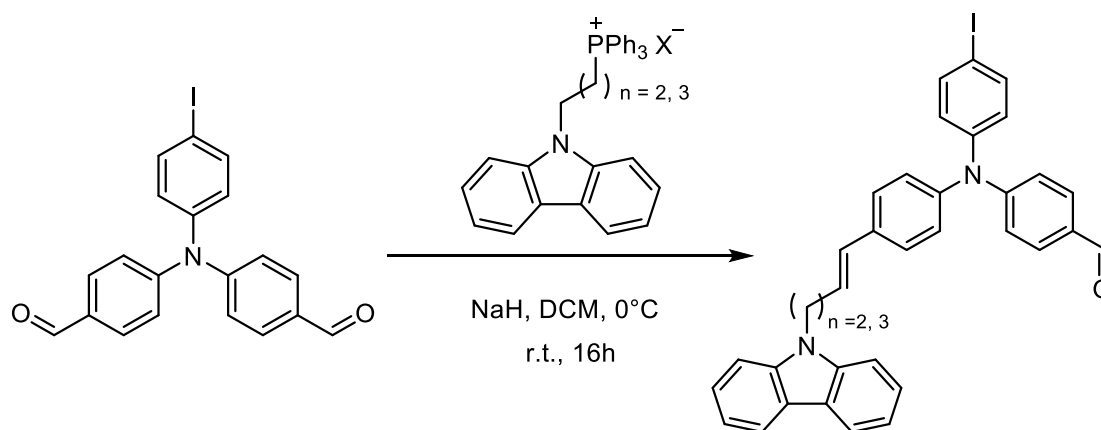
4-(5-(9H-carbazol-9-yl)pent-1-en-1-yl)-N-(4-iodophenyl)-N-(4-(4-methoxystyryl)phenyl)-aniline (**8d**)

8d (0.17 g) was prepared from the phosphonium **3d** (0.16 g, 0.38 mmol) and the aldehyde **7** in 73% yield.

^1H NMR (400 MHz, CDCl_3) δ (ppm): 6.80-8.20 (m, 24H), 6.45 (m, 2H), 6.20 (m, 2H), 4.37(m, 2H), 3.82 (m, 3H), 2.40 (m, 1H), 2.30 (m, 1H), 2.10 (m, 2H).

Wittig reactions

- Mono-Wittig reaction procedure



To a solution of **8** (95 mg, 0.22 mmol), phosphonium salt CBZ-*n*C-PPh₃-X (0.52 mmol) in dry DCM (10 ml), NaH (23 mg, 0.88 mmol) was added under argon at -15°C . The solution was stirred for 16h at room temperature under argon then diluted with DCM. It was washed with water then dried over MgSO_4 . The solvent was removed under reduced pressure. The mixture was purified by column chromatography (DCM/Petroleum ether = 1/1) to give the desired product as yellow solid.

(from CBZ-3C-PPh₃-Br)

^1H NMR (400 MHz, CDCl_3) δ 9.83 (s, 1H), 8.11 (ddt, $J = 7.6, 5.1, 1.0$ Hz, 2H), 7.77 – 7.66 (m, 2H), 7.66 – 7.55 (m, 2H), 7.30 – 7.16 (m, 4H), 7.10 – 6.96 (m, 6H), 6.94 – 6.81 (m, 2H), 6.50 – 6.39 (m, 1H), 6.14 (dt, $J = 15.7, 7.2$ Hz, 0H), 5.73 (dt, $J = 11.6, 7.3$ Hz, 1H), 4.49 – 4.40 (m, 2H), 2.99 – 2.71 (m, 2H).

^{13}C NMR (101 MHz, CDCl_3) δ 190.55, 152.69, 146.08, 144.46, 140.43, 138.88, 134.49, 134.21, 131.46, 130.76, 130.13, 130.02, 128.43, 127.81, 127.70, 127.58, 127.03, 126.22, 125.83, 125.82, 125.78, 123.11, 120.57, 120.43, 119.12, 108.81, 108.74, 38.30, 31.38.

4-((4-(5-(9H-carbazol-9-yl)pent-1-en-1-yl)phenyl)(4-iodophenyl)amino)benzaldehyde (12)

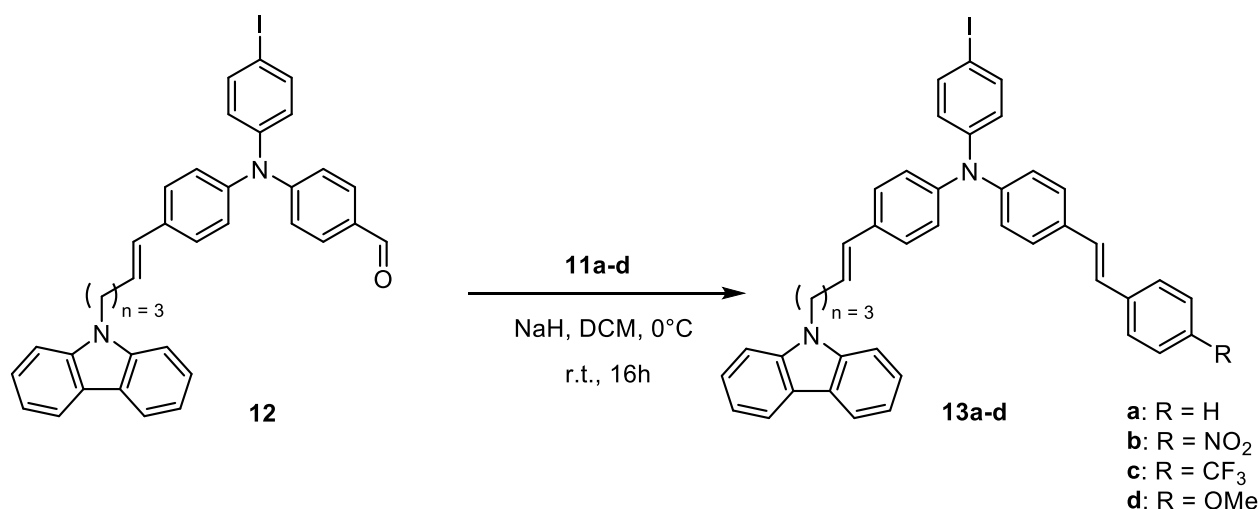
(from CBZ-4C-PPh₃-Br, **10**) (Yield: 97 mg, 70%)

^1H NMR (400 MHz, CDCl_3) δ 9.84 (s, 1H), 8.08 (ddt, $J = 24.9, 7.8, 1.0$ Hz, 2H), 7.78 – 7.58 (m, 4H), 7.51 – 7.34 (m, 4H), 7.30 – 7.14 (m, 3H), 7.12 – 6.96 (m, 4H), 6.45 – 6.30 (m, 1H),

6.15 (dt, $J = 15.8, 6.8$ Hz, 0.3 H), 5.69 (dt, $J = 11.7, 7.3$ Hz, 0.7 H), 4.38 (q, $J = 7.0$ Hz, 2H), 2.46 – 2.24 (m, 2H), 2.15 – 2.00 (m, 2H).

^{13}C NMR (101 MHz, CDCl_3) δ 190.22, 152.91, 146.44, 140.81, 139.02, 135.14, 134.65, 131.61, 131.41, 130.52, 130.30, 129.79, 129.46, 127.85, 127.72, 127.60, 126.43, 126.12, 125.84, 123.38, 123.32, 120.75, 120.69, 120.59, 120.57, 119.15, 108.90, 108.82, 88.41, 53.44, 42.73, 30.71, 29.90, 29.33, 28.74, 26.67.

- Bis-Wittig reaction procedure (**13a-d**)

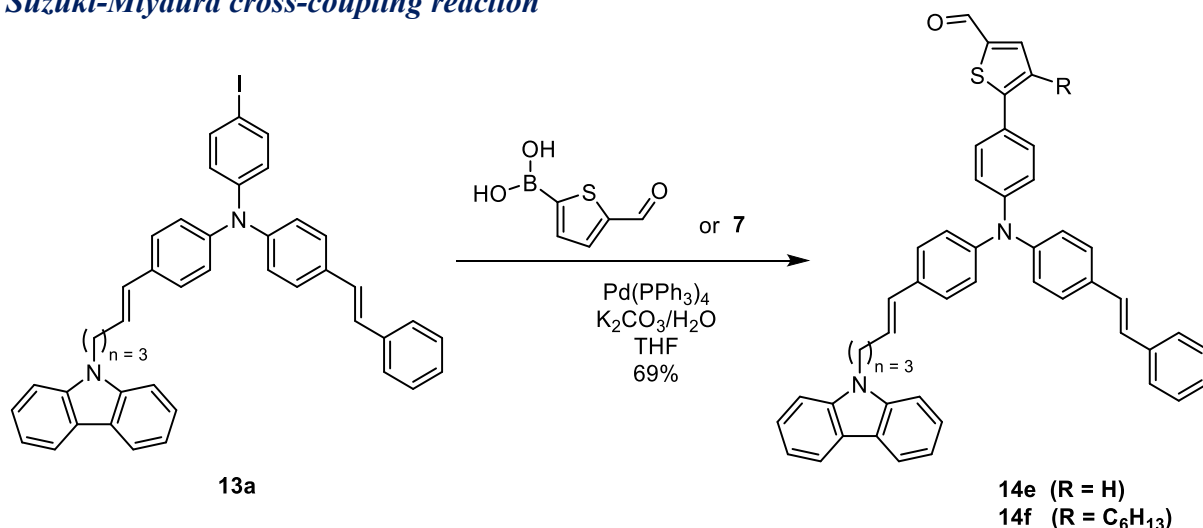


4-(5-(9H-carbazol-9-yl)pent-1-en-1-yl)-N-(4-iodophenyl)-N-(4-(styryl)phenyl)aniline (13a)

Under argon, aldehyde **12** (0.1g, 0.13 mmol), benzyltriphenylphosphonium bromide **11a** (0.14 g, 0.32 mmol), and NaH (0.013g, 0.52 mmol) was added into anhydrous DCM (10 mL) at 0°C . The solution was stirred for 16h at room temperature under argon then was extracted with DCM/ H_2O . The organic phase obtained was dried over MgSO_4 and the solvent was removed under reduced pressure. The mixture was purified by column chromatography (DCM/EP = 2/8) to give the desired product **13a** as pale-yellow solid (86 mg, 94%).

^1H NMR (400 MHz, CDCl_3) δ 8.21 – 7.93 (m, 2H), 7.61 – 7.26 (m, 9H), 7.26 – 7.10 (m, 4H), 7.09 – 6.95 (m, 4H), 6.92 – 6.77 (m, 5H), 6.54 (qd, $J = 12.3, 9.0$ Hz, 1H), 6.43 – 6.27 (m, 1H), 6.10 (dt, $J = 15.8, 6.7$ Hz, 0.3 H), 5.63 (dtd, $J = 11.5, 7.2, 5.7$ Hz, 0.7 H), 4.36 (qd, $J = 7.0, 4.3$ Hz, 2H), 2.46 – 2.23 (m, 2H), 2.16 – 1.97 (m, 2H)

Suzuki-Miyaura cross-coupling reaction



Under argon atmosphere, **13a** (105 mg, 0.14 mmol) and commercial 5-formyl-2-thiopheneboronic acid (33 mg, 0.21 mmol) were dissolved in a mixture of water (6 mL) and THF (30 mL). After it was stirred and bubbled by argon for 30 min, K₂CO₃ (1.00 g, 7.3 mmol) was added, followed by the palladium catalyst Pd(PPh₃)₄ (17 mg, 0.014 mmol). The mixture was heated under reflux for 4 h, followed by TLC. After cooling, THF was removed under reduced pressure, and the aqueous portion was extracted with CH₂Cl₂ (3 x 40 mL). The organic layers were dried over anhydrous MgSO₄ and the solvent removed under vacuum. The residue was purified by column chromatography using petroleum ether/DCM (1/1) to give the desired product **14e** as a yellow oil (67 g, 69%).

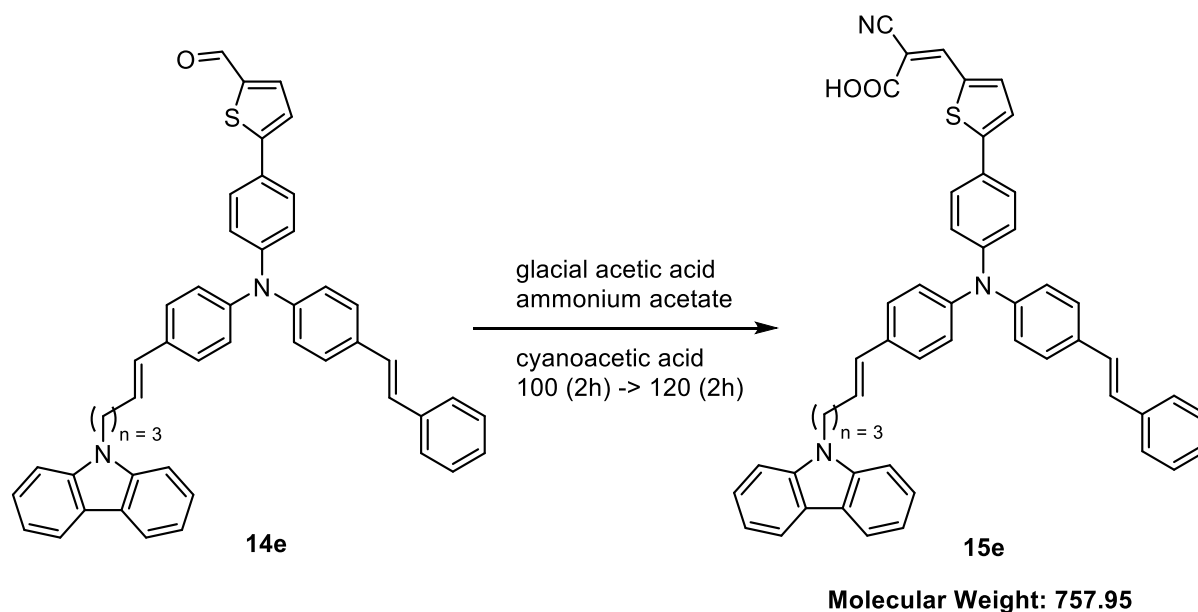
¹H NMR (400 MHz, CDCl₃) δ 9.78 (dd, *J* = 5.0, 2.5 Hz, 1H), 8.03 (d, *J* = 7.7 Hz, 1H), 7.97 (t, *J* = 7.3 Hz, 1H), 7.63 (dt, *J* = 7.1, 3.6 Hz, 1H), 7.53 – 6.93 (m, 23H), 6.92 – 6.80 (m, 2H), 6.59 – 6.40 (m, 1H), 6.37 – 6.21 (m, 1H), 6.13 – 5.96 (m, 0.4H), 5.67 – 5.48 (m, 0.6H), 4.39 – 4.23 (m, 2H), 2.40 – 2.29 (m, 1H), 2.24 – 2.16 (m, 1H), 2.08 – 1.93 (m, 2H).

¹³C NMR (101 MHz, CDCl₃) δ 182.37, 154.55, 149.02, 146.03, 142.04, 140.80, 137.84, 137.25, 133.35, 130.92, 130.54, 130.30, 130.06, 129.82, 129.71, 128.99, 128.87, 128.49, 128.31, 127.82, 127.68, 127.57, 127.30, 126.65, 125.82, 125.43, 125.15, 125.03, 124.82, 124.48, 124.40, 123.33, 123.20, 120.54, 119.10, 108.91, 108.82, 68.10, 59.92, 42.73, 38.47, 31.44, 30.69, 29.87, 29.34, 29.34, 26.68, 25.82.

The same synthetic procedure towards **14f**, while using **7** instead of commercial 5-formyl-2-thiopheneboronic acid. Yield: 82 mg, 76%.

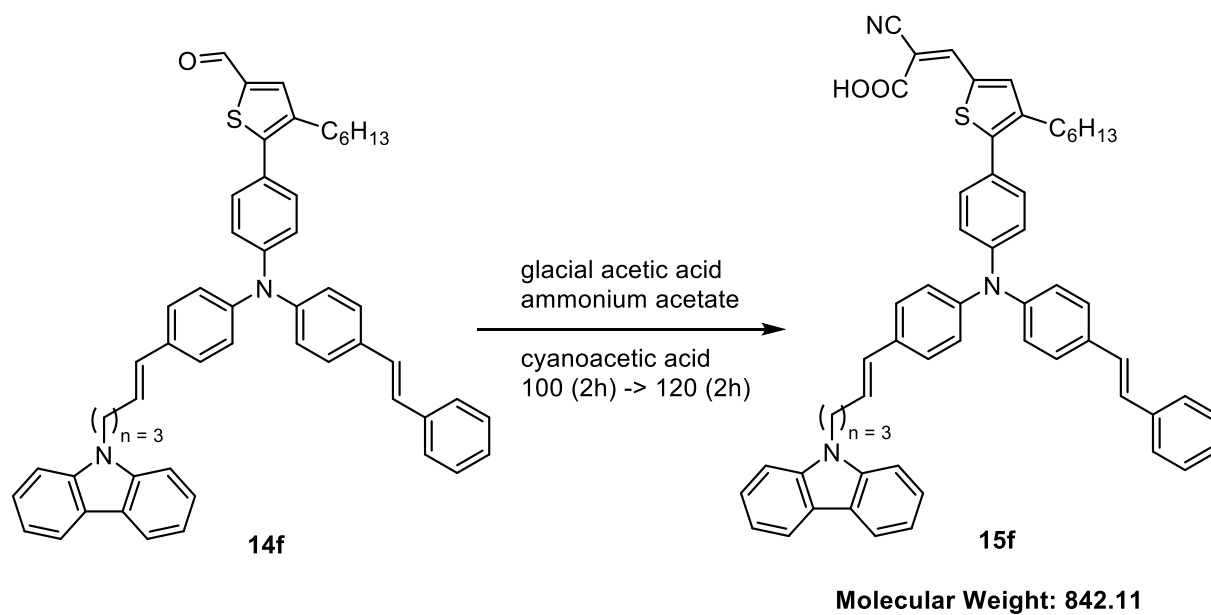
Final products (target dyes)

3-[5-[[4-(2-phenylethenyl)phenyl][5-(9H-carbazol-9-yl)pentenyl]aminophenyl]-2-thienyl]-2-cyano-2-propenoic acid (**15e** or **ZJX4015**)



A mixture of **14e** (0.1 mmol), cyanoacetic acid (43 mg, 0.5 mmol) and ammonium acetate (19 mg, 0.24 mmol) in glacial acetic acid (10 mL) was heated at 120°C for 4 hours under argon atmosphere (followed by TLC). After cooling down to room temperature, the mixture was extracted with DCM/H₂O. The organic layers were washed by water (5 x 100 ml) and dried over anhydrous MgSO₄ and the solvent removed under vacuum. The residue was purified by column chromatography and PLC using 5% of MeOH in DCM to give a red solid ZJX4015 or **15e** (56 mg, 74% yield). The product was confirmed by mass spectroscopy ($m/z_{\text{calc}} = 757.28$, $m/z_{\text{found}} = 757.28$, $[M]^{+/\bullet}$).

3-[5-[[4-(2-phenylethenyl)phenyl][5-(9H-carbazol-9-yl)pentenyl]aminophenyl]-(4-hexyl-2-thienyl)]-2-cyano-2-propenoic acid (**15f** or **ZJX4041**)



The same synthetic procedure towards product **15f**, while using **14f** as starting material. Yield: 65 mg, 77%.